TECHNISCHE UNIVERSITÄT MÜNCHEN

Fakultät für Medizin

Hedgehog and insulin signalling in β-cell biology and glucose metabolism

Felizitas Maria Schmitz

Vollständiger Abdruck der von der Fakultät für Medizin der Technischen Universität München zur Erlangung des akademischen Grades eines

Doktors der Naturwissenschaften

genehmigten Dissertation

Vorsitzender: Prof. Dr. Matthias Tschöp

Prüfer der Dissertation:

1. Prof. Dr. Heiko Lickert

2. Prof. Dr. Martin Hrabě de Angelis

Die Dissertation wurde am 31.08.2017 bei der Technischen Universität München eingereicht und durch die Fakultät für Medizin am 21.02.2018 angenommen.

Contents

1 List of abbreviations

5330417C22RIK	KIAA1324, EIG121 (oestrogen-induced gene 121)
AC	adenylate cyclase
ACET. TUB	acetylated tubulin
ACTH	adrenocorticotropic hormone
ADP	adenosine diphosphate
AGRP/NPY	NPY in agouti-related peptide
AICAR	5-aminoimidazole-4-carboxamide ribonucleotide
AJCC	American Joint Committee on Cancer
AKT	serine-threonine kinase AKT (PKB)
ALMS	Alström syndrome
AMPK	AMP-activated protein kinase
AP	adaptor protein
AP2	adaptor protein 2
ARF1	ADP ribosylation factor 1
ARL13B	ADP ribosylation factor like GTPase 13B
AS160	TBC1 Domain Family Member 4 (TBC1D4)
ATG16L1	autophagy-related 16 Like 1
ATG3	autophagy-related 3
ATG5	autophagy-related 5
ATG6	autophagy-related 6 (beclin 1)
ATG7	autophagy-related 7
ATP	adenosine triphosphate
AUC	area under the curve
AURA	major centrosomal mitotic kinase aurora kinase A
BAD	BCL2-associated agonist of cell death
BBS	Bardet–Biedl syndrome
BBS4	Bardet–Biedl syndrome 4
BECLIN 1	autophagy-related 6 (Atg6)
BFP	blue fluorescent protein
BMI	body mass index
BP	base pair
CAMKKB	calcium/calmodulin-dependent protein kinase kinase b
CAMP	cyclic adenosine monophosphate
CAV1	caveolin 1
CAV2	caveolin 2
CAV3	caveolin 3
CDE	clathrin-dependent endocytosis
CDK2	cyclin-dependent kinase 2
CDK4	cyclin-dependent kinase 4
CDKN1A	cyclin-dependent kinase inhibitor 1a
CDKN1B	cyclin-dependent kinase inhibitor 1b
CD-M6PR	cation dependent mannose 6-phosphate receptor
CETN2	centrin 2
C-FOS	cellular oncogene c-FOS

CIE	clathrin-independent endocytosis
CI-M6PR	cation-independent mannose 6-phosphate receptor (IGF2R)
CK1	casein kinase 1
CME	clathrin-mediated endocytosis
CNV	copy number variant
COLL IV	collagen IV
CONA	concanavalin A
COPI	coat protein complexe I
COPII	coat protein complexe II
CSF1R	colony stimulating factor 1 receptor
CYC	cyclopamine
DAPI	40, 6-diamidin-2-phenylindol
DHH	desert hedgehog
DMSO	dimethyl sulfoxide
DPP4	Dipeptidylpeptidase 4
E18.5	embryonic day 18.5
E2	oestrogen 2
EDU	5-ethynyl-2'-deoxyuridine
EE	early endosomes
EEA1	early endosome marker
EGFP	enhanced green fluorescence protein
EGFR	epidermal growth factor receptor
EIG121	oestrogen-induced gene 121; 5330417C22RIK
ELISA	enzyme-linked immunosorbent assay
ELK1	ETS transcription factor
EMP12	endomembrane protein 12
EPAC	cAMP-regulated guanine nucleotide exchange factor
ER	endoplasmic reticulum
ERBB2, EGFRB2	erb-B2 receptor tyrosine kinase 2
ERGIC	ER-Golgi intermediate compartment
ERα	oestrogen receptor α
ESC	embryonic stem cell
EXCHIP	exon chip analysis
FACS	fluorescence activated cell sorting
FFAR	G-protein-coupled free fatty acid receptor
FFAS	free fatty acids
FGF	fibroblast growth factor
FLTP	flattop
FOXO1	forkhead box O1
FSH	follicle-stimulating hormone
G-1-P	glucose-1-phosphate
G-6-P	glucose-6-phosphate
GCG	glucagon
GDP	guanosine diphosphate
GIP	gastrointestinal inhibitory polypeptide
GIPR	gastric inhibitory polypeptide receptor
GLI1,2,3	glioma-associated oncogene homolog 1,2,3

GLIS3	Gli similar proteins 3
GLP1	glucagon-like peptide-1
GLP1	glucagon-like peptide 1
GLP1R	glucagon-like peptide 1 receptor
GLUT2	glucose transporter type 2
GLUT4	glucose transporter type 4
GM130	golgi matrix protein 130
GNRH	gonadotropin-releasing hormone
GPCR	G protein–coupled receptor
GPCRY1	G protein–coupled receptors Y1
GPCRY1	G protein–coupled receptors Y1
GPI	glycosylphosphatidylinositol
GPRASP2	G protein-coupled receptor associated sorting protein 2
GRB10	growth factor receptor bound protein 10
GRB2	growth factor receptor bound protein 2
GRK2	G protein-coupled receptor kinase
GRP78	glucose-regulated protein 78 kDa
GSIS	glucose-induced insulin secretion
GSK3	glycogen synthase kinase 3
GSK3β	glycogen synthase kinase 3β
GTP	guanosine triphosphate
GTT	glucose tolerance test
GWAS	genome-wide association study
H & E	Hematoxylin and Eosin staining
HAP1	huntingtin-associated protein 1
HAT	hypoxanthine-aminopterin-thymidine
HBSS	Hank's balanced salt solution
HDL	high-density lipoprotein
HEF1	human enhancer of filamentation 1
HET	heterozygous
HFD	High-fat diet
HH	Hedgehog
HIF	hypoxia-inducible factors
HNF1α	hepatic nuclear factor 1 α
HPA	hypothalamic–pituitary–adrenal
HPG	hypothalamic–pituitary–gonadal
HPRT	hypoxanthine-guanine phosphoribosyltransferase
HSP90	heat shock protein 90
IF	immunofluorescence
IFT	intraflagellar transport
IGF1	insulin-like growth factor 1
IGF1R	insulin-like growth factor 1 receptor
IGF2	insulin-like growth factor 2
IGF2R	insulin-like growth factor 2 receptor (CI-M6PR)
IGFBP	IGF binding proteins
IGFR-L	insulin-like growth factor receptor-Like
IHC	immunohistochemistry

IHH	indian hedgehog
IL6Rα	interleukin-6 receptor subunit α
ILV	intraluminal vesicle
IMCD3	inner medullary collecting duct 3 cells
IMPC	International Mouse Phenotyping Consortium
INS	insulin
INSR	insulin receptor
IP	intraperitoneal or immunoprecipitation
iPSC	induced pluripotent stem cell
IRS	insulin receptor substrate proteins
IST	insulin secretion test
ITGB3	integrin subunit B 3
ITT	insulin tolerance test
KD	knock-down
KDEL	Lys-Asp-Glu-Leu
KI67	proliferation-related Ki67 antigen
KIAA1324	EIG121 (oestrogen-induced gene 121); 5330417C22RIK
KIF3A	kinesin family protein 3A
KIF7	kinesin family member 7
KO	knock-out
LAMP1	lysosomal-associated membrane protein 1
LAMP2	lysosomal-associated membrane protein 1
LC3A/B	autophagy-related protein LC3A
LDL	low-density lipoprotein
LE	late endosomes
LH	luteinizing hormone
LKB1	serine/threonine-protein kinase LKB1
LSM	laser scanning microscope
M6P	mannose 6-phosphate
MDM2	MDM2 proto-oncogene
MEF	mouse embryonic fibroblast cells
MEK1	dual specificity kinase MAPK kinase 1
MOC	Mander's overlap coefficient
MODY	Maturity Onset of Diabetes of the Youth
MTOR	mammalian target of rapamycin
MVB	multivesicular body
NAFLD	non-alcoholic fatty liver disease
NEDD4	neural precursor cell expressed developmentally down-regulated protein 4, E3 Ubiquitin
NEFA	non-esterified fatty acids
NEK	NIMA related kinase
NEO^{R}	neomycin phosphotransferase
NG2	chondroitin Sulfate Proteoglycan Ng2
NHS	N-Hydroxysulfosuccinimide
NKX2.2	NK2 homeobox 2
NKX6.1	Nk6 homeobox 1
NMR	Nuclear magnetic resonance spectroscopy

ORF	open reading frame
P0	postnatal day zero
PACAP	pituitary adenylate cyclase-activating polypeptide
PAX6	paired box homeotic gene-6
PCC	Pearson correlation coefficient
PCNT	pericentrin
PCSK2	neuroendocrine convertase 2
PDGFRα	platelet-derived growth factor receptor α
PDGFRβ	β-type platelet-derived growth factor receptor
PDK1	phosphoinositide-dependent kinase 1
PDX1	pancreatic and duodenal homeobox 1
PFA	paraformaldehyde
PGC1	peroxisome proliferator-activated receptor-γ coactivator 1
PI3K	phosphoinositide 3-kinase
PIFO	pitchfork
PIP2	phosphatidylinositol 4,5-bisphosphate
PIP3	phosphatidylinositol 3,4,5-trisphosphate
PKA	protein kinase A
PKB	protein kinase B (AKT)
PLK1	polo-like kinase 1
PM	plasma membrane
PP	pancreatic polypeptide
PTCH	patched
qPCR	real time quantitative PCR
RAB7	Ras-associated protein
RAF	proto-oncogene c-RAF
RAS	small G-protein Ras
RFX3	regulatory factor X 3
RTK	receptor tyrosine kinase
SAG	chlorobenzothiophene-containing Hh pathway agonist
SAR1	secretion associated ras-related GTPase 1
SD	standard deviation
SE	sorting endosomes
SEC	transport proteins SEC
SEM	standard error of the mean
SHC	Src homology-2
SHH	sonic hedgehog
SLC30A8	solute carrier family 30 member 8
SMA	smooth muscle actin
SMARCA1	ATPase chromatin subfamily A member 1
SMO	smoothened
SOS	guanine nucleotide exchange factor SOS
SST	somatostatin
SSTR3	receptor for somatostatin-14 and -28
SUFU	suppressor of fused homolog
T2D	Type 2 Diabetes
TBC1D4	TBC1 Domain Family Member 4 (AS160)

TCA	citric acid cycle
TFR	transferrin receptor
TGFβ	transforming growth factor β
TGN	*trans*-Golgi network
TGN46	*trans*-Golgi network 46
TIRF	total internal reflection fluorescence
TORC1	rapamycin complex-1
TRFP	tag red fluorescent protein (tagRFP)
TSC1/2	Rheb GTPase activating complex; tuberous sclerosis 1/2
T-TEST	Student's *t*-test
TYPE 1 DIABETES	T1D
TYPE 2 DIABETES	T2D
TBRIII	type III transforming growth factor receptor
UTR	untranslated region
VIP	vasoactive intestinal peptide
VLDL	very low density lipoprotein
WES	whole-exome sequencing
WGA	Wheat germ agglutinin
WGS	whole-genome sequencing
WHO	World Health Organization
WNT	wingless
WT	wildtype
βIGF1R	β-cell-specific deletion of IGF1R
βIRKO	β-cell-specific KO of INSR

2 Abstract

Type 2 diabetes is a chronic metabolic disease that is a leading cause of morbidity and mortality worldwide. It is characterized by hyperglycaemia due to peripheral insulin resistance and β-cell dysfunction. The main aims of this thesis were to investigate the biological and molecular function of a novel gene, the *insulin-like growth factor receptor-Like* (*Igfr-L*), and of cilia-dependent Hedgehog (Hh) signalling in the islet of Langerhans as well as their effect on glucose metabolism.

A subset of ciliopathy patients manifests metabolic disorders due to defective cilia that interfere with cellular homeostasis, numerous signalling pathways including Hh signalling, and cell-cycle regulation. We describe the generation of a Cre-inducible cilium-specific reporter mouse line expressing the ARL13B-tRFP fusion protein, which labels cilia with a strong fluorescence protein and verified its functionality by immunostainings and by live-cell imaging of various mono and multi-ciliated tissues. A well-characterized cilium-dependant signalling cascade is the Hh pathway that is crucial for embryonic development and controls tissue maintenance, cell proliferation and regeneration in adults. However, its relevance in the adult endocrine pancreas remains poorly explored. We demonstrated that Hh ligand stimulation induces cell proliferation of pancreatic endocrine cells *in vitro*, and showed that islets, derived from Kif7$^{+/-}$ mice, displayed a slight insulin secretion defect. Moreover, we identified Igfr-L as a novel receptor that is highly expressed in pancreatic β-cells and plays a major role in the control of glucose metabolism. Igfr-L$^{-/-}$ mice die postnatally with signs of lethargy, respiratory distress, cyanosis, hyperinsulinemia and hypoglycaemia. Pancreata of Igfr-L$^{-/-}$ mice exhibited elevated mRNA expression of glucose metabolism-associated genes at postnatal day P0. Additionally, adult Igfr-L$^{+/-}$ mice displayed impaired insulin sensitivity, mild hyperinsulinemia and slight glucose intolerance after 28 weeks of HFD feeding. *In vitro* studies in the β-cell line Min6, revealed that the Igfr-L is transported in the secretory pathway of the cell und likely shuttles between Golgi, the lysosome and the cell surface by clathrin-mediated endocytosis. We showed that Igfr-L negatively regulates insulin signalling and the key metabolic sensor Ampk. The Igfr-L is a transmembrane receptor that comprises a potential growth factor receptor cysteine-rich domain and a predicted mannose-6-phosphate binding domain, which are similar to domains found in receptor tyrosine kinases and the insulin-like growth factor receptor 2. Thus, we hypothesis that the Igfr-L acts as signalling co-receptor or scavenger receptor at the plasma membrane, thereby influencing insulin signalling and glucose metabolism.

In conclusion, we demonstrated that the *Igfr-L* gene encoding for a novel receptor that modulates insulin signalling and Hh signalling are involved in the regulation of glucose metabolism. Thus, both, the Igfr-L protein and Hh pathway, are molecular targets for diabetes treatment.

3 Introduction

3.1 Relevance and implications of diabetes mellitus

Diabetes mellitus is a chronic metabolic disease, which became a major healthcare problem with a growing prevalence worldwide. According to the World Health Organization (WHO) report in 2017, the number of people worldwide suffering from diabetes mellitus increased from 108 million in 1980 to 422 million in 2014. An estimated number of 1.5 million deaths were caused by this disease and almost 2.2 million deaths were attributable to high blood glucose in 2012 ("WHO | *Global report on diabetes*," 2017).

Diabetes mellitus is a group of metabolic diseases characterized by a disturbance in the energy homeostasis of the body as a result of hyperglycaemia (Alberti & Zimmet, 1998). Maturity Onset of Diabetes of the Youth (MODY) patients display mutations in single genes critical for β-cell function such as hepatic nuclear factor 1 α (*HNF1α*), pancreatic and duodenal homeobox 1 (*PDX1*) or glucokinase. This rare type of diabetes usually manifests in young patients with first symptoms under the age of 25. Type 1 diabetes (T1D) mellitus is an autoimmune disease, which causes the autoimmune progressive destruction of insulin-producing β-cells by CD4+ and CD8+ T cells and macrophages infiltrating the islets. This can eventually lead to an absolute deficiency in insulin in the body. T1D patients usually require daily insulin administration for survival. The main characteristic of Type 2 diabetes (T2D) is hyperglycemia due to peripheral insulin resistance and dysfunctional β-cells. Risk factors for T2D are lifestyle related and genetic predispositions including obesity, a poor diet, age, pregnancy and physical inactivity. Although T2D patients do not entirely depend on insulin treatment, a third of them need insulin on a regular basis to adjust their blood glucose levels. Untreated diabetes patients with chronic hyperglycemia can develop serious long-term complications including polydipsia, polyphagia, cardiovascular disease, stroke, chronic kidney disease, foot ulcers, vision loss and nerve damage, which can even lead to death. Current treatments cannot stop or revert diabetes progression, thus novel regenerative therapies are urgently needed.

3.2 The pancreas and its interplay with metabolic organs in the regulation of energy homeostasis

The pancreas plays a key role in the regulation of energy homeostasis by controlling nutrient digestion and glucose metabolism. The adult pancreas is divided into an exocrine compartment consisting of acinar and ductal epithelium and an endocrine structure comprising the islets of Langerhans. In the exocrine part, which form 85% of the mass of the pancreas, acinar cells are organized in grape-like structures surrounding the tips of the tubular ductal network. Centroacinar cells lie at the interface of acinar cell clusters and the epithelium at the terminal end of intralobular ducts. These intralobular ducts merge to form interlobular ducts, which are linked to the main duct, which in turn connect the pancreas to the duodenum (Bastidas-Ponce, Scheibner, Lickert, & Bakhti, 2017; Grapin-Botton, 2005). Acinar cells secrete digestive enzymes such as amylase, pancreatic lipase and trypsinogen into the ductal system. Ductal cells secret

mucin and an aqueous bicarbonate solution that neutralizes stomach acidity. The islet of Langerhans is a cluster of cells composed of five different cell types, which releases various hormones directly into the bloodstream. Islets are scattered in the whole pancreas representing approximately 1–2% of the organ volume. These micro-organs are highly vascularized by an extensive endothelial network and innervated by sympathetic, parasympathetic and sensory nerves. In adult mice, insulin-producing β-cells represent the main portion with 65–80% of total islet cells building the islet core. Glucagon-producing α-cells (15–20%), pancreatic polypeptide (PP)-producing γ-cells (3–5%), somatostatin producing δ-cells (3–10%) and ghrelin-producing ε-cells (<1%) are located in the islet periphery (Brissova et al., 2005; Islam, 2010). The interplay of different pancreatic endocrine hormones maintains blood glucose levels within a narrow range of 4–6 mM. The most critical hormones in the regulation of glucose metabolism are insulin and glucagon. Nevertheless, somatostatin, PP and ghrelin are also essential for a balanced homeostasis. Somatostatin inhibits the release of glucagon and insulin whereas the PP hormone regulates the exocrine and endocrine secretion activity of the pancreas and gut motor activity (Hauge-Evans et al., 2009; Khandekar, Berning, Sainsbury, & Lin, 2015). Ghrelin, which is also expressed in many other tissues in the body such as the gastrointestinal tract, adrenal cortex and kidney, stimulates the hypothalamus resulting in increased appetite, elevated gastric acid secretion and stimulated gastrointestinal motility (Gil-Campos, Aguilera, Cañete, & Gil, 2017).

Upon food ingestion, nutrients including glucose are absorbed by the gastro-intestinal system and transferred into the blood system. An elevated exogenous glucose level promotes insulin secretion by the pancreatic β-cell. Thereby, glucose is incorporated by the β-cells via the membranous glucose transporter type 2 (GLUT2) and metabolized intracellularly via the glycolysis and the citric acid cycle (TCA), resulting in an increase in the cytoplasmic adenosine triphosphate (ATP) to adenosine diphosphate (ADP) ratio (Henquin, 2009; Rorsman & Braun, 2013). This leads to the closure of ATP-sensitive potassium channels (K_{ATP} channels) followed by the depolarization of the cell membrane and to the opening of voltage-gated Ca^{2+} channels. Subsequently, insulin secretion is triggered by an increase in cytoplasmic Ca^{2+} concentration (Henquin, 2009; Rorsman & Braun, 2013). Elevated Ca^{2+} levels allow the fusion of insulin-containing vesicles with the plasma membrane and the subsequent release of insulin granules into the bloodstream (Henquin, 2000, 2009). Insulin secretion is a biphasic process with an initial rapid transient peak around 5-10 minutes after glucose stimulation being followed by a slowly developing second phase of release (>30 min) (Rorsman & Braun, 2013; Y. Shi et al., 2000).

Insulin in the blood system binds to the insulin receptor (InsR) at the cell surface of peripheral tissues like liver, skeletal muscle and adipose tissue activating the insulin signalling cascade in these cells (Figure 3.1). This enables the uptake of glucose from the bloodstream by the GLUT2 transporter in these metabolic tissues (Khan & Pessin, 2002; Kohn, Summers, Birnbaum, & Roth, 1996; Zisman et al., 2000). In the liver insulin enhances glycogenesis, a process in which glycogen is synthesised from glucose. Insulin inactivates glycogen phosphorylase and glycogen synthase kinase (GSK)-3 through the phosphoinositide 3-kinase (PI3K) pathway that in turn activates glycogen synthase (Han, Kang, Kim, Choi, & Koo, 2016; Rui, 2014). Moreover, incorporated glucose stimulates glycolysis by enhancing the expression of the hepatic glucokinase gene, a key

enzyme that converts glucose into glucose-6-phosphate (G-6-P). G-6-P is metabolized into pyruvate through glycolysis (Han et al., 2016; Rui, 2014). The cell further oxidizes pyruvate through the TCA cycle and oxidative phosphorylation to generate ATP in mitochondria. Additionally, glycolytic products are used to synthesize fatty acids by lipogenesis. Long-chain fatty acids help producing triacylglycerol, phospholipids, and cholesterol esters in hepatocytes that are then stored in lipid droplets or released into the circulation as very low density lipoprotein (VLDL) particles (Rui, 2014).

When blood glucose levels are low during sleep phases or in between meals, glucagon is secreted into the blood stream by pancreatic α-cells (Figure 3.1). Glucagon counteracts insulin actions by promoting breakdown of glycogen into glucose (glycogenolysis) in the liver and muscle cells and by raising *de novo* glucose synthesis (gluconeogenesis) in the liver, which allows the release of glucose into the circulation. In adipocytes, glucagon promotes lipolysis that causes the conversion of stored triglycerides into free fatty acids and glycerol. Free glycerol travels through the bloodstream to the liver where it can also be converted into glucose. Non-esterified fatty acids (NEFA) are released and metabolised into ketone bodies in the liver by mitochondrial β-oxidation and ketogenesis (Rui, 2014).

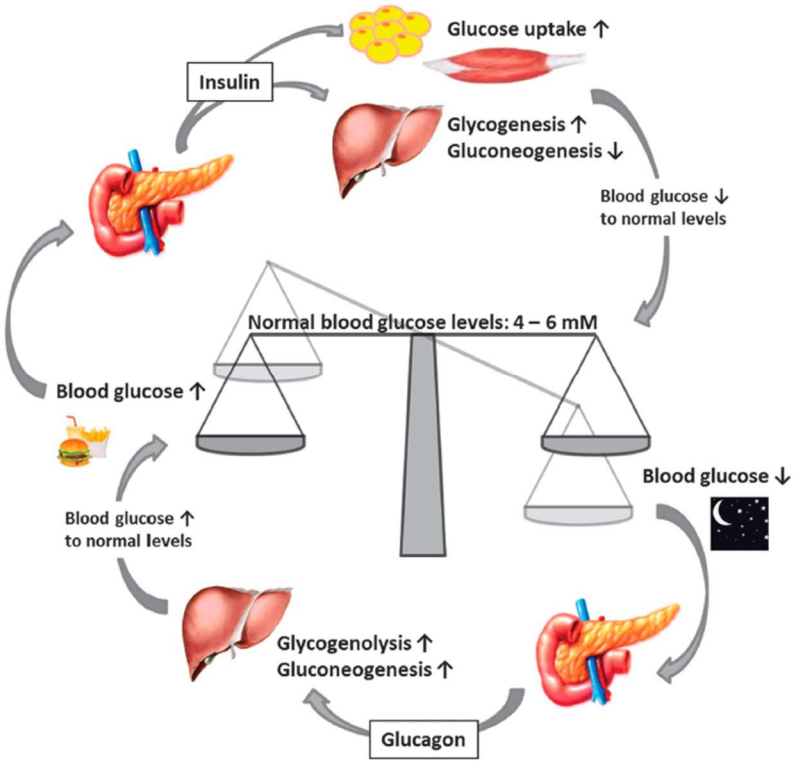

Figure 3.1: Regulation of glucose homeostasis by the pancreas and the peripheral metabolic organs, liver, skeletal muscle and adipose tissue.

Upon food intake, a rise in blood glucose levels induces the secretion of insulin from the pancreas into the blood stream. Insulin stimulates glucose uptake in the peripheral organs that leads to the induction of glycogenesis and the inhibition of gluconeogenesis in the liver. During starvation periods such as sleep

phases, the pancreas releases glucagon, which induces glycogenolysis and gluconeogenesis in the liver to maintain blood glucose levels. (The figure is adapted and modified from (Röder, Wu, Liu, & Han, 2016) Reprint by permission from Nature Publishing Group: Experimental & Molecular Medicine, copyright (2016))

3.3 Pancreatic β-cell failure in the development of T2D

Both insulin resistance and β-cell dysfunction contribute to the development of T2D. Insulin resistance, which is already distinct in prediabetic patients, involves the inability of metabolic organs like liver, muscle and adipose tissue to adequately respond to normal actions of insulin (Ferrannini, 2010; Samuel et al., 2012). β-cells react to insulin resistance by elevating their insulin production and secretion and by increasing their cell mass to compensate deteriorated insulin-related effects. In this phase of T2D development, patients display a normoglycemic state with a rise in insulin levels in the blood stream (hyperinsulinemia). As disease state progresses, β-cell function continues to decline and insulin production and secretion eventually becomes inadequate causing impaired glucose tolerance (Nolan & Prentki, 2008; Prentki & Nolan, 2006). Eventually, β-cell failure results in chronic hyperglycaemia and insulin resistance affecting the entire energy metabolism. Impaired insulin secretion often results in enhanced food intake due to decreased signalling in the hypothalamus leading to obesity and insulin resistance in the brain. Plasma glucose levels rise upon elevated glucose production in the liver and inefficient glucose uptake in liver and muscle cells. Additionally, adipocytes increase lipolysis releasing more non-esterified fatty acids (NEFA) into the circulation (Muoio & Newgard, 2008). Both, elevated circulating NEFA concentrations in the blood and increased weight gain inhibits the β-cell's adaptive response to insulin resistance. Chronic exposure to NEFAs, and high levels of glucose in turn contribute to β-cell dysfunction, especially aberrant secretory capacity, followed by detrimental loss of β-cell mass and survival. These pathomechanisms are also referred to as glucotoxicity and lipotoxicity (Del Prato, 2009; Janikiewicz, Hanzelka, Kozinski, Kolczynska, & Dobrzyn, 2015).

3.4 Cilia biology and cilia-related disease

Ciliopathies comprise a heterogeneous group of disorders associated with mutations in ciliary proteins, which result in dysregulated ciliogenesis or abnormal function of cilia. They involve a wide range of phenotypically and genetically overlapping human diseases like Bardet-Biedl syndrome (BBS), Joubert syndrome, Meckel-Gruber syndrome, nephronophthisis and Sensenbrenner syndrome. The clinical manifestations of these disorders include symptoms such as polycystic kidney disease, retinal degeneration, situs inversus, hydrocephalus, nephronophthisis, anosmia, hypogonadism and polydactyly (Hildebrandt, Benzing, Katsanis, & Katsanis, 2011; Oud, Lamers, & Arts, 2016). A subset of ciliopathies also manifest metabolic disorders, obesity and T2D related symptoms in humans. Beside other symptoms, BBS patients suffer from obesity and diabetes (Suspitsin & Imyanitov, 2016) with hyperphagia in some patients and defective sensory functions that would normally indicate satiation. Alström

syndrome (ALS) patients also feature a variety of endocrine related phenotypes including hyperinsulinemia, insulin resistance, T2D, hypertriglyceridemia and obesity (J. D. Marshall, Maffei, Collin, & Naggert, 2011). The link between ciliopathies and metabolic disorders implicates a functional role of cilia in the energy homeostasis of a cell.

The cilium itself is a highly conserved organelle found in most of eukaryotic cells, which projects from the cell surface like an antenna (Gerdes, Davis, & Katsanis, 2009; Pazour & Witman, 2003) (Figure 3.2A). It acts as mechano- and chemosensor by transducing extracellular cues such as mechanical flow into the cell or by mediating signalling induced by factors like hormones, growth factors and developmental morphogens (Goetz & Anderson, 2010; Singla & Reiter, 2006). The cilium core comprises nine parallel peripheral microtubule doublets, named the axoneme surrounded by a membrane that is continuous with the plasma membrane. The axoneme originates from the triplet microtubules structure of the basal body, the mother centriole (W. F. Marshall, 2008). Cilia are historically classified into two categories, motile and non-motile (primary) cilia. Motile cilia have a central pair of microtubules in the axoneme (9+2), which they connect to the outer ring of microtubule doublets via radial spoke proteins. Dynein arms attached to the microtubule doublets drive the ciliary bending motion (Ishikawa, 2017). In contrast, immotile primary cilia lack a central microtubule pair displaying a 9+0 arrangement. Cells with motile cilia often carry multiple cilia at their apical cell surface that cooperatively beat in a rhythmic manner to generate a fluid movement. Multi-ciliated cells are found in the respiratory epithelium where they are important for clearing mucus out of airways and in the ependyma of the brain where they are essential for the circulation of cerebrospinal fluid in the ventricular system. An exception in ciliary architecture constitutes the motile primary cilium at the node. Nodal cilia of vertebrates possess motile 9+0 cilia creating the leftward flow in the node establishing left-right body axis specification, a critical process during embryonic development (Babu & Roy, 2013; Komatsu & Mishina, 2013). The ciliary pocket at the base of cilia acts as a platform for cilia-associated vesicular trafficking (Benmerah, 2013). The movement of cargo proteins along microtubules via the intraflagellar transport (IFT) system is a molecular motor-driven process. It is catalysed by kinesin motor proteins (kinesin II) driving the anterograde transport and dynein motor proteins (dynein II) mediating the retrograde transport (Pedersen & Rosenbaum, 2008; Scholey, 2008). Transition fibers extend from the distal region of the basal body directly to the plasma membrane regulating protein entry and exit from the cilia compartment.

Primary cilia assemble after a cell has undergone differentiation or if a cell becomes quiescent. In the G0 and G1 phases of the cell cycle, the mother centriole of the centrosome migrates to the cell surface and differentiates into the basal body of which the primary cilium nucleates (Plotnikova, Pugacheva, & Golemis, 2009; Sanchez & Dynlacht, 2016) (Figure 3.2B). Disassembly of the primary cilium occurs upon cell cycle re-entry at the G1 to S phase transition. It is mediated by the major centrosomal mitotic kinase aurora kinase A (AurA), the polo-like kinase 1 (Plk1), and the NIMA related kinase (NEK) (Liang, Meng, Zhu, & Pan, 2016; Seeger-Nukpezah et al., 2012; Shalom, Shalva, Altschuler, & Motro, 2008). Proteins including Ca^{2+}/CaM, pitchfork (PIFO) and hypoxia-inducible factors (HIF) activate AurA through a human enhancer of filamentation 1

(HEF1) dependent or independent cascade (Kinzel et al., 2010; Plotnikova et al., 2012; Xu et al., 2010). The cilium associated centriole is released thereby allowing the centrosome to form a mitotic spindle.

The cilium is a complex signalling centre that regulates several signalling pathways important for development and tissue homeostasis (Gerdes et al., 2009; Goetz & Anderson, 2010). The ciliary membrane is enriched in receptors and channels which convey signals from the extracellular space into the cell (Pazour & Witman, 2003; Singla & Reiter, 2006). Cilium-associated signalling pathways are wingless (WNT), platelet-derived growth factor receptor α (PDGFRα), fibroblast growth factor (FGF), Notch, Hedgehog (HH) and inositol signalling (Goetz and Anderson 2010b).

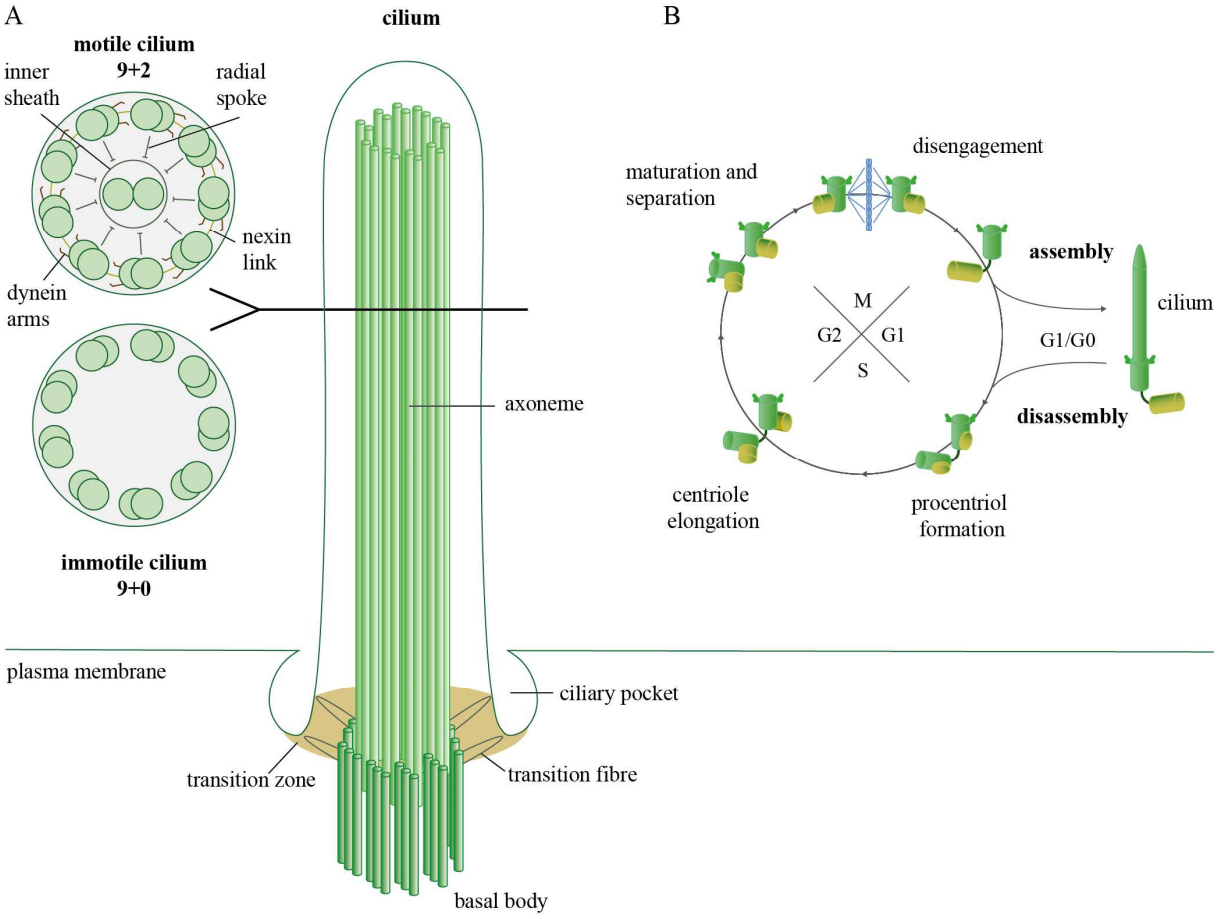

Figure 3.2: The architecture of a cilium and its link to the cell cycle

(A) Schematic image of the ciliary structure with cross-section diagramms of typical primary and motile cilia.
(B) Cilia assembly and dissasembly are tightly connected to the cell cycle and centrosome duplication.

3.5 Hedgehog signalling in vertebrates

A well-characterized signalling pathway, which was shown to be cilia-dependent, is the Hedgehog (HH) signalling cascade (Bangs & Anderson, 2017; Goetz & Anderson, 2010). HH signaling is evolutionarily highly conserved from Drosophila to humans and is regarded as a key regulator in

embryonic development (Briscoe & Thorond, 2013; Varjosalo & Taipale, 2008). The HH ligand acts as a long-range morphogen to control cell patterning and differentiation in several embryonic tissues such as the digit pattern in limbs or the organization of neuronal subtype identity in the central nervous system (Jiang & Hui, 2008). Additionally, the HH signalling pathway controls processes such as cell proliferation, stem cell homeostasis and plays a role in adult organ homeostasis and repair (Cochrane, Szczepny, Watkins, & Cain, 2015; Jia, Wang, & Xie, 2015; Petrova & Joyner, 2014). Moreover, it is involved in the development of many different types of cancers due to upregulation of the pathway (Jiang & Hui, 2008; Pak & Segal, 2016). HH signalling is controlled by three ligands, namely indian hedgehog (IHH), desert hedgehog (DHH) and sonic hedgehog (SHH). In vertebrates, SHH is mainly expressed in the developing nervous system and in many epithelial tissues. IHH acts primarily in bone development whereas DHH expression is limited to the peripheral nervous system and reproductive organs (Ingham & McMahon, 2001).

In the absence of HH ligands the 12-pass transmembrane protein patched (PTCH) localizes to the primary cilium base and inactivates the seven transmembrane receptor smoothened (SMO) by unknown mechanisms (Briscoe & Thorond, 2013) (Figure 3.3). The glioma-associated oncogene homolog (GLI) proteins, GLI1, GLI2 and GLI3 are transcription factors of the zinc finger protein family (Hui & Angers, 2011). GLI proteins are phosphorylated by the protein kinase A (PKA), the casein kinase 1 (CK1) and the glycogen synthase kinase 3β (GSK3β) at the base of cilia leading to the proteolytic cleavage of GLI3 and the complete degradation of GLI2 (Hui & Angers, 2011). This proteolytic processing causes the conversion from a full length active form (GliA) to a truncated repressor form (GliR), lacking the transcriptional activator domain (Hui & Angers, 2011). GLI processing is also promoted by suppressor of fused homolog (SUFU) and the kinesin family member 7 (KIF7) with SUFU forming complexes with GLI proteins (Cheung et al., 2009). The truncated repressor form of GLI (GLI-R) inhibits HH mediated target gene transcription in the nucleus (Hui & Angers, 2011).

The HH ligand activates the HH signaling cascade by binding to the PTCH receptor at the plasma membrane (Choy & Cheng, 2012) (Figure 3.3). Ligand binding causes the exit of PTCH from the cilium releasing its inhibition on SMO. Subsequently, SMO is phosphorylated by CK1 kinase and G protein-coupled receptor kinase (GRK2) enabling its translocation into the cilium (Wei Chen et al., 2004; Corbit et al., 2005; Kovacs et al., 2008). The SMO transport to the primary cilium is mediated by β-arrestins controlling the activity-dependent interaction of SMO and the motor protein kinesin family protein 3A (KIF3A) (Kovacs, Hara, Davenport, Kim, & Lefkowitz, 2009). Additionally, SMO translocation to the cilium is regulated by pitchfork (PIFO) and the G protein-coupled receptor associated sorting protein 2 (GPRASP2), which form a heterotrimeric complex with SMO. The authors showed that depletion of PIFO or GPRASP2 resulted in failure of SMO translocation to the cilium and in the lack of HH target gene activation suggesting the involvement of Pifo-Gprasp2 protein complex in SMO trafficking to the primary cilium (Jung et al., 2016). Furthermore, the activation of SMO results in the accumulation of GLI proteins in the tip of the cilium and the dissociation of the GLI–SUFU complex. KIF7 also localizes to the cilium and contributes to the activation of GLI proteins by assisting SMO in the dissociation of the GLI–SUFU

complex (Cheung et al., 2009). The full-length activator form of GLI (GLI-A) is transported from the cilium to the nucleus, where it activates transcription of HH target genes like cyclin D, cyclin E, proto-oncogene N-MYC, GLI1, PTCH1, paired box homeotic gene-6 (PAX6) and NK2 homeobox 2 (NKX2.2) in the nucleus (A M Kenney & Rowitch, 2000; Anna Marie Kenney, Cole, & Rowitch, 2003; Shahi et al., 2010).

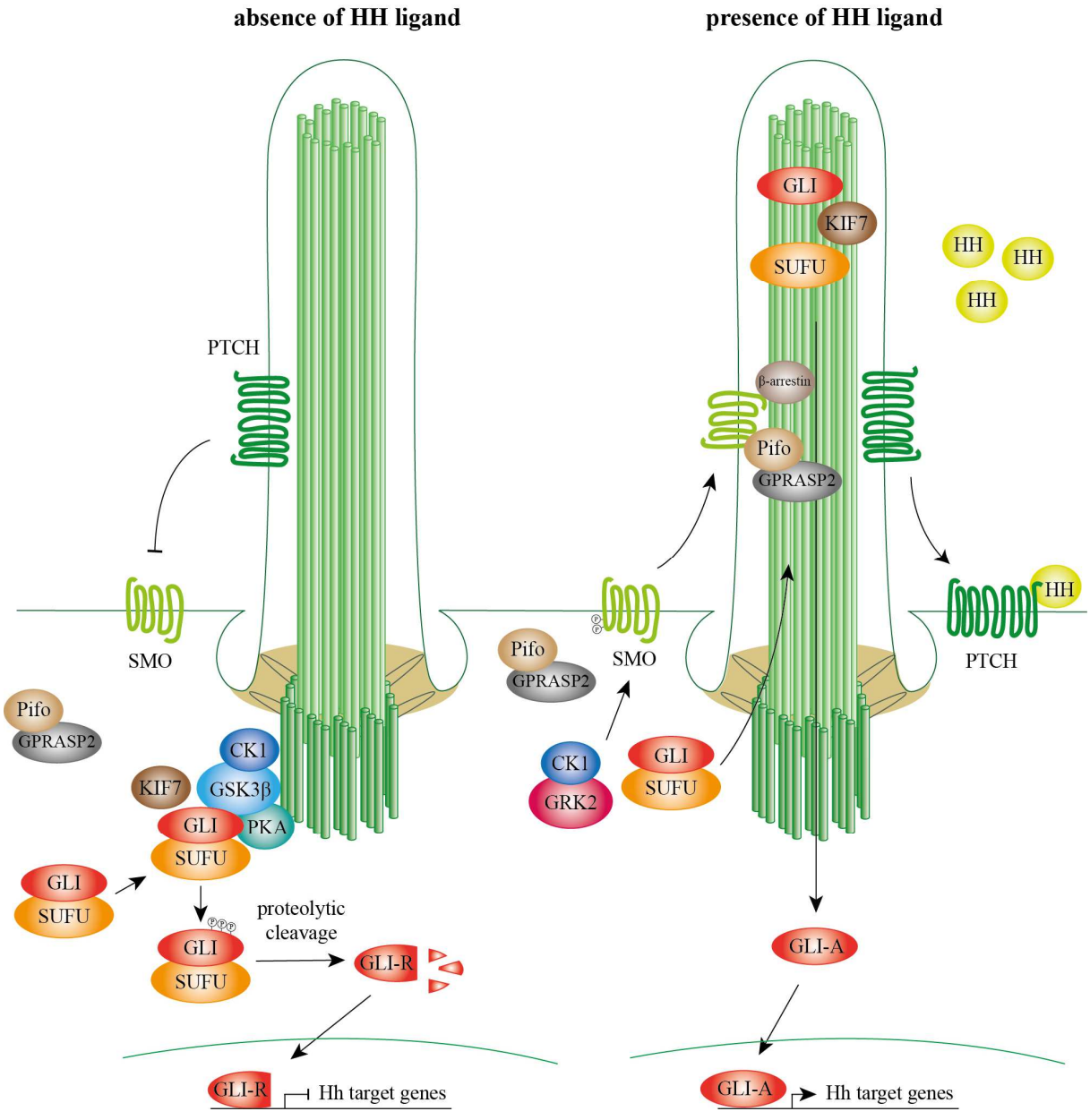

Figure 3.3: HH signalling pathway in vertebrates

Schematic illustration of the Hh signalling cascade in the absence and presence of Hh ligands.

Up to date, the function of Hedgehog (HH) signalling in the pancreas, especially in the β-cells was controversially discussed. However, in recent years there has been increasing amount of

literature providing evidence for hedgehog signalling in the islet of Langerhans (Hebrok, Kim, St Jacques, McMahon, & Melton, 2000; Janet Lau & Hebrok, 2010a). Ectopic Hh signaling in three weeks old mice, induced by a constitutively activated version of Gli2 and β-cell specific ablation of the primary cilium, leads to the formation of an undifferentiated β-cell population expressing progenitor markers (L. Landsman, Parent, & Hebrok, 2011). At adult stage, these mice display insulin secretion defects and impaired glucose tolerance. Similar metabolic phenotypes were observed for Ptch (Ptch+/-) and Smo (Pdx1 Cre Smo flox/null) mutant mice (Hebrok et al., 2000). In contrast, Smo (Pdx1 Cre Smo flox/null) mice that have reduced levels of Hh signaling also display glucose intolerance and increased insulin sensitivity (Janet Lau & Hebrok, 2010b). Thus, molecular mechanisms of Hh signalling in pancreatic endocrine cells and its influence on glucose metabolism is not fully elucidated.

3.6 Insulin receptor and insulin like-growth factor receptor signalling

The INSR/IGFR signalling pathway is essential for cellular growth and the maintenance of energy homeostasis, especially for the glucose metabolism in mammals. Insulin secreted by the pancreatic β-cell activates the insulin receptor (IR, INSR) in peripheral tissues, the brain and in the β-cell itself, regulating processes such as glucose uptake and glycogen storage. In contrast, the insulin-like growth factor 1 receptor (IGF1R) primarily plays a role in the control of cell proliferation and survival. A downregulated system caused by mutations in the insulin signalling pathway leads to insulin resistance and eventually to T2D, whereas overactivation of IGF1R signalling leads to overgrowth and cancer.

3.6.1 The structure of INSR, IGF1R and IGF2R and their ligands

The insulin/IGF signalling system includes the receptor tyrosine kinases (RTKs) INSR and IGF1R as well as the insulin like growth factor 2 receptor (IGF2R), also named cation-independent mannose 6-phosphate receptor (CI-M6PR) (Hubbard & Till, 2000). The INSR and IGF1R consist of a α and β subunit, which are covalently linked (Adams, Epa, Garrett, & Ward*, 2000; De Meyts & Whittaker, 2002). Both receptors form homodimers of two α and β subunits (heterotetramer α2β2) but can also dimerize in heterodimers by linking a αβ dimer of each receptor. Such hybrid receptors are held together by disulfide bonds and occur in cells expressing both receptors (Slaaby, 2015; Soos & Siddle, 1989). Alternative splicing in exon 11 of the INSR transcript results in two isoforms differing by the absence (INSR-A) or presence (INSR -B) of a 12-residue amino-acid sequence in the α-subunit (Seino & Bell, 1989). In comparison, the IGF2R is a single transmembrane glycoprotein that lacks intrinsic catalytic activity and exists as monomer but tends to dimerize at the plasma membrane (Hassan, 2003; York, Arneson, Gregory, Dahms, & Kornfeld, 1999). All three receptors bind their ligands but also related growth factors with different affinity, thereby activating downstream signalling. Insulin (INS) attaches to both INSR isoform A and B with similar affinity but binds the IGF1R and INSR/IGF1R heterodimers with less strength. The insulin-like growth factor 1 (IGF1) ligand mainly interacts with the IGF1R but also

binds IGF2R and INSR/IGF1R homo- and heterodimers (Roith, 2003). Insulin-like growth factor 2 (IGF2) interacts with all three receptors with highest binding efficiency for the IGF2R and the INSR-A isoform (Annunziata, Granata, & Ghigo, 2011b). Both IGF ligands circulate freely in the blood system and in extravascular fluids where they are bound and transported by six subclasses of IGF binding proteins (IGFBP) (Sara et al., 1983). Thereby, IGFBPs stabilize the ligand protein and prevent their degradation, which inhibit their physiological actions due to the restricted bioavailability (Bach, 2015).

The INSR and IGF1R exhibit a related protein domain organization with a high sequence homology in the receptor tyrosine kinase domain and low similarity in the ligand binding region (Adams et al., 2000). Both receptors contain leucine-rich repeats (large domains L1 and L2) flanking a highly conserved cysteine-rich domain in the α chain. Fibronectin type III domains C-terminal of L2 are the basis of disulphide bonds connecting the α chain with the fibronectin regions in the N-terminal region of the β-chain. C-terminal of the fibronectin domain, the β-subunit comprise a transmembrane helix followed by two regulatory regions, a trans-and juxtamembrane region, a tyrosine kinase catalytic domain and a C-terminal tail (Adams et al., 2000; De Meyts & Whittaker, 2002; Colin W Ward, Lawrence, Streltsov, Adams, & McKern, 2007). In contrast, the IGF2/M6P receptor is a type I transmembrane glycoprotein composed of a large extracellular region, a transmembrane region and a short cytoplasmic tail that lacks intrinsic catalytic activity. The extracellular region consists of 15 homologous repeat domains (mannose 6 phosphate (M6P) binding domains) in which binding of IGF2 primarily occurs in domain 11. IGF2 affinity is believed to be enhanced by a fibronectin type II-like region of repeat 13. Binding of M6P-marked lysosomal enzymes is mediated by domain three, five and nine (El-Shewy & Luttrell, 2009; Kornfeld, 1992).

3.6.2 Signal transduction and function of INSR, IGF1R and IGF2R

Although insulin and IGFs have distinct physiological roles, they activate the same key signalling pathways including phosphoinositide 3-kinase (PI3K)/ serine-threonine kinase AKT and small G-protein Ras / mitogen-activated protein (MAP) kinases to respond to extracellular stimuli (Siddle, 2011) (Figure 3.4). The PI3K/AKT pathway mainly leads to changes in metabolic activity, whereas the MAPK pathway majorly regulates cell growth and differentiation. The pathway selection upon receptor activation partially depends on the phosphorylation states of insulin receptor substrate proteins (IRS) and the Src homology-2 (SHC) protein, that bind the cytoplasmic domain of receptors (Taniguchi, Emanuelli, & Kahn, 2006). IRS proteins are highly phosphorylated on multiple serine/threonine residues by downstream kinases caused by autoregulatory feedback mechanisms. These phosphorylations mainly inhibit but also potentiate the activity of IRS proteins in some cases (Boura-Halfon & Zick, 2009; Sun & Liu, 2009). Several studies report that IRS1 majorly regulates signalling cascades linked to glucose homeostasis while IRS2 primarily mediates signal transduction controlling lipid metabolism (Taniguchi, Ueki, & Kahn, 2005; Thirone, Huang, & Klip, 2006). IRS proteins bind to the regulatory subunit of phosphatidylinositol-4,5-bisphosphate 3-kinase (PI3K) protein, which then catalyses the

conversion of the membrane lipid phosphatidylinositol 4,5-bisphosphate (PIP2) to phosphatidylinositol 3,4,5-trisphosphate (PIP3). This phospholipid recruits phosphoinositide-dependent kinase 1 (PDK1) that phosphorylates the serine/threonine kinase AKT (also named protein kinase B, PKB). AKT in turn activates a broad network of signalling cascades controlling a variety of downstream responses depending on the cell type (Manning & Toker, 2017a; Vasudevan & Garraway, 2010). In muscle and adipose tissue AKT controls glucose influx in cells by stimulating the insulin induced plasma membrane translocation of glucose transporter type 4 (GLUT4) (Whiteman, Cho, & Birnbaum, 2002). It also triggers glycogen synthesis by phosphorylating glycogen synthase kinase 3 (GSK3) (Lan, Qi, & Du, 2014). Moreover, AKT signalling suppresses the transcriptional program of the forkhead box O1 (FOXO1) transcription factor, thereby modulating various cell functions including metabolism (gluconeogenesis) and apoptosis promotion (Myatt & Lam, 2007).

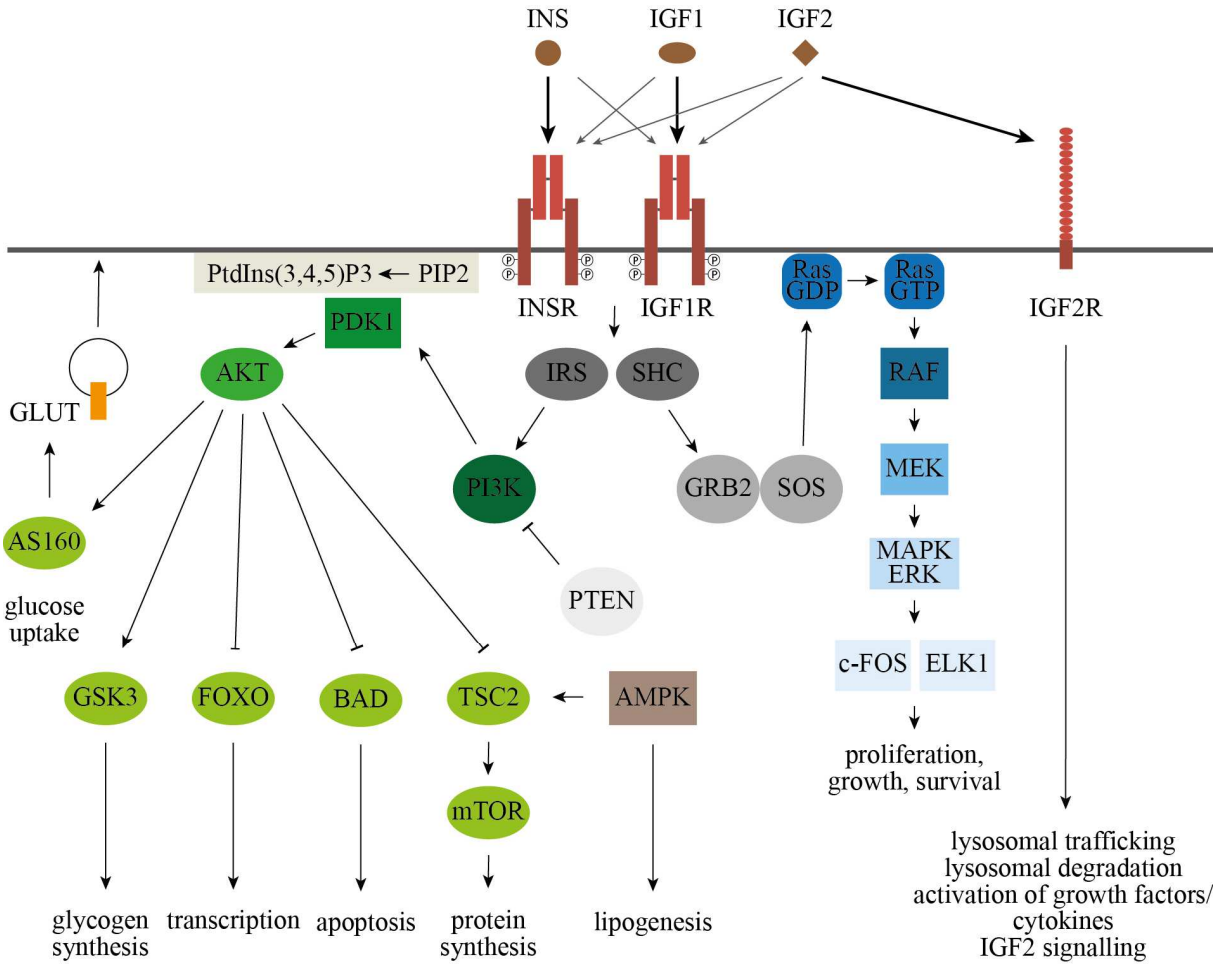

Figure 3.4: The INSR/IGF1R signalling system

INSR and IGF1R orchestrate a complex signalling network regulating metabolic processes and growth. Key pathways act via PI3K/Akt and Ras/MAP kinases. IGF2R controls mechanism involved in lysosomal function and growth factor/cytokine signalling.

AKT influences the activity of mammalian target of rapamycin (mTOR) via the phosphorylation of the Rheb GTPase activating complex (tuberous sclerosis 1/2, TSC1/2) that regulates the synthesis of proteins important for cell growth and metabolism (Taniguchi et al., 2006). Further, AKT substrates are the TBC1 domain family member 4 (TBC1D4/AS160), which controls glucose transport and the BCL2-associated agonist of cell death (BAD) that regulates apoptosis. (Manning & Cantley, 2007; Manning & Toker, 2017b; Vasudevan & Garraway, 2010).

In concert with other receptor tyrosine kinases, the INSR and IGF1R modulate the transcription of genes crucial for cell proliferation and survival using the Ras/MAP kinase pathway (Katz, Amit, & Yarden, 2007) (Figure 3.4). Receptor activation initiates the interaction of IRS and SHC proteins with the growth factor receptor bound protein 2 (GRB2). This adaptor protein is recruited to the plasma membrane in complex with the guanine nucleotide exchange factor SOS, where it phosphorylates the small G-protein Ras, which in turn binds and exchanges guanosine diphosphate (GDP) to guanosine triphosphate (GTP). Subsequently, Ras activates a signalling cascade including the proto-oncogene c-RAF (RAF), the dual specificity kinase MAPK kinase (MEK1) and ERK, a kinase of the MAPK family. MEK/ERK heterodimers translocate to the nucleus, where they phosphorylate a number of mitogenic substrates including cellular oncogene c-FOS and ETS transcription factor (ELK1) (Roskoski, 2012; Sturgill, 2008).

3.6.3 Expression and physiological function of INSR and IGF1R

In vertebrates, IR and IGF1R are expressed early in fetal tissues. While in adult differentiated cells IGF1R is found virtually in all tissues at significant levels, the INSR expression depends on its isoform (Giddings & Carnaghi, 1992). The InsR-B isoform appears in postnatal life in insulin target tissues like muscle, liver and fat suggesting a role in the regulation of metabolism. In contrast, INSR-A is abundant during prenatal life where it controls cell proliferation (Belfiore, Frasca, Pandini, Sciacca, & Vigneri, 2009). Mice with null mutations for the insulin receptor display a slight growth retardation at birth. After birth, metabolic abnormalities rapidly manifest within the first 7 days. Strong hyperinsulinemia and increased glucose levels upon feeding were measured, which results in β-cell failure within few days and is followed by death of diabetic ketoacidosis (Kitamura, Kahn, & Accili, 2003). Additionally, low glycogen stores, fatty livers and high serum triglycerides were observed. Mice lacking a functional IGF1R die at birth of respiratory failure and display a severe growth deficiency. Fetuses exhibit organ hypoplasia, ossification delay and epidermal abnormalities (Liu, Baker, Perkins, Robertson, & Efstratiadis, 1993).

3.6.4 Autocrine insulin signalling in the pancreatic β-cell

Autocrine insulin signalling in the pancreatic β-cell has been subject of controversial debate in recent years but a growing body of evidence implies its relevance in β-cell function (Goldfine & Kulkarni, 2012; I. B. Leibiger, Leibiger, & Berggren, 2008; Rhodes, White, Leahy, & Kahn, 2013). It is believed that β-cells are either exposed to extremely high insulin concentration since they

themselves are the source of insulin or that secreted insulin is rapidly dispensed into the circulation (Rhodes et al., 2013). A hyperinsulinemic milieu would result in physiological feedback inhibition signals in the cell, which ensure that insulin signalling is not chronically sustained in the β-cell contributing to an insulin-resistant state. This includes desensitization mechanisms like the downregulation of the insulin receptor expression and its internalization into endosomal compartments (Carpentier, Fehlmann, Van Obberghen, Gorden, & Orci, n.d.; Zick, 2005). Such autoregulatory feedback loops attenuate insulin signalling and would only be deactivated upon absence of insulin to restore insulin signal transduction (Heaton & Gelehrter, 1981). On the other hand, islets contain an extensive microcirculatory network essential for islet function, which might clear insulin from the islet vicinity allowing insulin signalling with physiological insulin concentrations.

A plethora of studies indicate that insulin-producing pancreatic β-cells are target of insulin action with effects on transcription, translation, glucose and lipid metabolism, ion flux, insulin biosynthesis, insulin secretion, β-cell mass, cell proliferation, cell size and apoptosis (Goldfine & Kulkarni, 2012; B. Leibiger, Wahlander, Berggren, & Leibiger, 2000; I. B. Leibiger et al., 2008; Uchizono, Alarcón, Wicksteed, Marsh, & Rhodes, 2007). *In vivo*, there are more indices for a functional role of insulin signalling in islets. Mice with a β-cell-specific KO of INSR (βIRKO) manifest glucose intolerance, display increased fasting insulin levels due to reduced insulin content and islet size as well as an impairment in glucose-induced first phase insulin secretion (R N Kulkarni et al., 1999a). A similar phenotype was also overserved for the β-cell-specific deletion of IGF1R (βIGF1r mice) including glucose intolerance and insulin secretion defects despite normal β-cells and islets (R N Kulkarni et al., 2002). However, these data need to be treated with caution, since the Cre-recombinase used was shown to not be exclusively β-cell-specific but is also active in parts of the brain, such as the hypothalamus (Song, Xu, Hu, Choi, & Tong, 2010; Wicksteed et al., 2010).

3.6.5 The function of the IGF2/CI-M6P receptor

IGF2R is a multifunctional receptor that controls various cellular functions related to lysosome biogenesis and the regulation of growth and development (Figure 3.4). It acts as clearance receptor by binding and internalizing extracellular IGF2 ligand, which is subsequently degraded in the lysosome. Thus, IGF2R controls extracellular IGF2 concentrations attenuating signalling of the INSR/IGF1R signalling pathway (James Brown, Jones, & Forbes, 2009; Kornfeld, 1992). Furthermore, IGF2Rs bind newly synthesized, M6P-tagged lysosomal enzymes via their M6P-binding domain and transport them from the *trans*-Golgi complex to the late endosome. In pre-lysosomal compartments, the acidic pH triggers the dissociation of the receptor ligand complex. From there enzymes are sorted to the lysosome. After enzyme release, unoccupied receptors are either recycled back to the *trans*-Golgi area or routed to the plasma membrane (J Brown, Jones, & Forbes, 2009; El-Shewy & Luttrell, 2009). Moreover, latest data suggested a functional role of IGF2R in the initiation of ERK1/2 signalling by transactivating G protein-coupled sphingosine 1-phosphate receptors at the plasma membrane (El-Shewy et al., 2006;

ElShewy, Lee, Obeid, Jaffa, & Luttrell, 2007). However, this remains controversial and poorly understood. Beside IGF2, the IGF2R also binds cytokines and peptide hormones like leukemia inhibitory factor, proliferin and transforming growth factor-β. By regulating their uptake and processing, IGF2R influences their physiological actions (Blanchard et al., 1999; Dennis & Rifkin, 1991; S. J. Lee & Nathans, 1988).

Similar to its IGF2 ligand, the concentration of IGF2R is high in fetal tissues and dramatically declines during the postnatal development (Lund et al., 1986; Moses et al., 1980; Sklar, Kiess, Thomas, & Nissley, 1989). Mice inheriting a disrupted *IGF2R* gene from their mother do not express the IGF2R protein in tissues since the gene is exclusively expressed from the maternal allele due to imprinting mechanisms (A. Ward, 1997). Mice deficient of IGF2R die perinatally due to cardiorespiratory failure. Fetuses are 30% larger than normal with up to 4.4 fold elevated IGF2 serum levels (M. M. Lau et al., 1994; Ludwig et al., 1996; Z.-Q. Wang, Fung, Barlow, & Wagner, 1994). Mutants also display organomegaly, a kinked tail, polydactyly, heart defects, edema, dyspnea and reduced fertility. Moreover, in IGF2R deficient mice lysosomal enzyme activities were moderately decreased in tissue samples and plasma enzyme concentrations were significantly elevated (Sohar, Sleat, Gong Liu, Ludwig, & Lobel, 1998). Additionally, single-nucleotide polymorphisms in IGF2R are associated with a variety of cancer types in tissue like breast, brain, gastrointestinal, ovarian and prostate (J Brown et al., 2009; Cheng et al., 2009; Lonn et al., 2008).

3.6.6 The metabolic regulator AMPK

The serine/threonine kinase AMP-activated protein kinase (AMPK) is a major cellular energy sensor and a master regulator of metabolic homeostasis controlling lipid metabolism, glucose homeostasis, insulin secretion in the pancreatic β-cell and inflammation including hepatic ketogenesis, cholesterol synthesis, lipogenesis, and triglyceride synthesis, adipocyte lipolysis, and skeletal muscle fatty acid oxidation (Garcia & Shaw, 2017; Winder & Hardie, 1999). AMPK is a central player involved in pathomechanisms of obesity, insulin resistance, type 2 diabetes, non-alcoholic fatty liver disease (NAFLD), and cardiovascular disease (Day, Ford, & Steinberg, 2017). Parts of the INSR/IGF1R signalling cascades are indirectly regulated by AMPK. This kinase inhibits mTOR by phosphorylating tuberous sclerosis 2 protein (TSC2) and raptor, that eventually results in decreased protein and lipid synthesis. The AMPK protein is a heterotrimeric enzyme comprised of a catalytic (α) and two regulatory (β and γ) subunits (Hardie, 2008). The enzyme is activated by two distinct pathways namely, a Ca^{2+}-dependent pathway regulated by calcium/calmodulin-dependent protein kinase kinase b (CaMKKb) and an AMP-dependent pathway mediated by the serine/threonine-protein kinase LKB1 (Sanders, Grondin, Hegarty, Snowden, & Carling, 2007). Kinase activation occurs upon binding of AMP to the γ subunit. Thus, signalling activity depends on the intracellular AMP/ATP ratio, which itself is regulated by physiological conditions such as hypoxia or glucose deprivation. Other factors stimulating AMPK activity are calcium concentration and the action of various hormones, cytokines, and adipokines.

3.7 Endocytosis and trafficking of receptor tyrosine kinases

Receptor tyrosine kinases (RTKs) are synthesized in the endoplasmic reticulum (ER) where folding, partial dimerization and further processing of precursor proteins occur under the guidance of the chaperones calnexin and calreticulin before they are transported to the Golgi apparatus (Bass, Chiu, Argon, & Steiner, 1998). Via the ER-Golgi intermediate compartment (ERGIC), proteins are delivered to the Golgi, in which they undergo multiple post-translation modifications such as disulfide bridge formation or glycosylation. From the *trans*-Golgi, receptors are further transported in the secretory pathway to the different cellular compartments including the plasma membrane, where they undergo constitutive endocytosis. At the cell surface receptors are accessible to extracellular ligands to incorporate signals into the cells (Gomez-Navarro & Miller, 2016a).

3.7.1 Receptor trafficking routes after endocytosis of RTKs

Endocytosis is a major regulator of RTK signalling. Studies proposed that receptor exist in a loose dimeric form at the plasma membrane prior to ligand binding (I. N. Maruyama, 2015). Ligand binding to the α subunit of receptors induces a conformational change of the receptor, which entails the autophosphorylation of the dimeric cytoplasmic domains at multiple tyrosine residues. Receptors are located in certain membrane domains such as lipid rafts apart from proteins of the endocytic machinery (Foti, Moukil, Dudognon, & Carpentier, 2004). The activated InsR, for example, segregates in membrane areas, where clathrin-coated pits are formed so that the ligand-receptor complex is endocytosed subsequently (Foti et al., 2004).

Internalization of receptor-ligand complexes is mediated by membranous vesicles, which subsequently fuse with early endosomes (EE) (Figure 3.5). This highly dynamic process occurs within the first 2-5 min after ligand stimulation. The acid environment of endosomes causes the release of some ligands, which remain in vesicular parts of endosomes. Unoccupied receptors and ligand-receptor complexes are able to immediately recycle to the cell surface through re-fusion of peripheral EEs with the plasma membrane or via retro-endocytosis that involves the transport of tubular carrier vesicles derived from peripheral endosomal compartments (tubular carriers: (Polishchuk, Capestrano, & Polishchuk, 2009)). A slower recycling pathway requires another sorting step in multivesicular bodies (MVBs) and sorting endosomes (SE) or via trafficking through pericentriolar recycling compartments. EE mature into SE/MVBs by incorporating RTKs into intraluminal vesicles (ILVs) via inward membrane invagination. Remodelling of membrane protein composition leads to the transformation of SE/MVBs into late endosomes (LE), which eventually fuse with lysosomal compartments. Lysosomes contain proteolytic enzymes that proteolytically degrade ligands and receptors. The receptor transportation through early and late endosomes to lysosomal compartments, entails a decline in pH. The acidic pH in lysosomes ensures proper function of hydrolytic enzymes.

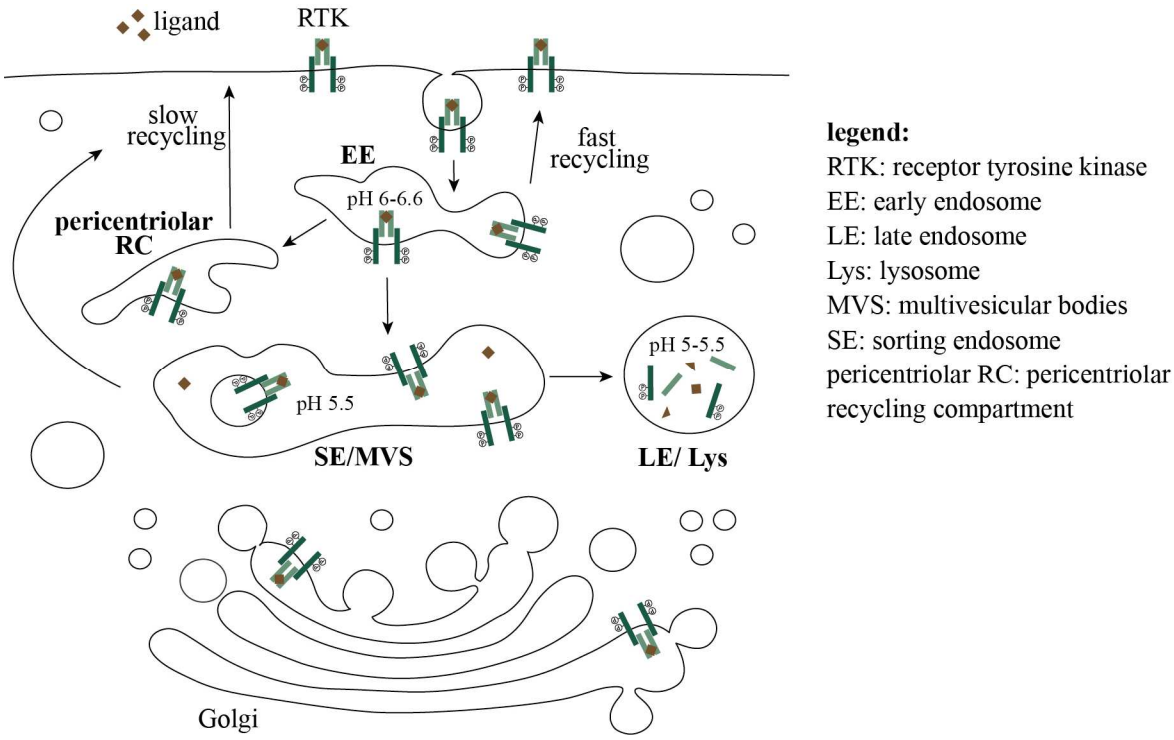

Figure 3.5: Receptor internalization, recycling and degradation

Ligand bound RTKs are internalized in membranous vesicles, which fuse with early endosomal compartments. Recycling to the cell surface occurs either at this stage or after trafficking to sorting endosomes (SE) or multivescular bodies (MVBs) or to the pericentriolar recycling compartment. Vesicular transport to lysosomal compartments causes the proteolytic degradation of receptors and ligands.

Receptor endocytosis is a highly dynamic process. The rates of constitutive internalization, recycling and lysosomal degradation defines the half-life of a receptor. Turnover rates range from $t_{½}$ one hour for the colony stimulating factor 1 receptor (CSF1R) in macrophages to 2-3 hours for the interleukin-6 receptor in MDCK cells and up to 24 h for the epidermal growth factor receptor (EGFR) when overexpressed in carcinoma cells (Gerhartz et al., 1994; P. S. W. Lee et al., 1999; Stoscheck & Carpenter, 1984).

3.7.2 Receptor endocytosis pathways and COP vesicle-mediated transport of RTKs

RTKs are internalized by clathrin-mediated endocytosis (CME) and clathrin-independent endocytosis (CIE) (Goh & Sorkin, 2013; Traub, 2009a) (Figure 3.6). The majority of RTKs were shown to be endocytosed and transported via CME. Clathrin-coated vesicles bud from multiple organelles and transport receptors from the *trans*-Golgi network (TGN) to endosomes as well as to and from the plasma membrane (PM). The CME pathway mediates the endocytosis of well-characterised receptors such as G protein–coupled receptors (GPCRs), RTKs, EGFR and transferrin receptor (TFR) at the plasma membrane. CME is initiated by the sequential assembly of coat components forming a clathrin-coated pit at the membrane that results in a coated vesicle of 100-200 nm in size. Membranous receptor proteins interact with adaptor proteins (AP),

thereby connecting with the coat complex (Collins, McCoy, Kent, Evans, & Owen, 2002; Kirchhausen, 2000). Adaptor proteins are recruited to the membrane via binding to phosphatidylinositol-(4,5)-bisphosphate (PIP2), a lipid molecule enriched in the plasma membrane. For coat assembly AP, proteins interact with clathrin proteins forming a triskelion. Three clathrin heterodimers consisting of one heavy and one light chain molecule, build a trimeric structure (Kirchhausen, 2000). Triskelions assemble into a curved lattice-like structure and form a coat around the vesicle. Dynamin, a large GTPase mediates the fission of the vesicle from the membrane by forming a helical polymer around the constricted neck of the budding vesicle (Praefcke & McMahon, 2004).

In contrast to CME, caveolae mediated endocytosis is poorly characterized. This pathway has been implicated in the endocytosis of EGFR, INSR, glycosylphosphatidylinositol (GPI)-linked proteins, integrins, glycosphingolipids and certain viruses such as SV40 (Boothe et al., 2016; Kumari, Mg, & Mayor, 2010). Caveolae form flask-shaped invaginations with a diameter of around 60–120 nm. Membrane regions, in which caveolae assemble, are enriched in certain sphingolipids, cholesterol and PIP2, representing so called lipid rafts (Fujimoto, Hayashi, Iwamoto, & Ohno-Iwashita, 1997; Fujita, Cheng, Tauchi-Sato, Takenawa, & Fujimoto, 2009). In the assembling process of caveolae vesicles at the plasma membrane, caveolin proteins, which are integral membrane proteins, directly bind to membrane cholesterol (Rothberg et al., 1992). It is thought that accumulation of caveolins induces membrane curvature. Caveolins act like wedges in the membrane thereby displacing outer leaflet lipids more than inner leaflet lipids (McMahon and Gallop 2005). There are three subtypes of caveolin proteins; Caveolin 1 (CAV1) is expressed in non-muscle cells, while caveolin 2 (CAV2) and caveolin 3 (CAV3) are expressed in muscle cells (Chadda et al., 2007).

The transport of proteins between the ER and the Golgi apparatus is mediated by the two coat protein complexes COPI and COPII (Gomez-Navarro & Miller, 2016a, 2016b) (Figure 3.6). COPII vesicles primarily regulate recruitment and budding of cargo at the ER that is destined for the Golgi (anterograde transport). In contrast, COPI complexes regulate traffic in the retrograde direction from the Golgi back to ER compartment or between different compartments of the Golgi (intra-Golgi transport). The COPII coat comprises five proteins, the secretion associated ras-related GTPase 1 (SAR1), and the transport proteins SEC23, SEC24, SEC13 and SEC31 (Brandizzi & Barlowe, 2013). The assembly is activated by SAR1 by converting GDP to GTP. GTP-bound SAR1 recruits SEC proteins in a sequential manner with SEC24 acting as cargo adaptor directly binding to the ER export signals of proteins (Gomez-Navarro & Miller, 2016a, 2016b). COPI complexes form through the action of ADP ribosylation factor 1 (ARF1), a small GTPase related to SAR1, and a heptameric protein complex called coatomer. Coatomers consists of seven subunits (zα, β, β', γ, δ, ε, and ζ-COP), which are assembled at the target membrane domain after ARF1 binding. Cargo proteins interact with the coatomer complex via KDEL (Lys-Asp-Glu-Leu) receptors (Gomez-Navarro & Miller, 2016a, 2016b).

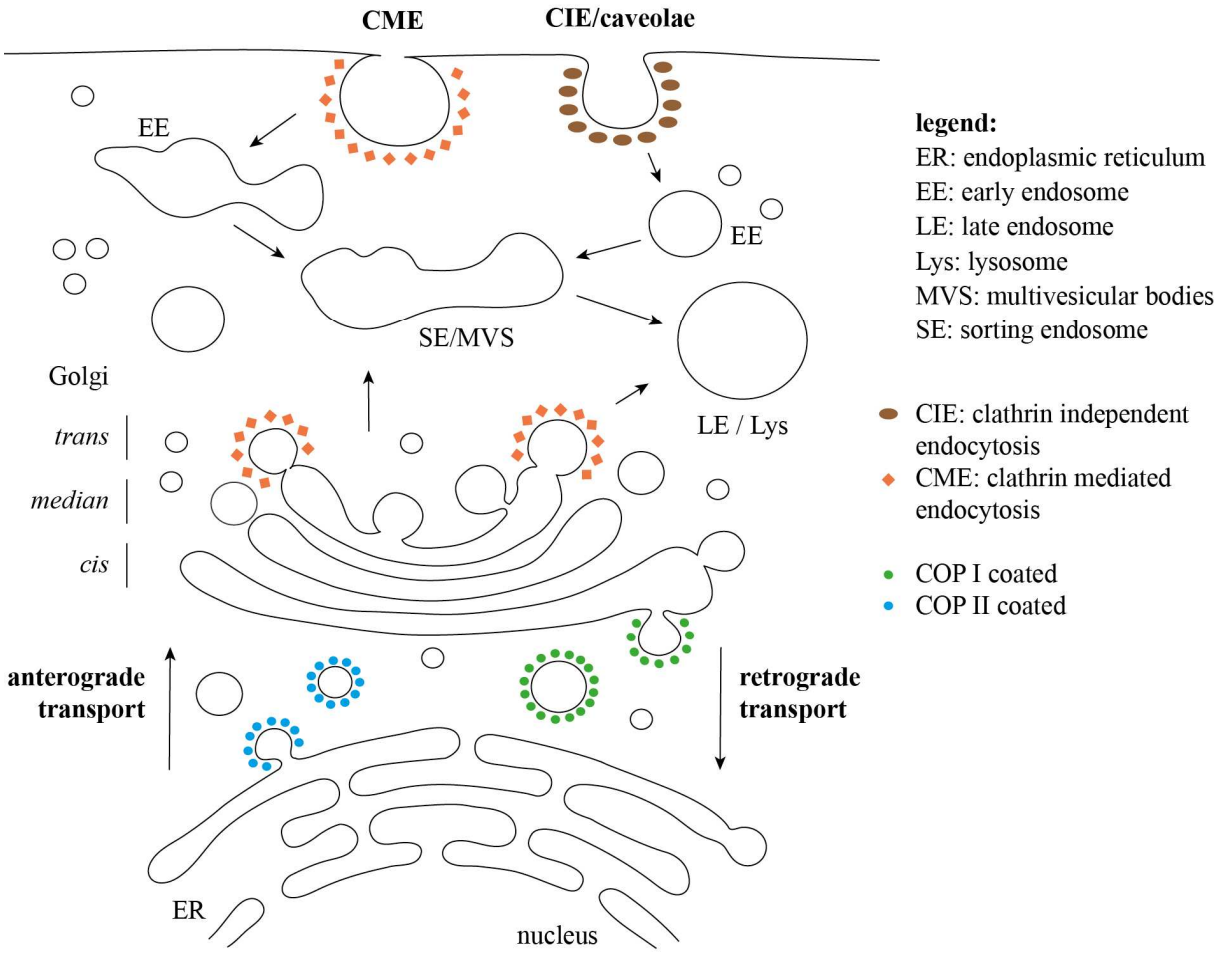

Figure 3.6: Mechanisms of endocytosis and receptor transport

RTKs are endocytosed and transported in the cell via CME or caveolae. The trafficking between Golgi and ER compartments is mediated by COP-coated vesicles.

3.7.3 Regulation of RTK-mediated signalling through endocytic and trafficking processes

Duration and activity of receptor-mediated signalling is regulated by many different mechanisms. Receptor-mediated activation of downstream signalling mainly occurs at the plasma membrane. However, there is also evidence that signalling prolongs after internalization. Several studies reported that INSR/IGFR-mediated phosphorylation of SHC, but not IRS proteins, is dependent on receptor internalization (Chow, Condorelli, & Smith, 1998; Foti et al., 2004; Hamer et al., 2002). Additionally, there is evidence that internalized INSR maintains its signalling activity in the endosome. Also, IRS-1 phosphorylation and PI3K activation as well as signalling to the SHC/ERK pathways might primarily take place after endocytosis in endosomes (Di Guglielmo et al., 1998).

Moreover, EGFR signalling activity as well as the endocytic route and pathway of the receptor is dependent on the availability of extracellular EGFR ligands. Upon low ligand concentration, the EGFR is internalized via CME, which mainly results in receptor recycling and sustained signalling inducing cell proliferation. In contrast, high dose of extracellular ligands leads to strong receptor ubiquitinoylation followed by CME or CIE-mediated internalization. CIE targets EGFR to

lysosomal degradation causing signal extinction, whereas CME maintains signalling by receptor recycling to the plasma membrane (Capuani et al., 2015; Orth, Krueger, Weller, & McNiven, 2006; Sigismund et al., 2013). Furthermore, physical and mechanical stimuli modulate endocytic routes and signalling. Elevated membrane tension of cells, found on the apical side of polarized cells or caused by mechanical stress, blocks CME at the cell surface. Actin polymerization at the intracellular side of the plasma membrane allows CME internalization in contrast to cells with low membrane tension, in which clathrin-coat assembly is sufficient to bend the membrane (Boulant, Kural, Zeeh, Ubelmann, & Kirchhausen, 2011). Moreover, low temperature decreases membrane fluidity and declines internalization rates of all endocytosis pathways (W. A. Dunn, Hubbard, & Aronson, 1980).

Furthermore, ubiquitylation plays a key role in controlling receptor trafficking and degradation. Growth factor receptor bound protein 10 (GRB10) is involved in controlling ligand-induced ubiquitination and stability of INSR and IGF1R that is mediated by the E3 ubiquitin protein ligase NEDD4 (neural precursor cell expressed developmentally down-regulated protein 4) (Huang & Szebenyi, 2010). Additionally, the E3 ubiquitin ligase activity of Cbl proto-oncogene (CBL) proteins is implicated in the catalysis of ubiqutinylation, thereby negatively regulating the tyrosine kinase activity of INSR and IGF1R (Kishi et al., 2007; Sehat, Andersson, Girnita, & Larsson, 2008). Last, the E3 ubiquitin ligase MDM2 proto-oncogene (MDM2) influences the ubiquitylation and degradation of IGF1R upon recruitment by β-arrestin (Girnita et al., 2005; Girnita, Girnita, & Larsson, 2003).

3.8 The *5330417C22RIK* gene: state of the art

Studies analysing the function of *5330417C22RIK* gene were first published by Deng et al., 2005. *KIAA1324* (*EIG121*), the human ortholog of the *5330417C22RIK* gene, was found as an estrogen-induced gene in female patients. Gene expression was elevated in the estrogen-dominated proliferative phase of premenopausal endometrium, in the postmenopausal endometrium of women receiving an oestrogen replacement therapy and in estrogen-related type I endometrial adenocarcinoma (Lei Deng et al., 2005). Furthermore, Jaillard et al., 2016 found copy number variants (CNVs) in the *KIAA1324* gene of female patients under the age of 40 years with ovarian failure (Jaillard et al., 2016). *EIG121* expression was detected in various cancer types, where it was differentially regulated suggesting it as a biomarker. High mRNA levels of *EIG121* in high-grade serous carcinoma tissue of the ovary and peritoneum, isolated from women, who underwent an ovarian cancer-surgery, predicted shorter patients survivals (Schlumbrecht, Xie, Shipley, Urbauer, & Broaddus, 2011). In contrast, high mRNA expression of *EIG121* in pancreatic neuroendocrine tumours was associated with favourable prognostic features for patients such as small size, low WHO grade and low stage in the American Joint Committee on Cancer (AJCC) system (Estrella et al., 2014). Furthermore, Kang et al., 2015 claimed that *KIAA1324* is a tumour suppressor gene, which reduces cancer progression in gastric cancer cells by influencing tumour invasion and drug resistance (J. M. Kang et al., 2015). In addition, *KIAA1324* directly interacts and inhibits the glucose-regulated protein 78 kDa (GRP78), thereby supressing proliferation through

inhibiting GRP78-mediated AKT activation. It also stimulates apoptosis by blocking the interaction of GRP78 and caspase 7. Similarly to pancreatic neuroendocrine tumours, low *KIAA1324* mRNA expression was associated with poor prognosis in gastric cancer patients (J. M. Kang et al., 2015). Moreover, EIG121 has an anti-proliferative effect when overexpressed in HEK human embryonic kidney cells (T-Rex-293). Overexpression of EIG121 further induced autophagosome formation and lysosomal degradation of proteins upon starvation, thus controlling autophagy (L Deng, Feng, & Broaddus, 2010). Autophagy regulation by EIG121 was also detected in cultured human endometrial adenocarcinoma JEC cell spheres and JEC obtained cancer stem cells. Additionally, EIG121 was shown to play a role in the autophagy-related maintenance of cancer stem cell homeostasis (Ran, Zhou, & Zhang, 2017).

In conclusion, the expression of the *5330417C22RIK* gene is differentially regulated in cancer tissues and might play a role in autophagy. But what is its physiological function in energy homeostasis and how does it act on a molecular level?

3.9 Aims of the thesis

The aim of this thesis was to investigate Hh and insulin signalling in β-cell biology and glucose metabolism. Mutations in cilia-associated proteins interfere with cellular homeostasis, numerous signalling pathways and the cell cycle. The role of the primary cilium and ciliary signalling in energy homeostasis is still controversially discussed. To facilitate the analysis of cilia and cilia-dependent Hh signalling *in vitro* and *in vivo*, we intend to generate and characterize a novel Cre-inducible knock-in ARL13B-tRFP cilia reporter mouse that fluorescently labels the cilium. The Hh signalling cascade is a cilium-dependent pathway that is essential for cell proliferation, tissue homeostasis and regneration in adults. However, little is known about its molecular and metabolic relevance in the adult endocrine pancreas. Thus, we decided to examine Hh signalling mechanisms in the adult islet of Langerhans and its influence on energy homeostasis. Furthermore, we characterized the novel gene, Insulin-like growth factor receptor-Like (*Igfr-L)*, which was shown to be highly expressed in epithelial cells during the secondary transition of pancreas development. Its expression and actions are essential for the survival of neonates. First bioinformatic analysis indicated high structural similarities to protein domains of receptor tyrosine kinases and the Igf2r suggesting a related function in insulin signalling and energy homeostasis. Unravelling the molecular function of Hh signalling and Igfr-L in the endocrine pancreas and their involvement in glucose metabolism will contribute to the understanding of the physiology and pathophysiology of type 2 diabetes and will provide novel molecular targets for therapy.

4 Results

4.1 Analysis of Hedgehog signalling in the islet of Langerhans and its impact on glucose metabolism

Until now, the functional role of Hedgehog signalling in the adult pancreas, especially in the β-cells was subject of controversial debate since Shh signalling is suppressed in embryonic development to allow the budding of the pancreas from the foregut endoderm. Additionally, literature providing evidence for the functional role of Hh in the adult islet of Langerhans appear to be partially contradictory. For example, ectopic expression of the Shh ligand in the rat β-cell line INS-1E induces insulin production and secretion at the transcriptional level (Melissa K. Thomas, Lee, Rastalsky, & Habener, 2001). In contrast, adult Ptch1 heterozygous mice display increased levels of Hh signalling but are glucose intolerant (Hebrok et al., 2000). To shed light on these discrepancies, we analysed Hh signalling in pancreatic endocrine cells and its effect on glucose metabolism.

4.1.1 Hh signalling activity in pancreatic cells is differentially regulated *in vitro* and *in vivo*

To confirm that the main Hh pathway components are expressed in pancreatic endocrine cells, we performed an immunofluorescence study on isolated islets of adult WT mice using antibodies marking Hh signalling components, β-cells (Nk6 homeobox 1, Nkx6.1), α-cells (glucagon, Gcg) and cilia (acetylated tubulin) (Figure 4.1A). Hh proteins Smo, Ptch, Pifo, Grasp2, Gli1, Gli2 and Gli3 are expressed in the pancreatic islets although the expression levels of the Gli transcription factors are very low. Smo, Ptch and Pifo were also expressed in cilia of islets cells. Additionally, Western blot analysis of pancreatic islet lysates confirmed the expression of the Hh proteins Kif7 and Sufu (Figure 4.1B).

Collectively, the expression of Hh signalling components suggests a possible functional role of this pathway in islet cells and ciliary localization of Smo indicates active Hh signal transduction.

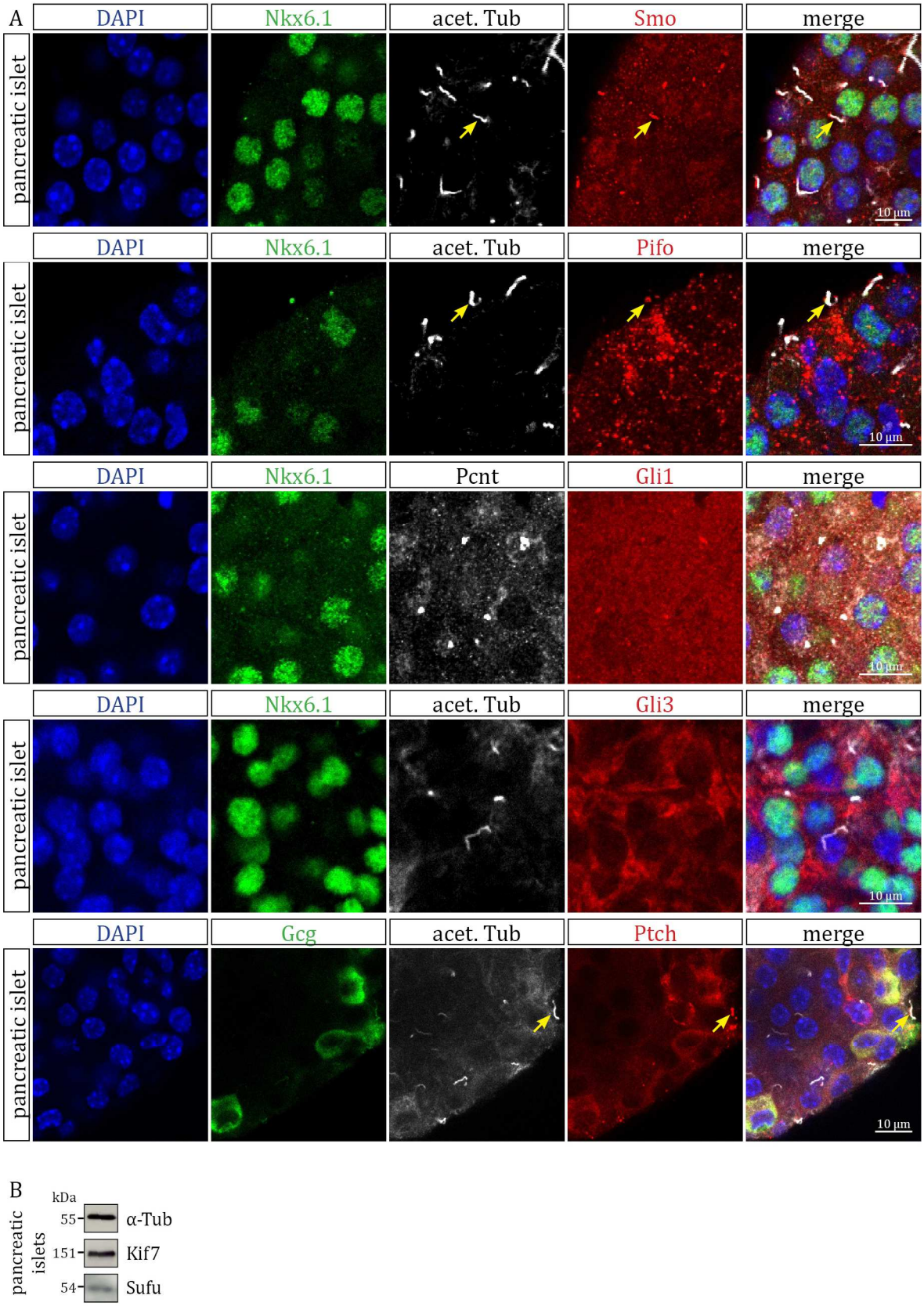

Figure 4.1: Hedgehog pathway components are expressed in the islet of Langerhans

(A) Representative laser scanning microscopy (LSM) images of pancreatic islets isolated from 2-3 months old WT CD1 mice. Smo, Pifo, Gli1, Gli2, Gli3 and Ptch (red) were coimmunostained with the β-cell marker

Nkx6.1 and the α-cell marker Gcg (green). Cilia (marked by a yellow arrows) were labelled with acetylated tubulin (acet. Tub) and centriols with pericentrin (Pcnt) (white). Loading was controlled by the detection of α-tubulin.
(B) Representative Western blot of pancreatic islet lysates derived from adult WT CD1 mice showing Kif7 and Sufu protein expression.

Furthermore, the transgenic Hh reporter mouse strain *Tg(GBS-eGFP)* was used for the examination of Hh signalling in pancreatic endocrine cells. The reporter transgene contains eight concatemerized fragments of a *FoxA2* enhancer with a binding site for the Hh transcription factor Gli1 located upstream of an open-reading frame for the *eGFP* fluorescent reporter gene. Thus, *eGFP* expression in cells reflects Hh target gene expression indicating active Hh signalling (Balaskas et al., 2012).

Immunohistochemistry (IHC) analysis of isolated islets derived from *Tg(GBS-eGFP)* mice revealed a subpopulation of endocrine cells expressing different levels of eGFP (Figure 4.2A). To explore whether Hh activity is constitutive active and/or restricted to certain cell types, live-imaging of isolated islets from *Tg(GBS-eGFP)* mice was performed for 60 hrs. Over time, eGFP signal appeared or vanished in a few single cells (Figure 4.2B, white and yellow arrows). Additionally, we observed fast migrating eGFP expressing cells within the islet suggesting a non-endocrine cell type, likely pancreatic stellate cells (blue and red arrows). Coimmunostainings of eGFP with specific markers for the different types of pancreatic islet cells demonstrated that Hh signalling was not only restricted to one endocrine cell type but was detected in α-, β-, δ- and PP-cells (Figure 4.2C).

This study implies that Hh signalling might be active in all endocrine cells. Moreover, the degree of Hh activity is heterogeneously and dynamically regulated within individual cells, which needs further exploration.

To investigate whether islet cells respond to extracellular Hh ligand stimulation, isolated islets from *Tg(GBS-eGFP)* reporter mice were induced by Shh ligand treatment for 72 hours and subsequently either fixed for immunofluorescence detection (Figure 4.3A) or lysed for protein analysis (Figure 4.3B). In both studies, eGFP expression was slightly increased upon Shh ligand stimulation reflecting an active pathway. To prove that Hh reporter activity is accompanied by active Hh signalling transduction, eGFP signal was compared to Hh target gene expression in isolated pancreatic islet cells. Upon Shh stimulation, mRNA expression levels of e*GFP*, *Gli1* and *Ptch1* elevated equally and declined by treatment of cyclopamine (Cyc), an Hh antagonist (Figure 4.3C). To conclude, endocrine islet cells are able to activate the Hh signalling cascade upon extracellular ligand stimulation *in vitro*.

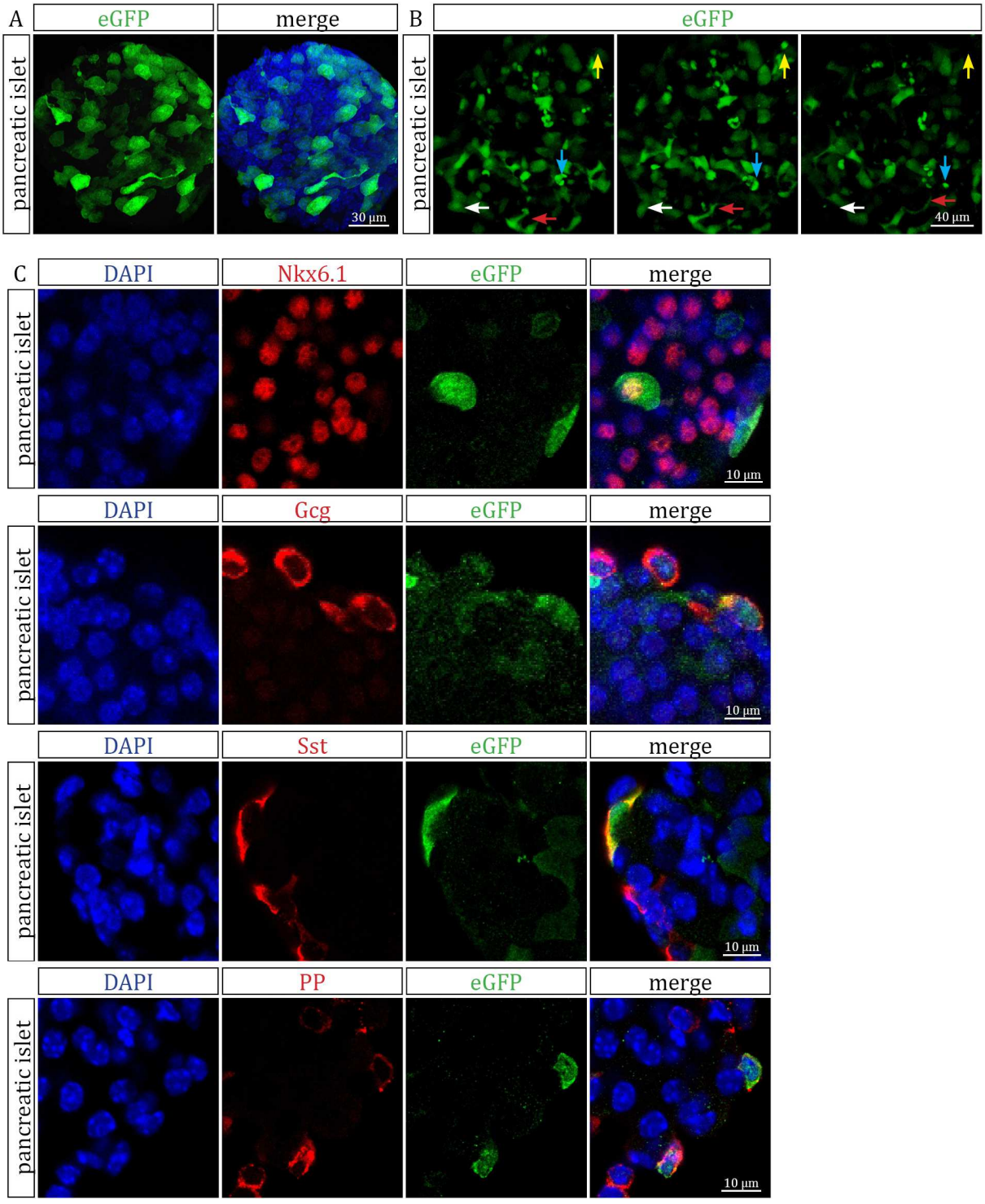

Figure 4.2: eGFP expression representing Hh activity is heterogeneously distributed in pancreatic endocrine cells *in vitro*

(A) Immunofluorescence images of a pancreatic islet derived from a transgenic reporter mouse *Tg(GBS-eGFP).* eGFP expression was detected by a GFP antibody (green).
(B) Still images of a time-lapse movie showing a cultured islets of Langerhans isolated from a *Tg(GBS-eGFP)* reporter mouse (movie see attachment page 175). White and yellow arrows indicate eGFP signal, which appeared or vanished, whereas blue and red arrows show migrating eGFP expressing cells.

(C) Representative LSM images of pancreatic islets isolated from adult WT CD1 mice. eGFP expression was detected via a GFP antibody (green) and coimmunostained with markers for β-cells (Nkx6.1), α-cells (Gcg), δ-cells (Sst) and PP-cells (PP) (red).

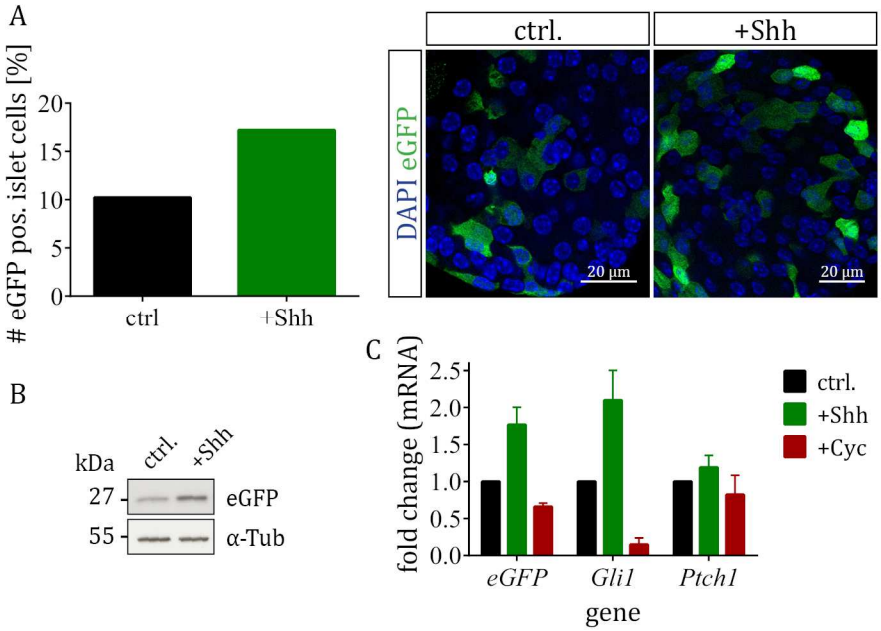

Figure 4.3 Hh signalling is inducible in pancreatic islets cells *in vitro*

(A) Pancreatic islets of adult *Tg(GBS-eGFP)* reporter mice were cultured in serum-free or in Shh ligand (500 ng/ml) complimented medium for 72 hrs. After taking LSM images of immunofluorescence stainings, the number of eGFP expressing islet cells were quantified for both conditions. (n (mice) = 2, mean)
(B) Representative Western blot image of islets isolated from adult *Tg(GBS-eGFP)* reporter mice. eGFP and α-Tub expression for serum-free and 72 hours Shh (500 ng/ml) stimulated condition.
(C) Real time quantitative PCR (qPCR) analysis of *eGFP, Gli1* and *Ptch1*. Pancreatic islets derived from adult *Tg(GBS-eGFP)* mice were cultured in serum-free conditions or treated with Shh ligand (500 ng/ml) or cyclopamine (10 µM) for 72 hrs. (n (mice) = 3, mean ± SD)

Previous experiments showed active Hh signal transduction in pancreatic islets *in vitro* (Figure 4.1). Hence, we immunostained β-cells in pancreatic cryosections derived from adult *Tg(GBS-eGFP)* reporter to verify active Hh signalling *in vivo*. Contrary to our assumption, we could not detect eGFP expression in either Nkx6.1 labelled β-cells or glucagon marked α-cells (Figure 4.4A). Only single non-endocrine cells in the islet or exocrine cells exhibited Hh activity.

To characterize which cell types exhibited active Hh pathway, pancreatic tissue sections of the *Tg(GBS-eGFP)* reporter was immunostained with markers for endothelial cells (Cd31, Cd31 antigen), pericytes (Ng2, chondroitin Sulfate Proteoglycan Ng2) and pancreatic stellate cells (Sma, α-smooth muscle actin) (Figure 4.4B). Endothelial cells line the interior surface of blood vessels and lymphatic vessels. Pericytes are contractile cells, which partially envelop endothelial cells, thereby regulating capillary blood flow and the maturation of endothelial cells (Bergers &

Song, 2005). To distinguish between pericytes and endothelial cells, we also immunostained the basal lamina (Collagen IV, Coll IV), which lies between both cell types. Pancreatic stellate cells have a star-like shape, are able to migrate, proliferate highly, become activated upon inflammation or injury and are important for the production of ECM (Apte, Pirola, & Wilson, 2012; Zang et al., 2015). We found eGFP expression in a subpopulation of endothelial cells and in some pericytes but did not observe eGFP expression in pancreatic stellate cells. This suggests that Hh signalling is only activated in rare cell types upon certain stimuli but is not constitutive active.

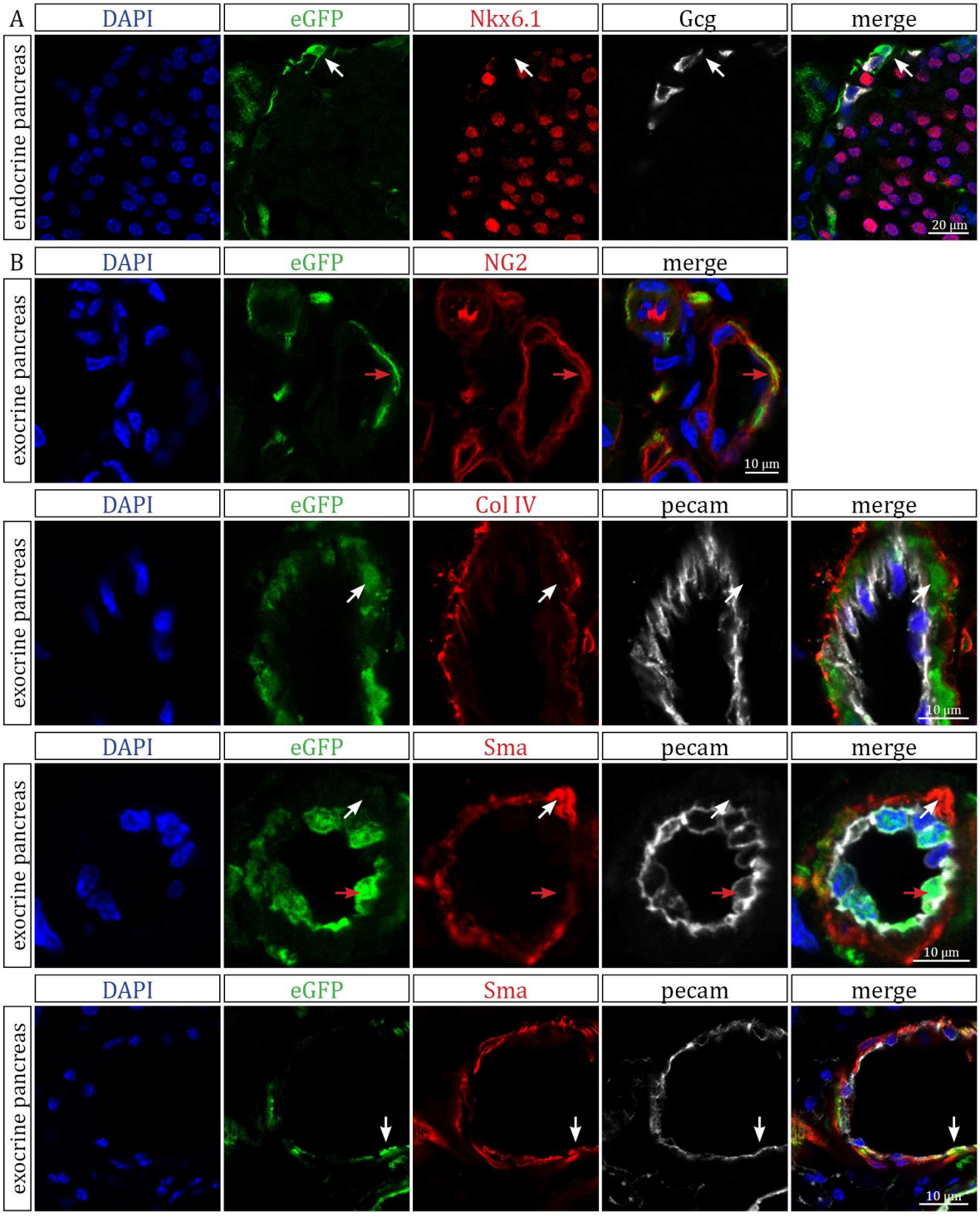

Figure 4.4: A small heterogeneous subpopulation of pancreatic cells exhibits Hedgehog activity *in vivo*

(A) Representative LSM images of pancreatic sections (adult *Tg(GBS-eGFP)* mice) immunostained for eGFP (green), α- (Glc, white) and β- (Nkx6.1, red) cells.
(B) Immunofluorescence stainings of eGFP (green), Ng2 (red), ColIV (red), Sma (red) and Pecam (white) in adult pancreas (*Tg(GBS-eGFP)* reporter mice.
(A,B) White arrows indicate eGFP expressing cells.

To test the possibility that the Hh pathway is activated only under specific circumstances *in vivo*, we investigated pancreatic endocrine cells in the *Tg(GBS-eGFP)* reporter mouse during development, aging and pregnancy. Hh signalling plays a major role in embryonic development and adult tissue homeostasis (McMahon, Ingham, & Tabin, 2003; Petrova & Joyner, 2014) and it regulates cell proliferation in adult organs (Dahmane & Ruiz i Altaba, 1999; Wechsler-Reya & Scott, 1999). Increased β-cell proliferation in mice is important for the increase of β-cell mass as a result of elevated metabolic demand in pregnancy (Sorenson and Brelje 1997). Thus, pancreata of pregnant females and embryonic pancreatic tissue at stages E14.5, P1-5 and 16 months old mice of *Tg(GBS-eGFP)* were analysed for Hh activity (data not shown). However, we could not observe differences in eGFP expression in these mice, suggesting that these circumstances do not induced Hh signalling *in vivo*.

Furthermore, the absence of eGFP expression in pancreatic endocrine cells *in vivo* might be due to inaccurate reflection of the endogenous expression. Additionally, it might be possible that Hh signalling is too low or only transiently active to turn on eGFP expression *in vivo*. The latter coincides with the observation that Gli transcription factors, which induce eGFP expression in *Tg(GBS-eGFP)* cells, are expressed at very low level in pancreatic endocrine cells (Figure 4.1).

In summary, we could not observe active Hh signalling in β-cells *in vivo* but discovered a small heterogenous subpopulation of pancreatic exocrine cells exhibiting Hedgehog activity.

4.1.2 Hh signalling elevates proliferation rate of endocrine islet cells *in vitro*

Hh signalling has been shown to promote cell proliferation in a variety of systems such as cancer progression and embryonic development (Dahmane & Ruiz i Altaba, 1999; Wechsler-Reya & Scott, 1999). To examine whether Hh activity enhances pancreatic endocrine cell proliferation, isolated islets from 3 months old WT mice were either stimulated with the Shh ligand or the Smo antagonist Cyc for 72 hours and subsequently immunostained with the cell cycle marker Ki67 (proliferation-related Ki67 antigen) (Figure 4.5). Interestingly, the number of Ki67 positive cells in Shh activated condition were slightly increased compared to untreated control conditions. In contrast, Cyc treatment resulted in a reduced proliferation rate. These results are consistent with the notion that Hh signalling activation can induce islet cell proliferation *in vitro*.

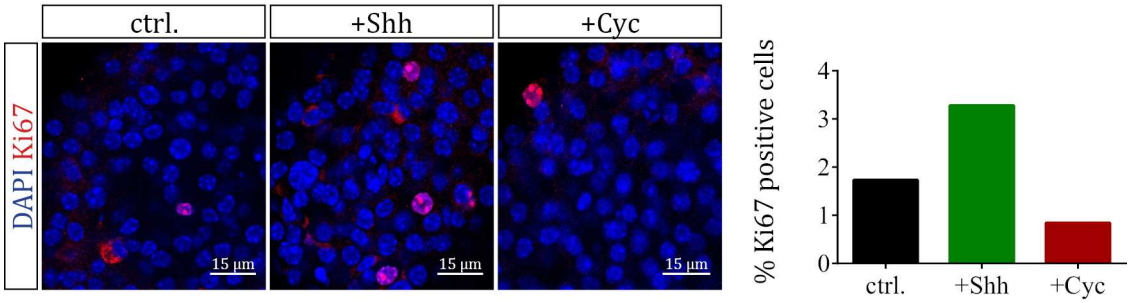

Figure 4.5: Shh stimulation increases proliferation rate of pancreatic islet cells

Representative LSM images of islet cells isolated from adult WT CD1 mice, which were cultured in control, Shh (500 ng/ml) stimulated and Cyc (10 µM) induced conditions for 72 hrs. The proliferation rate was determined by counting the number of Ki67 positive islet cells. (n (mice) = 2, mean)

4.1.3 Adult heterozygous Kif7 mice exhibit an insulin secretion defect

There is some evidence that the Hh pathway is involved in the regulation of glucose homeostasis in dysfunctional pancreatic endocrine cells. For example, ablation of Smo in Pdx1-Cre^{early} Smo $^{flox/null}$ mutant mice causes glucose intolerance and increased insulin sensitivity (J. Lau & Hebrok, 2010).

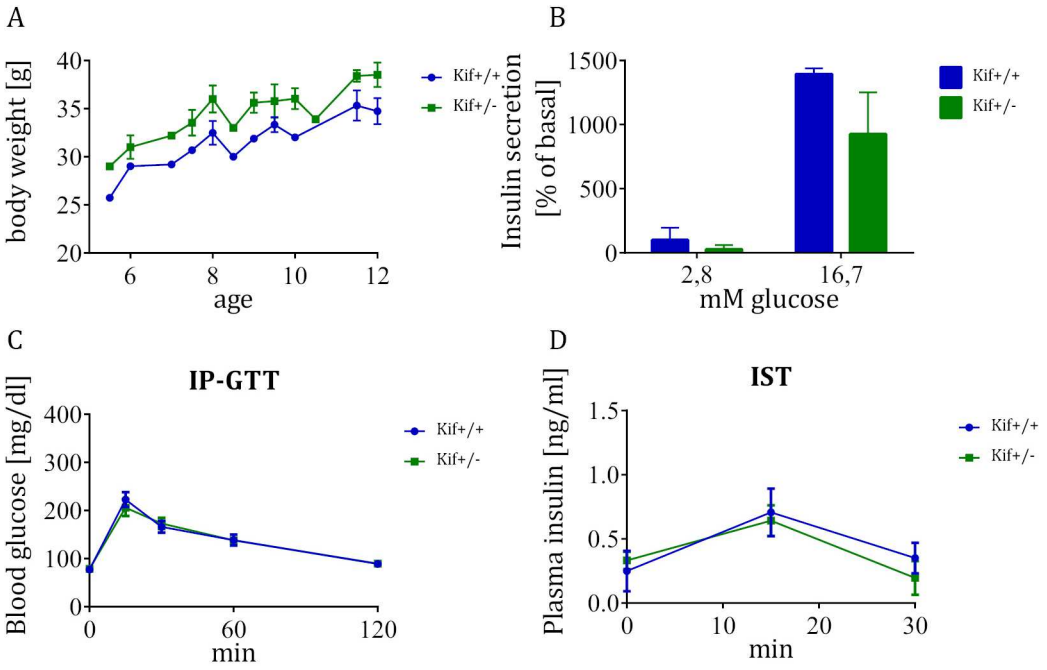

Figure 4.6: Male Kif7$^{+/-}$ mice exhibit a slight insulin secretion defect

(A) Weight monitoring over 8 weeks starting from the age of 4 weeks, comparing wild type and Kif7$^{+/-}$ mutant mice. (1-5n (mice) per time point, mean ± SEM)

(B) Glucose stimulated insulin secretion (GSIS) of isolated islets derived from 12-14 weeks old wildtype (Kif7$^{+/+}$) and Kif7$^{+/-}$ mice. (3n (mice), mean ± SEM)

(C) Intraperitoneal glucose tolerance test (ipGTT) of 12 weeks old wild type and Kif7$^{+/-}$ mice. (5n WT mice, n6 Kif7$^{+/-}$ mice, mean ± SEM)

(D) Insulin secretion test (IST): Plasma insulin levels were measured during the IP-GTT shown in (C). (n = 5 WT mice, n = 8 Kif7$^{+/-}$ mice, mean ± SEM)

To investigate Hh signalling in the regulation of glucose homeostasis *in vivo*, we employed Kif7$^{+/-}$ mice as a gene knock-out mouse model. The motor protein Kif7 is a conserved regulator of the Hh signalling pathway, which acts as a positive regulator by preventing the processing of Gli3 into its repressor form (Liem, He, Ocbina, & Anderson, 2009). Kif7$^{-/-}$ mice die at birth with severe malformations, including anencephaly and polydactyly (Cheung et al., 2009). Thus, we analyzed metabolic parameters in adult heterozygous male mice. Kif7$^{+/-}$ mutant mice exhibited slightly higher body weight relative to the WT animals at the age of 6-12 weeks (Figure 4.6A). To explore if heterozygosity of Kif7 influences β-cell function, we performed a glucose stimulated insulin secretion assay (GSIS) with isolated islets of adult Kif7$^{+/-}$ mice (Figure 4.6B). Insulin secretion of Kif7$^{+/-}$ islets was slightly reduced in low (2.8 mM) and high (16.7 mM) glucose medium. Furthermore, we performed a intraperitoneal glucose tolerance test (IP-GTT) and an insulin secretion test (IST) in a cohort of Kif7$^{+/-}$ mice (Figure 4.6C,D). However, this metabolic study did not reveal severe changes in glucose homeostasis.

In conclusion, partial lack of Kif7$^{+/-}$ causes a slight insulin secretion defect *in vitro*, which is presumably compensated *in-vivo* by systemic mechanisms.

4.2 A novel Cre-inducible knock-in ARL13B-tRFP fusion cilium reporter

Mammalian primary cilia have been shown to mediate transduction of Hh signals in the cell. Mutations in cilia-associated genes lead to a dysfunctional cilium including dysregulated ciliogenesis and abnormal cellular signalling, which causes a broad range of diseases, namely ciliopathies. Beside other symptoms, a subset of ciliopathy patients also exhibit metabolic disorders. To investigate the function of cilia in endocrine β-cells in a tissue-specific manner *in vitro* and *in vivo*, we generated a novel Cre-inducible cilia reporter mouse strain (Schmitz et al., submitted).

4.2.1 Generation of the ARL13B-tRFP reporter mouse line

We aimed to create a Cre-inducible reporter mouse strain in which the cilium and the basal body of a cell were simultaneously labelled with fluorescent proteins. Therefore, a construct was generated containing the sequence of the human ADP ribosylation factor like GTPase 13B (*ARL13B*) gene fused to the sequence of the tag red fluorescent protein (tagRFP; tRFP) as well as the blue fluorescent protein (BFP) sequence fused to the human centrin 2 (*CETN2*) gene. The ARL13B protein is a cilium specific GTPase, which regulates ciliogenesis and intraflagellar transport (Y. Li, Wei, Zhang, Ling, & Hu, 2010). CETN2, a structural component of the centrosome, is involved in the duplication and segregation of the centrosome (Rice & Agard, 2002) and therefore localizes to both, centrosomes and basal body.

We designed a targeting vector in which the open reading frame (ORF) of the *ARL13B-tRFP-2A-BFP-CETN2* reporter sequence was cloned in inverse orientation in front of a pCAG promoter inducing overexpression of the transgene (Dr. Ingo Burtscher, IDR, Helmholtz Zentrum, Munich) (Figure 4.7). Targeted mutagenesis in embryonic stem cells (ESCs) was performed to insert this construct sequence upstream of the endogenous *Hprt* (hypoxanthine-guanine phosphoribosyl-transferase) gene locus by homologous recombination (A. Gossler, Medizinische Hochschule Hannover, Germany). Upon integration, parts of the murine 5' upstream sequence of the Hprt locus including the first exon of the *Hprt* gene were replaced by its corresponding human sequence from the vector. For gene targeting, E14TG2a ESCs were used which have a partially mutated *Hprt* locus. Upon construct integrations the *Hprt* locus is repaired enabling the ESCs to survive in hypoxanthine-aminopterin-thymidine (HAT) secletion medium in culture (Thompson, Clarke, Pow, Hooper, & Melton, 1989). The ORF of the reporter sequence is flanked by WT and 2272 loxP sites. Cre-recombinase activity causes the inversion of the reporter sequence, which enables transcription by the pCAG promoter since the reporter sequence is orientated correctly. Subsequently, the neomycin phosphotransferase (*neo*^{r}) cassette 5' prime of the reporter sequence is excised by the Cre-recombinase using remaining loxP sites. This second recombination event ensures that further sequence inversions are prevented and the reporter sequence stays in correct orientation. The transcription of the reporter sequence results in a bicistronic mRNA, which is eventually co-translated in equimolar ratio. The sequences of the two fusion proteins ARL13B-tRFP and BFP-CETN2 are separated by a 2A site enabling a ribosomal skipping mechanism during translation. Normal peptide bond formation is impaired at this site, which ensures the separation of fusion proteins when translated consecutively (Donnelly et al., 2001).

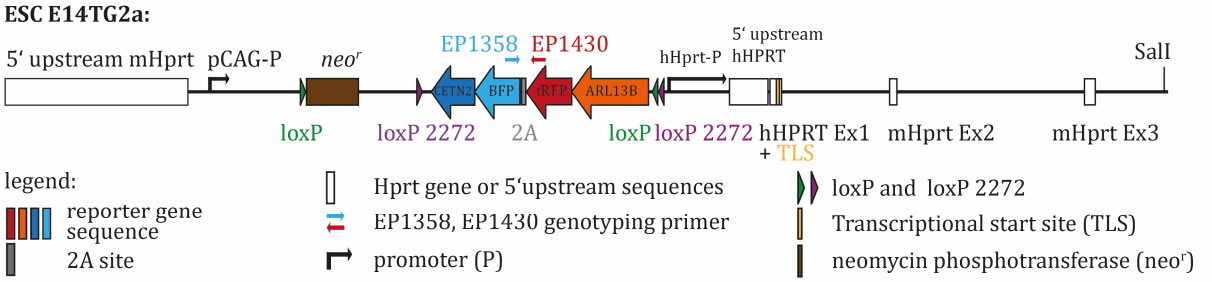

Figure 4.7: Targeting strategy for the generation of the ARL13B-tRFP reporter mouse

The ARL13B-tRFP-2A-BFP-CETN2 targeting vector is schematically illustrated. The construct was integrated in the 5' upstream region of the Hprt locus by homolgous recombination in ESCs replacing the first exon and parts of the 5' upstream region with the human HPRT sequence. The *ARL13B-tRFP* and *BFP-CETN2* fusion sequences are under contol of a pCAG promoter (*CAG*= The *CMV* early enhancer/chicken β-actin promoter; *CMV* = cytomegalovirus). 5' Upstream sequence, Hprt exons, 2A site, *neo*^{r} selection cassette and reporter sequences are illustrated with white or coloured boxes. The restriction enzyme SalI was used for vector linearization before transfection in ESCs. Binding sites for genotyping primer EP1358 and EP1430 are located in the BFP or tRFP sequence, respectively. The illustration was depicted in scale.

To examine proper integration of the targeting construct in ESCs, collaboration partners (A. Gossler, Medizinische Hochschule Hannover, Germany) performed a long-range PCR and identified six ESC clones with integrated reporter sequence (Figure 4.8A). We used clones #4 and #6 to generate mouse germline chimeras by ESC aggregation (Angelika Ziegler and Bianca Vogel, ISF/IDR Helmholtz Zentrum, Munich). Mice were genotyped using primers located in the BFP and tRFP reporter sequence, respectively (Figure 4.8B). Heterozygous ARL13B-tRFP mice were crossed into cell type-specific Cre lines such as ROSA-Cre (ARL13B-tRFP^{Rosa}), Fltp(T2AiCre) (ARL13B-tRFP^{Fltp}) or Foxa2T2AiCre (ARL13B-tRFP^{Foxa2}). In male progenies of ARL13B-tRFP x ROSA-Cre crossings, the reporter recombined in every cell of the body, whereas female offspring displayed a mosaic reporter expression pattern. In females, the X-chromosome, on which the *Hprt* gene is located, undergoes random X-inactivation causing transgene expression in 50% of the cells.

Next, we investigate proper synthesis of ARL13B-tRFP and BFP-CETN2 reporter proteins by performing a Western blot using mouse embryonic fibroblasts (MEFs) derived from WT and ARL13B-tRFP (ARL13B-tRFP^{Rosa}) embryos at embryonic stage E13.5 (Figure 4.8C). Endogenous Arl13b and the reporter fusion protein ARL13B-tRFP migrate higher than its calculated molecular weight at 60 kDa and 110 kDa most likely due to post-translational modifications of the Arl13b protein such as palmitoylation (Mariani et al., 2016). Likewise, endogenous Cetn2 and the fusion protein BFP-CETN2 is detected at 20 kDa and 57 kDa in MEFs.

To confirm proper protein expression and correct subcellular localization of the transgenes, we performed immunofluorescence stainings (IFs) on mouse tissue sections. However, only fluorescent signal for the ARL13B-tRFP reporter protein but not for the BFP-CETN2 fusion protein was detectable (data not shown). The absence of BFP fluorescence signal might either result from a mutated DNA reporter sequence or due to an instable mRNA or protein. Sequencing of the transgene sequence isolated from ARL13B-tRFP mice confirmed a correct nucleotide sequence (data not shown) and accurate construct integration in the mouse genome. Thus, we verified mRNA expression of *BFP-CETN2* reporter gene via real time quantitative PCR (qPCR) using RNA isolated from MEFs (Figure 4.8D). Indeed, mRNA expression of *BFP* was detectable in MEFs expressing the reporter sequence. We also tested the proper expression of the BFP-CETN2 reporter by stably transfecting murine inner medullary collecting duct 3 (IMCD3) cells with the ARL13B-tRFP-2A-BFP-CETN2 targeting vector. Western blot analysis (Figure 4.8C) validated strong reporter protein expression and live-cell epifluorescence microscopy (Figure 4.8E) verified correct localized ARL13B-tRFP and BFP-CETN2 reporter proteins in cilia or basal bodies of IMCD3 cells, respectively (Dr. Ingo Burtscher, IDR). The reduced expression level of the reporter protein in MEFs compared to IMCD3 cells suggests that the BFP-CETN2 fusion protein expression is too low to be detected in murine cells or tissues.

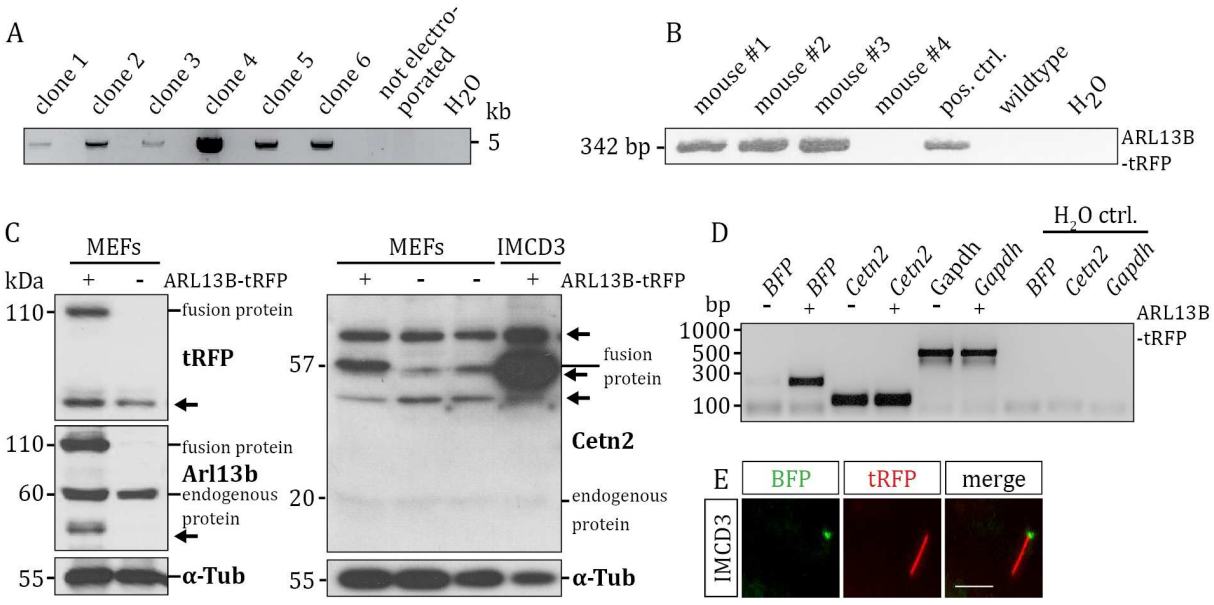

Figure 4.8 Generation of the ARL13B-tRFP reporter mouse line

(A) Agarose gel image of long range PCR products to identify ESC clones harboring the ARL13B-tRFP construct. (performed by the collaboration partner A. Gossler, Medizinische Hochschule Hannover, Germany)
(B) PCR genotyping of ARL13B-tRFP mice using EP1358 and EP1430 primers to distinguish WT mice from mice expressing the ARL13B-tRPF reporter. The PCR product is detected at a size of 342 bp in reporter expressing mice.
(C) Representative Western blot image of MEFs and IMCD3 protein lysates using anti-Arl13b, anti-tRFP and anti-Cetn2 antibodies to prove correct reporter protein expression. An anti-α-tubulin antibody demonstrates proper loading of protein lysates. Note, black arrows indicate unspecific bands.
(D) qPCR analysis detecting mRNA expression of *BFP* and *Cetn2* in RNA samples isolated from WT or reporter expressing MEFs.
(E) Live-cell epifluorescence microscopy images of IMCD3 cells, which integrated the ARL13B-tRFP-2A-BFP-CETN2 construct after transfection. tRFP signal was detected in the cilium (red) and BFP signal was observed in the basal body (green). (scale: 10 µm)

A fluorescence reporter provides the advantage to distinguish cells via fluorescence-activated cell sorting (FACS) depending on their active reporter expression. To prove this for the ARL13B-tRFP reporter, we FACS sorted cultured MEF cells, which were derived from male wildtype or male and female reporter expressing embryos. Indeed, we detected stronger signal intensity for reporter expressing male cells (Figure 4.9, P3) in comparison to WT cells (Figure 4.9, P2) for which we detected autofluorescence signal. Because female MEFs only express the reporter in 50% of their cells, we were able to separate cells in two populations, cells with or without active reporter expression.

Despite the fact, that the BFP-CETN2 reporter protein was not detectable in mouse tissue, the ARL13B-tRFP reporter constitutes a valuable tool for the investigation of ciliary function.

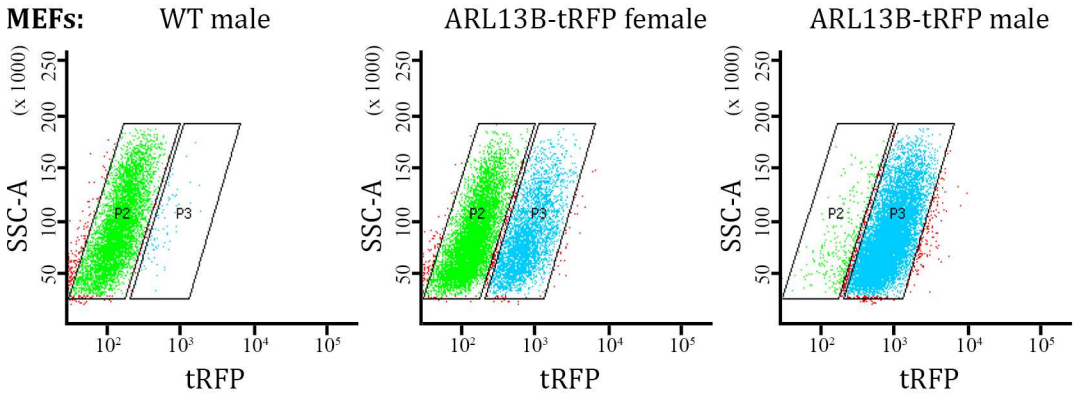

Figure 4.9: FACS sorting easily separates cells depending on the reporter expression

FACS analysis of MEFs isolated from WT and male or female ARL13B-tRFP^{RoseCre} E13.5 embryos. tRFP signal intensity was plotted against side scatter (SSC) signal to distinguish cells depending on the reporter expression. Female cells express the ARL13B-tRFP reporter in half of the cells due to X-inactivation of the reporter locus.

4.2.2 Functional analysis of the ARL13B-tRFP mouse strain

Next, we aimed to preclude possible effects of the overexpressed reporter protein on the viability and fertility of animals and on the ciliary function including cellular signalling and ciliary length. Indeed, male and female offspring of ARL13B-tRFP x RosaCre matings were fertile and viable. Germline transmission of the cilia reporter construct in ARL13B-tRFP^{Rosa} mice did not affect fertility in male offspring. Spematocytes isolated from male ARL13B-tRFP^{Rosa} reporter mice did not show reduced motility when compared to cells of wildtype littermates (Figure 4.10).

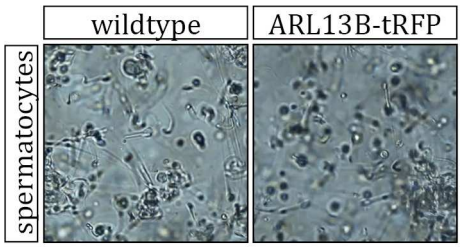

Figure 4.10: ARL13B-tRFP^{Rosa} mice are fertile and viable

Representative bright field images of live-cell movies displaying spermatocytes isolated from male WT and ARL13B-tRFP^{RoseCre} mice (movie see attachment page 175).

Arl13b overexpression induces cilia length increase in zebrafish embryos and in the murine fibroblast cell line NIH 3T3 by regulating ciliary membrane extension (Lu et al., 2015). Hence, we investigated ciliary length of female ARL13B-tRFP MEFs by performing immunofluorescence stainings (Figure 4.11A). Cilia of cells with active reporter expression did not exhibit a significant increase in length relative to cilia of cells in which the reporter expression was suppressed by X-inactivation (Figure 4.11B).

Further, Arl13b regulates Shh signal transduction in the cilium (Horner & Caspary, 2011; Mariani et al., 2016). To examine if Arl13b overexpression influences Shh pathway activity in ARL13B-tRFP reporter expressing cells, Shh signalling was either stimulated with the Shh ligand and the Smo agonist SAG or inhibited with Cyc in MEFs (Figure 4.11C). Male WT or reporter expressing MEFs showed equally increased protein expression of the Shh target gene Gli1 upon active Hh signalling implying that canonical Shh signalling is not significantly influenced by the reporter expression (Figure 4.11D).

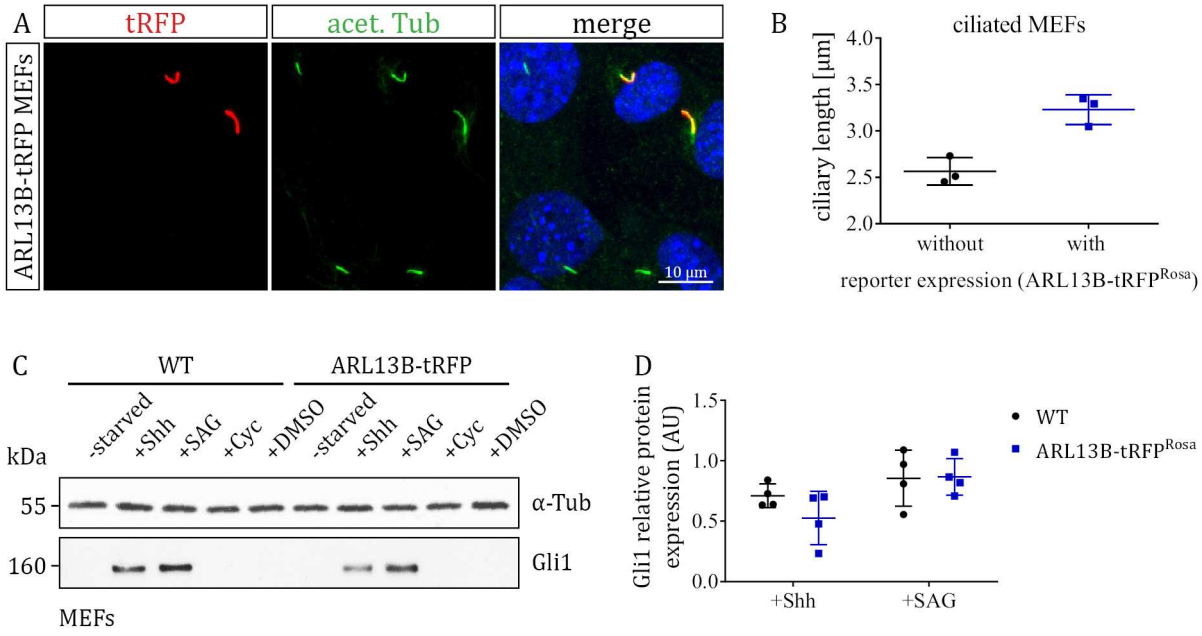

Figure 4.11: ARL13B-tRFP^{Rosa} reporter expression does not significantly influence ciliary length and Shh signalling in MEFs

(A) Representative Immunofluorescence staining of female ARL13B-tRFP^{RosaCre} MEFs. All cilia were immunostained with an anti-acetylated tubulin antibody (acet. Tub, green), whereas cilia expressing the ARL13B-tRFP fusion protein were sepcifically labeled with an anti-tRFP antibody (red).
(B) Quantification of ciliary length measured in immunofluorescence stainings of MEFs (A). Cilia of cells within the same cell line were compared according to an active or inactive reporter expression (n (experimental weeks) = 3, mean ± SD, paired t-test)
(C) Western blot analysis of WT and ARL13B-tRFP reporter expression in MEFs. Cells were starved in serum-free medium overnight. Subsequently, Shh signalling was stimulated with the Shh ligand (500 ng/ml) and the smoothened agonist SAG (1 µM) and suppressed with cyclopamine (Cyc, 10 µM) for 24 hrs to examine the protein expression of the Shh target gene Gli1. Equal loading of protein lysates was controlled by detecting the α-tubulin protein (α-Tub).
(D) Quantification of Gli1 expression detected in (C). (n = 4 (n = 2 clones plus n = 2 experimental weeks), mean ± SD, unpaired t-test)

Taken together, ARL13B-tRFP^{RosaCre} reporter animals are fertile and viable and overexpression of the reporter protein does not significantly influence Shh signalling and ciliary length.

4.2.3 The ARL13B-tRFP reporter protein accurately localizes to cilia in mono-and multi-ciliated tissue

Upon Cre-recombinase mediated inversion of the reporter sequence in ARL13B-tRFP^{Cre} mice reporter expression is activated. To exclude leaky reporter transcription, reporter protein expression was validated in ARL13B-tRFP^{Fltp} mice and compared to ARL13B-tRFP mice in which the reporter transcription was not enabled by a recombinase (Figure 4.12). Immunostainings of female isolated pancreatic islets exhibited reporter expression only in mice carrying a recombinase-activated reporter sequence suggesting correct reporter induction.

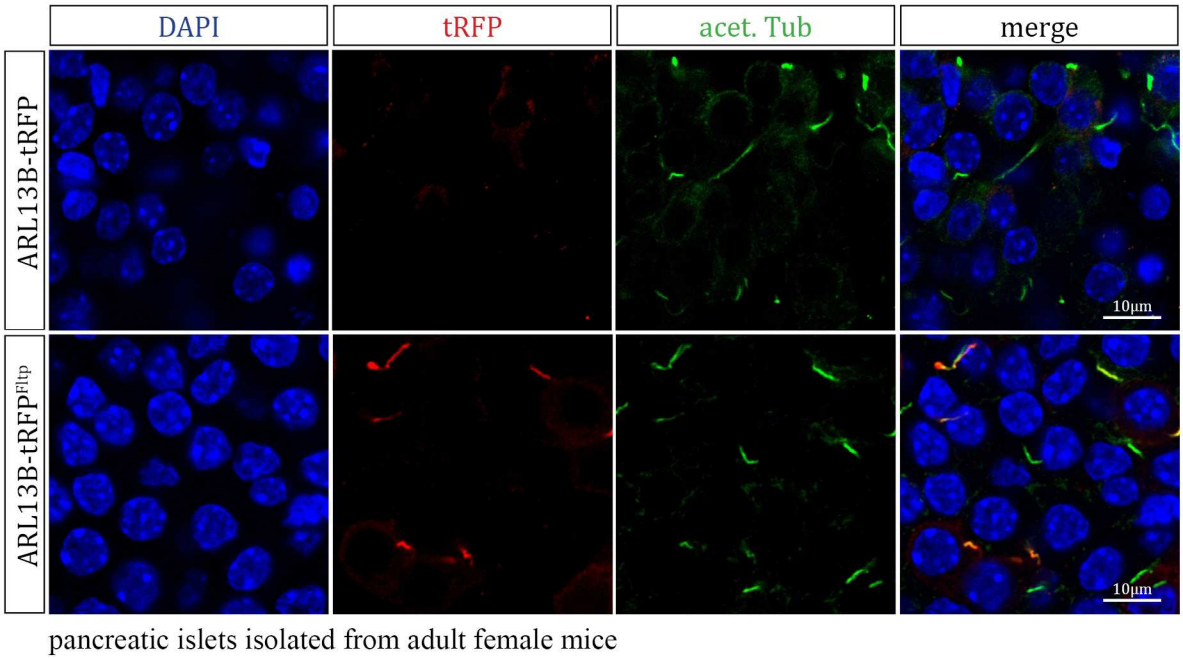

Figure 4.12: ARL13B-tRFP^{Fltp} reporter expression is specifically induced depending on the availability of Cre-recombinase activity

Representative LSM pictures of pancreatic islets isolated from adult female ARL13B-tRFP^{Fltp} and ARL13B-tRFP mice.

Detection of the reporter was verified in immunohistochemistry and in live-cell imaging facilitating the study of ciliary function in fixed tissue and in explant tissue culture.

Proper expression and localization of the ARL13B-tRFP reporter protein in cells carrying single primary cilia and multi-ciliated tissue was further validated by an immunofluorescent approach (Figure 4.13). We labelled cilia with an anti-acetylated tubulin antibody and coimmunostained with an anti-tRFP antibody to detect the reporter protein in cryosections of pancreas, lung and brain as well as in whole-mount preparations of embryos.

Pancreatic islets of female pups at postnatal day 2 (P2) (ARL13B-tRFP^{Fltp}) exhibited correctly localized reporter signal in the primary cilia of reporter expressing cells (Figure 4.13A). Similarly, we detected a strong and specific reporter signal in cilia of Foxa2 marked axial mesoderm cells at

the node of E7.5 female embryos (ARL13B-tRFP^{Foxa2}) (Figure 4.13B). Motile kinocilia of the ependyma in 3.5 months old female reporter mice (ARL13B-tRFP^{Foxa2}) also displayed accurately localized reporter protein (Figure 4.13C). Additionally, we observed high reporter expression in the multiciliated respiratory epithelium of P2 female lungs (ARL13B-tRFP^{Foxa2}) (Figure 4.13D).

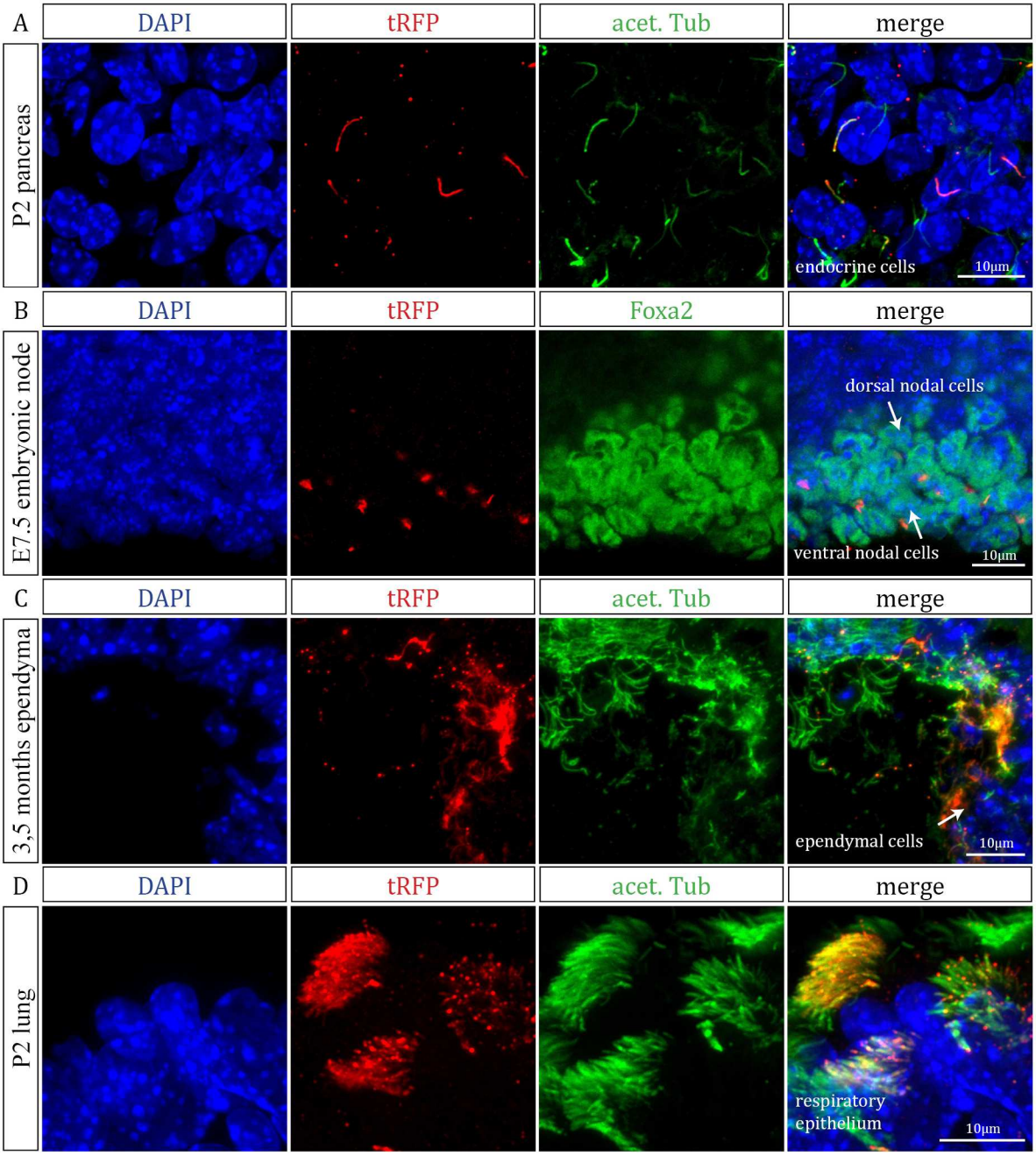

Figure 4.13: ARL13B-tRFP reporter protein precisely localizes to the primary cilium in mono- and multi-ciliated tissue

(A) Immunofluorescent picture of embryonic pancreatic sections (ARL13B-tRFP^{Fltp}) isolated at P2.
(B) Whole mount immunofluorescence stainings of E7.75 mouse embryos (ARL13B-tRFP^{Foxa2}) showing posterior view of the nodal area.
(C) Immunofluorescent image of brain tissue sections derived from 3.5 months old ARL13B-tRFP^{Fltp} mice.

(D) Representative LSM images of P2 lung sections (ARL13B-tRFP^{Fltp}).
(A-D) ARL13B-tRFP (tRFP antibody, red) was coimmunostained with antibodies either against the ciliary acetylated tubulin (aTub, green) or against the endoderm marker Foxa2 (green). All images are maximum projections of several z-stacks.

To investigate if the ARL13B-tRFP reporter mouse line was suitable for live-cell imaging *ex vivo*, we performed time-lapse confocal microscopy for organ cultures and cultured embryos. Pancreatic islets were isolated from 3.5 months old mice (ARL13B-tRFP^{Fltp}) (Figure 4.14A). Cilia protruding from the tissue surface of cultured islets exhibited a bright fluorescent reporter signal. Likewise, we recorded a time-lapse movie of endoderm cells on the surface of cultured embryos at the late gastrulation stage E7.75 (ARL13B-tRFP^{Foxa2}) (Figure 4.14B). Next, we isolated lungs from E13.5 embryos (ARL13B-tRFP^{Rosa}) and cultured them overnight (Figure 4.14C). Epithelial cells at the inner apical site of grown tubules carried multiple moving cilia, which were imaged over time. We detected a strong and specific signal for cilia of culture lung tissue that lasted several hours.

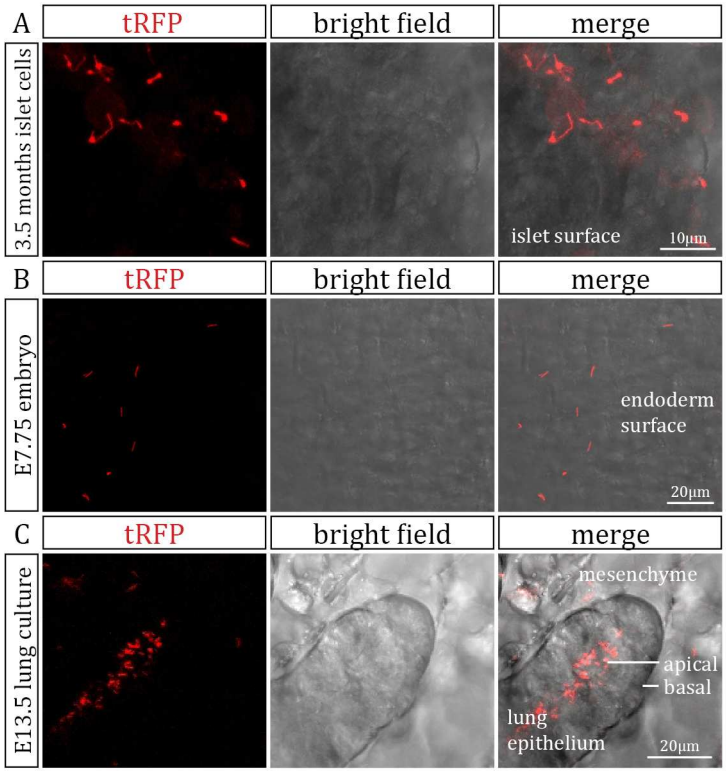

Figure 4.14: Time-lapse confocal microscopy of cilia in explant cultures expressing the ARL13B-tRFP fusion protein

(A-C) Still images of time lapse movies displaying cultured lung tissues, isolated islets of Langerhans and cultured embryos. Bright field (BF) and fluorescent signal (tRFP) images are presented. All images are maximum projections of several z-stacks. (movies see attachment page 175)
(A) Pancreatic islets of Langerhans isolated from a 3.5 months old mouse (ARL13B-tRFP^{Fltp}).
(movie: 1 frame/ 10 min)
(B) Endoderm surface of an embryo at stage E7.75 (ARL13B-tRFP^{Foxa2}). (movie: 1 frame/ 10 min)
(C) Cultured lung tissue derived from a E13.5 embryo (ARL13B-tRFP^{Rosa}). (movie: 11.3 frames/ min)

In summary, the ARL13B-tRFP reporter is strongly expressed in mono- and multi-ciliated cells and accurately localizes to motile and non-motile cilia. We detected a bright reporter signal in immunofluorescence analysis of fixed tissue and during live-cell imaging of explant tissue culture. Thus, the ARL13B-tRFP reporter mouse strain is a valuable tool for the investigation of ciliary structure and function in a tissue-specific manner to understand processes, such as ciliary protein trafficking or cilium-dependent signalling *in vitro* and *in vivo*.

4.2.4 The ARL13B-tRFP reporter enables the monitoring of cilia assembly and disassembly in living cells

The primary cilium and cell-cycle progression are tightly linked since cilia are assembled when cells exit the cell cycle as a result of mitogen deprivation or differentiation cues (Sanchez and Dynlacht 2016). However, underlying principles of this interdependency are not completely understood.

We studied the process of cilia assembly and disassembly in MEFs in a 2D culture system by performing live-cell imaging (Figure 4.15). About 40 min prior to the beginning of mitosis, a long cilium was observed. Over the next 20 minutes, it reduced its length until only a single dot was visible. During mitotic division, when cells exhibited a morphological round shape, no fluorescent reporter signal was detectable. In telophase, a single dot of reporter signal reappeared in both daughter cells, which elongated to a fully-grown primary cilium over the next 3.5 hours.

To conclude, the ARL13B-tRFP mouse strain is suitable for the investigation of ciliogenesis and ciliary function *in vivo* and *ex vivo* using live-cell imaging.

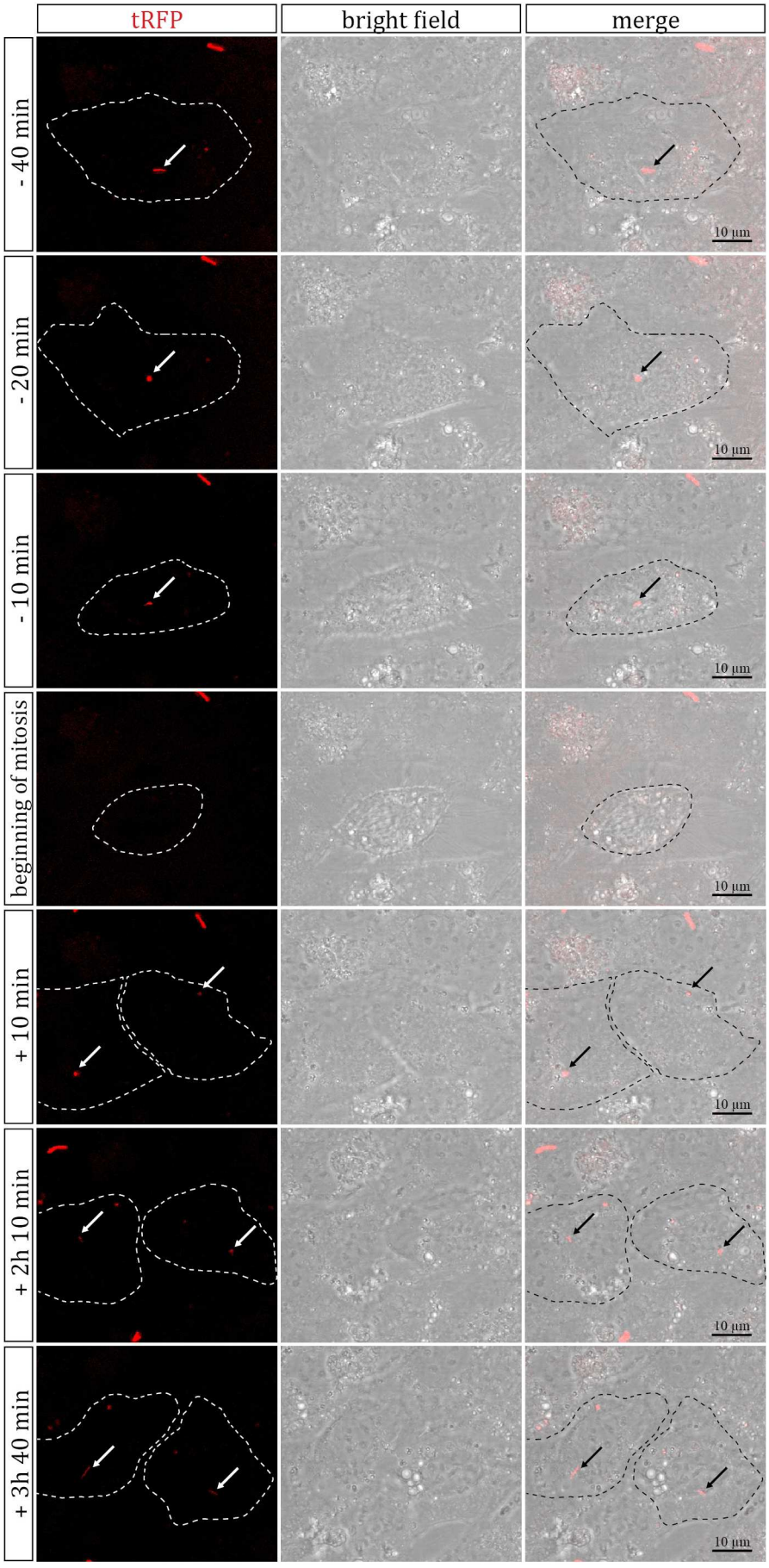
tRFP
bright field
merge
- 40 min
- 20 min
- 10 min
beginning of mitosis
+ 10 min
+ 2h 10 min
+ 3h 40 min
10 µm

Figure 4.15 Live-cell imaging of cilia assembly and disassembly during the cell cycle of MEFs

Time-laps movie of cultured MEFs (ARL13B-tRFP^{RosaCre}) for which bright field (BF) signal and fluorescent signal (tRFP) was detected. Representative images of a dividing cell about 10 min, 20 min and 40 min prior to the beginning of mitosis, during mitosis and 10 min, 2h 10min and 3h 40min after mitosis are shown. (movie: 1 frame/ 10 min; movie see attachment page 175)

4.3 Characterization of a putative modulator of the InsR/Igfr signalling system *in vivo* and *in vitro*

4.3.1 Bioinformatic analysis of the *5330417C22RIK* gene and protein

To identify novel regulatory genes involved in the endocrine lineage formation of the pancreas, we previously performed an mRNA expression profile using a microarray-based screen in our laboratory. We detected abundant mRNA expression of the *5330417C22RIK* gene specifically in the pancreatic epithelium when compared to the mesenchyme (Willmann et al., 2016). To examine the biological function of the *5330417C22RIK* gene in more detail, KO mice were generated.

As a first step, we performed a bioinformatical characterization summarizing database knowledge to get insight into the function of the gene and protein based on predictions. The analysis of the gene locus und structure gave us information about its transcriptional regulation and possible alternative splice variants. Homology studies of orthologous amino acid sequences from other species indicated to which extent the 5330417C22RIK protein is evolutionary conserved. Further, predicted topology, domain structures and potential post-translational modifications for the 5330417C22RIK protein gave hints to its functional properties, subcellular localization, interaction partner or its involvement in signalling pathways.

4.3.1.1 The *5330417C22RIK* gene

The *5330417C22RIK* gene is named after its RIKEN clone 5330417C22. In *mus musculus* it is located at chromosome 3 at position 108,455,694-108,536,536 bp of the reverse strand of the DNA and is found at 47.14 cM in the genetic map. The *5330417C22RIK* gene comprises 22 exons (Figure 4.16, black boxes) of which two exons (19 and 20) lie in close proximity to each other. Additionally, it possesses a predicted promoter site (green box) 5' of the first exon and several promoter flanking (light green boxes) and enhancer regions (yellow boxes) within the gene sequence (Figure 4.16).

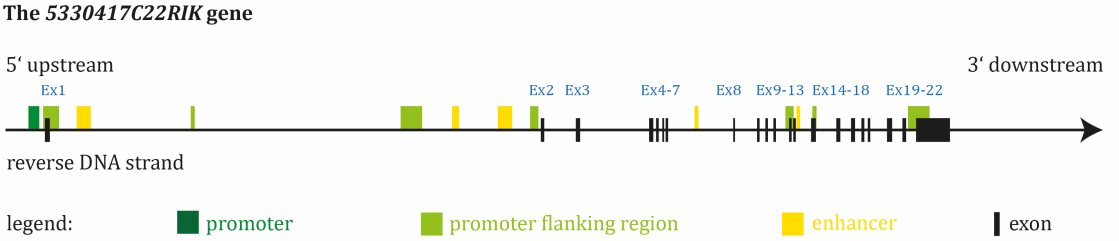

Figure 4.16: The *5330417C22RIK* gene with its predicted exon-intron sequences and promoter and enhancer regions.

Schematic representation of the *5330417C22RIK* gene locus. The gene contains 22 exons and is located on the reverse strand of the DNA at chromosome 3. Promoter, promoter flanking regions, enhancer regions and exons are depicted in coloured boxes. Modified from Ensemble database (http://www.ensembl.org; 17.5.17)

Seven transcripts processed by alternative splicing are predicted for this gene (Figure 4.17 and Table 4.1) of which only three are protein coding. The largest predicted transcript (*5330417C22RIK-202*) has a length of 5836 bp and is encoded by 22 exons resulting in a protein product of 1013 amino acid (aa). Its translation start site (start codon) is located in the beginning of exon 1 and its stop codon resides in the beginning of exon 22 leaving 5’ and 3’ untranslated regions at both ends (framed boxes). In comparison, the second transcript (*5330417C22RIK-201*) and its protein is shorter in length (3321 bp, 911 aa) since exon 2 is spliced out, exon 22 is shortened and the translational start site resides in the beginning of exon 3. The third predicted transcript (*5330417C22RIK-203*) entails a sequence of 2896 bp (939 aa) and comprises 21 exons of which exon 7 is removed by alternative splicing and exon 21 is shortened. Start and stop codon in this variant match with the first transcript isoform.

Table 4.1: Predicted transcripts for the *5330417C22RIK* gene.

Three predicted, protein coding transcripts for the *5330417C22RIK* gene are listed including their number of exons and the transcript and protein length. Modified from Ensemble database (http://www.ensembl.org; 17.5.17).

Number	Name (mus musculus)	Transcript ID	Exons (protein coding exons)	Transcript length	Protein length
#1	*5330417C22RIK-202*	ENSMUST00000106625.9	22 (22)	5836 bp	1013 aa
#2	*5330417C22RIK-201*	ENSMUST00000048012.12	21 (20)	3321 bp	911 aa
#3	*5330417C22RIK-203*	ENSMUST00000106626.2	21 (21)	2896 bp	939 aa

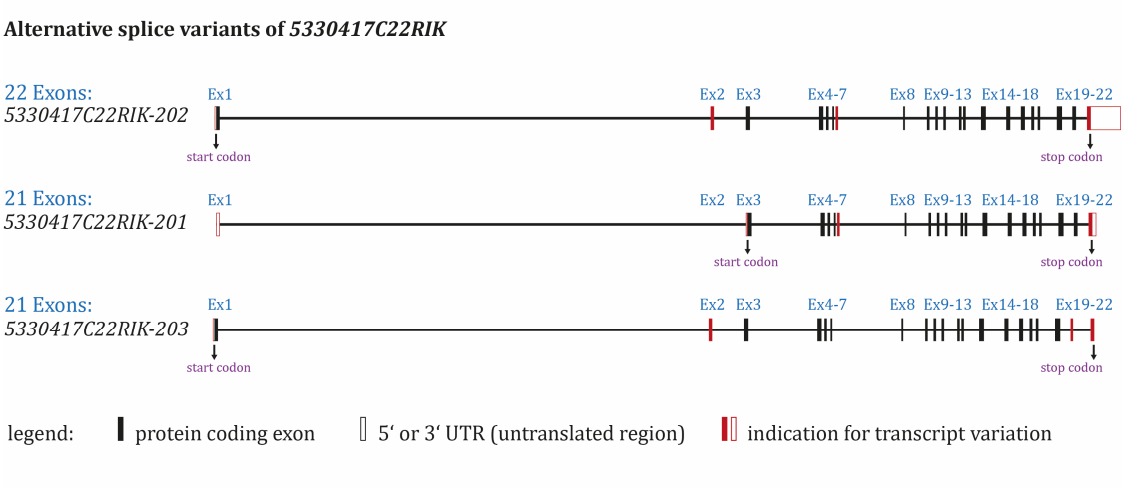

Figure 4.17: Schematic picture of predicted alternative splice variants for the *5330417C22RIK* gene.

Full boxes represent protein coding exons whereas untranslated regions (UTRs) are depicted by framed boxes. Red coloured exons highlight differences between transcript variants. Modified from Ensemble database (http://www.ensembl.org; 17.5.17)

Taken together, the *5330417C22RIK* gene consists of 22 exons, which are transcribed and consequently spliced into mainly three predicted transcript variants with different lengths.

4.3.1.2 The 5330417C22RIK protein

The 5330417C22RIK protein is evolutionarily highly conserved as it was shown by the presences of 73 predicted orthologs for the 5330417C22RIK protein and 1 paralog (5330417C22RIK Like) in vertebrates and invertebrates. High protein sequence homology is found in several vertebrates including C. lupus (dog: 90.3%), B. taurus (cow: 90.3%), G. gallus (chicken: 68.9%), X. tropicalis (frog: 61.7%) and D. rerio (zebrafish: 56.3%) (protein identity in % derived from NCBI HomoloGen search, https://www.ncbi.nlm.nih.gov/homologene/23249). Its human ortholog KIAA1324, also named EIG121 (Estrogen-induced gene 121), maba1 and UPF0577 (UPF0577 Protein KIAA1324), shares a protein sequence identity of 90.8% with Mus musculus. The amino acid sequence alignment of these two species reveals the highest homology in their C-termini (marked by asterisks, Figure 4.18).

The A2AFS3-1 (UniProt ID A2AFS3 isoform 1; http://www.uniprot.org/uniprot/A2AFS3) amino acid sequence derived from the UniProt database was used for the sequence alignment and following bioinformatical analysis in this chapter. UniProt predicts a 1009 aa long protein (A2AFS3-1) and claims it as the “canonical sequence”. This aa sequence corresponds to the *5330417C22RIK-201* (911 aa) transcript predicted by the Ensemble online database, but the resulting protein sequence starts with the translation start site in exon 1 and not in exon 2 as it is predicted for the *5330417C22RIK-201* transcript. Additionally, the UniProt A2AFS3-1 sequence excludes four amino acids in the middle of the sequence.

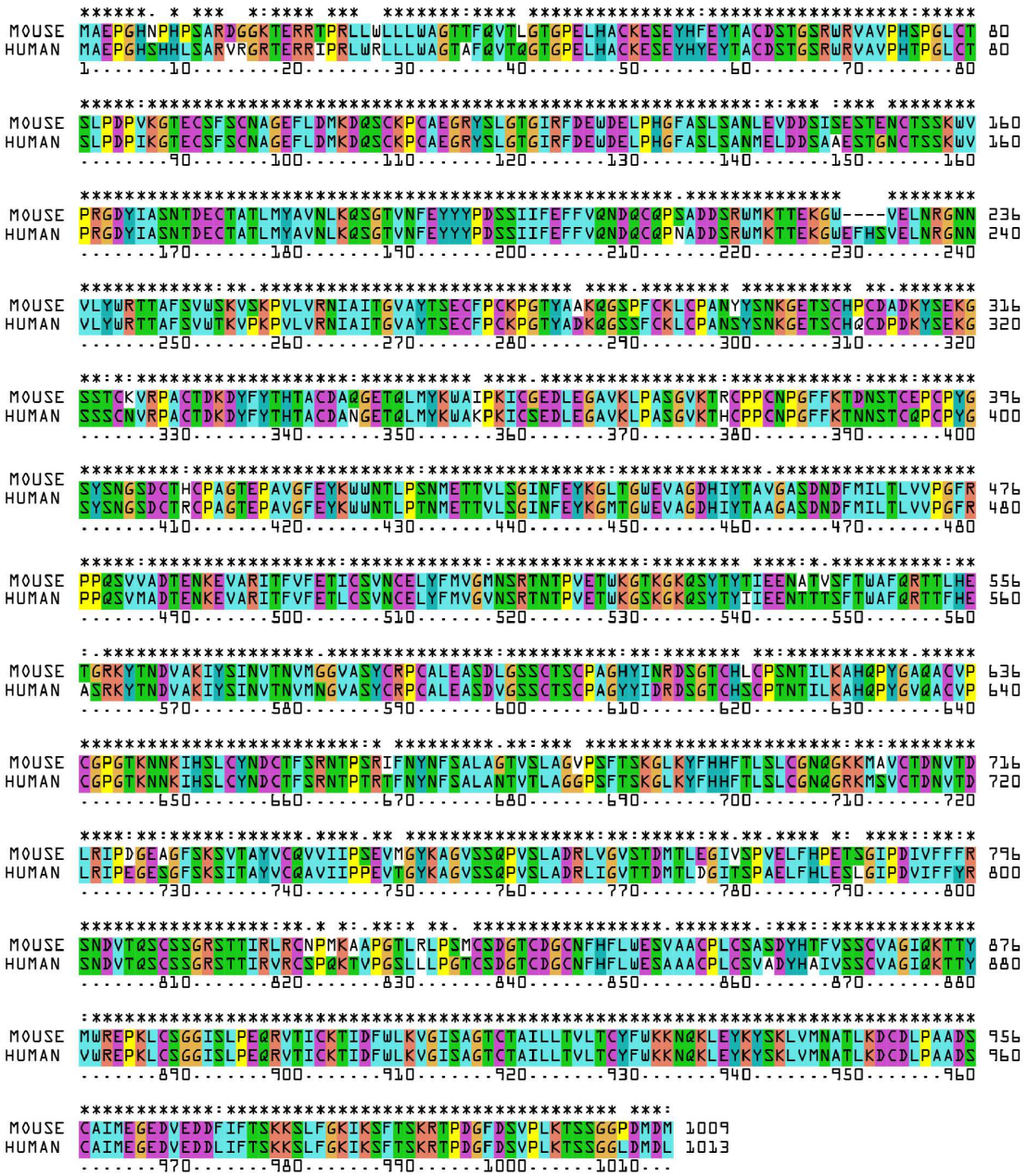

Figure 4.18: High protein sequence identity between mouse and human 5330417C22RIK.

For the ClustalX sequence alignment the amino acid sequences were downloaded from the database UniProt (http://www.uniprot.org; 18.5.17, UniProt ID human Q6UXG2-1; UniProt ID mouse A2AFS3-1). "*" means that aa residues are identical. ":" or "." refer to a “strong” aa group (>0.5) or “weaker” aa group (<0.5), which are conserved and defined by a PAM250 MATRIX score of ClustalX. Aa are labelled in colour according to their physicochemical properties: A, I, L, M, F, W, V in blue (hydrophobic), N, Q, S, T in green (polar), R, K in red (basic), C in magenta or blue, E, D in magenta (acid), H, Y in cyan, P in yellow.

The 5330417C22RIK protein has a molecular weight of 110.682 kDa with a basal isoelectric point of pH 5.98. Four topologically distinct domains are predicted for this protein (Figure 4.19). Its N-terminus starts with a 35 aa long signal peptide followed by a 871 aa long extracellular region, a 21 aa long helical transmembrane domain and a short 82 aa long cytoplasmic tail. The signal peptide found at the N-terminus is present in newly synthesized type 1 proteins, which are

targeted to the secretory pathway by its transmembrane domain (Agarraberes & Dice, 2001; Kunze & Berger, 2015). Thus, the protein is predicted to reside inside membranous organelles such as the endoplasmic reticulum (ER), the Golgi apparatus, the endosome and the plasma membrane. Furthermore, Tang et al., 2010 claimed that the protein is secreted from the cell to the extracellular space (Tang et al., 2010).

Moreover, the 5330417C22RIK protein is a substrate of potential post-translational amino acid modifications in its intracellular and extracellular regions (iPTM and UniProt databases). There are predicted N-linked glycosylation sites at asparagine residues 153, 387 and 400 (Figure 4.19, red dots). Bioinformatical analysis predicts a cysteine-rich domain including three possible disulfide bonds at cysteine residues 274-291 aa, 304-326 aa and 307-338 aa (black brackets) in the extracellular region. Further, the iPTM database predicts a phosphorylation site at Y935 and a ubiquitination site at K936 in the intracellular tail of the protein (yellow and brown square).

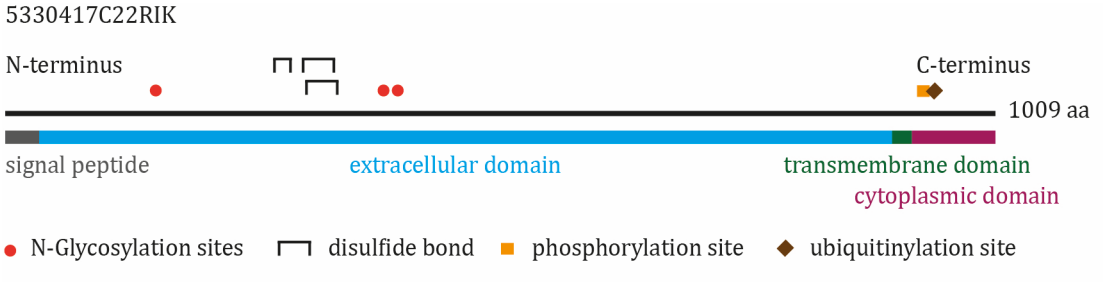

Figure 4.19: Predicted topology and post-translational aa modifications of the 5330417C22RIK protein.

The aa sequence was downloaded from the database UniProt (http://www.uniprot.org/uniprot/A2AFS3; 18.5.17; UniProt ID A2AFS3). N-glycosylation site (red dots) and disulfide bond (black brackets) predictions are derived from UniProt. The iPTM database (http://research.bioinformatics.udel.edu/iptmnet/entry/A2AFS3; 18.5.17; UniProt ID mouse A2AFS3) provides predicted phosphorylation sites (orange square) and ubiquitinylations sites (brown square).

The protein domain structure was analysed using Ensemble (www.ensembl.org) and Hhpred (www.toolkit.tuebingen.mpg.de) databases (Figure 4.20). The latter is an online tool for protein homology detection and structure predictions of highly conserved and distantly related proteins comparing aa sequences from different species. In the extracellular domain of 5330417C22RIK two potential, functional distinct regions were identified by Ensemble, namely a mannose-6-phosphate receptor binding domain and a growth factor receptor cysteine-rich domain (Figure 4.20A). The mannose-6-phosphate receptor binding domain is found in the cation-independent mannose-6-phosphate receptor (CI-M6PR, Igf2r) and the cation-dependent mannose-6-phosphate receptor (CD-M6PR) (El-Shewy & Luttrell, 2009). M6PRs specifically bind phosphomannosyl residues of lysosomal enzymes in the Golgi apparatus and at the cell surface and transport them to the acidic pre-lysosomal compartments where the low pH mediates dissociation of the complex (El-Shewy & Luttrell, 2009). The structure of the growth factor

receptor cysteine-rich domain includes a β-hairpin with adjacent disulphide bonds (McInnes & Sykes, 1997). This domain exists in proteins involved in signal transduction pathways mediated by receptor tyrosine kinases such as insulin-like growth factor-binding proteins (Igfbp), the type-1 insulin-like growth -factor receptor (Igf1r) and members of the epidermal growth factor (Egf) receptor family in which this domain contributes to ligand binding and receptor dimerization (Garrett et al., 1998; C W Ward, Hoyne, & Flegg, 1995; Zeslawski et al., 2001).

Similarly, Hhpred assigns regions with sequence similarities to domains of the CI-M6PR and CD-M6PR and to cysteine-rich domains of proteins such as tumor necrosis factor receptor superfamily (Tnfr), β-nerve growth factor (Ngf), glutamate metabotropic receptor 3 (Grm3), Ephrin Type-A Receptor 1(Epha4), B and T lymphocyte attenuator (Btla), extracellular calcium-sensing receptor 1 (Pcar1) and epidermal growth factor receptor (Egfr) (Figure 4.20B). A sequence alignment of regions of the M6P receptors and the mannose-6-phosphate receptor binding domain of 5330417C22RIK reveals a calculated probability of 95.16 for the CI-M6PR and 94.41 for the CI-M6PR with protein sequence identities of 0.334 and 0.371 (Figure 4.20C). In line, a probability of 98.62 and a sequence similarity of 0.485 is computed for the cysteine-rich domain in the Tnfr. Hhpred includes secondary structure predictions in its calculations for probability values. Thus, high structural similarities are predicted despite low protein sequence similarities.

A thorough analysis of the 5330417C22RIK protein sequence revealed potential binding motifs for proteins involved in the intracellular transport of cargo proteins (Figure 4.21). We found two KKxx dilysine motifs in the extracellular region of the receptor protein, which was originally identified in endoplasmic reticulum protein retention receptors (KDEL receptor). These receptors are bound by coatomers at their dilysine residues in the carboxyl terminus promoting their Golgi-ER retrograde transport (W. Ma & Goldberg, 2013; Yang et al., 2002). Coatomers are the core components of the coat protein I (COPI) complexes. Directly adjacent to the first dilysine motif, we located a potential KXE/D motif. This motif regulates retrograde transport within the Golgi apparatus in the Arabidopsis endomembrane protein 12 (EMP12), but is also highly conserved in all eukaryotic EMPs (Gao et al., 2014a). Furthermore, we identified a potential binding motif for the μ2 subunit of the adaptor protein 2 (AP2) in the cytoplasmic domain of the 5330417C22RIK protein proximally to the membrane (Figure 4.21). AP2 is a heterotetrameric (α2, β2, μ2, σ2) protein complex that is essential for clathrin-mediated endocytosis (CME) in the cell (Traub, 2009b). The consensus sequence for the binding of the μ2 subunit comprises a YxxØ sequence in which x can be any amino acid and Ø a bulky hydrophobic amino acid (F, Phenylalanine; I, Isoleucine; M, Methionine; L, Leucine or V, Valine).

A

B **Hhpred: Protein homology detection and structure prediction:**

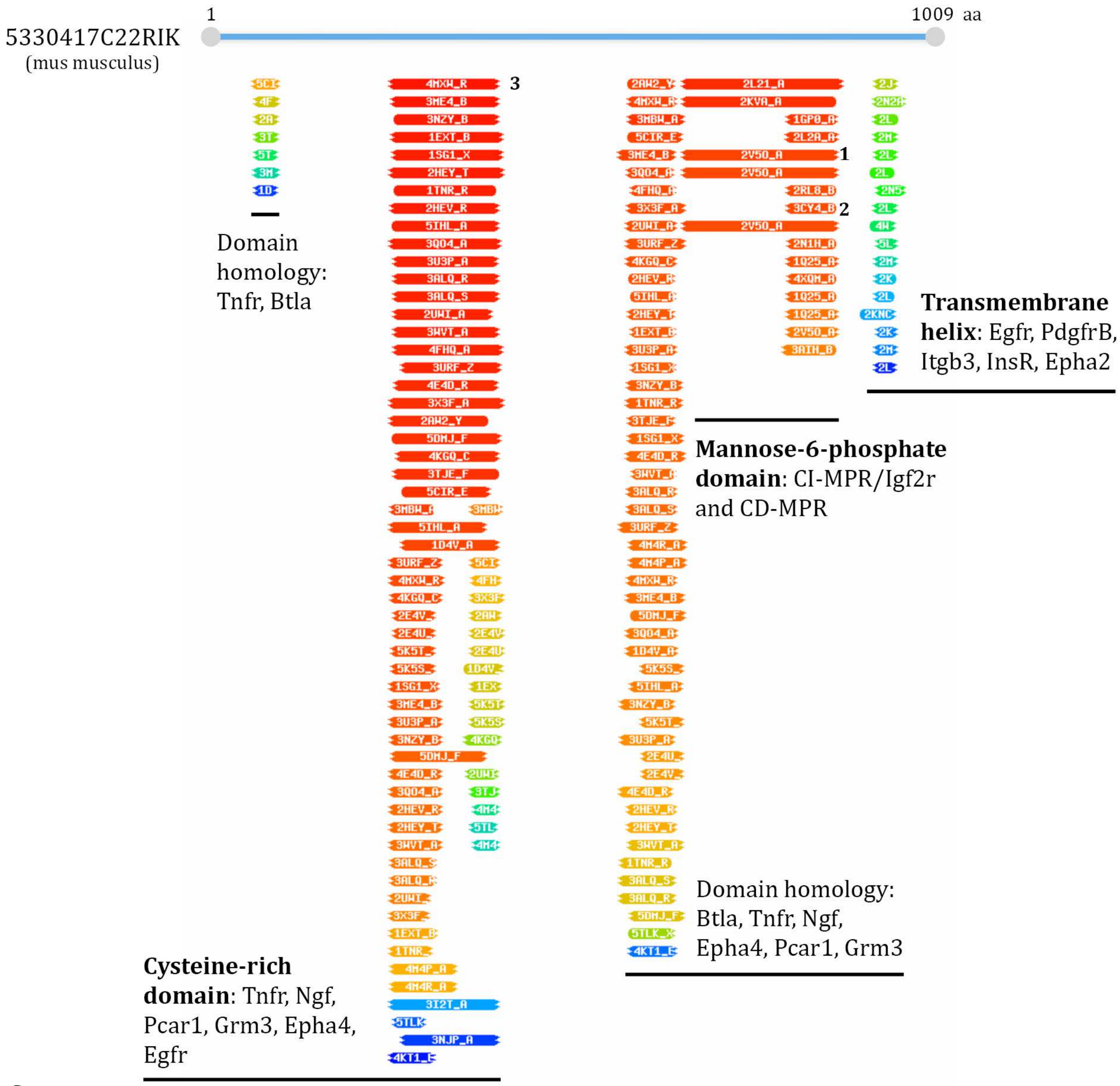

C

1. alignment CI-M6PR (homo sapiens)

probability: 95.16 score: 71.22 sequence similarity: 0.334

```
ss_pred                    CCeeeecCCCceEEEecHHhcccceEecccccc-----ccccceeeEEEEEcCCcCCce-eEEEEcCccceecCCCCCCCcceeeEEEEEEEEeeccccCCcceeeeeceehhheeEEeccCCccCCcc
5330417C22RIK   653        DCTFSRNTPSRIFNYNFSALAGTVSLAGVPSFT-----SKGLKYFHHFTLSLCGNQGKK-MAVCTDNVTDLRIPDGEAGFSKSVTAYVCQVVIIPSEVMGYKAGVSSQPVSLADRLVGVSTDMTLEGIV
consensus       653        dc~~~~~~~~~~~~Ydfs~L~~~~~~~g~~~ft------~~g~~y~h~FniSlcg~~~~~--a~c~dn~t~~~~~~~~~~~~~~v~~~vC~~t~~p~~~~~~~~~~~~q~~~lgd~l~~vt~~~~~~~~~
consensus       144        ~C~~~~-----~~~~yDLs~L~~~~~~~~~~~~~~~~~~~~~~----~~~~~NiC~~l~~~~~~~C~~~~-------------------~~C-------------~~~~~~~~~~lG~~~~~~~~~~~~~--
hCI-M6PR        144        ECSVRN----GSSIVDLSPLIHRTGGYEAYDESEDDASDTN----PDFYINICQPLNPMHAVPCPAGA------------------AVC------------KVPIDGPPIDIGRVAGPPILNPIANE--
ss_dssp                    CCEEEE----TTEEEECGGGCCSSSCEEECCCC------CC----CCEEECSSSCCCCCTTCCCCTTC------------------SEE------------ECCSSSCCEEEEEECSCCEECSSSCC--
ss_pred                    ccEeec----CCeEEeccccceeecCCcEEecCCCCCCCCCC----CcEEEEecCCCCCCCCCCCCCCCC------------------eEE------------EecCCCCceeeeecCCCEEeCCCCe--

ss_pred                    CccccccCCCCCCCCcEEEEeecCCCCccCCCc----eEEEEEEEECCCCCCCCeeecCccCCCCCCCCceEEEEEEeCccCCC
5330417C22RIK              SPVELFHPETSGIPDIVFFFRSNDVTQSCSSG----RSTTIRLRCNPMKAAPGTLRLPSMCSDGTCDGCNFHFLWESVAACPL     854 (1009)
consensus                  ~~~~~~~~~~~~~~d~~f~~~s~~~t~~C~~g----rst~I~lrCdp~~~~~g~~~~p~~Cp~gtcDgC~f~flW~S~~ACPl     854 (1009)
consensus                  ---------------l~l~Y----~~g~~C~~~~~~~~st~I~f~Cd~~~~~~~p~~~~~~---------~~C~y~f~w~T~~ACp~     290 (627)
hCI-M6PR                   ---------------IYLNF---ESSTPCLADKHFNYTSLIAFHCKRGVSMGTPKLLRT-------SECDFVFEWETPVVCPD     290 (627)
ss_dssp                    ---------------EECEE---ECSSCCSCC---CCEEEEEEEECCSSCCCCEEECCC-------TTTEEEEEEEEGGGSCC
ss_pred                    ---------------EEEEe---cCCCCCCCCCCeeEEEEEEEEcCCCCCCCcEEecC-------CCcEEEEEEeccccCCC
```

2. alignment CD-M6PR (bos taurus)

probability: 94.41 score: 56.98 sequence similarity: 0.371

```
ss_pred          cEEEEeecCCCCccCC-----CceEEEEEEECCCCCCC--CeeecC--ccCCCCCCCCceEEEEEeCccCC
5330417C22RIK    790 DIVFFFRSNDVTQSCS-----SGRSTTIRLRCNPMKAAP--GTLRLP--SMCSDGTCDGCNFHFLWESVAACP    853 (1009)
consensus        790 d~~f~~~s~~~t~~C~------~grst~I~lrCdp~~~~~~~g~~~~p-~~~Cp~gtcDgC~f~flW~S~~ACP    853 (1009)
consensus         91 ~~~l~Y---~~g~~c~~~~~~~~r~t~I~~~C~~~~~~~~~~~~~~~~~~~~~~~~~~c~y~f~~~t~~aCp    154 (154)
hCD-M6PR          91 WIMLIY---KGGDEYDNHCGREQRRAVVMISCNRHTLADNFNPVSEERGKV------QDCFYLFEMDSSLACS    154 (154)
ss_dssp          EEEEEE---EECCBCSSSGGGCBCCEEEEEEECTTCSSEEEEEEEECCSS------SCCEEEEEEEGGGCC
ss_pred          eEEEEE---eCCCccccCCCCcccEEEEEEeCCcccCCCcceEEeccccc------cCcEEEEEeccccC
```

3. alignment TNFR superfamily (homo sapiens)

probability: 98.62 score: 115.92 sequence similarity: 0.485

```
ss_pred          ceeeeCCCCccccCCCCCcceeCCCCcccCCC-----CcccceCCCCeeecCC--CcccceecCCCccCccceeeeeccCCCCeeEEEEeecCcccCCCCCCceeCCCCCCccC---CCCCCCceec-----
5330417C22RIK    268 SECFPCKPGTYAAKQGSPFCKLCPANYYSNKG-----ETSCHPCDADKYSEKG--SSTCKVRPACTDKDYFYTHTACDAQGETQLMYKWAIPKICGEDLEGAVKLPASGVKTRC---PPCNPGFFKT-----
consensus        268 s~C~pCp~Gt~s~~~Gss~C~pCP~gtYs~~g-----a~~C~pCp~~tys~~g--s~~C~~rp~Ct~~Dy~~~~tpCd~~g~~~~~ykwiePkiC~~~~~~av~LP~~~~~~~C-----~~~CnpG~~~~~~~-----
consensus         23 ~~C-~C~~g~y~~~~~~~~C~~Cp~G~~~~~~c~~~~~~C~~C~~gty~~~~~~~~~C~~C~~C~~~~~~~~~~ct~t~----------~~~C-~C~~G~~~~~~~~~c~~C~~c~~C~~G~~~~~~~t
hTNFR             23 QTC-RDQEKEYYEPQHRICCSRCPPGTVVSAKCSRIRDTVCATCAENSYNEHWNYLTICQLCRPCDPVMGLEEIAPCTSKR----------KTQC-RCQPGMFCAAWALECTHCELLSDCPPGTEAELKDEV
ss_dssp          C-C-CSSSSBCCBTTTTBCCBCBCTTEEESSCCCSSCCCCCEEECCTTEECCSSBCCSSCEECCCCCCC----CCCCCBTTB----------CCCC-CC-----C------CCSSSSCCCCCTTEEC-----C
ss_pred          ccc-CCCCCeEEcCCCCeeCCCCCCCEEEeeCCCCCCCCeeeeCCCCeeecCCCCCCCCCCCCCCcEEEECCCCCC----------Cccc-ccCCCceecCCCCccccchhhccCCCCceeeecCCC

ss_pred          --CCCceeeCCCCceeCCC----cceeCCC
5330417C22RIK    --DNSTCEPCPYGSYSNGS----DCTHCPA    408 (1008)
consensus        --~~~~C~~CP~GtYS~G~-----~C~~CP~    408 (1008)
consensus        ~~~~~C~~C~~Gtys~~~~~~~~C~~ct~    172 (193)
hTNFR            GKGNNHCVPCKAGHFQNTSSPSARCQPHTR    172 (193)
ss_dssp          CSSCCCCEECCTTEECCSCCTTCCCEECCC
ss_pred          CCCCceeeeCCCCccccCCCCCCCceeCcc
```

Figure 4.20: Predicted domain structure of the 5330417C22RIK protein.

(A) Beside a transmembrane domain, the Ensemble database predicts two functional protein regions for the 5330417C22RIK receptor, a growth factor receptor cysteine-rich domain and a mannose-6-phosphate receptor binding domain. Modified from the Ensemble database (http://www.ensembl.org; 17.5.17; 5330417C22RIK-201)

(B) The Hhpred online tool predicts sequence and structural similarities with transmembrane domains, mannose-6-phosphate domains and cysteine-rich domains for different proteins of related species. Colour coding indicates the power of sequence probability (red high and blue moderate probability). Modified from the MPI Bioinformatics Toolkit prediction tool "Hhpred"; (http://toolkit.tuebingen.mpg.de/hhpred; 06.06.17; aa sequence used from UniProt mouse ID A2AFS3) Abbreviations: erb-B2 receptor tyrosine kinase 2 (ErbB2, EgfrB2), B-type platelet-derived growth factor receptor (PdgfrB), integrin subunit B3 (Itgb3)

(C) Sequence alignments were derived from Hhpred homology predictions displayed in (B). The "probability" (in percent) calculates if the database match is a true positive and that the sequence is homologous to the query sequence at least in some core part. It includes the "score" value, which is computed by a primary sequence and secondary structure comparison. The "sequence similarity" is the degree of resemblance between two sequences including direct aa matches and aa with preserved physiochemical properties. 'ss_pred' sequence denotes the PSI-PRED (PSI-blast based secondary structure PREDiction) secondary structure predictions and confidence values whereas 'ss_dssp' is the secondary structure assigned by DSSP (hydrogen bond estimation algorithm). The "consensus" sequence uses capital letters for well conserved aa and lower case for partially conserved aa.

Moreover, we also found a potential receptor dimerization motif in the transmembrane helix of the Igfr-L protein sequence (Figure 4.21). Human EGFR isoforms exhibit one or two GxxxG motifs within their transmembrane domain, which significantly contribute to receptor homo- and heterodimerization (Escher, Cymer, & Schneider, 2009; Sharpe, Barber, & Grant, 2002).

All five identified motifs are also conserved in the human IGFR-L protein sequence affirming their importance for the protein function (Figure 4.18).

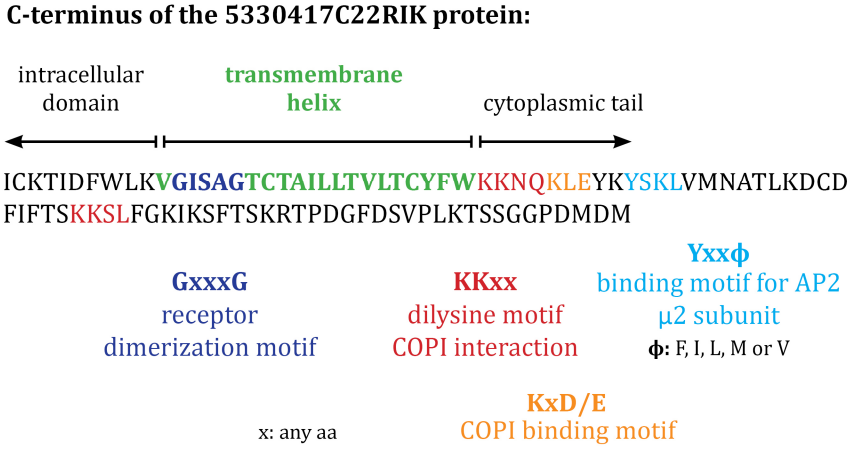

Figure 4.21: The extracellular domain of the 5330417C22RIK protein contains potential binding motifs for the AP2 protein complex and for COPI vesicles near the membrane, whereas the transmembrane helix exhibits a potential receptor dimerization motif.

Schematic picture of the C-terminal amino acid sequence of the 5330417C22RIK protein with potential binding sites for the endocytosis adaptor protein AP2 and ER-Golgi trafficking protein complex COPI as well as a receptor dimerization motif. The aa sequence was downloaded from the database UniProt (http://www.uniprot.org/uniprot/A2AFS3; 18.5.17; UniProt ID A2AFS3)

Taken together, the 5330417C22RIK protein is a highly conserved receptor with a large extracellular region, a short transmembrane domain and a short cytoplasmic tail. The signal peptide at the N-terminus and the transmembrane domain of the protein suggests the receptor trafficking in the secretory pathway. Coatomer binding motifs and the sorting signals for AP2 binding found in the extracellular region of 5330417C22RIK strengthen the hypothesis that the receptor is transported through the Golgi-ER area and is endocytosed by CME. The GxxxG motif found in the transmembrane helix of the Igfr-L implicates that the receptor might not only exist as monomers but also forms homo- or heterodimers in the membrane. Additionally, the receptor has predicted post-translational aa modifications including N-linked glycosylation sites, a phosphorylation site and an ubiquitylation site, which might be relevant for the proper function of the protein. Bioinformatical analysis revealed high similarity to a growth factor receptor cysteine-rich domain and a mannose-6-phosphate receptor binding domain in the extracellular region of the protein. Due to its high similarity of these regions to receptor domains of Igf1r, the Egfr and M6PRs (Igf2r), we speculate that the 5330417C22RIK receptor might have similar molecular and physiological function. Hence, we named the product of the *5330417C22Rik* gene **Insulin-like growth factor receptor-Like** (**Igfr-L**) protein.

4.3.1.3 mRNA and protein expression of Igfr-L in Homo sapiens and Mus musculus

Next, we searched databases for Igfr-L mRNA and protein expression in mouse and human tissues to possibly draw first conclusions on the biological function of the receptor protein (Figure 4.22). Interestingly, mRNA and protein expression of Igfr-L (mouse and human) is mainly detected in different parts of the brain, the gastrointestinal tract including stomach, intestine, duodenum and colon, as well as in sex specific organs, such as the prostate, the uterus, the ovary, the testis (Figure 4.22A and B). Further, it is also found in organs like the lung, the olfactory apparatus, the spinal cord and the skin. Remarkably, this expression profile shows receptor expression in endocrine and exocrine glands like the pituitary gland (hypophysis), salivary gland (parotid and submandibular glands), the pineal gland, the pancreas, the stomach, the intestine, the adrenal gland and gonads. Additionally, collaboration partners found high Igfr-L expression in the arcuate nucleus of the hypothalamus that regulates food intake and satiety (Dr. Gustav Collden, Institute for diabetes and obesity, Helmholtz Zentrum, Munich).

In summary, the expression pattern of Igfr-L indicates a potential involvement of the receptor in the function of endo- and exocrine cells.

4.3.2 Generation of mono- and polyclonal Igfr-L antibodies

Since the commercialization of the first therapeutic monoclonal antibody in 1986, the production and clinical administration of therapeutic antibodies treating a wide range of diseases has increased significantly. In this context, Igfr-L might be a new target. Moreover, the biochemical and cell biological analysis of proteins requires the use of antibodies. Thus, we generated and tested antibodies for their specificity to the Igfr-L in Western blot and immunofluorescence analysis. Several polyclonal anti-rabbit antibodies were produced by Pineda (Antikörper Service Pineda, Berlin, Germany) (Table 4.2, Pineda animal 1). We chose the epitope from the intracellular region of the human receptor sequence due to its high sequence identity to the mouse amino acid sequence (Figure 4.18). Moreover, we generated four unpurified monoclonal antibodies (Table 4.2) in our in-house antibody facility (Helmholtz Zentrum Munich, Institute for Molecular Immunology, antibody core facility), which were produced by immunizing mice (31A11-61111 and 36D7-11) or rat (16F6-311 and 14F1-1141) with an Igfr-L peptide sequence derived from the cytoplasmic tail of the Igfr-L protein. Antibodies raised against the extracellular domain of Igfr-L receptor were generated in rabbits in collaboration with Dr. Coskun (Paul Langerhans Institut Dresden) and the Max-Planck Institute Antibody Facility in Dresden. They obtained serum for two polyclonal anti-rabbit antibodies (Table 4.2, 1374 and 1692).

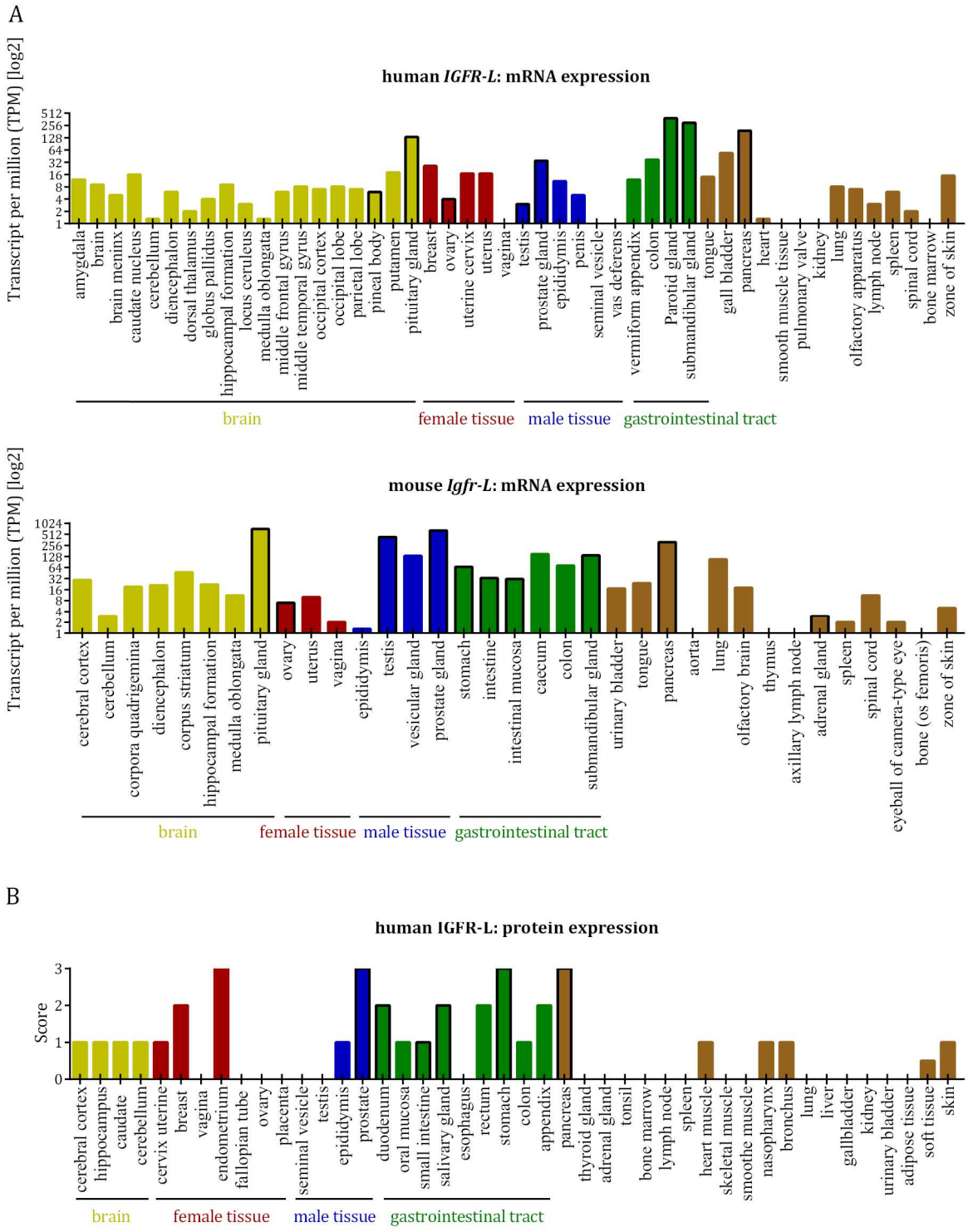

Figure 4.22: Igfr-L is mainly expressed in the brain, in gender specific organs, in the gastrointestinal tract as well as in endo-and exocrine glands.

(A) mRNA expression profile of human and mouse Igfr-L. Modified from EMBL-EBI Expression Atlas (http://www.ebi.ac.uk/gxa/home; 30.5.17; Data: FANTOM5 project)

(B) Protein expression profile of the IGFR-L based on immunofluorescence stainings. Score 0-3 indicates the strength of immunofluorescence signal. Modified from the Human Protein Atlas (http://www.proteinatlas.org/; 30.5.17)

(A, B) Analysed tissues are divided into color-coded groups according to which functional features they have in common. Brown bars represent remaining organs. Framed bars mark endocrine and exocrine glands.

Table 4.2: List of antibodies tested in immunofluorescence and Western blot.

Name	Species	Clonality	Subclass	IGFR-L antigen (human)	Purification status	Collaboration partner/producer
14F1-1141	rat	monoclonal	IgG 2a	peptide of cytoplasmic domain	supernatant	HMGU antibody core facility
16F6-311	rat	monoclonal	IgG 2a	peptide of cytoplasmic domain	supernatant	HMGU antibody core facility
31A11-61111	mouse	monoclonal	IgG 2b	peptide of cytoplasmic domain	supernatant	HMGU antibody core facility
36D7-11	mouse	monoclonal	IgG 2b	peptide of cytoplasmic domain	supernatant	HMGU antibody core facility
animal 1	rabbit	polyclonal		peptide of cytoplasmic domain	affinity purified	Antikörper Service Pineda
1374	rabbit	polyclonal		recombinant protein of extracellular domain	serum	Dr. Coskun/ Max-Planck Institute Antibody Facility
1692	rabbit	polyclonal		recombinant protein of extracellular domain	serum	Dr. Coskun/ Max-Planck Institute Antibody Facility

We tested these antibodies for their specificity by Western blot (Figure 4.23A) and immunofluorescence (IF) stainings (Figure 4.23B) using WT and Igfr-L KO Min6. Min6 Igfr-L KO cells were generated in our laboratory by Dr. Amir Morshedi employing the Crisp-Cas9 technology. The WT Cas9 enzyme, which cut about 40-50 bp up- and downstream of the start codon directed by two guiding RNAs, was deployed. After construct transfection Min6 cells were sorted by fluorescence activated cell sorting (FACS) and subsequently cultured. Several WT and KO clones were picked (KO: D5, E10, F9, G9, G11 and WT: B7, B8, B9, B10) to exclude clonal variation in later experiments.

Indeed, all antibodies tested displayed specificity in Western blot and on a subcellular level (IF) simultaneously demonstrating their binding affinity to the mouse protein (Figure 4.23A and B). Only antibody 1374 and 1692 show faint bands of similar migration height as the Igfr-L KO Min6 cell lysates. In SDS-PAGE (sodium dodecyl sulphate-polyacrylamide gel electrophoresis) the receptor migrates at a size of 130 kDa despite its calculated molecular mass of 110.682 kDa indicating post-translational modifications as predicted by bioinformatical analysis (Figure 4.19). At subcellular level, immunostaining experiments revealed that the receptor is localized in the proximity of the nucleus.

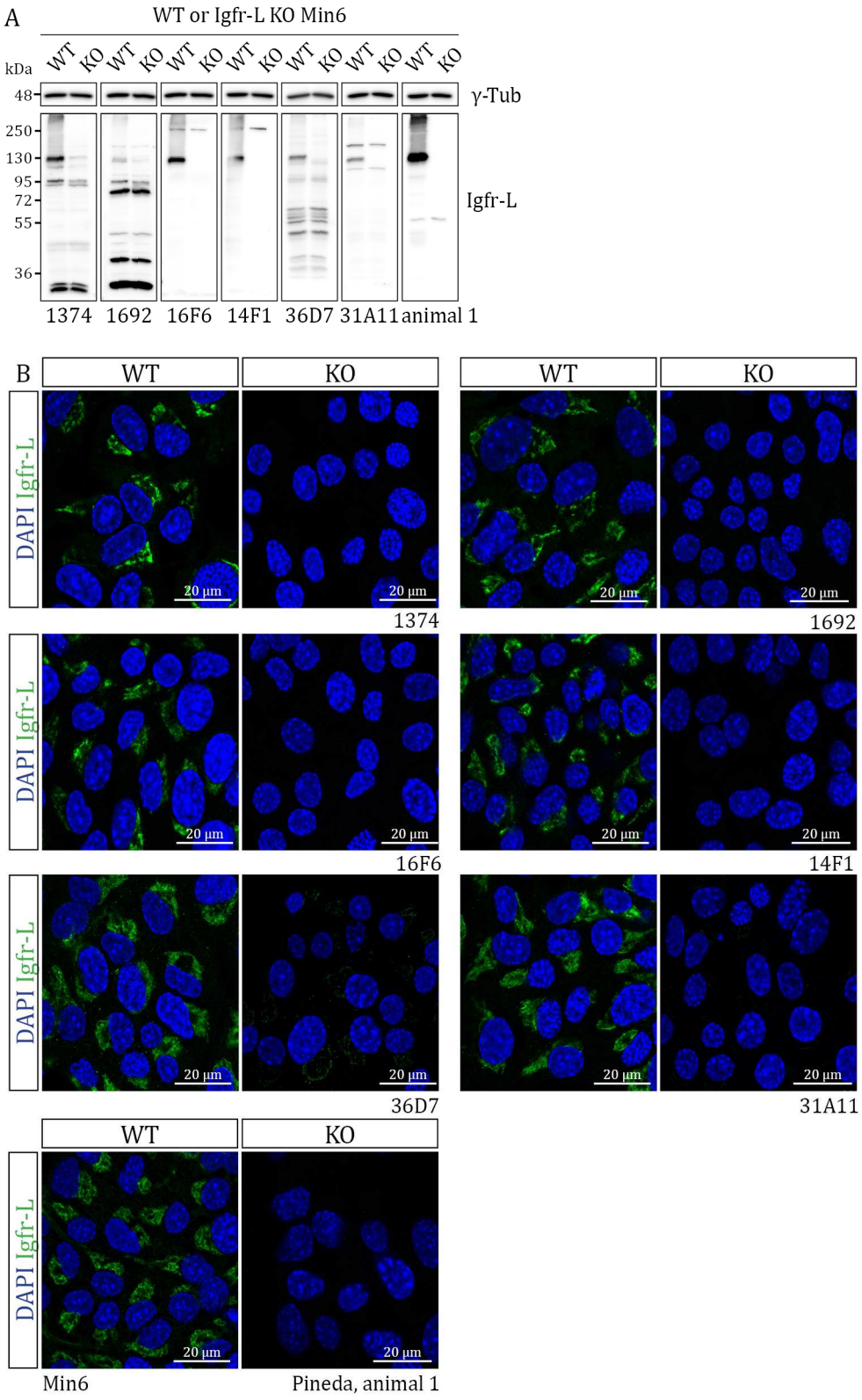

Figure 4.23: Igfr-L antibody specificity in Western blot and in immunocytochemistry in WT and Igfr-L KO Min6 cells.

(A, B) Representative Western blots (A) and immunofluorescence analysis (B) for the specificity assessment of Igfr-L antibodies in WT (B8) and Igfr-L KO (E10) Min6 cells.

4.3.3 Analysis of postnatal death of Igfr-L$^{-/-}$ mice

To investigate the biological function of the *Igfr-L* gene *in vivo*, Igfr-L$^{-/-}$ mice were generated from ESC clones derived from the European Conditional Mouse Mutagenesis Program (EUCOMM, http://www.mousephenotype.org/). The EUCOMM clone 5330417C22RIK$^{tm1a(EUCOMM)Hmgu}$ (clone number H03) was chosen for ESC aggregation.

Strikingly, Igfr-L$^{-/-}$ mice die postnatally within the first hours after birth with signs of lethargy, hypoglycaemia, hyperinsulinemia, respiratory distress and cyanotic episodes with bluish discoloration of the skin, which is likely due to the respiratory or metabolic distress (PhD project Fataneh Fathi Far). Additionally, most of the mutant pups do not display milk in their stomach. The analysis of tissue morphology by Haematoxylin and Eosin histological stainings of Igfr-L mutant mice at embryonic day 18.5 (E18.5) showed no obvious abnormalities (Dr. Aurelia Raducanu IDR, Helmholtz Zentrum, Munich).

4.3.3.1 Pancreata of Igfr-L$^{-/-}$ mice exhibit elevated mRNA expression of glucose metabolism associated genes and cell cycle inhibitors postnatally

To examine the consequences of Igfr-L deletion *in vivo*, we performed a real-time quantitative polymerase chain reaction (qPCR) study using RNA isolated from pancreata at E18.5 and postnatal day zero (P0) (Figure 4.24). We analysed 33 genes involved in pancreas development, pancreatic endocrine cell maturation and differentiation, glucose and insulin metabolism, as well as cell polarity and cell proliferation. At E18.5, all genes except *Pcsk2* (prohormone convertase 2) were not or were only slightly deregulated in Igfr-L$^{-/-}$ pancreata.

Strikingly, after birth many of these genes were either slightly or significantly differentially expressed. Except glucagon-like peptide 1 receptor (*Glp1r*), which is activated by the Glp1 (glucagon-like peptide 1) ligand and which stimulates signalling cascades leading to glucose induced insulin secretion (GSIS), mRNA expression of all deregulated genes was enhanced (X. Ma, Guan, & Hua, 2014). Solute carrier family 30 member 8 (*Slc30a8*) is a major component of insulin maturation and storage processes (Chimienti, Favier, & Seve, 2005). The ATPase chromatin subfamily A member 1 (*Smarca1*) is involved in the chromatin remodelling complex of different tissues including endocrine pancreas during development and at adult stage (Haumaitre, Lenoir, & Scharfmann, 2009). Gastric inhibitory polypeptide receptor (*Gipr*) plays a role in stimulating insulin release in the presence of elevated glucose (S.-J. Kim et al., 2005). *InsR* activates insulin signalling pathway upon insulin binding and thus controls glucose uptake and release (Khan & Pessin, 2002; Siddle, 2011). Receptor for somatostatin-14 and -28 (*Sstr3*) binds the peptide hormone somatostatin thereby inhibiting insulin and glucagon secretion (Braun, 2014). Interleukin-6 receptor subunit α (*Il6ra*) was demonstrated to play a role in the immune response and was shown to directly affect β-cells by enhancing GSIS via the PLC-IP(3)-dependent pathway (Suzuki et al., 2011). *Pcsk2* contributes to the processing of hormone precursors including proglucagon in pancreatic α-cells (Rouillé, Martin, and Steiner 1995). Cyclin dependent kinase inhibitor 1A (*Cdkn1a*) and cyclin dependent kinase inhibitor 1b (*Cdkn1b*) inhibit cyclin-

cyclin-dependent kinase 2 (*Cdk2*) or cyclin-dependent kinase 4 (*Cdk4*) complexes regulating cell cycle progression at G1 (Ekholm & Reed, 2000).

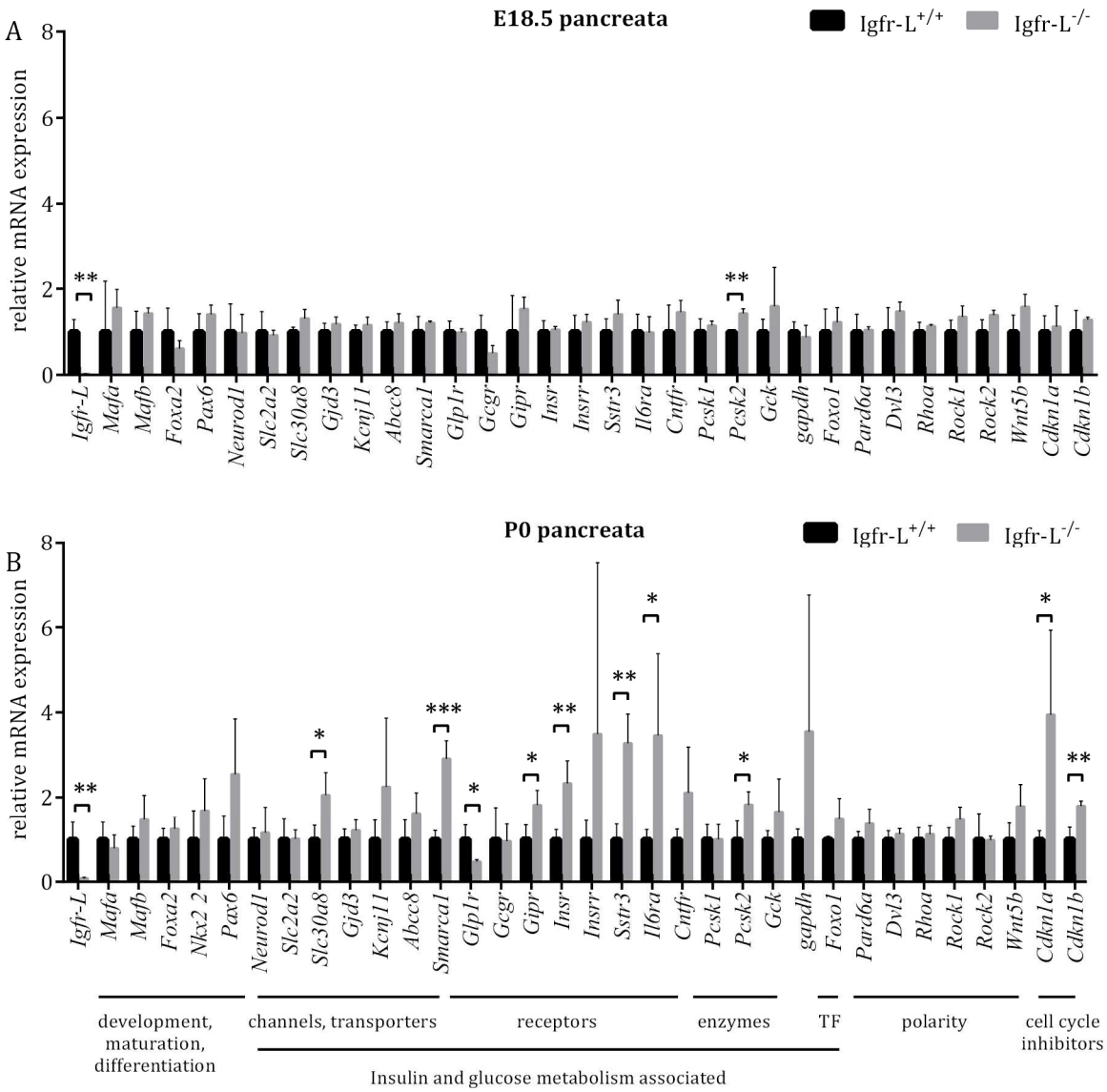

Figure 4.24: Igfr-L$^{-/-}$ mice exhibit elevated mRNA expression of glucose metabolism associated genes at stage P0 in the pancreas

(A, B) Real-time qPCR analysis of wildtype (Igfr-L$^{+/+}$) and Igfr-L$^{-/-}$ E18.5 pancreata (A) and P0 pancreata (B). *18S, Hprt* and actin β *(Actb)* genes were used as reference in the calculation of relative mRNA expression. (n (mice) = 3, mean + SD, unpaired *t*-test)

Taken together, differentially expressed genes in postnatal pancreata indicate a potential involvement of Igfr-L in pancreatic cell cycle progression and in insulin and glucose metabolism.

4.3.3.2 Partial Igfr-L depletion does not influence autophagy related processes in Min6 cells

Deng et al., 2010 claimed that the human homolog of the Igfr-L receptor, EIG121, protects cells from starvation by enhancing autophagy processes. They revealed that knock-down of EIG121 blocked the degradation of autophagy-related protein LC3A/B (LC3A/B) upon nutrition depletion (L Deng et al., 2010). Prolonged hypoglycaemia is a cause of premature death induced by the sudden interruption of trans-placental nutrient supply at birth (Kuma et al., 2004). Postnatally, new-borns transiently go through a starvation period until gluconeogenesis and glycogenolysis are activated in the liver (Darlington, 1999; Kotoulas, Kalamidas, & Kondomerkos, 2006). Autophagy is induced in response to starvation and is highly active 3-6 hours postpartum, thus generating the energy necessary for survival. Autophagy-related 5 (Atg5) homozygous mutants die within the first 12 hrs after birth due to a blockage of autophagosome fusion, which results in low energy levels (Kuma et al., 2004). To investigate if the Igfr-L deletion leads to autophagy defects *in vitro*, we analysed protein expression of autophagy-related proteins in WT and Igfr-L depleted Min6 cells by siRNA mediated knock-down (Figure 4.25). Autophagy related 16 like 1 (Atg16l1), autophagy-related 7 (Atg7), autophagy-related 3 (Atg3), Lc3A/B and Atg5 did not show altered protein expression levels when compared to the control samples. Only beclin 1 (autophagy-related 6, Atg6) protein expression is slightly reduced upon Igfr-L depletion. A main inducer for autophagy is nutritional deprivation in most of the eukaryotic cells. Consequently, we starved Min6 cells in Hank's balanced salt solution (HBSS) buffer for 15, 30, 60 and 120 min excluding glucose and growth factors. Also, starvation conditions did not cause deregulated protein expression of Atg3 and Lc3A/B in Igfr-L depleted cells. Long-term starvation however, decreased expression levels of autophagy regulated proteins in all samples. This confirms latest, controversially discussed, data from Goginashvili et al., 2015 in which they report that Min6 cells feature an atypical autophagy control (Goginashvili et al., 2015). Contrary to most of mammalian cell types, pancreatic β-cells might not activate but suppress macroautophagy upon starvation and instead gain their energy supply by lysosomal degradation of nascent secretory insulin granules.

In summary, partial depletion of Igfr-L does not influence the regulation of autophagy in Min6 cells. A study of autophagy processes in other cell types might shed light on the question whether autophagy is the cause of death in Igfr-L$^{-/-}$ neonates.

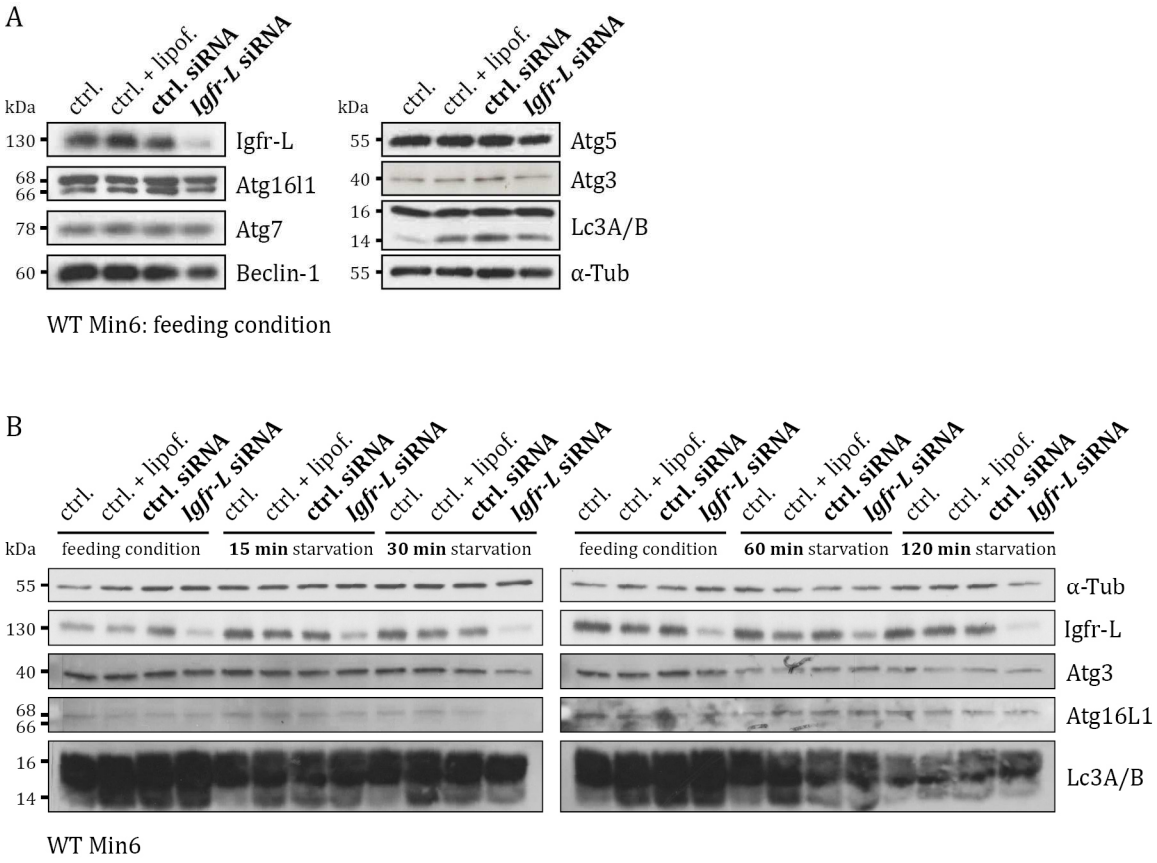

Figure 4.25: siRNA mediated depletion of Igfr-L does not influence autophagy in Min6 cells in feeding condition and upon nutrient deprivation.

(A) Representative Western blot images of WT Min6 cells cultured in feeding conditions. "ctrl": control, "ctrl. + lipof.": control sample with lipofectamin in transfection medium, "ctrl. siRNA": control siRNA, "*Igfr-L* siRNA": siRNA for *Igfr-L*. Autophagy associated proteins were detected.
(B) Protein expression study using Western blot of WT Min6 cells in feeding conditions and upon starvation (15, 30, 60 and 120 min).

4.3.4 Metabolic study of adult Igfr-L$^{+/-}$ male and female mice

After birth neonates undergo a starvation period due to the cut off from the placental nutrient supply and maternal metabolic exchange resulting in hypoglycaemia. Mutations interfering with the energy equilibrium of an organism can seriously challenge the survival of new-borns (Turgeon & Meloche, 2009). Several findings indicated that a dysbalanced glucose homeostasis might be the cause of postnatal death of Igfr-L$^{-/-}$ pups. Elevated mRNA expression of genes like the *InsR*, *Slc30a8* or *Glp1r* in Igfr-L$^{-/-}$ P0 pancreata suggests a potential involvement of Igfr-L in glucose metabolism (Figure 4.24). Further, bioinformatic analysis of the Igfr-L domain structure predicted a potential growth factor cysteine-rich domain as it is found in receptor tyrosine kinases of the insulin signalling pathway (Figure 4.20). Insulin signalling plays a major role in triggering glucose uptake into peripheral tissues and in controlling lipid metabolism. Additionally, the International Mouse Phenotyping Consortium (IMPC) reported elevated circulating glucose levels in adult Igfr-L heterozygous male and female mice

(http://www.mousephenotype.org/data/ genes/ MGI:1923930). Considering these hints, we decided to metabolically phenotype Igfr-L mutant animals to further explore the potential role of Igfr-L in energy homeostasis. Since many metabolic investigations are only feasible in adult animals and because of KO mice are dying perinatally, we used adult Igfr-L heterozygous mice for metabolic analysis. Igfr-L$^{-/-}$ mice studied in previous experiments (Figure 4.24) showed small amounts of residual Igfr-L protein in tissue samples (data not shown) most likely due to splicing mechanisms, which bypass the stop codon 5' upstream of the *Igfr-L* gene within the integrated EUCOMM construct enabling receptor gene transcription. To ensure complete absence of protein expression the critical exon (exon 3), which is flanked by *loxP* sites was removed from the *Igfr-L* gene by crossing the 5330417C22RIK$^{tm1a(EUCOMM)Hmgu}$ mouse line with the RosaCre mice (5330417C22RIK$^{\Delta Ex3}$). Therefore, we analysed 5330417C22RIK$^{\Delta Ex3}$ mice in all following *in vivo* studies.

4.3.4.1 Glucagon and ketone bodies levels are normal in adult Igfr-L$^{+/-}$ mice

InsR KO mice exhibit normal metabolic features after birth but develop early postnatal diabetes and die of ketoacidosis (Kitamura et al., 2003). Assuming the possibility that Igfr-L pups might display similar physiological and metabolic phenotype like the InsR mutants, we thus examined β-ketones (β-hydroxybutyrate) concentrations in blood plasma samples collected from 3 month old Igfr-L$^{+/-}$ male and female mice (Figure 4.26A). However, we did not observe abnormal β-ketone levels in Igfr-L$^{+/-}$ animals when compared to the controls. Further, we found glucagon mRNA expression deregulated in P0 pancreata of Igfr-L$^{-/-}$ mice (data not shown). The pancreas releases glucagon into the blood circulation upon low glucose levels causing the conversion of glycogen into glucose in the liver (Heppner et al., 2010). Hence, we measured glucagon levels in blood plasma of WT and Igfr-L heterozygous animals but could not detect significant differences (Figure 4.26B).

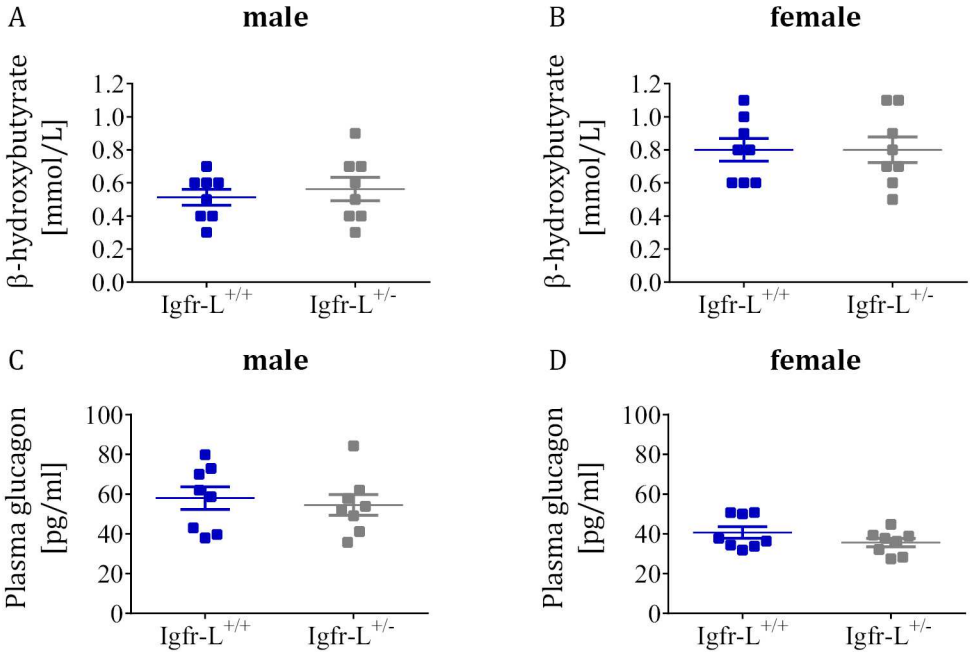

Figure 4.26: Plasma ketone bodies and glucagon levels are not changed in 3 months old Igfr-L$^{+/-}$ mice.

(A, B) Measurement of plasma ketone bodies (β-hydroxybutyrate) in 3 months old male (A) and female (B) Igfr-L$^{+/-}$ mutant mice.
(C, D) Analysis of plasma glucagon levels in 3 months old male (C) and female (D) Igfr-L$^{+/-}$ mutant mice.
(A-D) n (mice) = 8, mean ± SEM

4.3.4.2 Igfr-L$^{+/-}$ mice show impaired insulin sensitivity upon 28 weeks of HFD

To further characterize a potential involvement of the Igfr-L in glucose homeostasis, we examined metabolic parameters by performing glucose tolerance tests (GTT), insulin secretion tests (IST), insulin tolerance tests (ITT) and Nuclear magnetic resonance (NMR) spectroscopy in adult Igfr-L heterozygous mice (Figure 4.27). From the age of 3 months on, mice were fed a 58% kcal high-fat diet (HFD) to metabolically challenge mutant animals. We monitored metabolic parameters before starting the HFD feeding ("0 weeks of HFD"; 12 weeks of age), after 12 weeks of HFD (6 months old mice) and after 28 weeks of HFD (9 months of age). Standard procedures for HFD mouse models recommend the analysis of male cohorts because oestrogen, the major female gender determining hormone, is suggested to protect against the manifestation of insulin resistance (Pettersson, Walden, Carlsson, Jansson, & Phillipson, 2012; H. Shi & Clegg, 2009). However, previous literature reported that the expression of EIG121, the human ortholog of the Igfr-L, is regulated by oestrogen. Enhanced EIG121 expression in endometrial cancer tissue was caused by an oestrogen replacement therapy prescribed to postmenopausal women (Lei Deng et al., 2005). This discovery might imply gender-specific metabolic control mechanisms in Igfr-L mutant mice. Hence, we decided to assemble a mouse cohort of age-matched male and female WT and heterozygous Igfr-L (Igfr-L$^{+/-}$) animals.

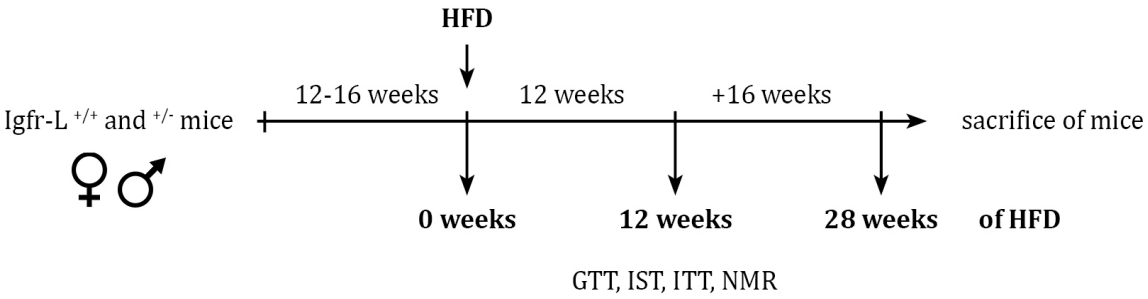

Figure 4.27: Experimental design of metabolic analysis of Igfr-L$^{+/-}$ male and female mice.

During the entire period of HFD feeding, we monitored the body weight and blood glucose levels of non-starved male and female mice. As expected Igfr-L heterozygous males and females gained a weight up to 50-60g but did not show significant differences when compared to WT controls (Figure 4.28A,B). In contrast to female animals, males displayed slightly increased non-starved blood glucose levels during the late phase of HFD (Figure 4.28C,D).

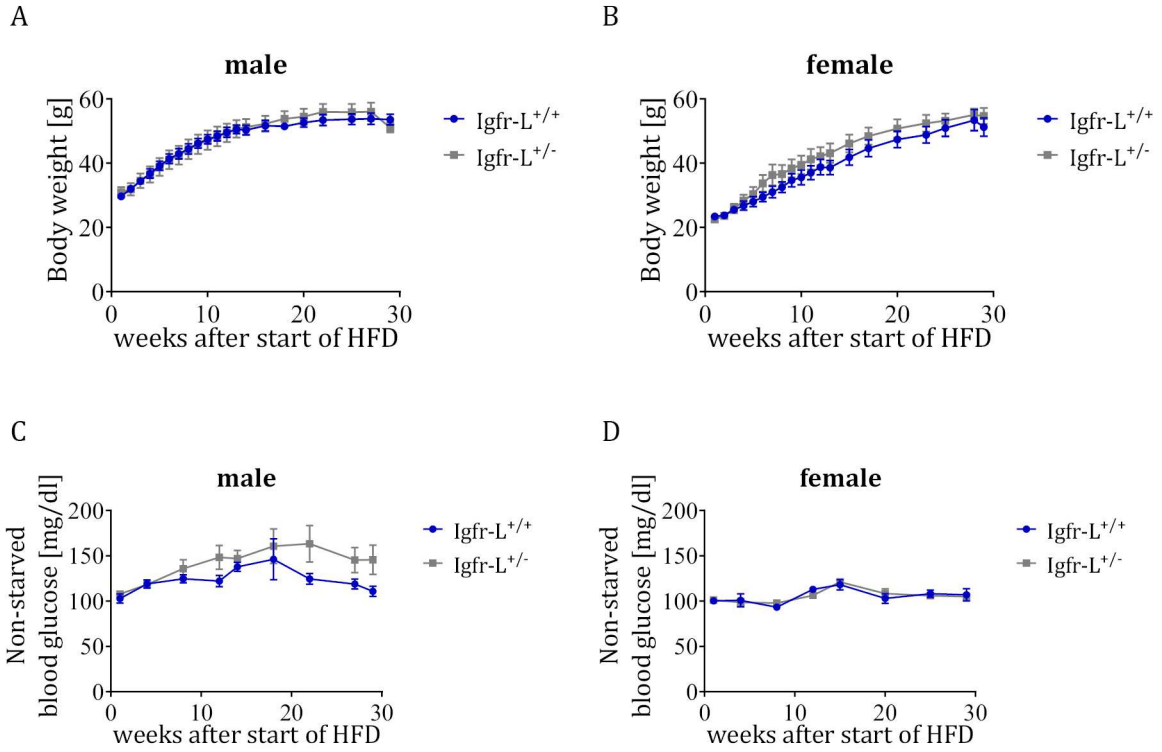

Figure 4.28: Slight elevation in blood glucose levels in non-starved Igfr-L$^{+/-}$ males during 28 weeks of HFD.

(A, B) Monitoring of body weight during 28 weeks of HFD feeding in WT and Igfr-L$^{+/-}$ male and female mice.
(C, D) Blood glucose levels during 28 weeks of HFD in non-starved male and female mice.
(A-D) HFD was introduced at the age of 12 weeks. (n (mice) = 8, mean ± SEM, two-way ANOVA)

To investigate glucose tolerance and insulin sensitivity in Igfr-L$^{+/-}$ mice, we performed intraperitoneal glucose tolerance tests (IP-GTT) and intraperitoneal insulin tolerance tests (IP-ITT) (Figure 4.29A-F). Additionally, blood samples were collected at time point 0, 15 and 30 min of GTTs to measure secreted insulin in the blood plasma (insulin secretion test, IST). We did not detect altered glucose tolerance, insulin secretion or insulin sensitivity in 3 month old male and female Igfr-L$^{+/-}$ mice (Figure 4.29A-F, 0 weeks of HFD). Heterozygosity for Igfr-L in mice might be sufficient for a functional metabolic system. However, high-fat diet feeding induces obesity and metabolic disorders in rodents, which might possibly reveal pathophysiological conditions in heterozygous mice. Thus, we exposed animals of both cohorts to a 58% kcal HFD for 12 weeks (Figure 4.29A-F). HFD challenged male and female animals displayed normal glucose levels upon insulin or glucose injection but minor hyperinsulinemia after 5.5 hours starvation, which persisted within the first 30 min upon glucose injection (Figure 4.29B,E). Furthermore, Igfr-L$^{+/-}$ female mice displayed diminished glucose clearance after insulin administration and showed a small tendency towards a glucose intolerance in the GTT.

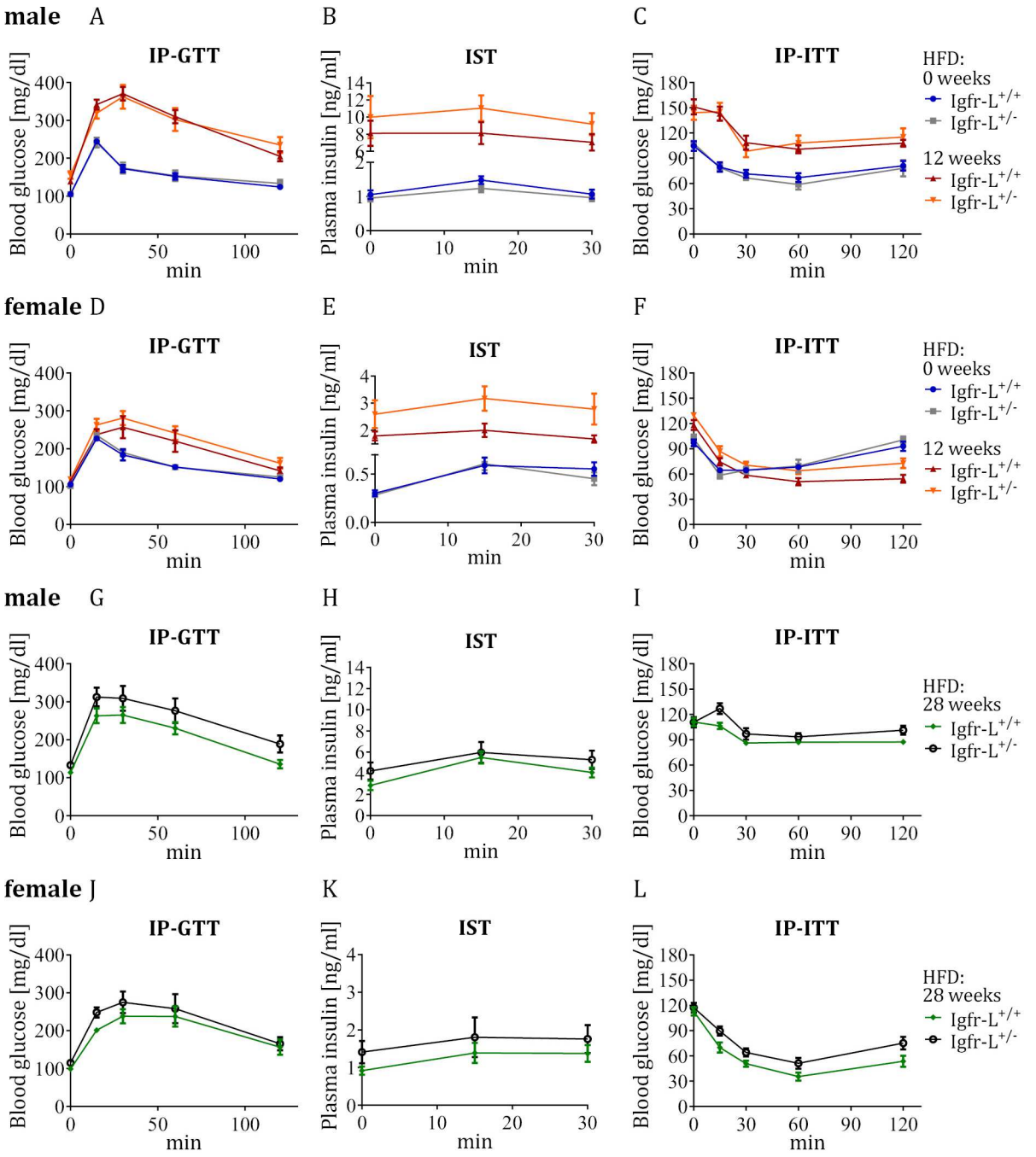

Figure 4.29: Igfr-L$^{+/-}$ male and female mice display an impaired insulin sensitivity after 28 weeks of HFD.

(A, D, G, J) Intraperitoneal glucose tolerance test (IP-GTT)
(B, E, H, K) Insulin secretion test (IST): Blood plasma samples were taken simultaneously to the measurements of glucose levels during IP-GTT
(C, F, I, L) Intraperitoneal insulin tolerance test (IP-ITT)
(A-L) Igfr-L$^{+/-}$ male and female mice before HFD (0 weeks), after 12 weeks and after 28 weeks of HFD. (n (mice) = 7 or 8, mean ± SEM, two-way ANOVA)

The Kulkarni group described (El Ouaamari et al. 2016) a model of 30 weeks long HFD, which leads to chronic insulin resistance caused by hyperinsulinemia. The latter is a result of enhanced

β-cell proliferation and increased β-cell mass. Thus, we prolonged the metabolic challenge by chronically feeding cohort mice a HFD for additional 16 weeks to potentially induce a more pronounced phenotype. After 28 weeks of HFD insulin secretion defects were less pronounced in contrast to the last measurement at 12 weeks of HFD but glucose tolerance and insulin sensitivity were deteriorated (Figure 4.29G-L).

When comparing calculated area under the curve (AUC) values for all performed metabolic tests (GTT, IST, ITT), we could confirm significantly decreased glucose clearance upon insulin injection in females after 12 weeks and for both genders after 28 weeks of dietary food intake (Figure 4.30A-F).

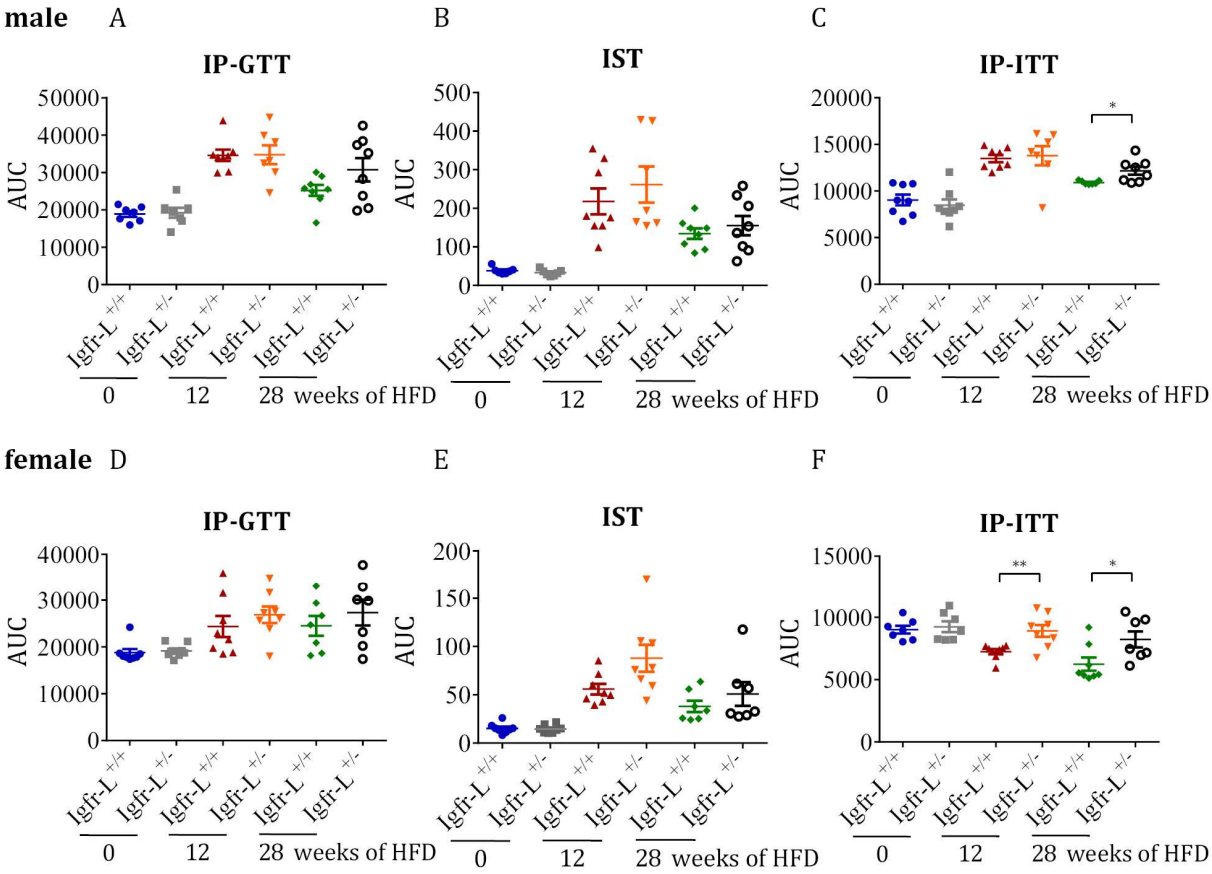

Figure 4.30: Area under the curve (AUC) calculations for IP-GTT, IST and IP-ITT confirm insulin sensitivity impairments after 28 weeks of HFD.

(A-F) Data correspond to experimental results shown in Figure 4.29. (n (mice) = 7 or 8, mean ± SEM, unpaired *t*-test)

Collectively, Igfr-L$^{+/-}$ male and female animals develop a systemic impairment of insulin sensitivity with first symptoms appearing after 12 weeks of HFD and fully manifested after 28 weeks of high caloric food intake. Insulin resistance is characterized by decreased insulin sensitivity, which causes a decline in glucose uptake in peripheral tissues resulting in hyperglycaemia. Consequently, β-cells compensate for elevated blood glucose levels by elevating

insulin secretion (Cerf, 2013). T2D is a consequence of chronic insulin resistance and is thought to involve both, a decline in insulin sensitivity and a decrease in β-cell function, although the order of events is not entirely clear, yet (Prentki & Nolan, 2006). Therefore, we next analysed both, peripheral organs and pancreatic β-cells to understand the primary cause of an impaired insulin sensitivity and hyperinsulinemia in Igfr-L$^{+/-}$.

4.3.4.3 Reduced Igfr-L expression influences β-cell function

Hyperinsulinemia can be caused by a hypersecretion of insulin from β-cells due to increased insulin content or an insulin secretion defect and can result in an enlarged β-cell mass in the pancreas (Cerf, 2013, 2015).

To examine insulin content, we isolated islets of Langerhans from mice, which were fed with HFD for 28 weeks (Figure 4.31A) and determined insulin levels by enzyme-linked immunosorbent assay (ELISA). We observed that insulin concentrations in heterozygous male or female islets were unchanged when compared to control islets. Moreover, we analysed insulin secretion of isolated pancreatic islets in response to low and high glucose over time. For this, we used a microfluidic system that supplies islets with a constant flow of Hank's balanced salt solution (HBSS) buffer supplemented with glucose, thus enabling the detection of first and second phase insulin secretion in a time-resolved manner. Pancreatic islets isolated from Igfr-L$^{+/-}$ male animals after 28 weeks of HFD were starved in 3 mM glucose and stimulated with 11 mM glucose medium. Both, WT and Igfr-L heterozygous islets secreted high amounts of insulin upon glucose induction displaying a merged first and second phase insulin secretion peak, which is the consequence of chronic HFD exposure. However, in high glucose conditions, Igfr-L$^{+/-}$ islets secreted slightly elevated amount of insulin, especially in the first phase of insulin secretion. To control whether insulin secretion independent of glucose is unaffected, islets were stimulated with 25 mM KCl. Both, WT and Igfr-L$^{+/-}$ islets respond to KCl induction with equal amount of secreted insulin.

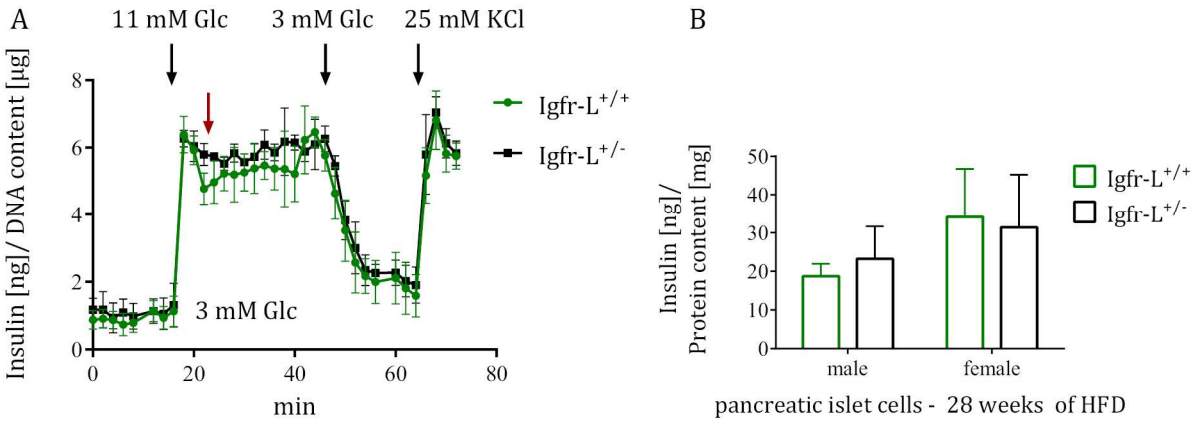

Figure 4.31: Islet of Langerhans isolated from male Igfr-L $^{+/-}$ mice exhibit a slight defect in first phase insulin secretion.

(A) Time-resolved glucose induced insulin secretion (GSIS). Isolated control and Igfr-L$^{+/-}$ male islets were cultured in 3 mM glucose, followed by a 11 mM glucose stimulus. After a regeneration phase with 3 mM glucose complemented culture buffer, islets were induced with 25 mM KCl. Secreted insulin concentrations were measured in the buffer supernatant. Black arrows indicate changes in glucose concentrations. The red arrow highlights a slight decrease in insulin secretion in the first phase of insulin secretion of Igfr-L$^{+/-}$ islets. (n (mice) = 4, mean ± SD)
(B) Insulin content of pancreatic islets isolated from WT and Igfr-L$^{+/-}$ male and female mice. (n (mice) = 3, mean ± SD)

To investigate if the hyperinsulinemia in Igfr-L$^{+/-}$ mice might be a result of increased β-cell mass caused by hyperproliferation, we performed a proliferation study for pancreatic β-cells of male and female animals sacrificed after 28 weeks of HFD (Figure 4.32A). Mice were injected with 5-ethynyl-2'-deoxyuridine (EdU) 24 hours prior sacrifice. However, the proliferation rate of HET males and females did not show a significant difference when compared to WT controls. Only β-cells of HET male mice exhibited a slight decrease in EdU incorporated β-cells. Calculated mean values vary strongly despite counting a sufficient number of β-cells per pancreas. This is due to the extremely low overall proliferation rate of adult pancreatic islets (Gunasekaran & Gannon, 2011).

To further elucidate whether Igfr-L might have an influence on the proliferation rate of cells, we used WT and Igfr-L KO Min6 cells and compared the proliferation rate upon 2 hours of EdU administration. EdU immunostainings of the parental WT cell line, four control clones and five KO clones were evaluated to exclude clonal variation (Figure 4.32B). In fact, Igfr-L KO mutant clones revealed a higher number of EdU positive cells when compared to control clones.

Considering the lethal phenotype of new-born mice upon Igfr-L knock-out, we also assumed a strong phenotype in heterozygous animals. However, we detected only a moderately dysbalanced glucose homeostasis and a slight insulin secretion defect. To examine if Igfr-L heterozygous mutant mice compensate for the partial lack of Igfr-L by upregulating their Igfr-L protein expression, we isolated pancreatic islets of male and female mice (28 weeks of HFD diet) and performed Western blot analysis (Figure 4.33A). The protein expression levels of Igfr-L differ by 25.3% in heterozygous males and 35.6% in heterozygous female animals (Figure 4.33B). Similarly, we observed the same differences in signal intensities of the Igfr-L in immunostainings of WT and Igfr-L$^{+/-}$ pancreatic β-cells (Figure 4.33C,D). This indicates the significance of the Igfr-L for cells because they adapt to the heterozygous state of the Igfr-L allele by either increasing Igfr-L expression to more than 50% or by increasing stability of the Igfr-L pool in the cells.

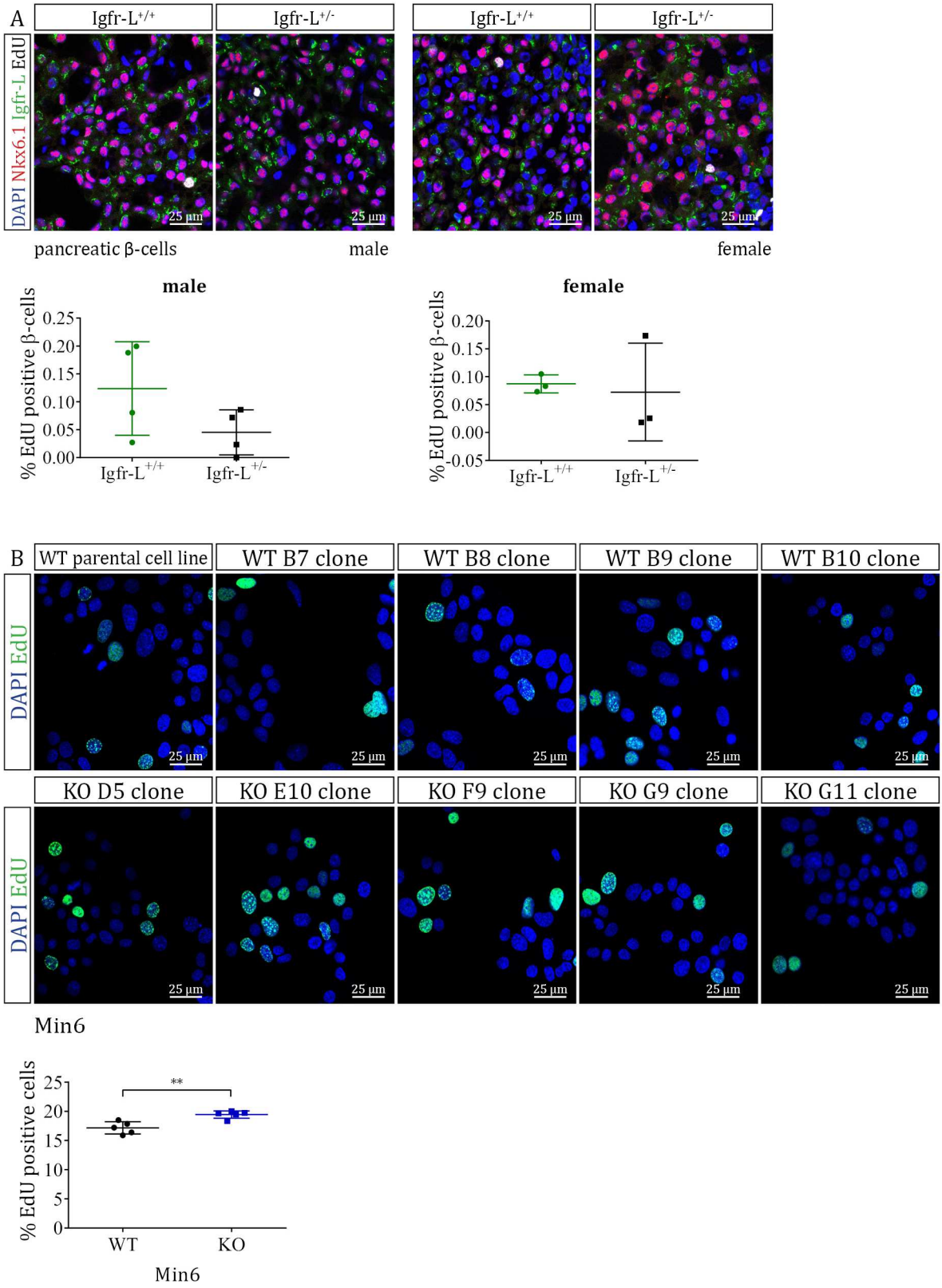

Figure 4.32: Elevated proliferation rate in Igfr-L KO Min6 cells

(A) LSM images of pancreatic sections derived from Igfr-L$^{+/-}$ male and female mice, which were sacrificed 24 hours after EdU administration. Quantification of EdU incorporation: (n = 4 (male mice) and 3 (female mice), mean (6000-11,000 cells counted per n) ± SD)

(B) Representative immunostainings of Min6 control and Igfr-L KO cells. Cells were incubated with Edu for 2 hrs. Quantification of EdU incorporation: (n (clones) = 5, mean (of 3 different weeks for each clone) ± SD, unpaired t-test)

Endocrine hormones of the islet of Langerhans mutually influence their secretion and counteract their physiological actions (Yovos, 2011). Insulin is secreted upon physiological hyperglycaemia inducing glucose uptake in peripheral tissue (Röder et al., 2016). In contrast, the α-cell hormone glucagon promotes gluconeogenesis and inhibits glycolysis counteracting insulin action (Heppner et al., 2010). Glucagon, insulin and PP secretion is suppressed by somatostatin action (Hauge-Evans et al., 2009). An atypical islet architecture and composition influences this complex interplay of endocrine hormones as it was shown for diabetic *db/db* mice (A. Kim et al., 2009). To investigate if the slightly increased insulin secretion, which we observed in islets of heterozygous adult animals upon HFD (Figure 4.31A), is caused by an altered islet composition or by an abnormal distribution of endocrine cell types, we studied pancreatic sections of male and female Igfr-$L^{+/-}$ animals after 28 weeks of HFD (Figure 4.33E,F). However, we did not observe obvious alterations in islet architecture or expression levels of the main endocrine hormones including insulin, glucagon or somatostatin.

In summary, reduced Igfr-L expression leads to a moderate increase in insulin secretion of pancreatic β-cells. Further studies will follow to verify if this defect is due to an increased β-cell mass or an impaired secretory machinery of β-cells.

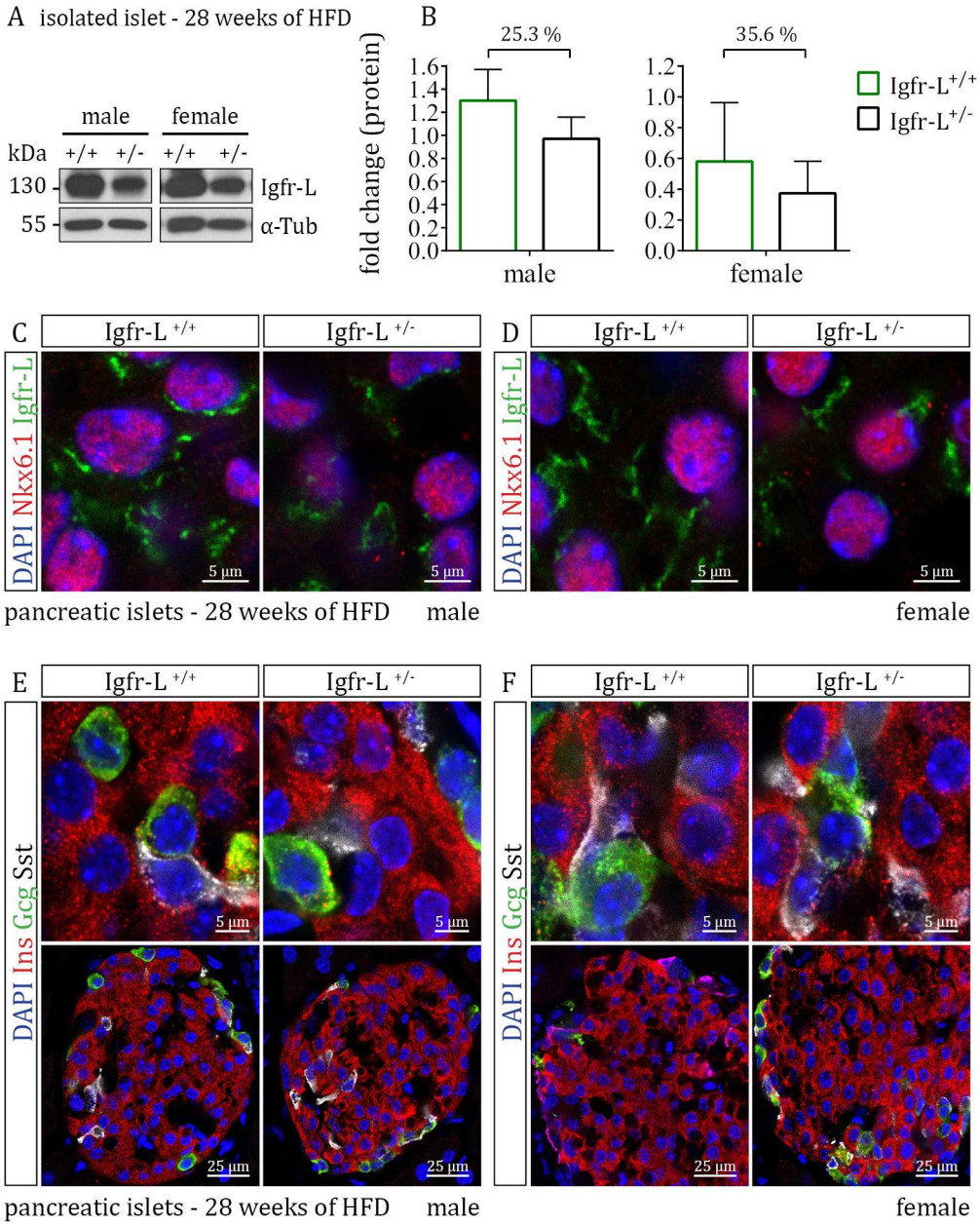

Figure 4.33: Protein expression of Igf-L and islet architecture analysis in heterozygous adult male and female mice.

(A) Igfr-L protein expression analysis in isolated pancreatic islets (Western blot)
(B) Quantification of Igfr-L protein analysed in (A). (n (mice) = 3, mean ± SD)
(C, D) Representative laser scanning microscopy (LSM) images of pancreatic sections. Igfr-L (green) was coimmunostained with the β-cell marker Nkx6.1 (red).
(E, F) Immunofluorescence images of pancreatic sections. Different types of pancreatic endocrine cells were detected using antibodies for insulin (red, β-cells), glucagon (green, α-cells) and somatostatin (white, δ-cells).
(A-F) WT and Igfr-L$^{+/-}$ male and female mice after 28 weeks of HFD.

4.3.4.4 Impact of Igfr-L on the regulation of lipid metabolism

In the metabolic syndrome, a dysregulated lipid metabolism can cause ectopic lipid occurrence in peripheral tissues and the circulatory system triggering oxidative stress, inflammation, and altered cellular signalling influencing insulin action (Glass & Olefsky, 2012; Muoio & Newgard, 2008). This leads to an aberrant glucose homeostasis and eventually to T2D.

To investigate whether the impaired insulin sensitivity (Figure 4.30) is a consequence of an elevated fat storage or dysfunctional lipid metabolism in Igfr-L$^{+/-}$ animals, we measured body fat composition by NMR spectroscopy (Figure 4.34). As expected the lean to fat mass ratio changes upon HFD. Especially in females, the ratio is reversed after 28 weeks of HFD. But no differences in body composition were detected in heterozygous male or female mutant mice when compared to WT animals, suggesting that overall fat storage is not the primary cause of observed impaired insulin sensitivity.

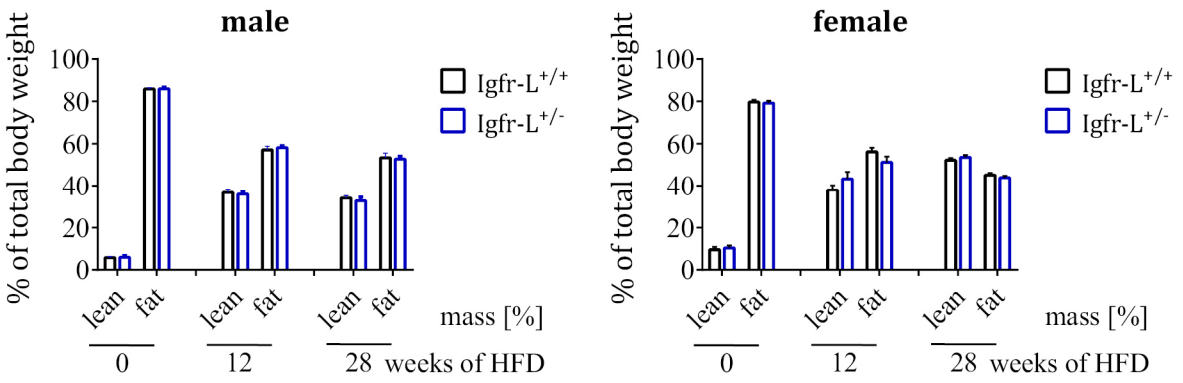

Figure 4.34: No deviation in fat or lean mass in Igfr-L$^{+/-}$ male and female mice after 28 weeks of HFD.

NMR spectroscopy analysis of Igfr-L$^{+/-}$ male and female mice before HFD and 12 and 28 weeks after HFD. (n (mice) = 8, mean ± SEM)

Insulin resistance and T2D is often accompanied by the fat deposition in multiple peripheral organs including liver, muscle, pancreas, kidney and heart as a result of a high demand in energy storage. This often leads to increased organ size. Non-alcoholic fatty liver disease (NAFLD) is associated with hepatic obesity and insulin resistance in rodents and is characterized by decreased insulin signalling in the liver (Birkenfeld & Shulman, 2014; Lambert, Ramos–Roman, Browning, & Parks, 2014).

By assessing the weight of metabolically active organs, such as the pancreas, the liver and epididymal fat tissues of Igfr-L$^{+/-}$ mice after 28 weeks of HFD, we tried to assess a potential role of the Igfr-L in lipid metabolism (Figure 4.35). Interestingly, for Igfr-L mutant females we observed an increase in liver weight. However, analysis of liver sections using H&E stainings did

not reveal any morphological differences. Additional examination will be necessary to verify that elevated liver weight might be caused by hepatosteatosis.

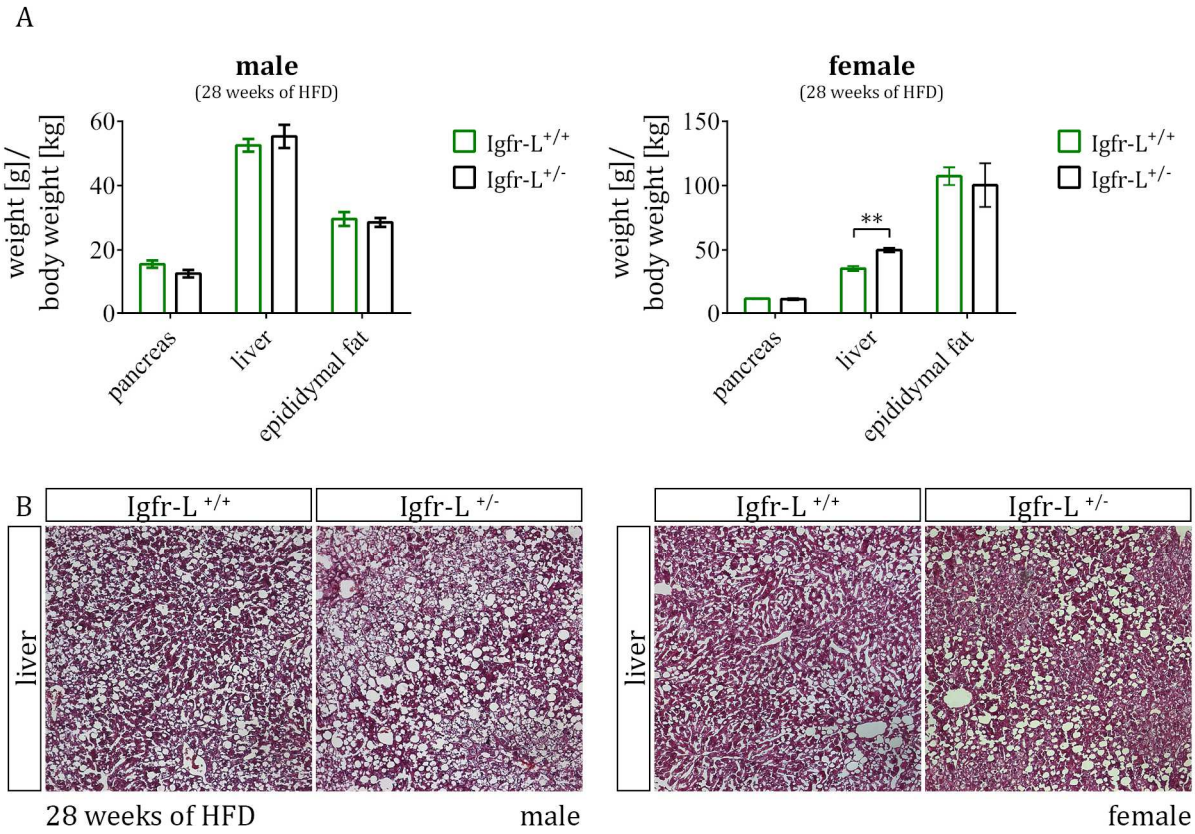

Figure 4.35: Increased liver weight in Igfr-L$^{+/-}$ females after 28 weeks of HFD.

(A) Organ weight of pancreas, liver and epididymal fat pads (males: n = 4 (pancreas and epididymal fat) n = 8 (liver), females: n = 3 (all tissues), mean ± SEM, unpaired t-test)
(B) Hematoxylin and Eosin (H & E) staining of liver cryo sections
(A, B) Igfr-L$^{+/-}$ male and female tissue after 28 weeks of HFD.

In T2D and the metabolic syndrome hyperglycaemia and insulin resistance promote the development of diabetic dyslipidaemia, which causes the reduction of plasma high-density lipoprotein (HDL) cholesterol, hypertriglyceridemia and often a slightly increased plasma concentration of low-density lipoprotein (LDL) cholesterol (Ginsberg, 1991; Howard, 1999). In adipose tissue, insulin inhibits the hormone-sensitive lipase promoting the storage of triglycerides in adipocytes and reducing the secretion of non-esterified fatty acids (NEFA) from adipose tissue. Additionally, it induces clearance of LDL from the blood by increasing LDL-receptor expression and activity (Chait, Bierman, & Albers, 1979). To examine possible abnormalities in lipid metabolism, we analysed blood plasma samples from six hours starved WT and Igfr-L heterozygous male and female animals for following parameters: triglycerides, NEFA, total cholesterol, HDL and LDL (Figure 4.36A-L). Only, measured triglyceride values were significantly reduced in heterozygous females. However, at this experimental stage this result is hard to explain since impaired insulin sensitivity is usually accompanied by elevated triglycerides in the blood.

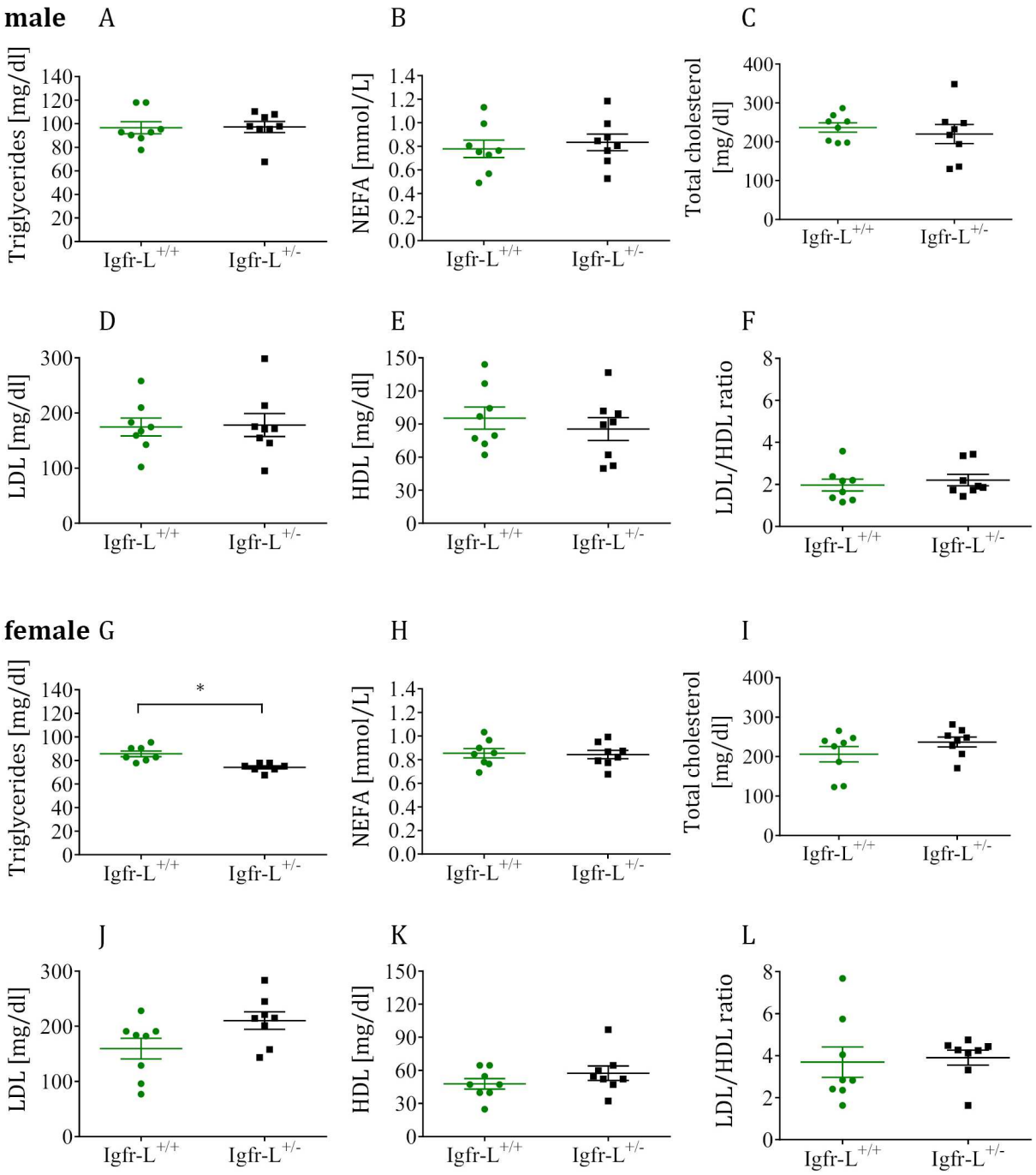

Figure 4.36: Plasma triglycerides levels are decreased in Igfr-L heterozygous females.

(A, G) Plasma triglycerides analysis
(B, H) Plasma non-esterified fatty acids (NEFA) measurement
(C, I) Plasma total cholesterol determination
(D, J) Plasma low density lipoprotein (LDL) study
(D, K) Plasma high density lipoprotein (HDL) investigation
(F, L) LDL/HDL ratio
(A-L) Plasma samples for the analysis were taken from Igfr-L$^{+/-}$ male (A-F) and female (G-L) mice after 28 weeks of HFD. (n = 8 (all except n = 7 for triglycerides of females), mean ± SEM, unpaired t-test)

To conclude, Igfr-L heterozygous female mice develop enlarged livers and manifest diminished triglyceride plasma concentrations upon 28 weeks of HFD. Additional experiments will shed light on how these findings are interconnected with an impairment of insulin sensitivity and insulin secretion in Igfr-L heterozygous animals.

4.3.4.5 Association of human IGFR-L locus with dysbalanced cholesterol metabolism, deregulated insulin sensitivity, coronary artery disease and T2D

To investigate the relevance of murine metabolic phenotype in humans, we searched for statistical association of human IGFR-L with T2D and related traits in patients using the database T2D Knowledge Portal (www.type2diabetesgenetics.org) (Figure 4.37). T2D Knowledge Portal analyses human genetic information linked to type 2 diabetes and related traits, such as T2D incidence, plasma glucose, insulin sensitivity, BMI (body mass index) or gender. It uses datasets of different experimental types (genotyping and sequencing studies) like genome-wide association study (GWAS), whole-genome sequencing (WGS), whole-exome sequencing (WES) or exon chip analysis (ExChip) and includes large data sets of over 100.000 genetic samples. Indeed, the IGFR-L locus associates with disbalanced parameters such as LDL cholesterol, total cholesterol, HDL cholesterol, insulin sensitivity, with coronary artery diseases and T2D strengthening the assumption that IGFR-L might be involved in the development of T2D and the regulation of lipid metabolism.

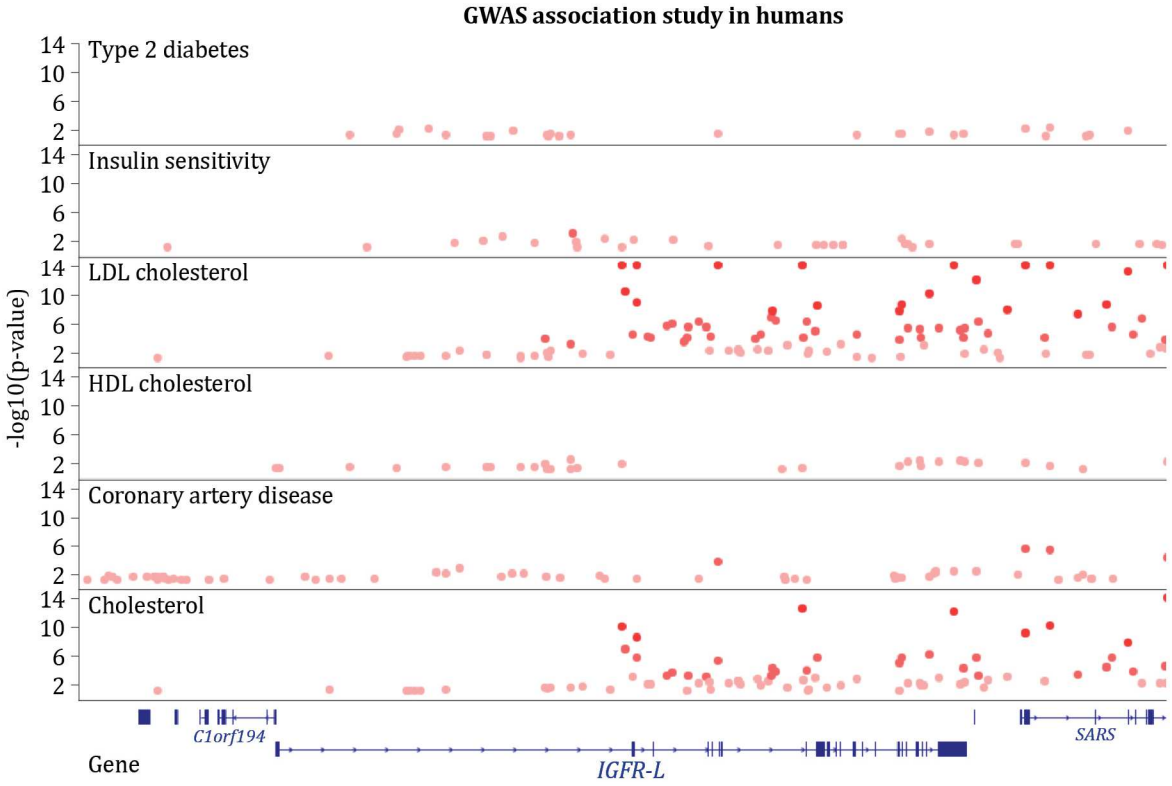

Figure 4.37: The human *IGFR-L* gene locus is associated with abnormal cholesterol metabolism, deregulated insulin sensitivity, coronary artery disease and T2D.

The Type2 Diabetes knowledge portal provides data for association studies linking IGFR-L to T2D and related traits. 146kb of chromosome 1, which includes the IGFR-L locus is shown: chr1:109,629,789-109,776,198. Association with variants of the different phenotypes have a p-value of 0.05 or lower. Modified from Type2 Diabetes knowledge portal (AMP-T2D Program; T2D-GENES Consortium, SIGMA T2D Consortium. KIAA1324, http://www.type2diabetesgenetics.org/gene/geneInfo/KIAA1324, 2017 May 10)

4.3.5 The molecular function of Igfr-L

Until now, the literature reports little about the molecular function of the Igfr-L. Kang et al., 2015 claimed that the Igfr-L human ortholog, KIAA1324, binds the chaperone protein glucose-regulated protein 78 kDa (GRP78) thereby inhibiting GRP78–caspase 7 interaction and AKT activation. This results in the suppression of oncogenic activities of GRP78 by regulating apoptosis and proliferation mechanisms (J. M. Kang et al., 2015).

Since we discovered Igfr-L in a screen for novel pancreatic endocrine regulators and it is highly expressed in the pancreas during development, we first characterized the molecular, cell biological and biochemical properties of Igfr-L in pancreatic β-cells using the murine insulinoma cell line Min6.

4.3.5.1 Igfr-L is highly expressed in murine and human cells

By immunofluorescence approach we compared expression and localization of Igfr-L in murine Min6 cells, in the human pancreatic β-cell line EndoC-βH1 and in the human breast cancer cell line MCF7 (Figure 4.38A-C). Indeed, the receptor is highly expressed in both human and mouse cell lines and shows similar localization near the nucleus, likely in the ER and Golgi compartment.

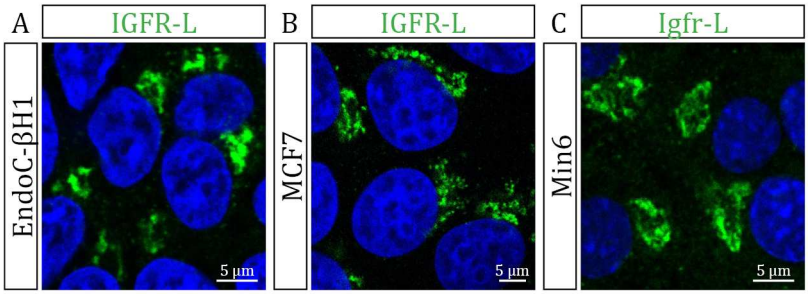

Figure 4.38: Igfr-L is highly expressed in murine and human cells displaying similar localization pattern.

(A-C) Representative laser scanning microscopy (LSM) images of cultured human EndoC-βH1 (β-cells) (A), human MCF7 (breast cancer cells) (B) and mouse Min6 (β-cells) (C) cells. Igfr-L immunostaining is shown in green.

4.3.5.2 Igfr-L mainly localizes to the Golgi complex and partially resides in the endosome, lysosome and at the plasma membrane

The subcellular localization often provides first hints for the molecular function of proteins including trafficking behaviour. Bioinformatic analysis of the Igfr-L predicted a receptor protein, which is targeted to the secretory pathway due to its N-terminal signal peptide and transmembrane domain (Figure 4.19). Consequently, we coimmunostained WT Min6 cells with Igfr-L antibodies and antibodies against marker proteins for different subcellular compartments (Figure 4.39A-I). To measure the degree of colocalization, we calculated the Pearson correlation coefficient (PCC, R-value) and the Mander's overlap coefficient (MOC, tM1 and tM2 values) using the ImageJ plugin Fiji Coloc2. Intensity values derived from ImageJ calculations are depicted in a scatter plot using the software R. Scatter plots graphically represent colocalizing pixels of a merged image with pixel signals plotted according to their intensity values. The Igfr-L displayed large overlap with the trans-Golgi marker Tgn46 (*trans*-Golgi network 46) in coimmunostainings (Figure 4.39A). A PCC value of R = 0.85 and tM2 value of 0.94 was calculated. Igfr-L also showed strong colocalization with the *cis*-Golgi marker Gm130 (golgi matrix protein 130; R = 0.71 and tM2 = 0.78) and the *cis*-median Golgi marker giantin (R = 0.79 and tM2 = 0.95) (Figure 4.39B,C). In contrast, a R-value of 0.20 and a tM2 of 0.66 for Ergic (endoplasmic reticulum-golgi intermediate compartment) states rather poor overlap suggesting that the receptor passes through but does not stay in this intermediate compartment very long (Figure 4.39D). Retrograde cargo transport between ER and Golgi and protein traveling within the Golgi is mediated by COPI vesicles. Such coatomer protein complexes are recognized in its native form by a Cm1 antibody. As expected, good colocalization with this marker was detected for Igfr-L receptor (R = 0.63 and tM2 = 0.77) (Figure 4.39G). The PCC values for the overlap with the early endosome marker Eea1 (early endosome antigen 1) and the late endosome marker Rab7 (Ras-associated protein Rab7) indicate little colocalization (Eea1 R = 0.27 and Rab7 R = 0.26) (Figure 4.39E,F). However, high MOC values prove otherwise (Eea1 tM1 = 0.86 and Rab7 tM2 = 0.74), implying that a small protein fraction with low intensity levels travels in these sub-compartments. The two major lysosomal-associated membrane protein 1 and 2 (Lamp1 and Lamp2) exhibit considerable sequence homology and are thought to have similar domain structure and biochemical properties (Eskelinen, 2006). However, their subcellular localization slightly deviates (Figure 4.39H, I). Coimmunostainings with the lysosomal markers Lamp1 and Lamp2 revealed small overlap for Lamp2 (R = 0.27 and tM2 = 0.63) but no overlap for Lamp1 (R = -1.49 and tM2 = 0.54) (Figure 4.39H,I). This might indicate that a subset of Igfr-L is routed to lysosomal compartments preferring vesicular structures with the lysosomal membrane protein Lamp2.

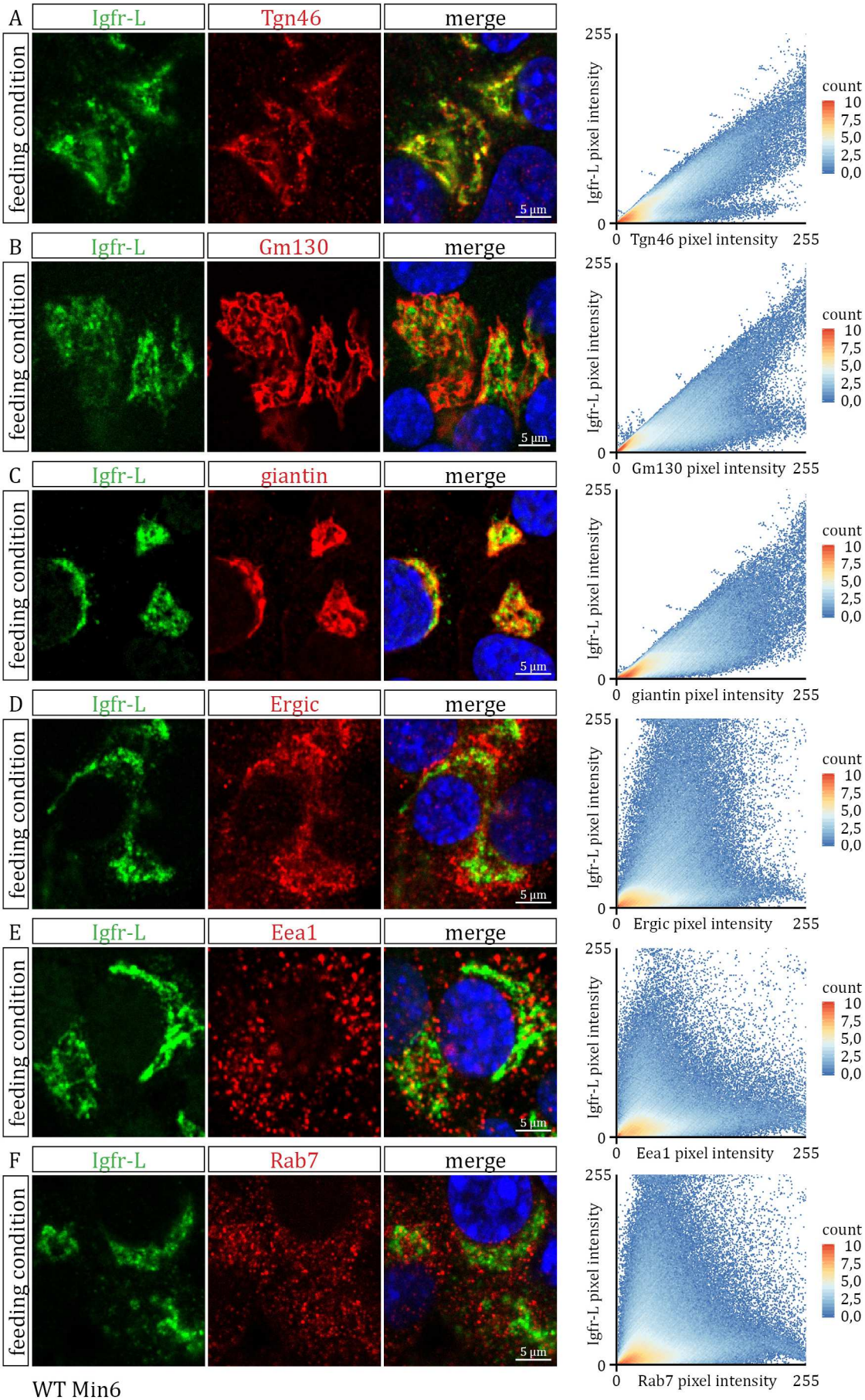
A
Igfr-L
Tgn46
merge
feeding condition
5 µm
B
Igfr-L
Gm130
merge
feeding condition
5 µm
C
Igfr-L
giantin
merge
feeding condition
5 µm
D
Igfr-L
Ergic
merge
feeding condition
5 µm
E
Igfr-L
Eea1
merge
feeding condition
5 µm
F
Igfr-L
Rab7
merge
feeding condition
5 µm
WT Min6
255
Igfr-L pixel intensity
0
0 Tgn46 pixel intensity 255
count
10
7,5
5,0
2,5
0,0
0 Gm130 pixel intensity 255
0 giantin pixel intensity 255
0 Ergic pixel intensity 255
0 Eea1 pixel intensity 255
0 Rab7 pixel intensity 255

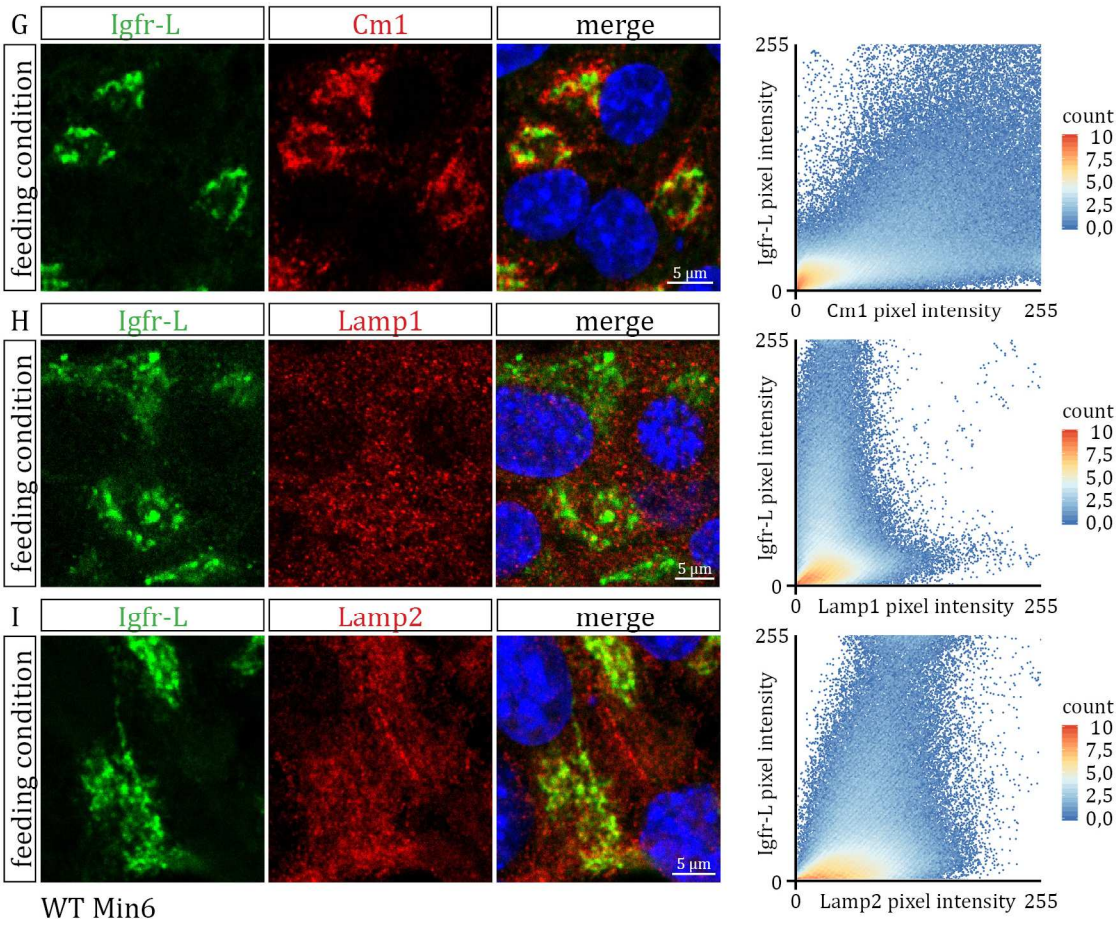

J

Channel (Ch)/ Image		Pearson correlation coefficient (PCC)	Mander's overlap coefficient (MOC)	
1	**2**	**Pearson's R value** (above Costes threshold)	**Manders' tM1** (above Costes threshold of Ch2)	**Manders' tM2** (above Costes threshold of Ch1)
Tgn46	**Igfr-L**	0.83	0.92	0.94
GM130	**Igfr-L**	0.71	0.86	0.78
giantin	**Igfr-L**	0.79	0.82	0.95
ERGIC	**Igfr-L**	0.20	0.54	0.66
EEA1	**Igfr-L**	0.27	0.79	0.86
Rab7	**Igfr-L**	0.26	0.65	0.74
CM1	**Igfr-L**	0.63	0.85	0.77
Lamp2	**Igfr-L**	0.27	0.37	0.63
Lamp1	**Igfr-L**	-1.49	0.38	0.54

Figure 4.39: The main pool of Igfr-L localizes in the Golgi apparatus, whereas a small subpopulation is found in the lysosome and the endosome.

(A-J) Representative laser scanning microscopy (LSM) images of WT Min6 cells (A-I). Igfr-L (green) was coimmunostained with antibodies marking different cellular organelles (red): Tgn46 (*trans*-Golgi), Gm130 (*cis*-Golgi), giantin (*cis*-and *medial*- Golgi), Ergic, Eea1 (early endosome), Rab7 (late endosome), Cm1 (coatomer, COPI vesicles), Lamp 1 and Lamp2 (lysosome). The degree of colocalizing marker signal is represented by a scatter plot (A-I), the PCC and the MOC (J). PCC values: "+1" perfect correlation, "0" no

correlation and "-1" perfect inverse correlation; MOC values: tM1 is the percentage of above background pixels in image/channel 1 that overlaps above-background pixels in image 2. tM2 is calculated vice versa. Computations were performed using ImageJ plugin Fiji Coloc2 (Costes background subtraction). Scatterplots depict colocalizing pixel intensity detected for both channels of merged images. Intensity counts are plotted in log scale and are colour coded (red high and blue low number of counts). (n = 2 (experimental weeks) except n = 1 for Tgn46 and Cm1, mean)

The main receptor pool of M6PRs exists intracellularly whereas only 12% is found at the cell surface (Bleekemolen, Stein, von Figura, Slot, & Geuze, 1988). Similarly, the Igfr-L resides mainly in the *cis*-Golgi area. The detection of receptor sub-populations in smaller cellular compartments proves difficult with common IF staining methods. Hence, we chose a technique that enabled us to enhance the IF signal for the receptor fraction present at the plasma membrane.

Living WT Min6 cells were incubated with an Igfr-L antibody specifically binding the extracellular domain of the receptor (Igfr-L ecto) at 4 °C for 30 min (Figure 4.40A). The temperature drop inhibits endocytosis retaining receptors at the cell surface. Thus, Igfr-L proteins at the plasma membrane were bound by receptor antibody (Igfr-L ecto), which was subsequently detected with a fluorescent labelled secondary antibody in immunofluorescence stainings. Min6 cells were coimmunostained with the plasma membrane markers Wheat germ agglutinin (WGA) and concanavalin A (ConA, mannose specificity) and with Igfr-L antibody recognizing the total receptor pool (Figure 4.40B,C). ConA and WGA are lectins interacting with glycoproteins and glycolipids that are enriched at the plasma membrane. As WGA is specific for N-acetyl-D-glucosamine and sialic acid and the Golgi is involved in the post-translational glycosylation of proteins, it also labels the Golgi apparatus in permeabilized cells.

The amount of Igfr-L receptor at the cell surface differs in each cell (white arrows). This might be due to distinct metabolic or signalling states of individual cells, which require heterogeneous receptor expression levels and varying requirements of the receptor at the plasma membrane.

In summary, the Igfr-L mainly resides in the Golgi apparatus with the highest concentration in the *trans*-Golgi area. Small subpopulations of the receptor are found at the plasma membrane, in the early and late endosome and partially localize to the lysosome.

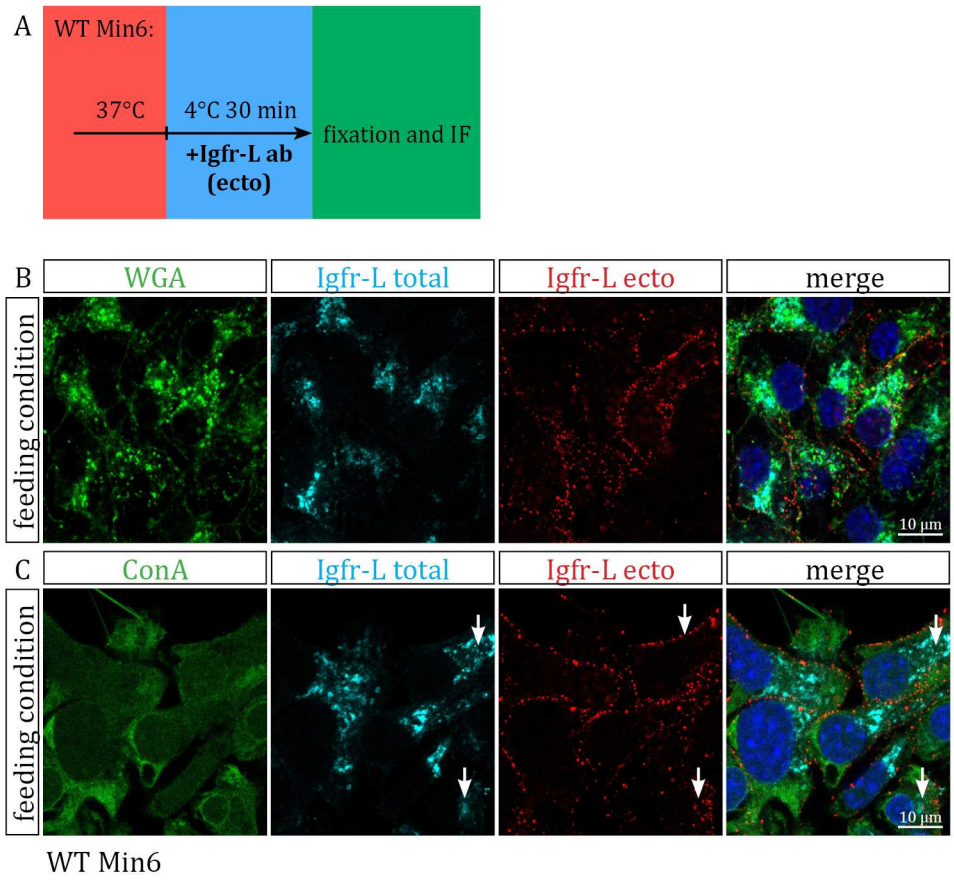

Figure 4.40: A small sub-population of Igfr-L localizes to the plasma membrane.

(A) Experimental design: WT Min6 cells were kept at 4°C for 30 min to inhibit endocytic processes and incubated with an Igfr-L antibody (Igfr-L ecto) specific for the ectodomain of the receptor protein. This allows the binding of Igfr-L ecto to a small subpopulation of receptor localized at the plasma membrane. For subsequent immunofluorescence, receptor signal on the cell surface was enhanced compared to the total receptor pool.
(B) Representative immunofluorescence images of WT Min6 cells using plasma membrane markers WGA and ConA (green) and the Igfr-L receptor antibody. Total pool of Igfr-L (Igfr-L total, cyan) and membrane localized Igfr-L (Igfr-L ecto, red) were detected. White arrows indicate Igfr-L localized to either plasma membrane or Golgi complex.

4.3.5.3 Igfr-L negatively regulates InsR/Igf1r signalling and the key metabolic regulator Ampk in feeding condition and upon starvation

Bioinformatic analysis predicted a growth factor cysteine-rich domain and a mannose-6-phosphate domain in the extracellular region of the Igfr-L protein. Structurally similar domains are found in receptor tyrosine kinases of the Ins/Igf signalling system where they are involved in ligand binding, receptor dimerization and trafficking (Adams et al., 2000; Tatulian, 2015). To examine if the Igfr-L protein plays a role in the regulation of the InsR/Igfr signalling pathway, we studied expression and activity levels of key players upon active or attenuated signal transduction.

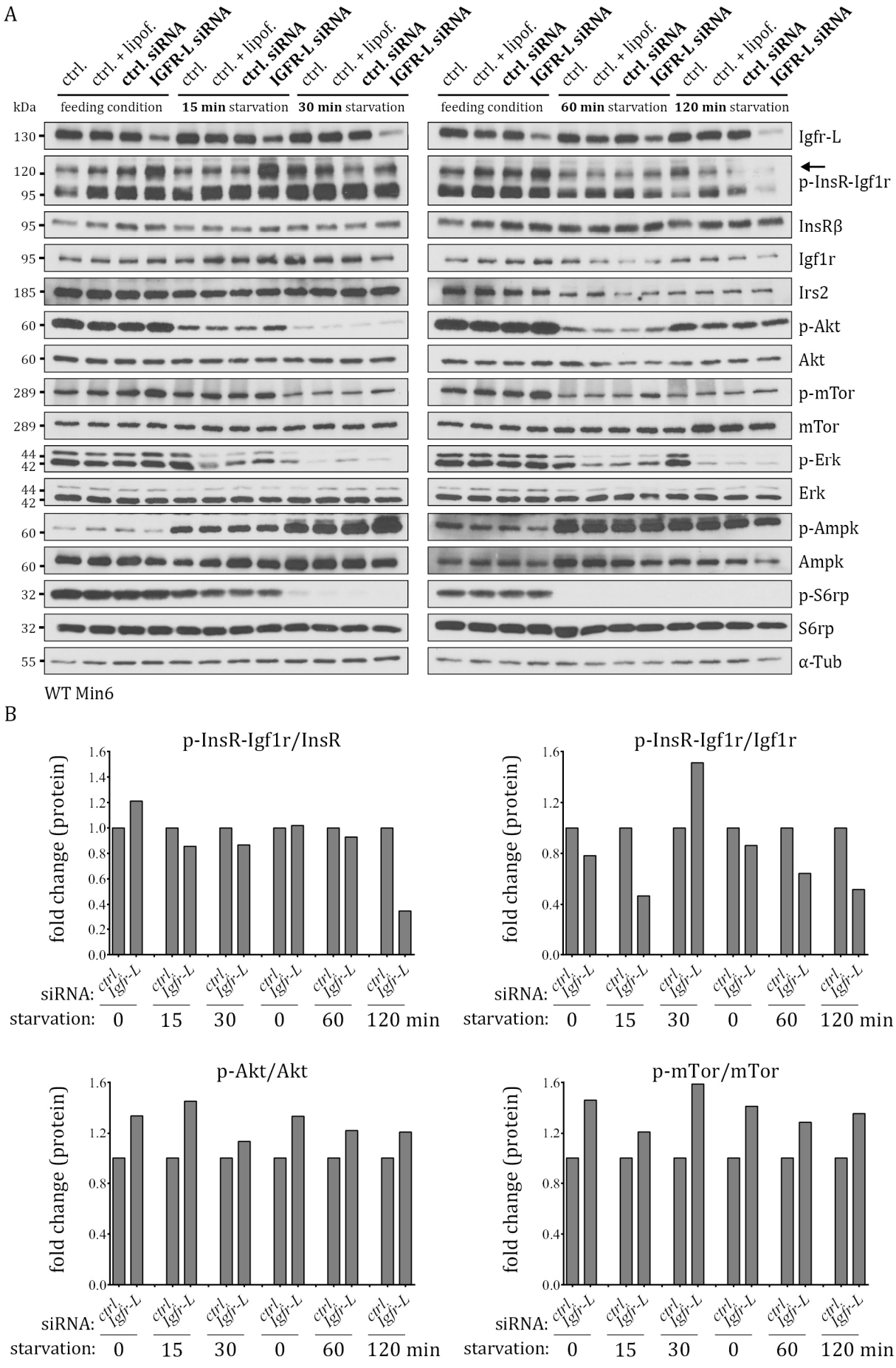
A
ctrl.
ctrl. + lipof.
ctrl. siRNA
IGFR-L siRNA
kDa
feeding condition
15 min starvation
30 min starvation
60 min starvation
120 min starvation
130
120
95
185
60
289
44
42
55
Igfr-L
p-InsR-Igf1r
InsRβ
Igf1r
Irs2
p-Akt
Akt
p-mTor
mTor
p-Erk
Erk
p-Ampk
Ampk
p-S6rp
S6rp
α-Tub
WT Min6
B
p-InsR-Igf1r/InsR
p-InsR-Igf1r/Igf1r
p-Akt/Akt
p-mTor/mTor
fold change (protein)
siRNA:
ctrl.
Igfr-L
starvation:
0
15
30
0
60
120 min

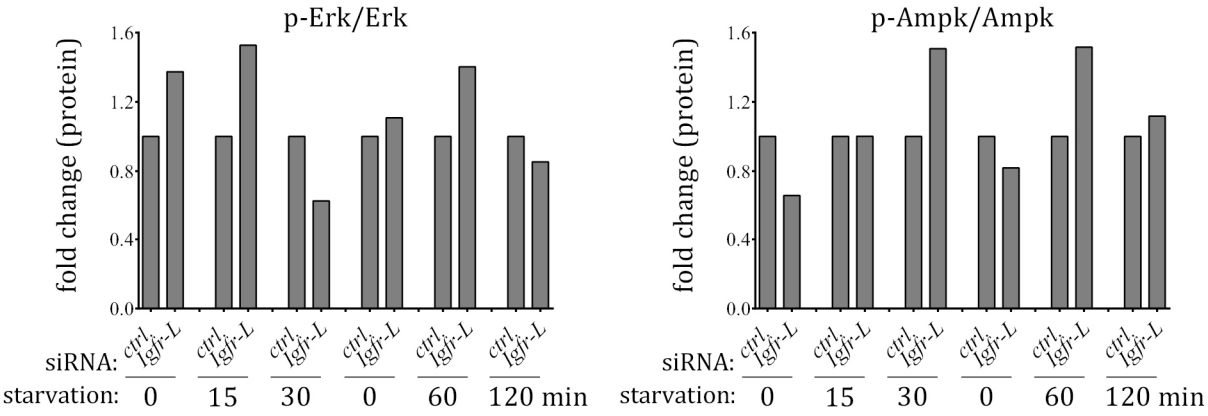

Figure 4.41: siRNA mediated knock-down of Igfr-L activates InsR/Igf1r signalling in feeding condition and during nutritional starvation.

(A) Western blot analysis of WT Min6 cells cultured in feeding conditions and upon 15, 30, 60 and 120 min nutritional deprivation. siRNA mediated knock-down of Igfr-L was performed: "Ctrl" control, "ctrl. + lipof." control sample with lipofectamine in transfection medium, "ctrl. siRNA" control siRNA, "*Igfr-L* siRNA" siRNA for Igfr-L. The black arrow indicates an unspecific protein band.
(B) Quantification of Western blots presented in (A) (protein bands for ctrl. siRNA and *Igfr-L* siRNA samples only). 0 min starvation correspond to feeding condition. Phospho-proteins were normalized to the loading control and the amount of total protein. (n = 1)

Therefore, we cultured WT Min6 cells in either growth factor rich medium (feeding medium) to maintain an activated InsR/Igfr pathway or in nutrient depleted medium (starvation) to diminish signal transduction. Further, we performed a small interference RNA (si-RNA) mediated knock-down of Igfr-L in cells and analysed protein lysates by Western blotting (Figure 4.41A,B). An average knock-down efficiency of 60% caused an upregulation of Akt and mTor phosphorylation in Igfr-L knock-down samples relative to the ctrl siRNA samples in feeding conditions. This elevated activity lasted during the first 60 min of starvation despite a general attenuation of signal activity over time. The phosphorylation levels of Ampk were quite low in feeding conditions but after 30 and 60 min of starvation we observed a general increase in Ampk phosphorylation. However, the Ampk phosphorylation in Igfr-L knock-down samples was elevated after 30 and 60 min of starvation when compared to control samples. The activity of Erk was differentially regulated in feeding and starvation condition and does not show a clear trend during 120 min of nutrient depletion. The phosphorylation of the InsR was not affected upon Igfr-L knock-down whereas the activity of Igf1r tended to be reduced. For the InsR-Igf1r phosphorylation we detected a second unspecific band migrating higher than the receptor itself at around 120kDa with an increased signal intensity in Igfr-L knock-down samples. This might be a protein recognized and regulated by the same kinase upon activation of the insulin signalling pathway with a substrate sequence similar to the phosphorylation motif found in InsR/Igf1r.

To confirm a potential role of Igfr-L in the InsR/Igfr signalling system we analysed Igfr-L KO Min6 cells in feeding and short-term starvation conditions (15 min) (Figure 4.42A,B). In contrast to Igfr-L knock-down experiments, we did not detect increased Akt or mTor activity but elevated phosphorylation of Ampk and InsR/Igf1r upon deletion of Igfr-L. After 15 min of nutrient depletion upregulated Ampk activity was maintained whereas Erk phosphorylation was reduced.

In conclusion, Igfr-L is involved in the modulation of the InsR/Igf signalling during active and attenuated signalling states by regulating the activity of its key components and the metabolic regulator Ampk. However, we observed that Igfr-L depletion differently influences the activity of signalling proteins in cells in which the receptor expression was depleted by siRNA-knock-down compared to cells in which the receptor expression was completely missing (Min6 KO). This discrepancy might be a result of an adaptation mechanism over time. Gradually, cells adjust to the absence of Igfr-L and alter their signal transduction thereby changing from an acute influence to a chronic effect on the signalling (see discussion and (Rhodes et al., 2013)). Additionally, to induce a full or partial receptor ablation, different techniques were used, which might also influence cellular signalling behaviour.

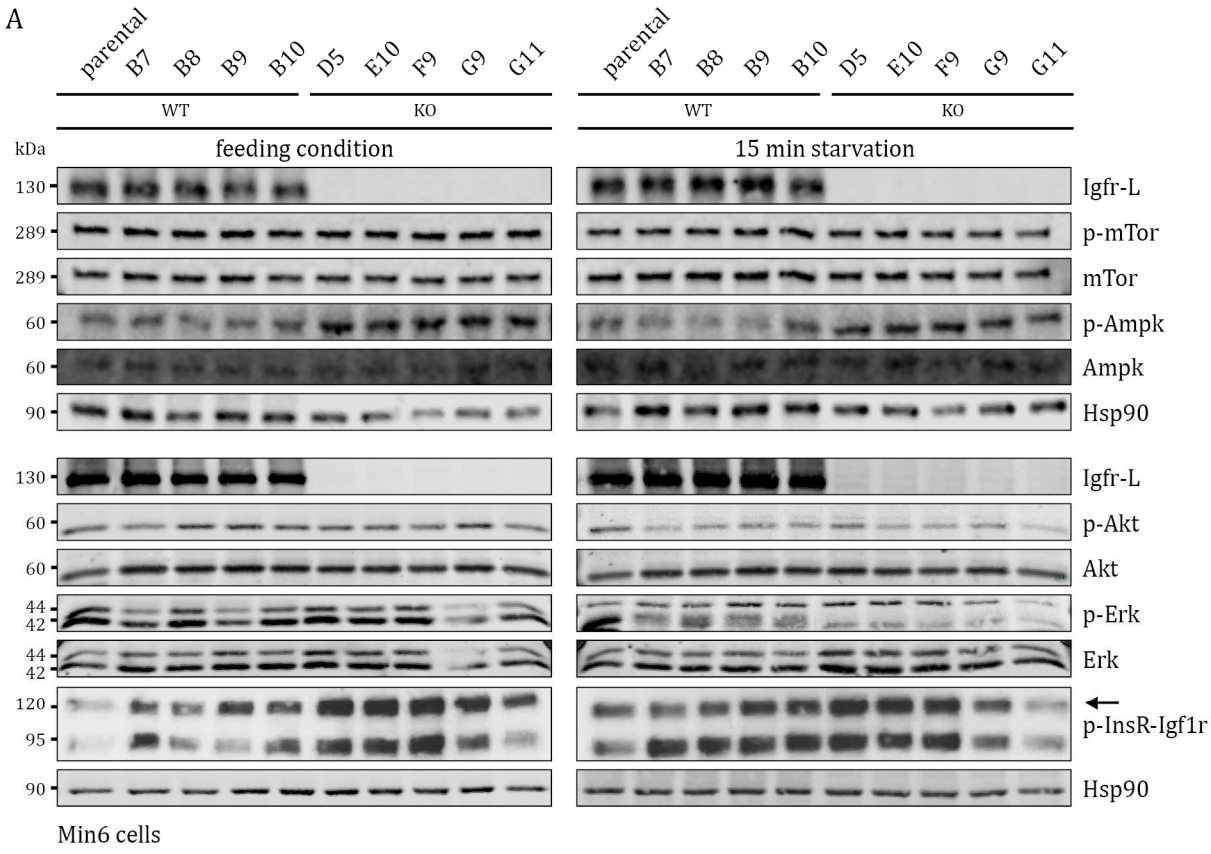
A
parental
B7
B8
B9
B10
D5
E10
F9
G9
G11
WT
KO
feeding condition
15 min starvation
kDa
130
289
289
60
60
90
130
60
60
44
42
44
42
120
95
90
Igfr-L
p-mTor
mTor
p-Ampk
Ampk
Hsp90
Igfr-L
p-Akt
Akt
p-Erk
Erk
p-InsR-Igf1r
Hsp90
Min6 cells

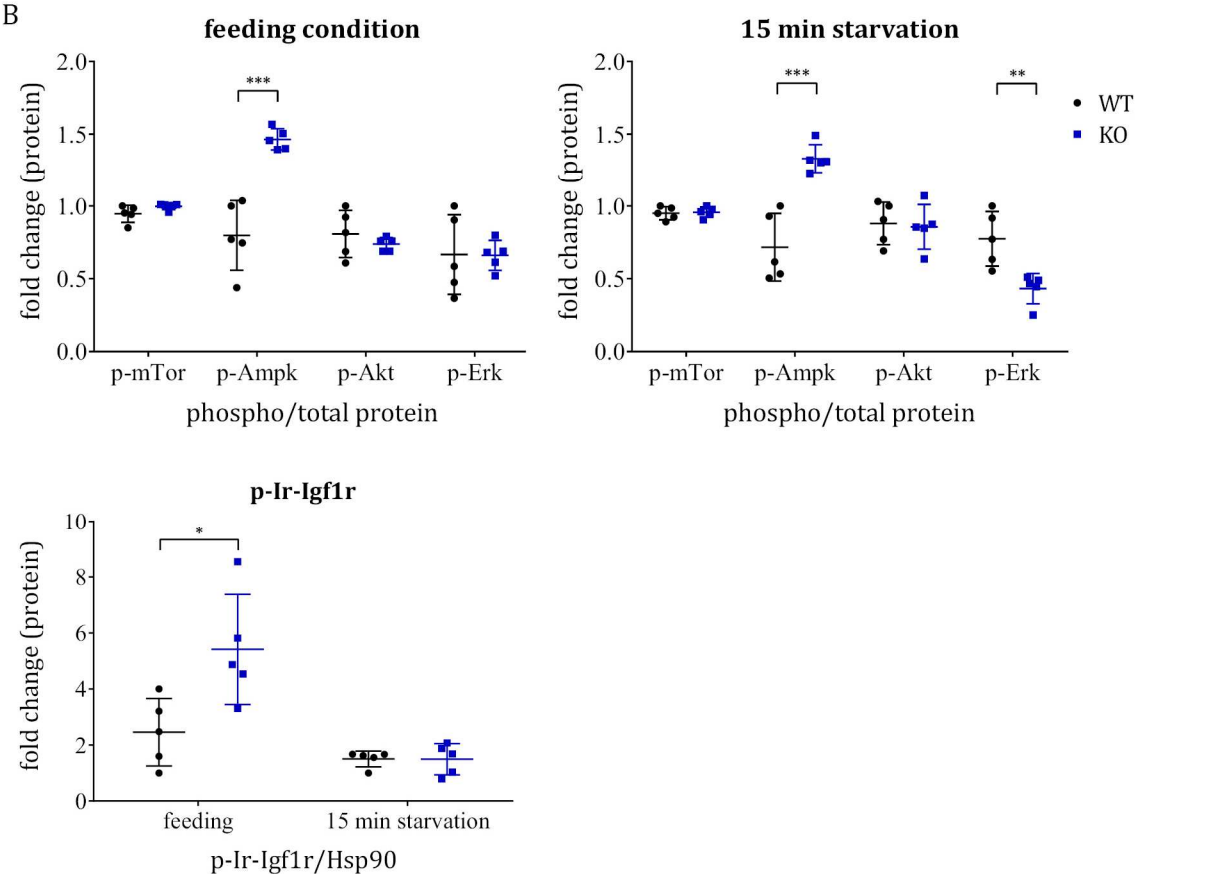
B
feeding condition
15 min starvation
fold change (protein)
2.0
1.5
1.0
0.5
0.0
***
**
p-mTor
p-Ampk
p-Akt
p-Erk
phospho/total protein
WT
KO
p-Ir-Igf1r
10
8
6
4
2
0
*
feeding
15 min starvation
p-Ir-Igf1r/Hsp90

Figure 4.42: Igfr-L negatively regulates InsR/Igf1r signalling and the key metabolic regulator Ampk.

(A) Representative Western blot images of parental WT Min6 cell line, control WT clones (B7, B8, B9, B10) and Igfr-L KO clones (D5, E10, F9, G9, G11) cultured in feeding medium or 15 min starving conditions. The black arrow indicates an unspecific protein band.
(B) Quantification of Western blots presented in (A). The parental WT cell line and control clones (WT) as well as KO clones (KO) were summaries for statistical calculations. Phospho-proteins were normalized on the loading control heat shock protein 90 (Hsp90) and total protein. (n = 5 clones (mean of 1-3 experimental weeks), mean ± SD, unpaired t-test)

4.3.5.4 Growth factor depletion affects subcellular localization of Igfr-L

The signalling activity of receptor tyrosine kinases (RTKs) is regulated by the presence and abundance of extracellular ligands (Goh & Sorkin, 2013). Ligand binding induces receptor dimerization followed by a transactivation of intracellular tyrosine kinase domains, which activates downstream signalling. Subsequently, receptors are internalized and sorted in the cytoplasm. The rates of internalization, recycling, and lysosomal degradation thus determines the half-life of a RTKs and their subcellular localization (Goh & Sorkin, 2013).

Previous experiments implicated an involvement of the Igfr-L in the regulation of the Ins/Igf pathway. Hence, we analysed the impact of attenuated and active Ins/Igf signalling on the intracellular distribution of Igfr-L by either starving WT Min6 cells or by exposing cells to Ins, Igf1 or Igf2 ligands after a 120 min period of nutrient deprivation (Figure 4.43A). Surprisingly, 135 min nutrient depletion caused a “contraction” of the Igfr-L to the Golgi area and a “compaction” of the Golgi apparatus itself when compared to the feeding condition (Figure 4.43B). The detected Igfr-L distribution pattern appears less granular with fewer dotty vesicles around the Golgi area. Stimulation with Ins, Igf1 and Igf2 ligands did not affect subcellular localization of Igfr-L. Additionally, cells were metabolically challenged by a high glucose treatment. Glucose itself might affect β-cells but also induces insulin secretion upon high extracellular concentrations activating autocrine signalling. However, 16.7 mM of extracellular glucose did not cause obvious changes in subcellular localization of Igfr-L. These observations imply that receptor availability is required in peripheral areas of the secretory pathway in glucose and growth factor complemented cellular environment but retracts to the Golgi apparatus upon nutrient depletion. However, the immunofluorescence technique might not be sensitive enough to detect small changes in receptor localization at the cell surface.

A

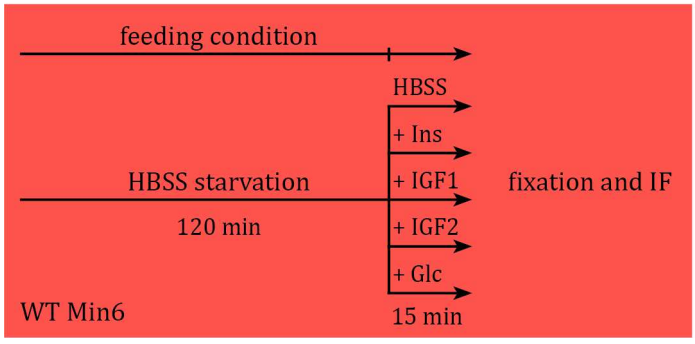

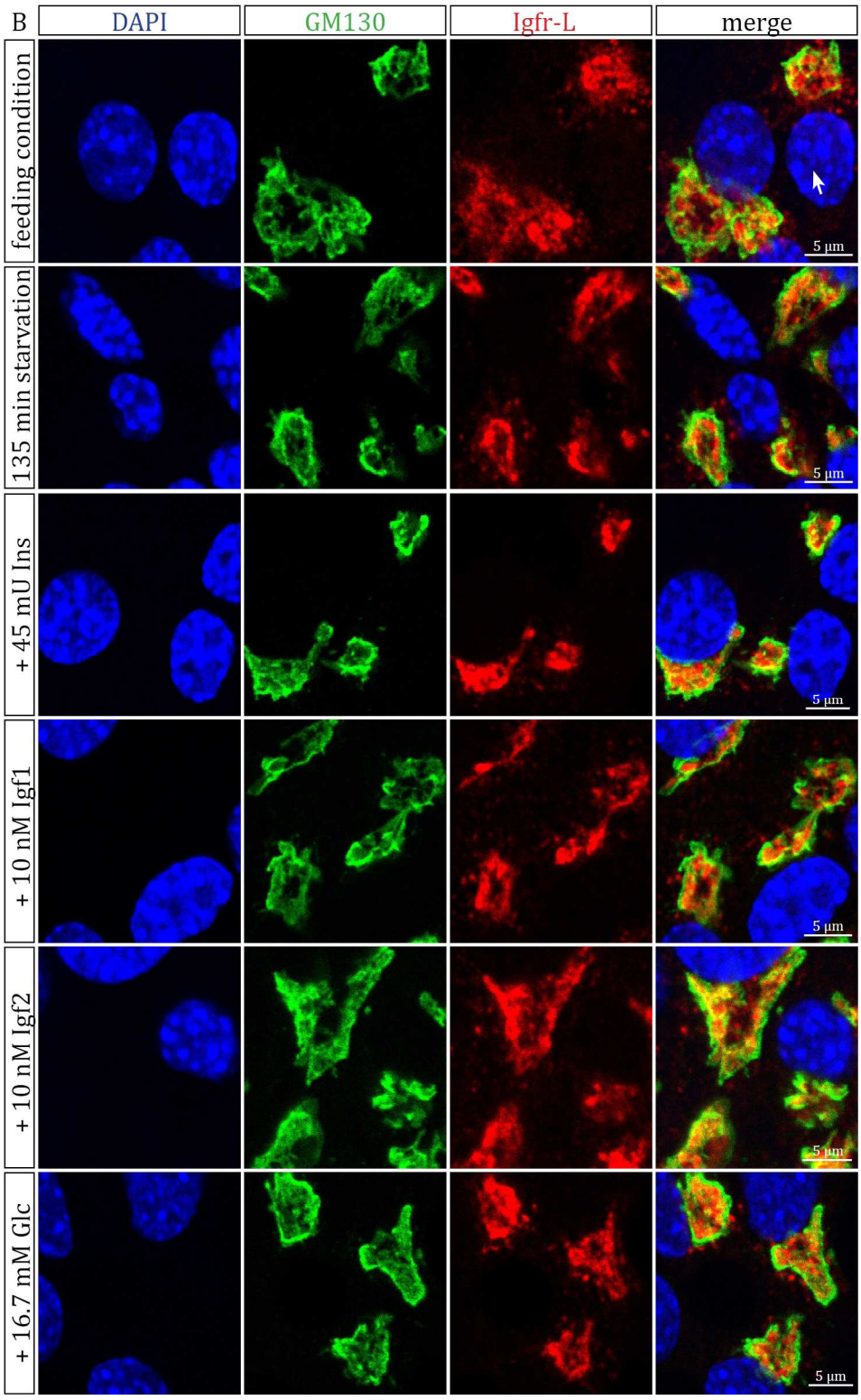

Figure 4.43: Igfr-L "contracts" its subcellular distribution to the compacted Golgi complex caused by nutrient deprivation.

(A) WT Min6 cells were cultured in feeding condition or starved for 120 min and subsequently stimulated with 45 mU Ins, 10 nM Igf1 and 10 nM Igf2 ligand or 17 mM glucose for 15 min.

(B) Representative laser scanning microscopy (LSM) images of WT Min6, which were exposed to the stimulation assay. Cells were coimmunostained with antibodies against Igfr-L (red) and the *cis*-Golgi (Gm130, green).

To further explore a possible interdependency of Igfr-L and the Ins/Igf signalling, we performed a si-RNA-mediated knock-down of Igfr-L in Min6 cells and examined subcellular distribution of insulin and Igf2r proteins using an immunofluorescence approach (Figure 4.44A,B). However, no change in localization was detected for either Igf2r or Ins in Igfr-L-depleted cells.

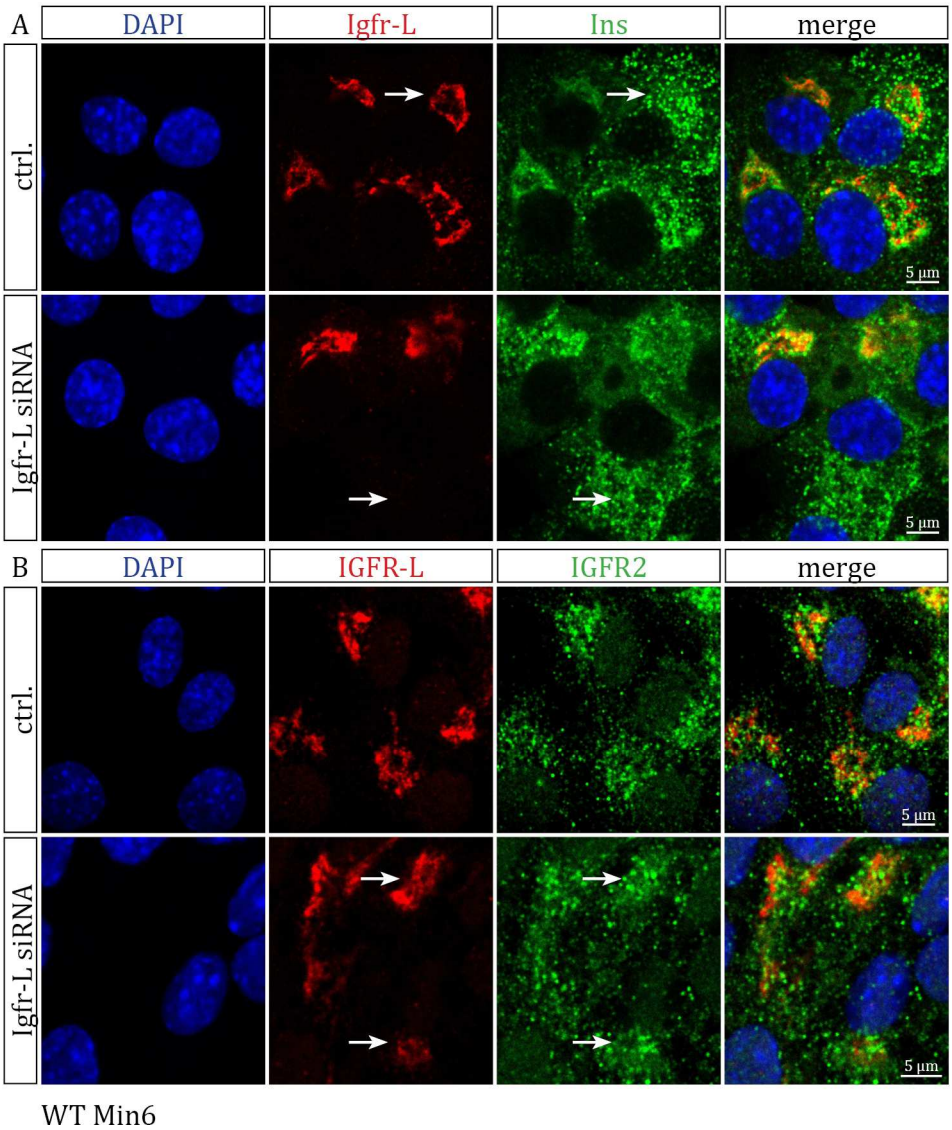

Figure 4.44: siRNA mediated knock-down of Igfr-L does not affect subcellular localization of insulin or Igf2r.

(A, B) Immunofluorescence images of WT Min6 cells cultured in control conditions and upon siRNA mediated knock-down of Igfr-L.

4.3.5.5 Plasma membrane localized Igfr-L is potentially internalized by clathrin-mediated endocytosis and is mainly directed to the Golgi complex after internalization from the cell surface

Previous experiments demonstrated the localization of Igfr-L at the plasma membrane and in the different compartments of the secretory pathway (Figure 4.39), proving that the Igfr-L travels through the membranous network within the cell.

To understand trafficking dynamics of the Igfr-L in greater detail, we studied the endocytosed receptor pool by performing endocytosis assays in WT Min6. Living cells were incubated at 4 °C for 30 min to inhibit endocytic processes (Figure 4.45A). We complemented the culture medium with an Igfr-L antibody, which recognizes the extracellular domain of the Igfr-L protein (Igfr-L ecto). This enables receptor-antibody binding at the cell surface. After replacing the medium with antibody free culture medium, cells were placed at 37 °C for up to 60 min allowing the receptor-antibody complex to be endocytosed by the cell. In subsequent immunofluorescence stainings the endocytosed Igfr-L ecto antibody was detected by a fluorescently labelled secondary antibody. Additionally, we coimmunostained cells with antibodies against the Igfr-L protein and the *cis*-Golgi (Gm130), the lysosomal marker Lamp2 and Cm1 that labels native coatomer complexes (Figure 4.45C,D). Afterwards, Igfr-L trafficking velocity and routing was determined by quantifying the colocalization with these markers (PCC values) over time (Figure 4.45E). To exclude that the Igfr-L ecto antibody does not unspecifically interact with other proteins at the plasma membrane, receptor endocytosis was controlled using Igfr-L KO cells (Figure 4.45B). Further, we excluded a potential influence of the serum components by treating control cells with pre-immune serum during the endocytosis assay. At time point zero, the antibody bound Igfr-L is situated at the plasma membrane (Figure 4.45C, white arrow). As time proceeds, the receptor rapidly travels into the cytoplasm most likely carried by membranous vesicles since it is detected as dots. Within the first 15 min, the receptor is found throughout the cytoplasm with first receptor dots reaching the Golgi area (Figure 4.45C). After 30 and 60 min, the endocytosed receptor pool mainly concentrates in the Golgi complex strongly overlapping with the *cis*-Golgi marker GM130 (Figure 4.45C).

A

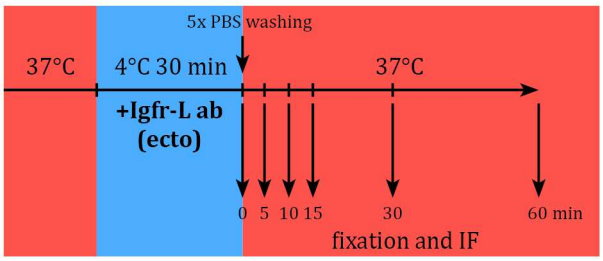

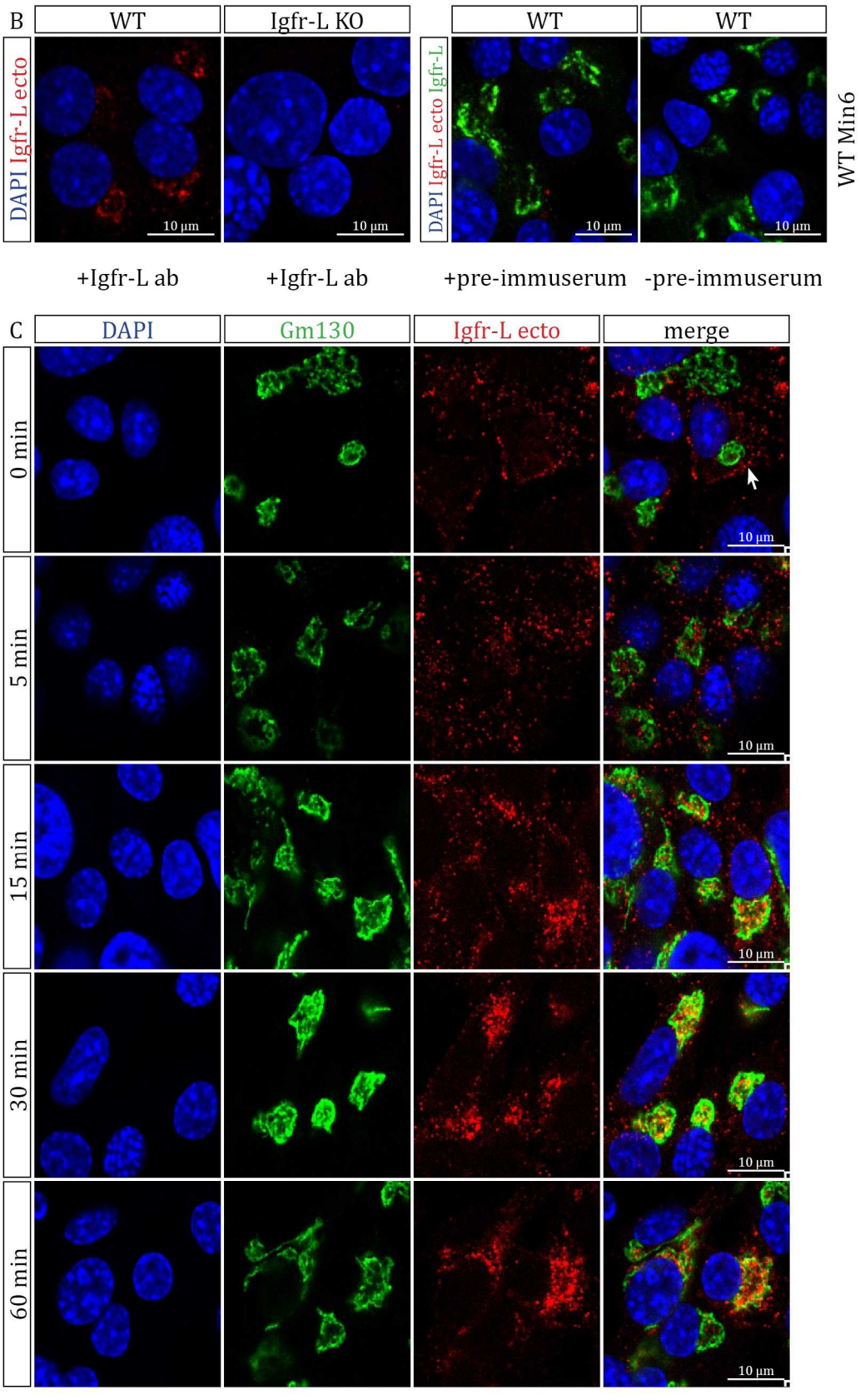
B
WT
Igfr-L KO
WT
WT
DAPI Igfr-L ecto
DAPI Igfr-L ecto Igfr-L
WT Min6
10 µm
+Igfr-L ab
+Igfr-L ab
+pre-immuserum
-pre-immuserum
C
DAPI
Gm130
Igfr-L ecto
merge
0 min
5 min
15 min
30 min
60 min
WT Min6

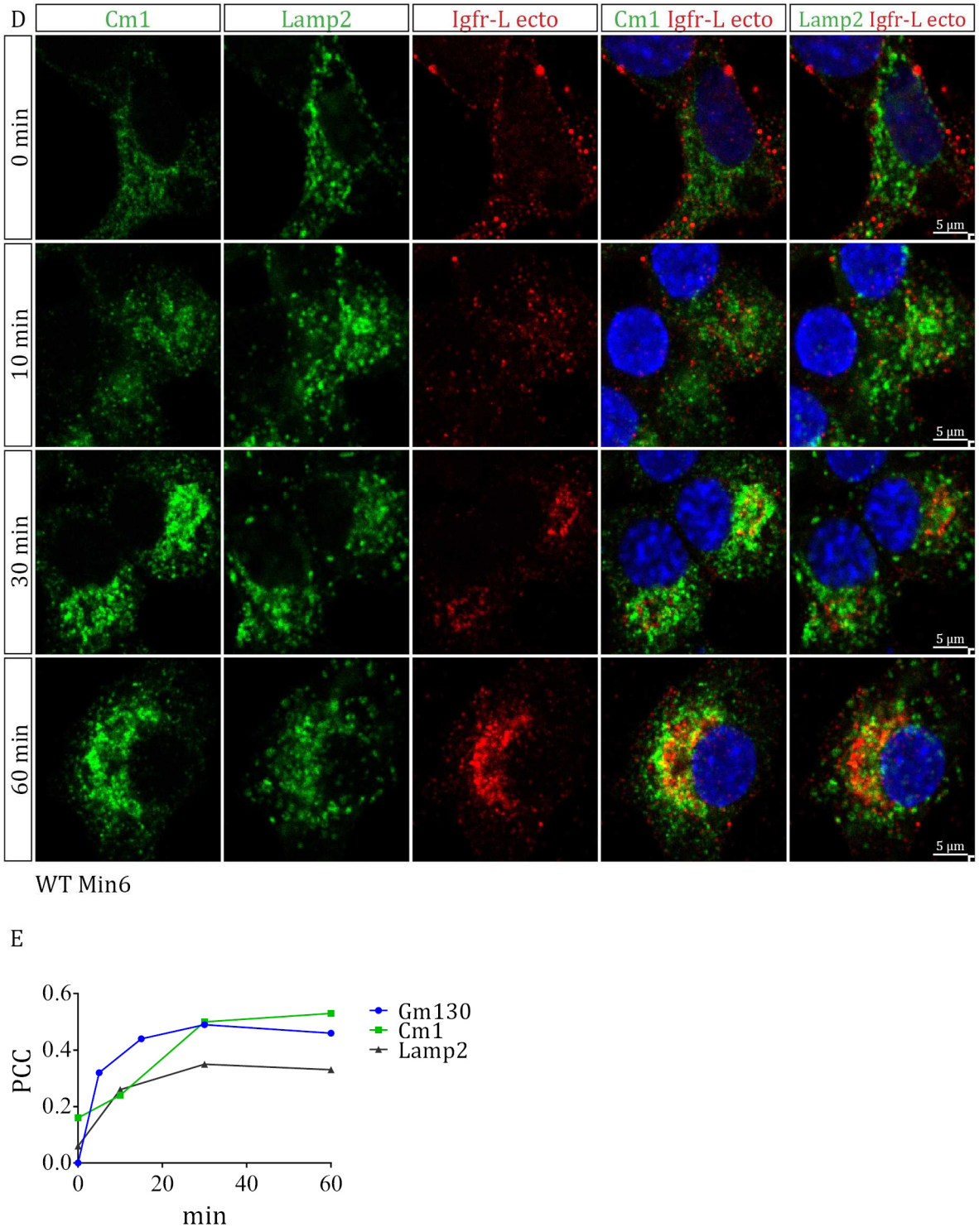

Figure 4.45: Igfr-L is primarily transported from the plasma membrane to the Golgi complex after endocytosis.

(A) Experimental design for the endocytosis assay in WT Min6 cells presented in (B-D). Cells were cultured in feeding medium complemented with IGFR-L ecto antibody at 4 °C for 30 min. This allows antibody binding to the ectodomain of the Igfr-L receptor at the cell surface. After removing the Igfr-L antibody from the medium cells were incubated at 37 °C for 0, 5, 10, 15, 20, 30 or 60 min. The antibody-receptor complex is endocytosed by the cell.

(B) LSM images of WT and Igfr-L KO Min6 cells for which an endocytosis assay was performed (60 min time point). Unspecific endocytosis of the Igfr-L ecto antibody and unspecific effects of serum proteins (unpurified Igfr-L antibody) was controlled.
(C) Representative Immunofluorescence images of WT Min6 at endocytosis time points 0, 5, 15, 30 and 60 min.
(D) Representative LSM images of WT Min6 at endocytosis time point 0, 10, 20, 30 and 60 min.
(B-D) Endocytosed Igfr-L ecto antibody (red) was coimmunostained with the *cis*-Golgi marker Gm130, the lysosomal marker Lamp2 or the coatomer marker Cm1 (green).
(E) The Pearson correlation coefficient (PCC) was calculated to determine colocalization of Igfr-L with Gm130, Lamp2 and Cm1 using ImageJ plugin Fiji Coloc2 (Costes background subtraction). (n = 2 (experimental weeks) for Cm1 and n = 1 for Lamp2 and GM130, mean)

A slightly delayed overlap was observed for the Igfr-L/Cm1 colocalization study (Figure 4.45D). Cm1 marks vesicles, which are trafficking retrograde from the Golgi and to the ER compartment whereas the GM130 antibody labels *cis*-Golgi membranes. This might suggest that the Igfr-L is routed from the peripheral sites of the secretory pathway to the cis-Golgi area via coated vesicles of a different pathway before it is also found in COPI coated vesicles. Coimmunostainings with Lamp2 aimed to clarify if the receptor also travels to the lysosomal compartments after endocytosis (Figure 4.45D). In fact, a smaller receptor fraction was also routed to the lysosomal area.

Collectively, these observations indicate that the Igfr-L is mainly directed to the Golgi apparatus after internalization from the cell surface but is also partially transported to the lysosome.

The major mechanisms mediating receptor internalization at the plasma membrane are clathrin-mediated endocytosis (CME), caveolae-dependent endocytosis (CDE) and micropinocytosis. These pathways dynamically control receptor signalling by regulating their internalization and subcellular routing (Barbieri, Di Fiore, & Sigismund, 2016). By immunofluorescence study, we investigated the endocytic pathway mediating Igfr-L internalization. WT Min6 cells were coimmunostained with antibodies against the Igfr-L and caveolin-1 (Cav1), a coat protein enriched in caveolar vesicles (Figure 4.46A,B). A PCC coefficient of -0.07 signifies no overlap of both markers despite a MOC value of 0.54 suggesting that the receptor might not use CDE.

A

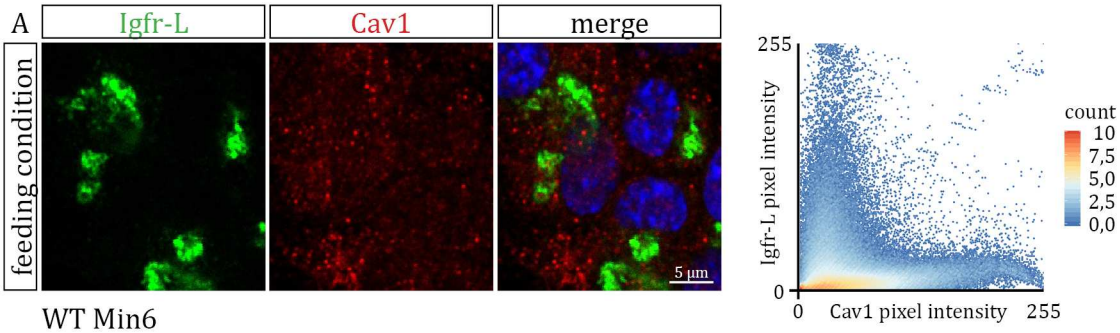

B

Channel (Ch)/ Image		Pearson correlation coefficient (PCC)	Mander's overlap coefficient (MOC)	
1	**2**	Pearson's R value (above Costes threshold)	Manders' tM1 (above Costes threshold of Ch2)	Manders' tM2 (above Costes threshold of Ch1)
Cav1	**Igfr-L**	-0.07	0.35	0.54

Figure 4.46: Igfr-L is likely not internalized by caveolae mediated endocytosis.

(A, B) Representative laser scanning microscopy (LSM) images of WT Min6 cells (A). Igfr-L (green) was coimmunostained with cavoelin1 (red). The degree of colocalizing marker signal is represented by a scatter plot (A), the Pearson correlation coefficient (PCC) and the Mander's overlap coefficient (B). Calculations were performed using ImageJ plugin Fiji Coloc2 (Costes background subtraction). The scatterplot depicts colocalized pixel intensity detected for both channels of the merged image. Intensity counts are plotted in log scale and are colour coded (red high and blue low number of counts). (n2 (experimental weeks), mean)

To further explore if the Igfr-L utilizes CME or clathrin-independent endocytosis (CIE) pathways, we blocked endocytosis in WT Min6 using pathway specific inhibitors (Figure 4.47A). Cells were separately incubated with different types of drugs at 37 °C for 60 min. Subsequently, we supplemented the culture medium with an Igfr-L antibody, which specifically recognizes the extracellular domain of the receptor (Igfr-L ecto antibody). The antibody receptor complex was endocytosed from the cell surface within the next 30 min. The cellular distribution pattern of endocytosed and total receptor was analysed by coimmunostaining cells with the *cis*-Golgi marker Gm130. Methyl-β-cyclodextrin acts on lipid rafts where it removes cholesterol from the membrane, thus interfering with both, CME and caveolae vesicle formation (Dutta & Donaldson, 2012). Inhibition with this drug caused the accumulation of Igfr-L at the plasma membrane (Figure 4.47B, white arrow). To confirm that Igfr-L is not transported by caveolae-dependent endocytosis, cells were exposed to Filipin-III. At low concentration, this compound inhibits CIE by binding to sterols in the membranes (Dutta & Donaldson, 2012). Filipin III mediated inhibition did not induce obvious subcellular localization changes of the total and the endocytosed receptor pool in relation to no-inhibitor and dimethyl sulfoxide (DMSO) control samples. Chlorpromazine blocks CME by translocating the scaffold protein AP2 from the cell surface to intracellular endosomes (Dutta & Donaldson, 2012). Igfr-L exhibits a more vesicular and less condensed cellular distribution pattern within and surrounding the Golgi area upon chlorpromazine inhibition (Figure 4.47, white arrow). The receptor did not concentrate at the plasma membrane

as it was observed upon Methyl-β-cyclodextrin inhibition probably due to differences in the mode of action of the two drugs. In summary, our data suggest that the internalization of Igfr-L occurs through CME.

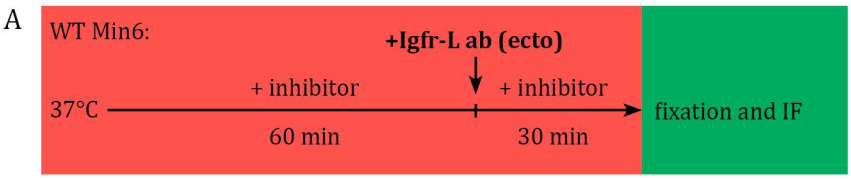

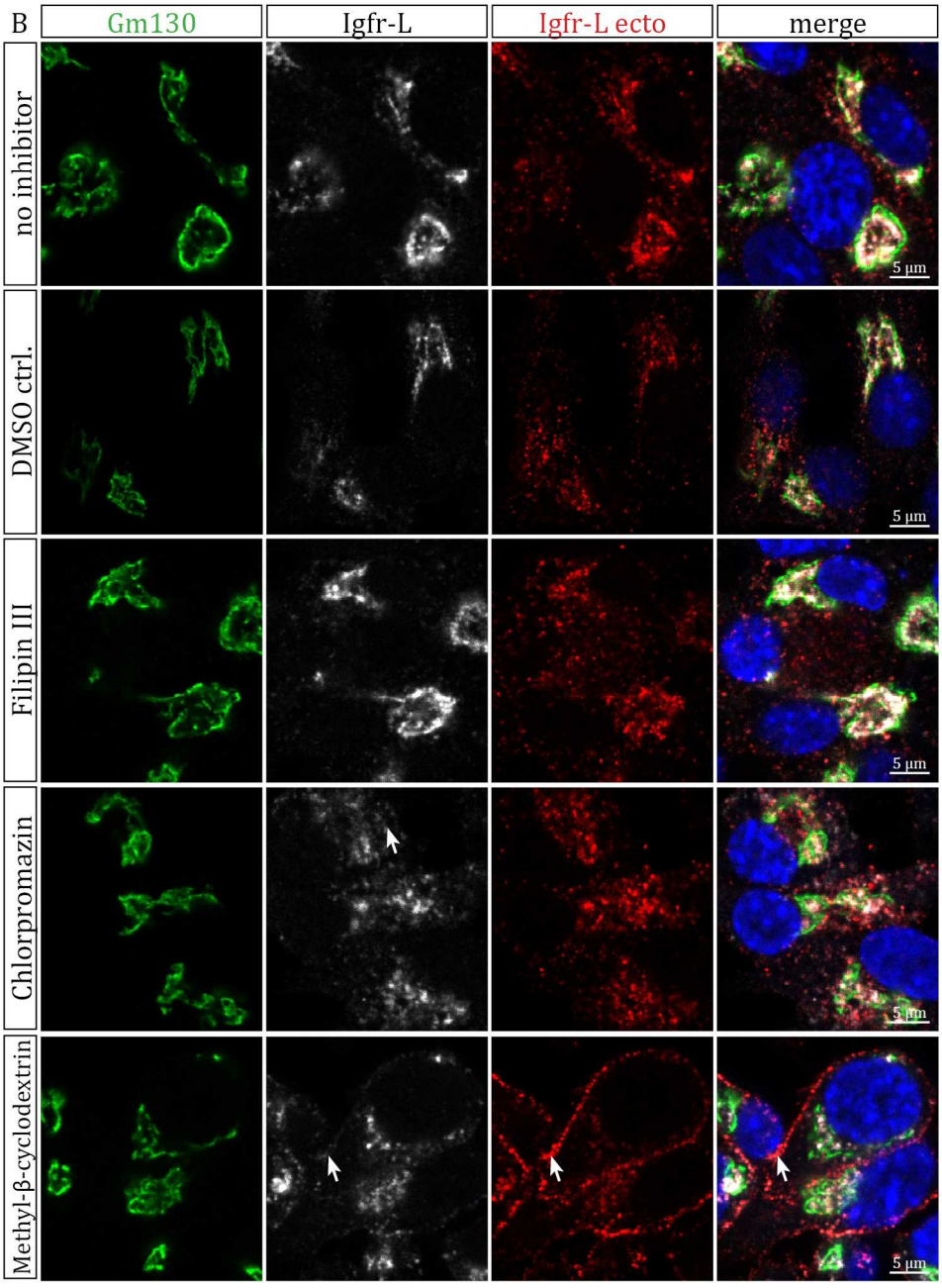

WT Min6

Figure 4.47: Igfr-L is likely internalized by clathrin-mediated endocytosis.

(A) Experimental overview of the endocytosis assay in WT Min6 cells presented in (B).
Cells were cultured in inhibitor complemented medium for 90 min. (3 µg/ml Filipin III, 15 µM Chlorpromazin, 10 mM Methyl-β-cyclodextrin) In the last 30 min Igfr-L ecto antibody was added to the culture medium. This allows Igfr-L antibody (Igfr-L ecto) binding to the ectodomain of the Igfr-L receptor at the cell surface and subsequent internalization of the antibody-receptor complex.
(B) Representative LSM images of WT Min6, which were exposed to the endocytosis assay. Internalized Igfr-L ecto antibody (red) was coimmunostained with the cis-Golgi marker Gm130 (green) and an Igfr-L antibody detecting the total protein (Igfr-L total, white). White arrows indicate abnormal receptor localization in inhibitor treated cells.

Receptor tyrosine kinases (RTKs) and other integral membrane proteins undergo constitutive endocytosis. Internalization, recycling and degradation rates depend on the nature of RTKs, the cell type, ligand availability and the metabolic state of the cell (Goh & Sorkin, 2013). Previous experiments indicated a change in trafficking dynamics of Igfr-L upon nutrient deprivation (Figure 4.43). To specify if plasma membrane location of the Igfr-L is metabolically regulated, we performed surface biotinylation assays in WT Min6 cells (Figure 4.48A). We starved cells in HBSS buffer with or without 25 mM glucose (no growth factors) for 15, 30, 60 and 120 min. Following, Min6 cells were cooled to 4 °C to inhibit endocytic processes and incubated in N-hydroxysulfosuccinimide (NHS)-biotin complemented buffer for 10 min enabling biotin to bind to cell surface proteins. NHS-biotin is a cell impermeable compound that covalently attaches biotin to proteins by modifying exposed primary amino groups through its succinimidyl (NHS) estergroup. Using a neutravidin-IP pull down assay, biotin-labelled plasma membrane proteins were isolated exploiting the high binding affinity of biotin for streptavidin. Subsequently, we performed Western blotting to detect the protein of interest. To assure that these alterations in surface localization did not result from changes in protein expression, input lysates were also analysed. Our data showed that the InsR stays at the cell surface during starvation but slightly withdraws from the membrane after 120 min (Figure 4.48B). Interestingly, the Igfr-L retracted from the plasma membrane upon nutrient deprivation but remained longer at the cell surface when cells were exposed to high glucose concentrations. Further investigation will clarify whether the starvation process and the presence of glucose induces higher receptor internalization or supresses recycling to the plasma membrane (Figure 4.48C).

Taken together, the Igfr-L is mainly directed to the Golgi apparatus after endocytosis in feeding conditions with a subpopulation of receptor traveling to the lysosome. Receptor trafficking routes are likely to be regulated by the CME pathway. Furthermore, the abundance of Igfr-L at the plasma membrane seems to be regulated by nutrient deprivation and the presence of glucose.

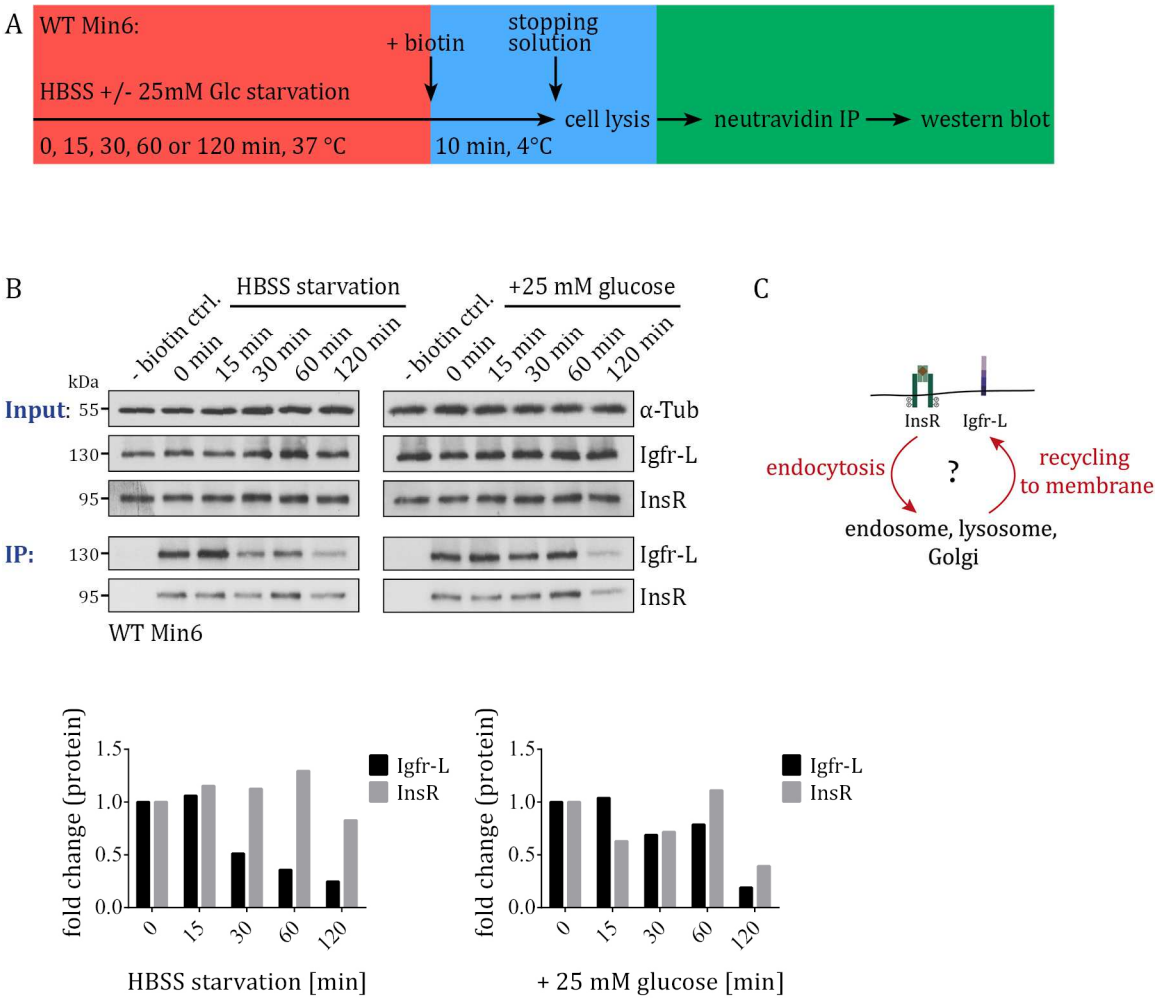

Figure 4.48: Plasma membrane localization of Igfr-L is regulated by starvation and glucose.

(A) Schematic image of the experimental procedure: Min6 cells were cultured in HBSS starvation medium complemented with 0 or 25 mM glucose for 0, 15, 30, 60 and 120 min. NHS-biotin was added to the buffer for additional 10 min (4 °C) enabling biotin to covalently attach to surface proteins. The temperature drop prevents internalization of biotinylated proteins. Subsequently, biotin bound proteins were isolated from the lysate by a neutravidin immunoprecipitation (IP) and detected via Western blot.
(B) Western blot analysis of neutravidin IP including quantification. (n = 2 experimental weeks)
(C) Schematic picture of InsR and Igfr-L plasma membrane (PM) localization and their possible trafficking routes.

5 Discussion

5.1 The ARL13B-tRFP cilia reporter is a valuable tool for the analysis of ciliary biology

We generated and extensively validated a novel Cre-inducible knock-in cilium reporter mouse line expressing the ARL13B-tRFP fusion protein, which labels cilia with a bright fluorescence protein. Using immunostainings, we confirmed bright and specific reporter expression in cilia of mono and multi-ciliated tissues including pancreatic islets, ependyma in the brain, respiratory epithelium and the embryonic node. Also, the reporter provides the advantage to perform time-lapse analysis as demonstrated by live-cell imaging of cilia in cultured embryos and organ explant cultures. Live-cell imaging was possible over several hours without observing obvious bleaching of the fluorescence signal. In contrast to other previously published cilium mouse reporters such as *Arl13b-EGFP^{tg}*, *hArl13b-mCherry-GECO1.2* (Delling et al., 2013) and ARL13B-mCherry (Bangs et al., 2015) mice, reporter expression in ARL13B-tRFP animals is Cre-inducible allowing the analysis of cilia in a temporally- and spatially-controlled manner. The ARL13B-tRFP reporter mouse also differs from other cilia reporter in various other aspects. It contains a tRFP that can be combined with GFP, a frequently used reporter protein, which is a clear advantage over the CiliaGFP (Sstr3::GFP) (O'Connor et al., 2013) and *Arl13b-EGFP^{tg}* (Delling et al., 2013) reporter mouse lines. In addition, we verified that male mice with germline expression (ARL13B-tRFP^{Rosa}) are viable and fertile in comparison to CiliaGFP animals.

Furthermore, there are multiple applications possible for this mouse model to investigate cilia biology. We verified that Hh signalling was unaffected upon ligand stimulation in reporter expressing cells suggesting a functional cilium despite transgenic reporter expression. The ARL13B-tRFP reporter allows the investigation of processes such as ciliary protein trafficking, cilium-dependent signalling and the analysis of ciliary structure. Thus, the reporter can be used for assessing Hh signalling in the pancreatic β-cell and its influence on glucose metabolism. Additionally, we monitored cilium assembly and disassembly in embryonic fibroblast cells using live-cell imaging. Ciliogenesis and cell-cycle progression are tightly linked, but many aspects of this reciprocal relationship are still unclear. Cilia assemble when cells exit the cell cycle as a result of mitogen deprivation or differentiation cues, whereas cilia disassembly occurs after mitogen stimulation of quiescent cells (Goto, Inaba, and Inagaki 2017; Sanchez and Dynlacht 2016). The analysis of cilia using the ARL13B-tRFP reporter might shed light on the interdependency of primary cilia and cell proliferation.

Moreover, Flattop (Fltp) is a basal body docking protein essential for cilia positioning (Gegg et al., 2014). Fltp expression in the endocrine pancreas defines a subpopulation of β-cells with mature features in comparison to proliferation-competent cells. These two populations differ in distinct molecular, physiological and ultrastructural features (Bader et al., 2016). β-cells with higher proliferative potential should be less ciliated than mature cells due to the reciprocal relationship of cell cycle and ciliogenesis. To verify this hypothesis, the cilium reporter mouse model can be applied.

The analysis of cilia using the reporter mouse model might also lead to a better understanding and characterization of ciliopathies including Bardet–Biedl syndrome (BBS) and Alström syndrome (ALMS). Beside other symptomes, BBS and ALMS patients display metabolic disorders, obesity and T2D related symptoms. In recent years, the role of primary cilia and related proteins in energy homeostasis became focus of scientific attention due to the high incidence of obesity and T2D in patients and mouse mutants with compromised ciliary function. A major regulator in glucose metabolism is the pancreas with its insulin secreting β-cells. β-cells as well as ductal cells of the pancreas are ciliated. Many ciliopathies that affect the pancreas manifest pancreatic cysts originating from duct cells, pancreatic duct dilation or an enlarged pancreas. (Oh, Vasanth, & Katsanis, 2015). The impact of defective cilia or related proteins on the endocrine pancreas is less well understood. Beside pancreatic ductal defects in mice, the deletion of regulatory factor X 3 (RFX3) and Gli similar proteins 3 (Glis3) genes, which are transcription factors essential for normal ciliary function, result in declined insulin secretion with impaired glucose tolerance (Ait-Lounis et al., 2007; H. S. Kang et al., 2009). However, it is unclear if observed phenotype is a direct or indirect effect caused by ciliary proteins functioning both at the cilium and other organelles. Gerdes et al., 2014 reported that young Bardet–Biedl syndrome 4 $(Bbs4)^{-/-}$ mice displayed impaired glucose handling before the onset of obesity. *In vivo* and *ex vivo* insulin secretion tests showed severely blunted first-phase insulin secretion in $Bbs4^{-/-}$ mice relative to controls. They also observed that the InsR is transported to the cilium in insulin stimulated β-cells and that ciliary/basal body integrity is necessary for activating Akt and PI3K, key factors of insulin signalling. They further demonstrated that Goto–Kakizaki rats, which constitute a T2D model, exhibited less ciliated β-cells and dysregulated ciliary/basal body gene expression in pancreatic islets (Gerdes et al., 2014).

In conclusion, the cilium-reporter mouse line is a versatile and valuable tool for the investigation of cilium biology *in vitro* and *in vivo*. This might give insight in pathomechanisms of obesity and T2DM associated with ciliopathies.

5.2 Relevance of Hh signalling in the islet of Langerhans and its implication on glucose metabolism

One of the pathways that is orchestrated at the cilium is Hh signalling. In recent years, the functional role of Hh signalling in the pancreas was subject of controversial debate since the absence of Shh signalling is required for the early development of the pancreas. Activin, a ligand of the transforming growth factor β (Tgfβ) signalling pathway, permits budding of the developing dorsal pancreatic anlage from the posterior foregut endoderm by repressing Shh signalling (Hebrok, Kim, & Melton, 1998). However, there has been increasing evidence in the literature that Hh signalling is not only required for the normal development of the pancreas, but is also necessary for the proper function of the mature organ, especially the islet of Langerhans (Cervantes, Lau, Cano, Borromeo-Austin, & Hebrok, 2010; L. Landsman et al., 2011; Limor Landsman, Parent, & Hebrok, 2011).

The key receptors of Hh signalling, Ptch and Smo, as well as members of the Hh family of signalling molecules, Ihh and Dhh, are expressed in pancreatic endocrine cells of adult mice (Hebrok et al., 2000; M K Thomas, Rastalsky, Lee, & Habener, 2000). We confirmed the expression of Hh signalling components in pancreatic endocrine cells including key genes such as *Smo*, *Ptch*, *Pifo*, *Gli1* and *Gli3* that are crucial for Hh pathway activity. Smo localized to the cilium implied active Hh signalling in endocrine cells. Using the *Tg(GBS-eGFP)* reporter mouse model, we demonstrated that a heterogeneously distributed, small subpopulation of pancreatic endocrine cells, including all types of hormone expressing cells, displayed Hh signalling. Isolated islets were competent to receive Hh signalling after ligand stimulation *in vitro*. However, we only observed single cells with active Hh pathway in the exocrine pancreas *in vivo*. In some pericytes and endothelial cells of the exocrine pancreas, we detected eGFP expression, suggesting Hh pathway activation. Endothelial cells line the interior surface of blood vessels and lymphatic vessels, whereas pericytes are contractile cells, which partially envelop endothelial cells, thereby regulating capillary blood flow and the maturation of endothelial cells (Bergers & Song, 2005). The Hh signalling cascade is important for the bidirectional signalling of endothelium and pericytes. It is also involved in vasculogenesis during development and in ischemia-induced postnatal neovascularization (Fabian et al., 2012; Nagase, Nagase, Machida, & Fujita, 2008; Pola et al., 2001; Straface et al., 2009). At a cellular level, recombinant Shh was shown to induce proliferation and survival of mural cells including pericytes and smooth muscle cells (F. Li et al., 2010; G. Wang et al., 2010). Thus, Hh signalling might play a role in vessel formation and in the crosstalk of pancreatic endothelial cells and pericytes in the endo- and exocrine pancreas.

Furthermore, Hh signalling was shown to induce cell proliferation in a variety of processes including cancer and embryonic development (Briscoe & Thérond, 2013; Pak & Segal, 2016). Constitutive activation of the Hh pathway was detected in pancreatic cancer, where it contributes to the induction of a malignant phenotype, is responsible for maintaining pancreatic cancer stem cells and stimulates cell proliferation and metastasis (Bai et al., 2016; HAO, TIAN, QIN, XIE, & YANG, 2013; Onishi & Katano, 2014). So far, it was unclear if Hh signalling also regulates cell cycle progression in pancreatic α and β-cells. We showed that Shh ligand stimulation induced cell proliferation in pancreatic islet cells *in vitro* using immunofluorescence analysis. Recently, Wang et al. 2016 claimed that replicating α-cells display active Hh signalling. Using single cell transcriptomics of human endocrine pancreas, they found one proliferating α-cell expressing Hh pathway components in a non-diabetic adult donor sample when comparing proliferating and quiescent α-cells (Y. J. Wang et al., 2016). Using the GBS-GFP reporter, we also demonstrated that few α and β-cells exhibited Hh signalling *in vitro*. These findings might indicate that Hh signalling induces cell proliferation of pancreatic α and β-cells.

Moreover, we observed a slight insulin secretion defect of isolated islets derived from $Kif7^{+/-}$ mice. However, this effect was likely compensated *in vivo* since $Kif7^{+/-}$ animals exhibited normal glucose metabolism relative to WT controls. Nevertheless, many published studies imply a potential role of Hh signalling in the regulation of glucose metabolism. Ectopic Hh signalling in the β-cell induced by a constitutively activated version of Gli2 and β-cell specific ablation of the primary cilium entailed the formation of a dedifferentiated β-cell population expressing progenitor

markers in three weeks old mice. At later stage, these dedifferentiated β-cells developed insulin secretion defects leading to a glucose intolerant state of transgenic animals (Limor Landsman et al., 2011). A mutated version of the *Ptch1* gene or a heterozygous state for *Ptch1* in mice caused the decrease of both the endocrine and exocrine cell mass in the pancreas (Nakayama et al., 2008). Additionally, adult *Ptch1* heterozygous mice, exhibiting increased levels of Hh signalling, displayed impaired glucose homeostasis (Hebrok et al., 2000). In contrast, mutant mice with Smo eliminated in the pancreatic epithelium (Pdx1 Cre Smo $^{flox/null}$), which led to decreased Hh activity, showed reduced insulin secretion and suffered from glucose intolerance and elevated insulin sensitivity (J. Lau & Hebrok, 2010). Mice with a hypomorphic deletion of Pifo displayed an impairment in insulin secretion of pancreatic β-cells and developed glucose intolerance under HFD condition as a result of β-cell mass decline caused by a reduced cell proliferation (PhD thesis Daniela Padula, 2014, Helmholtz Zentrum München). Gprasp2 mutant mice exhibited obesity after five months of age under normal chow conditions with an increase in islet size and hepatosteatosis. However, upon HFD feeding, animals overcame obesity with lower basal glucose levels after fasting and glucose intolerance as well as defects in the insulin secretion pathway when compared to WT controls (PhD thesis Daniela Padula, 2014, Helmholtz Zentrum München). Thomas et al., 2000 studied mechanistic details of Hh signalling in β-cells showing that ectopic expression of Shh increases rat insulin I promoter activation in INS-1 cells, thus promoting insulin production and secretion at transcriptional level (M K Thomas et al., 2000). These results support the notion that Hh signalling regulates insulin production and secretion in normal adult β-cells.

In summary, our data and the literature implicate that Hh signalling plays a role in the adult pancreas and in the regulation of glucose homeostasis. Moreover, Hh signalling likely regulates proliferation in β-cells. Thus, the Hh pathway could be therapeutically targeted to increase β-cell mass in diabetic patients.

5.3 Igfr-L, a putative modulator of the InsR/Igfr system and glucose homeostasis

To identify novel regulators of the endocrine lineage in the pancreas, we performed a mRNA expression profile using a microarray-based screen. We found that the Igfr-L is differentially expressed in pancreatic epithelium of E14.5 embryos relative to the mesenchyme. Several lines of evidence suggested that this novel receptor might be important for β-cell development and/or function as well as for the control of systemic metabolism. Firstly, the Igfr-L is specifically expressed in the pancreatic epithelium during the secondary transition of the pancreas. Secondly, the receptor exhibits a domain structure similar to receptor tyrosine kinases and the Igf2r. Last, GWAS studies revealed that the human IGFR-L locus associates with dysbalanced cholesterol metabolism, deregulated insulin sensitivity, coronary artery disease and T2D. Therefore, we analysed the function of Igfr-L in InsR/Igfr signalling and in glucose homeostasis.

5.3.1 Potential causes for postnatal death of Igfr-L$^{-/-}$ pups

To investigate the biological function of the *Igfr-L* gene *in vivo*, we generated Igfr-L$^{-/-}$ mice. Remarkably, Igfr-L$^{-/-}$ mice die postnatally within the first hours of life. It has been shown that a plethora of factors can affect physiological processes in the body causing death in neonates including cardiac, neuromuscular, pulmonary, skeletal, epidermal and renal defects as well as metabolic and endocrine dysregulations. Phenotypical features observed in several new-born KO mouse models are suckling defects, respiration problems, dehydration, weakness and hypoglycaemia (Turgeon & Meloche, 2009). Igfr-L$^{-/-}$ neonates displayed signs of lethargy, hyperinsulinemia, hypoglycaemia, respiratory distress and cyanotic episodes with bluish discoloration of the skin implying a potential respiratory, pulmonary, cardiac or metabolic phenotype (PhD project Fataneh Fathi Far, IDR, Helmholtz Zentrum, Munich). The Igfr-L is highly expressed in the pancreatic epithelium during the secondary transition at E14.5 suggesting an involvement of Igfr-L in the endocrine lineage formation of the pancreas. However, E18.5 Igfr-L$^{-/-}$ pups did not exhibit obvious morphological abnormalities in organs such as the pancreas, lung and the cardiovascular system. Additionally, we observed that the majority of mutant neonates lacked milk in their stomach that might be indicative for abnormal feeding behaviour. For instance, it was demonstrated, that ablation of the huntingtin-associated protein 1 (*Hap1*) gene leads to early postnatal death caused by a decrease in food intake (Chan et al., 2002; Sheng et al., 2006). Premature death caused by the inability to feed is not only due to the absence of nourishment, but can also be a result of dehydration since the liquid derived from the milk is essential for homeostatic processes in new-born pups (Papaioannou & Behringer, 2005). The Igfr-L is highly expressed in the hypothalamic region of the brain, which controls the appetite and food intake implying a potential impaired feeding behaviour. A balanced energy homeostasis is crucial for the survival of pups. Before birth, embryonic homeostasis including nutrient supply, metabolic exchange and waste disposal, is regulated by the maternal placenta. Mutations in genes controlling glucose metabolism in neonates was shown to be causative for postnatal death. For example, eIF2α mutant pups develop severe hypoglycaemia by 6-8 hours after birth due to a reduced glycogen storage and the inability to induce gluconeogenesis efficiently, a phenotype shown to be independent of suckling problems (Scheuner et al., 2001). A key organ in the regulation of glucose homeostasis is the endocrine pancreas. The hyperinsulinemia, observed in Igfr-L mutant pups, is likely due to elevated insulin secretion from pancreatic β-cells leading to hypoglycaemia. The analysis of pancreata, isolated from Igfr-L$^{-/-}$ animals at P0, revealed a significant increase in mRNA expression levels of several insulin and glucose metabolism-associated genes including *InsR*, *Sstr3* and *Slc30a8*, confirming a dysregulated energy homeostasis. Furthermore, symptoms such as lethargy, respiratory distress and cyanotic episodes observed in Igfr-L mutant pups, might also be a symptom of hypoglycaemia. Similar phenotypes were found in high mobility group protein 1 (Hmgb1) mutant animals, which exhibit hypoglycaemia after birth resulting in death within 24 hours despite normal nursing by the mother (Bianchi et al., 1999). Hmgb1 is a chromatin protein that organizes DNA and controls gene transcription, thereby regulating inflammatory processes.

To conclude, the Igfr-L is highly expressed in endo- and exocrine tissues. Therefore, the dysfunction of any of these organs can lead to postnatal lethality. A detailed CKO analysis needs to follow to pinpoint the tissue-specific function of the gene. However, it is likely that the pancreas, which regulates systemic glucose control or the hypothalamus that regulates feeding behaviour, are the primary cause. First data indicated that the β-cell specific deletion of Igfr-L (Ins1CreERT) leads to a slight hypoglycaemia and to enhanced glucose tolerance, which coincides with the phenotype of Igfr-L$^{-/-}$ neonates.

5.3.2 Influence of Igfr-L on energy homeostasis

We further investigated a potential involvement of Igfr-L in the control of glucose metabolism by analysing several metabolic parameters in adult heterozygous mice. Male and female Igfr-L$^{+/-}$ animals developed a systemic impairment of insulin sensitivity with a weak glucose intolerance and mildly increased hyperinsulinemia upon 28 weeks of HFD feeding. A slightly elevated insulin secretion in starving condition as well as after glucose administration, already manifested after the first 12 weeks of HFD feeding relative to WT controls. Upon analysing the functional role of Igfr-L in pancreatic β-cells, we observed that the receptor negatively regulates InsR/Igf1r signalling. Likewise, β-cell-specific KO mouse models demonstrated the importance of InsR/Igf1r system-associated genes for glucose homeostasis. Mice with β-cell-specific KO of InsR (β-IRKO) develop progressive glucose intolerance, elevated fasting insulin levels and impaired glucose-induced first-phase insulin secretion (R N Kulkarni et al., 1999a). A similar phenotype was also observed for Igf1r KO animals. Igf1r KO mice acquire an age-dependent impairment of glucose tolerance due to an abolishment in the first phase of glucose-induced insulin secretion (Rohit N. Kulkarni et al., 2002; Xuan et al., 2002). Phenotypical similarities of Igfr-L$^{+/-}$ mice after 28 weeks of HFD feeding and β-IRKO/Igf1r KO animals including mild glucose intolerance and increased plasma insulin levels, suggest that these receptors might function in the same signalling pathway. However, we also detected insulin sensitivity defects in Igfr-L$^{+/-}$ animals in contrast to β-IRKO/Igf1r KO animals that requires further investigation, but might be caused by chronic hyperinsulinemia.

Hyperinsulinemia observed in Igfr-L$^{+/-}$ animals can be induced by an insulin secretion defect of β-cells or an increased β-cell mass. Isolated islets, derived from Igfr-L$^{+/-}$ male animals after 28 weeks of HFD, secreted slightly more insulin upon glucose stimulation relative to WT controls, especially in the first phase of insulin secretion. An enlargement in β-cell mass is often due to a rise in cell proliferation. Although, we detected enhanced β-cell proliferation in Igfr-L KO Min6 cells, we did not detect a significant change in β-cell proliferation in Igfr-L$^{+/-}$ male and female animals. Thus, enhanced insulin secretion is likely the primary cause for hyperinsulinemia detected in Igfr-L heterozygous mice.

Moreover, in T2D patients, insulin resistance plays a key role in the development of dyslipidemia, which includes elevated triglycerides, low HDL cholesterol and relatively normal LDL cholesterol (Goldberg, 2001). A deregulated lipid metabolism often results in an increased fat deposit in peripheral organs. Igfr-L heterozygous animals displayed normal pancreas and epididymal fat

tissue weight as well as unaltered lean-to-fat mass ratio after 28 weeks of HFD feeding. However, Igfr-L$^{+/-}$ female livers were enlarged suggesting fat infiltration, which is consistent with observed impaired insulin sensitivity. Additionally, female animals exhibited declined plasma triglyceride levels, which is unexpected since T2D-induced dyslipidaemia and insulin resistance is usually accompanied by high triglycerides in the blood circulation. Igfr-L KO caused activation of the metabolic sensor Ampk in Min6 cells. Ampk is known to stimulate fatty acid oxidation and ketogenesis and to inhibit lipogenesis, cholesterol synthesis and triglyceride synthesis (Garcia & Shaw, 2017). Short-term overexpression of a constitutively active form of Ampk in hepatocytes, decreased plasma triglyceride levels and induced a fatty liver with unaffected plasma total cholesterol and HDL cholesterol concentrations (Foretz et al., 2005). However, these mice also displayed hypoglycaemia not observed in Igfr-L heterozygous mutant mice. 5-aminoimidazole-4-carboxamide ribonucleotide (AICAR) infusion, an AMP analog, which stimulates Ampk, also resulted in decreased plasma triglycerides (Bergeron et al., 2001). Thus, hyperactivity of Ampk might be causative for decreased plasma triglyceride levels and increased liver size in female Igfr-L$^{+/-}$ animals, suggesting that Igfr-L controls lipid metabolism by an Ampk-dependent mechanism. GWAS association studies further indicated a link between Igfr-L and lipid metabolism as well as energy homeostasis. The *EIG121* locus, the human ortholog of Igfr-L, associates with abnormal cholesterol metabolism, deregulated insulin sensitivity, coronary artery disease and T2D.

Furthermore, there might be other mechanisms how Igfr-L influences glucose metabolism. Igfr-L is highly expressed in the diencephalon, particularly in the arcuate nucleus of the hypothalamus. Further, it is found in the main endocrine glands in the body such as the pituitary gland (hypophysis), the pancreas, adrenal gland and gonads. A well-known interrelationship that functionally connects these organs is the hypothalamic–pituitary–gonadal (HPG) axis and hypothalamic–pituitary–adrenal (HPA) axis. The hypothalamus links the nervous system to the endocrine system via the pituitary gland (hypophysis). Secretion of gonadotropin-releasing hormone (GnRH) from the arcuate nucleus in the hypothalamus stimulates the pituitary gland to secrete gonadotropin hormones, namely follicle-stimulating hormone (FSH) and luteinizing hormone (LH) (Kota et al. 2013; Plant 2015). In the gonads, LH and FSH induce the release of the sex steroids such as androgens and oestrogens regulating gonadal function in both genders. The HPG axis plays a major role in the control of the reproductive system, development, the immune system, aging and energy homeostasis. Upon GnRH stimulation, the anterior pituitary gland also secrets the adrenocorticotropic hormone (ACTH), which induces the secretion of adrenaline and the steroid hormones aldosterone, cortisol and androgens in the adrenal cortex. The HPA axis controls critical steps in digestion, the immune system, emotions, sexuality, energy storage and energy expenditure (Handa and Weiser 2014; Keller-Wood 2015). In conclusion, Igfr-L might regulate energy homeostasis by controlling the endocrine system via HPA/HPG axis associated tissues.

Deng et al., 2005 claimed that oestrogen induces expression of EIG121 (Lei Deng et al., 2005). Oestrogen functions in the hypothalamus to regulate food intake and energy expenditure. In metabolic organs oestrogen is involved in the prevention of lipid accumulation and inflammation

as well as in insulin sensitivity. Global knockout of the oestrogen receptor α (ERα) in both, male and female mice, causes increased body weight and adiposity predominately through reduced energy expenditure and slight increase in food intake. Animals further displayed elevated fasting insulin, impaired glucose tolerance and marked skeletal muscle insulin resistance (Heine, Taylor, Iwamoto, Lubahn, & Cooke, 2000; Ribas et al., 2010). Additionally, oestrogen controls insulin secretion, nutrient homeostasis and survival in pancreatic β-cells (Mauvais-Jarvis, Clegg, & Hevener, 2013; Tiano & Mauvais-Jarvis, 2012). Oestrogen 2 (E2) treatment elevates insulin secretion in perfused rat pancreas and in cultured rodent islets (Faure & Sutter-Dub, 1979; Senzen, 1978). These indications suggest that Igfr-L might be involved in oestrogen-mediated control of energy homeostasis.

Moreover, we found gender-specific differences when analysing metabolic parameters of Igfr-$L^{+/-}$ mice, which were fed a HFD. Oestrogen usually protects against high-fat diet-induced insulin resistance and glucose intolerance in female animals (Riant et al., 2009). However, female Igfr-$L^{+/-}$ mice already manifest impaired insulin sensitivity after 12 weeks of HFD relative to WT controls, whereas Igfr-$L^{+/-}$ males, display deteriorated insulin sensitivity after 28 weeks of HFD feeding. Additionally, only Igfr-$L^{+/-}$ female mice exhibit increased liver weight and declined plasma triglycerides. A sexual dimorphism in the regulation of glucose homeostasis was also detected in Igf1r heterozygous mice (Garg, Thakur, Alex McMahan, & Adamo, 2011). Beside a small reduction in postnatal growth, both, male and female Igf1r$^{+/-}$ animals develop insulin resistance with age, whereas only males are glucose intolerant. Therefore, a potential effect of oestrogen on the physiological function of Igfr-L might explain gender-specific differences in glucose and lipid metabolism observed in Igfr-$L^{+/-}$ animals.

5.3.3 Igfr-L-mediated regulation of InsR/Igfr signalling

The endocrine part of the pancreas plays a major role in the regulation of glucose metabolism by secreting insulin into the blood stream upon high glucose concentration causing the uptake of glucose in peripheral tissues such as liver, muscle and adipocytes. Many studies provided evidence that insulin not only acts in a paracrine manner but also activates autocrine insulin signalling in β-cells where it regulates transcription, translation, glucose and lipid metabolism, ion flux, insulin biosynthesis, insulin secretion, β-cell mass, cell proliferation, cell size and apoptosis (I. B. Leibiger et al., 2008).

The Igfr-L receptor is highly expressed in pancreatic β-cells implying an important role in β-cell physiology. Interestingly, Igfr-L negatively regulates InsR/Igf1r signalling in the murine β-cell line Min6. Knock-down of Igfr-L caused an increase in Akt and mTor activity in standard feeding conditions and upon nutrient deprivation. In contrast, complete inhibition of Igfr-L expression (Igfr-L KO) led to an elevated phosphorylation of InsR/Igf1r receptors and the metabolic regulator Ampk in feeding conditions, and resulted in upregulated Ampk activity but reduced Erk phosphorylation upon short-term starvation. The discrepancy observed upon decreased Igfr-L expression and complete absence of Igfr-L protein might be a result of an adaptation mechanism. Long-term absence of Igfr-L receptor might modify the Igfr-L mediated effect on InsR/Igf1r

signalling from an acute to a chronic state. Hyperphosphorylation of the InsR/Igf1r receptor due to short-term Igfr-L downregulation activated downstream signalling pathway components including the key players Akt and mTor. However, chronic pathway activity will induce negative feedback mechanisms to downregulate the pathway that might affect the metabolic state of the cell leading to Ampk activation. Autoregulatory feedback loops for the InsR/Igfr signalling pathway were shown in β-cells since the β-cell itself is the source of insulin, which activates insulin signalling in an autocrine manner (Rhodes et al., 2013). Such mechanisms ensure the attenuation of the signal transduction in β-cells in a hyperinsulinemic milieu so that signalling is not chronically sustained, which would lead to an insulin-resistant state. During autoregulatory desensitization processes, downstream kinases such as Erk1/2, PKCζ and the target of rapamycin complex-1 (TORC1) phosphorylate the InsR and IRS proteins, which promotes their dissociation and cause their degradation (Rhodes et al., 2013). Inhibition of insulin action also includes the internalization of the InsR/Igf1r into the endosomal compartment and the downregulation of InsR transcription (Carpentier et al. n.d.; Zick 2005).

But what does Igfr-L-mediated regulation of InsR/Igf1r, Akt and mTor means for the functionality of β-cells? Isolated islets, derived from Igfr-$L^{+/-}$ male mice, which underwent 28 weeks of HFD feeding, exhibited slightly elevated insulin secretion relative to WT controls. Islets of different β-cell-specific KO mice including InsR, Igf1r and Irs2 display insulin secretory defects (Kubota et al., 2004; R N Kulkarni et al., 1999b; Xuan et al., 2002). Conversely, increased activity of the InsR/Igf1R pathway, as observed in Igfr-L-depleted β-cells, might stimulate insulin secretion (Cantley et al., 2007; R N Kulkarni et al., 1999a, 2002; Otani et al., 2004; Xuan et al., 2002). In β-cells, the Irs-PI3K axis of the InsR/Igf1r system mediates positive feedback on insulin exocytosis by increasing Ca^{2+} levels after insulin stimulation (Aspinwall et al., 2000). However, this concept is not unambiguously accepted in the scientific field. It was also demonstrated that acute stimulation of K_{ATP} channels by insulin antagonizes the effect of glucose on insulin secretion, by causing a hyperpolarization of β-cells followed by the inhibition of Ca^{2+} channels and the reduction of cytosolic Ca^{2+} that eventually leads to the inhibition of insulin release (Ullrich, 2015). Nevertheless, Igfr-L might control insulin secretion by influencing Akt activity in β-cells.

Moreover, we detected an increase in β-cell proliferation upon Igfr-L depletion in Min6 cells. Beside the fact that the MAP kinases branch of insulin signalling is the main regulator of cell proliferation (mitogenic processes) in many cell types, Akt also plays a major role in regulating the cell cycle of β-cells (I. B. Leibiger et al., 2008; Taniguchi et al., 2006). The expression of a constitutive active form of Aktα in β-cells of transgenic mice caused an increase in β-cell mass due to hypertrophy and hyperplasia (Bernal-Mizrachi, Wen, Stahlhut, Welling, & Permutt, 2001; Tuttle et al., 2001). Conversely, β-cell-specific ablation of PDK1, a kinase, which activates Akt in insulin signalling, resulted in both reduced β-cell proliferation and reduced β-cell size leading to a T2D-like phenotype in mice (Hashimoto et al., 2006). Fatrai et al., 2006 claimed that Akt stimulates β-cell proliferation by controlling cyclin D1, cyclin D2, and p21 levels and the activity of cyclin-dependent kinase 4 (Cdk4) in mice (Fatrai et al., 2006). In accordance with our results, Kang et al., 2015 reported that the human ortholog of Igfr-L, EIG121, functions as tumor suppressor blocking the proliferation of gastric cancer cells. By directly binding to GRP78, EIG121

supresses GRP78-mediated activation of AKT (J. M. Kang et al., 2015). These findings imply that Igfr-L controls cell proliferation by modulating Akt activity in β-cells, which might be caused via desensitizing the upstream receptors InsR and Igf1r.

mTor plays a key role in the regulation of β-cell mass and is likely involved in compensatory β-cell adaptation in the development of T2D (Xie & Herbert, 2012). The inhibition of mTOR by rapamycin causes loss of β-cell function and viability in pancreatic β cell lines as well as in murine and human islets indicating that the maintenance of mTOR activity is critical for the integrity of β-cells (Bell et al., 2003). Thus, Igfr-L might be involved in the control of β-cell mass by regulating mTor activity. This might occur by attenuating the activity of the upstream receptors InsR and Igf1r.

In summary, all these indices imply a potential role of Igfr-L in the regulation β-cell proliferation, and insulin secretion by influencing the InsR/Igf1r signalling pathway. Blocking the Igfr-L might positively affect β-cell biology regarding insulin secretion, insulin sensitivity and cell proliferation. Thus, the Igfr-L is a therapeutic target to prevent β-cell failure.

5.3.4 Protein structure and subcellular trafficking dynamics of Igfr-L

Bioinformatic analysis predicted that the Igfr-L is a transmembrane receptor with a large extracellular region and a small cytoplasmic tail. The protein structure displays high similarities to RTKs and M6PRs (Figure 5.1). The N-terminal region of the Igfr-L protein comprises a growth factor receptor cysteine-rich domain, which is related to the Tnfr and Egfr and occurs in many other RTKs including Igf1r and InsR. This domain is important for hormone-binding and ligand specificity of RTKs (C W Ward et al., 1995).

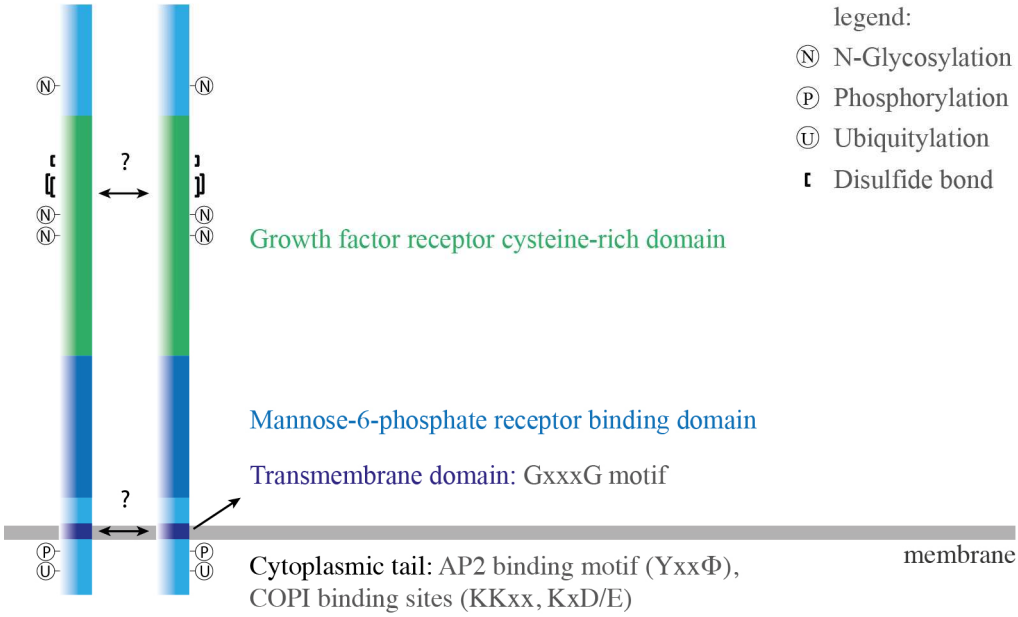

Figure 5.1: Schematic image of the Igfr-L protein structure including predicted topology and post-translational modifications as well as potential binding motifs.

C-terminal to the cysteine-rich domain, the Igfr-L contains a M6P-binding domain, which is highly conserved in CI-M6PR/Igf2r and CD-M6PR receptors. M6P-binding domains mediate the binding and sorting of lysosomal enzymes as well as the interaction of Igf2 ligand. Thus, it is also likely that the M6P-binding domain in the extracellular region of Igfr-L contributes to ligand interaction.

The resemblance of Igfr-L domain structure with RTKs and M6PRs implies an analogues molecular function. In addition, subcellular localization and trafficking behaviour might be similar regulated due to domain similarities. The subcellular localization of RTKs is tightly controlled due to its influence on the activity of downstream signalling. Ligand availability, for example, defines internalization rate of RTKs. After endocytosis receptors are directly recycled back to the cell surface or routed to the lysosome, where growth factors are degraded leading to the attenuation of downstream signalling (Goh & Sorkin, 2013). Colocalization studies revealed that the majority the Igfr-L protein in β-cells localizes to the Golgi complex with highest incidence in the *trans*-Golgi area (Figure 5.2). This coincides with the finding that the Igfr-L displays COPI binding motifs (KKxx and KxD/E binding sites) in its cytoplasmic tail (Figure 5.1). COPI-coated vesicles not only mediate the retrograde transport of vesicles from the Golgi to the ER but also regulate vesicular trafficking within Golgi stacks (Gao et al., 2014b; W. Ma & Goldberg, 2013). A main function of the Golgi apparatus is the post-translational modification of newly synthesised proteins transported from the ER to the Golgi including glycosylation and phosphorylation. The Igfr-L has predicted sites for post-translational amino acid modifications including N-linked glycosylation, phosphorylation and ubiquitylation. Indeed, collaboration partners showed that the Igfr-L is glycosylated, which might be relevant for the proper function of the protein (unpublished data, Dr. Ü. Coskun, Paul Langerhans Institut Dresden).

Moreover, the *trans*-Golgi network is the major sorting compartment of the secretory pathway for proteins, lipids and membrane traffic in the cell. Both, the Igf2r/CI-M6PR and the CD-M6PR bind M6P-tagged lysosomal enzymes in the *trans*-Golgi and transport them to endosomes and ultimately to pre-lysosomal compartments, where acid hydrolases degrade various biomolecules such as peptides, nucleic acids, carbohydrates, and lipids (El-Shewy & Luttrell, 2009). We also detected Igfr-L in different compartments of the secretory pathway including early and late endosomes and in parts of the lysosome (Figure 5.2). Considering its subcellular localization and the high similarity of its M6P binding domain to M6PRs, it is likely that the Igfr-L functions as sorting protein involved in the distribution of M6P-tagged proteins in the cell.

Although, the majority of Igfr-L protein is retained in the Golgi apparatus, immunofluorescence analysis verified a small fraction of Igfr-L protein transported to the cell surface likely via endosomal compartments. The CI-M6PR/Igf2r displays a related subcellular distribution. At steady state, about 90% of CI-M6PR/Igf2r receptors localize to the *trans*-Golgi network and endosomal compartments, whereas the rest is routed to the plasma membrane (El-Shewy & Luttrell, 2009). The Igf2r/CI-M6PR continuously shuttles between these cellular pools suggesting a similar trafficking behaviour for the Igfr-L. Indeed, endocytosis assays confirmed that the Igfr-L is constitutively internalized and primarily transported from the cell surface to the Golgi complex. Partially, the Igfr-L protein is also routed to the lysosome after endocytosis at the cell surface. Yet,

it is unclear whether the receptor is directly transported to the lysosomal compartment or if it first shuttles to the Golgi apparatus before it is further routed to the lysosome. Cell surface availability and constitutive internalization suggests an important function of the Igfr-L at the plasma membrane. The growth factor cysteine-rich domain and the M6P-binding domain might mediate binding of growth factors or growth factor receptors at the cell surface, which would induce internalization and routing to the lysosome.

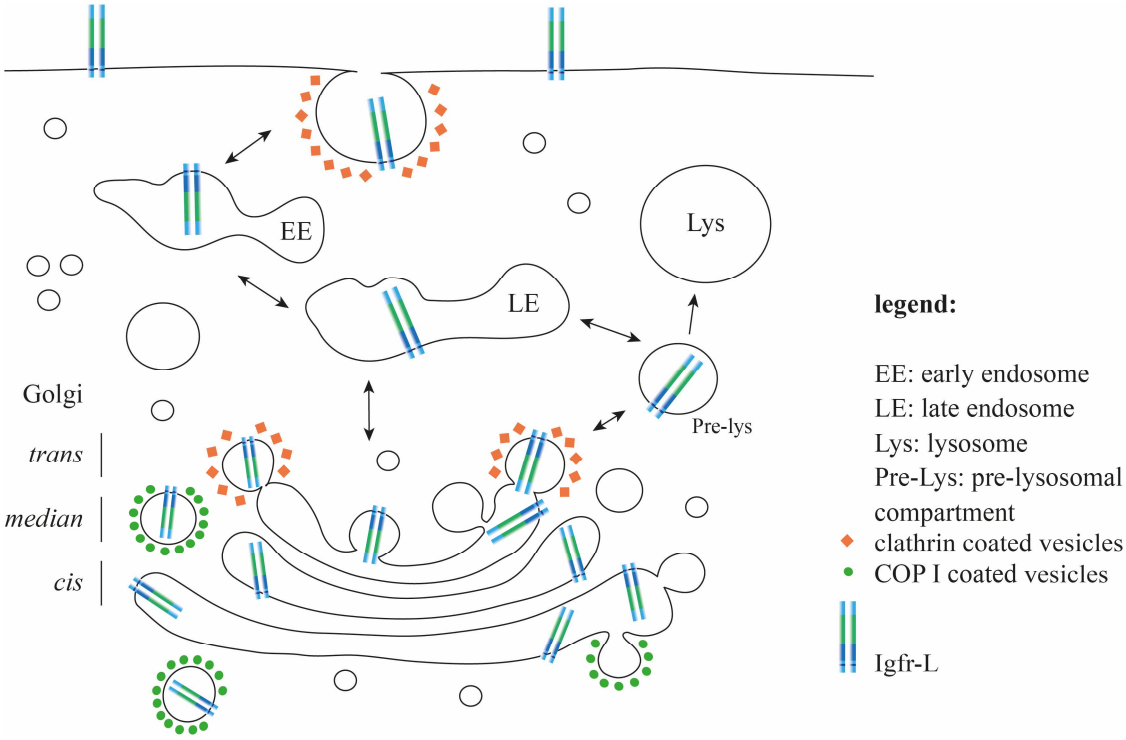

Figure 5.2: Schematic illustration of Igfr-L subcellular localization and trafficking routes

5.3.5 Regulation of cell surface location of Igfr-L by the presence of extracellular glucose

Beside other factors, the internalization rate of RTKs depends on ligand availability and the metabolic state of cells (Goh & Sorkin, 2013). When characterising trafficking dynamics of the Igfr-L, we observed a decrease of Igfr-L protein at the cell surface upon cell starvation using surface biotinylation assays. In contrast, the number of InsR at the plasma membrane was unchanged upon nutrient depletion. At high extracellular glucose concentrations, the Igfr-L remained longer at the plasma membrane but left the cell surface after 120 min, similar to the InsR. These observations coincide with the change in subcellular localization of the Igfr-L caused by starvation detected in immunofluorescence stainings. The Igfr-L “retracts” its subcellular distribution to the compacted Golgi area. It is unclear whether nutrient depletion and glucose regulate the rate of the Igfr-L internalization or its recycling and transport to the plasma membrane.

In steady state, InsR is nearly absent from the cell surface, whereas insulin removal from the culturing medium causes the accumulation of InsR at the plasma membrane (Ullrich, 2015). The Igfr-L might bind extracellular ligands or interact with other receptor tyrosine kinases such as

the InsR and Igf1r at the cell surface. Thus, one might expect that Igfr-L receptor abundancy increases at the plasma membrane upon nutrient depletion since cells ensure that extracellular growth factors are detected by receptors. However, we observed the opposite suggesting that the Igfr-L might be involved in the later phase of InsR/Igf1r signalling, namely in the downregulation of the pathway upon prolonged signalling (120 min). Igfr-L negatively regulates InsR signalling inhibiting the activity of InsR, mTor and Akt. High glucose concentration induces insulin secretion leading to autocrine InsR signalling in β-cells. Thus, Igfr-L might control negative feedback loops of InsR/Igfr signalling, which attenuates signalling and prevents long-term hyperactivity by causing the internalization of InsR. If true, this would also explain that Igfr-L but not InsR leaves the cell surface upon nutrient depletion since cells do not require a downregulation of the InsR pathway by Igfr-L in starving conditions.

Moreover, it is also likely that plasma membrane location of Igfr-L is controlled by the metabolic state of cells. InsR signalling regulates glucose uptake in cells by activating the PI3K/Akt pathway leading to the phosphorylation of AS160 and eventually to the translocation of GLUT transporters to the plasma membrane. High extracellular glucose concentration elevates the abundancy of CI-M6PR/Igf2r at the plasma membrane and enhances binding of Igf2 ligand. Zhang et al., 1997 claimed that this is induced by the generation of diacylglycerol in glucose metabolism, which leads to the activation of PKC and eventually results in increased phosphorylation of CI-M6PR/Igf2r (Zhang, Berggren, & Tally, 1997). However, further experiments analysing the influence of Igfr-L on metabolic processes including PKC activity will be necessary to shed light on the regulation of Igfr-L cell surface localization. Dynamics of the Igfr-L at the plasma membrane could be analysed in the future by using super resolution microscopy such as total internal reflection fluorescence (TIRF) microscopy. Single molecule imaging could also unravel the Igfr-L localization at the cell surface in different conditions, such as the presence of various growth factors in the medium.

5.3.6 Igfr-L endocytosis and trafficking by CME

In the cytoplasmic tail of the Igfr-L we identified a potential binding motif (Yxxϕ) for the μ2 subunit of the adaptor protein 2 (AP2). AP2 links many RTKs and the CI-M6PR/Igf2 to clathrin-coated vesicles (Ghosh, Dahms, & Kornfeld, 2003; Goh & Sorkin, 2013). We showed that the Igfr-L is likely internalized via CME at the plasma membrane of Min6 cells using inhibitors specifically supressing different trafficking and endocytosis pathways in the cell.

Most of the well-characterized RTKs and various other receptors are transported by clathrin-coated vesicles in the cell (Goh & Sorkin, 2013). However, in recent years numerous studies provided evidence that many of these receptors also use clathrin-independent pathways for intracellular trafficking and cell surface endocytosis. The Igf1r is internalized through clathrin-dependent endocytosis (CDE) and independent (CIE) endocytosis (Monami, Emiliozzi, & Morrione, 2008). In HaCat cells, Igf1r is internalized together with caveolin, and downregulation of caveolin 1 (Cav1) inhibits Igf1r signal transduction in H9C2 rat cardiomyoblasts (Salani et al., 2010; Salani, Briatore, Garibaldi, Cordera, & Maggi, 2008). Likewise, the InsR was thought to be

primarily transported by clathrin-coated vesicles. However, first evidence for caveolae-dependent endocytosis of the InsR were already found several years ago. The InsR interacts with caveolin 1 and co-localizes with caveolae at the plasma membrane of adipocytes (Gustavsson et al., 1999; Nystrom, Chen, Cong, Li, & Quon, 1999). Colocalization of InsR and Cav1 was recently verified in pancreatic β-cells by imaging a fluorescently labelled InsR using TIRF microscopy (Boothe et al., 2016). Until now, it is unclear if caveolae and CME-mediated trafficking differentially influences InsR or Igf1r actions.

In recent years a growing body of evidence suggested that endocytosis pathways, used by receptors for internalization at the plasma membrane, affect downstream signal activity and specificity (Barbieri et al., 2016). For instance, the Egfr internalization route depends on extracellular ligand concentrations. At low extracellular Egf concentration, the Egfr is endocytosed by CME leading to receptor recycling and a maintained signalling, which stimulates proliferation. At high extracellular Egf dose, about 40 % of Egfrs are internalized by CIE due to increased receptor ubiquitination. CIE targets Egfrs to degradation in the lysosome causing signal extinction (Barbieri et al., 2016).

Additional studies, such as transmission electron microscopy (TEM) could reveal if the Igfr-L also uses other endocytic pathways for internalization at the cell surface. The usage of different endocytosis pathways might influence the Igfr-L-mediated regulation of InsR/Igfr signalling.

5.3.7 Mechanistical model of Igfr-L regulating InsR/Igfr signal transduction

We demonstrated, that the Igfr-L negatively regulates InsR/Igf1r signal transduction including the kinase activity of Akt, mTor and InsR/Igf1r. RTKs activate downstream signalling via their tyrosine kinase, catalytic domain in the intracellular domain of the protein. Ligand binding leads to a conformational change of InsR/Igf1r receptors, which induces intrinsic kinase activity of InsR/Igf1r β-subunits. Autophosphorylated tyrosines at the β-subunit act as docking sites for signalling proteins, such as IRS proteins leading to the activation of downstream signalling. In contrast to RTKs, the Igfr-L lacks an intrinsic kinase activity. However, the similarities in topology and protein structure to receptor tyrosine kinases and the CI-M6PR/Igf2r, especially the growth factor cysteine-rich region and M6P-binding domain, might imply that the Igfr-L influences downstream signalling activity by acting as signalling co-receptors or as scavenger receptor (Figure 5.3).

Signalling co-receptors are either anchored to the cellular membrane by glycosylphosphatidylinositol (GPI) anchors and thus do not contain a cytoplasmic domain, or are transmembrane receptors with a short intracellular region lacking intrinsic kinase activity. Typically, co-receptors display a large extracellular region participating in ligand binding or complex formation with other receptors (Kirkbride, Ray, & Blobe, 2005). Examples for signalling co-receptor are receptors from the Egfr or Tgfβ superfamily as well as of the Hh signalling system (Kirkbride et al., 2005).

Most commonly, both, co-receptors and signalling receptors interact with ligands but are not able to bind ligands independently. Ligand-mediated receptor interaction can either be direct or indirect via adapter proteins. Complex formation of co-receptors and signalling receptors can lead to enhanced ligand affinity or altered ligand specificity affecting downstream signal activity and pathway usage (Kirkbride et al., 2005). For instance, induced expression of the TβRIII co-receptor in vascular endothelial cells elevates the responsiveness of cells to the TgfβII ligand (Sankar, Mahooti-Brooks, Centrella, McCarthy, & Madri, 1995). In addition, the ErbB2 receptor is an orphan receptor without known ligand but with receptor tyrosine kinase domain, which is only active when heterodimers are formed with other Egfr family members (Burgess et al., 2003; Citri & Yarden, 2006). In contrast, B2 receptor tyrosine kinase 3 (ErbB3) contains an inactive kinase domain but forms active heterodimers with other members of the ErbB family, thereby transducing signals. Similarly, it might be possible that the Igfr-L directly or indirectly interacts with other RTKs such as the InsR or Igf1r at the plasma membrane affecting receptor-ligand binding, which would lead to the downregulation of InsR/Igf1r signalling. When directly interacting with signalling receptors, the Igfr-L could act as monomer or homodimer. In the transmembrane domain of Igfr-L, we found a GxxxG motif, which was originally identified in Egfrs, where it contributes to receptor homodimerization (Gerber, Sal-Man, & Shai, 2004). The growth factor cysteine-rich domain in the Igfr-L might also enhance homo- or heterodimer formation. X-ray crystal structure studies showed that the cysteine-rich domain II in ErbB receptors affect receptor dimerization activated by Egf binding (Cho and Leahy 2002; Ferguson et al. 2003). The CD-M6PR is present primarily as non-covalent homodimer in the membrane (Nancy M Dahms and Hancock 2002). Likewise, the CI-M6PR/Igf2r tends to form homodimers on the cell surface although it behaves as a monomer in detergent solutions (Hassan 2003a; York et al. 1999) For the ErbB receptor family it was assumed that the majority of receptors exist as monomers at the cell surface prior to ligand binding, and that ligand association would stimulated receptor dimerization (I. Maruyama, 2014). As a result, intracellular kinase domains come into proximity activating receptor trans-phosphorylation. However, an increased number of studies have demonstrated that ErbB receptors exist as dimers at the plasma membrane before ligand interaction (Hiroshima, Saeki, Okada-Hatakeyama, & Sako, 2012; Tao & Maruyama, 2008).

Moreover, many co-receptors attenuate signalling by regulating endocytic processes of their signalling receptors. For example, phosphorylation of the type III transforming growth factor receptor (TβRIII) co-receptor by the signalling receptor TβRII, leads to β-arrestin 2-mediated co-internalization of TβRIII and TβRII and the downregulation of TGFβ signalling (W. Chen et al., 2003; Tazat, Hector-Greene, Blobe, & Henis, 2015). The Igfr-L was shown to be routed to lysosomal compartments after endocytosis, which might imply that it interacts with RTKs, thereby modulating receptor endocytosis and transport to lysosomes as well as limiting the time of receptor action at the plasma membrane (Figure 5.3).

Because co-receptors do not induce signalling cascades independently, it is often thought that co-receptors are non-essential or redundant. However, many findings supported the opinion that co-receptors are essential for functional signalling systems in the cell. The TβRIII co-receptor is crucial for embryonic development since TβRIII KO causes lethality at E13.5 owing to

proliferative defects in the heart and apoptosis in the liver (Stenvers et al., 2003). Likewise, Igfr-L KO mice die postnatally. Furthermore, the availability of co-receptors specifies, which tissue or cell type is responsive to extracellular signals. Due to its expression pattern, the Igfr-L might mainly act as co-receptor in endocrine and exocrine tissues affecting either ligand specificity and affinity of RTKs or receptor endocytosis.

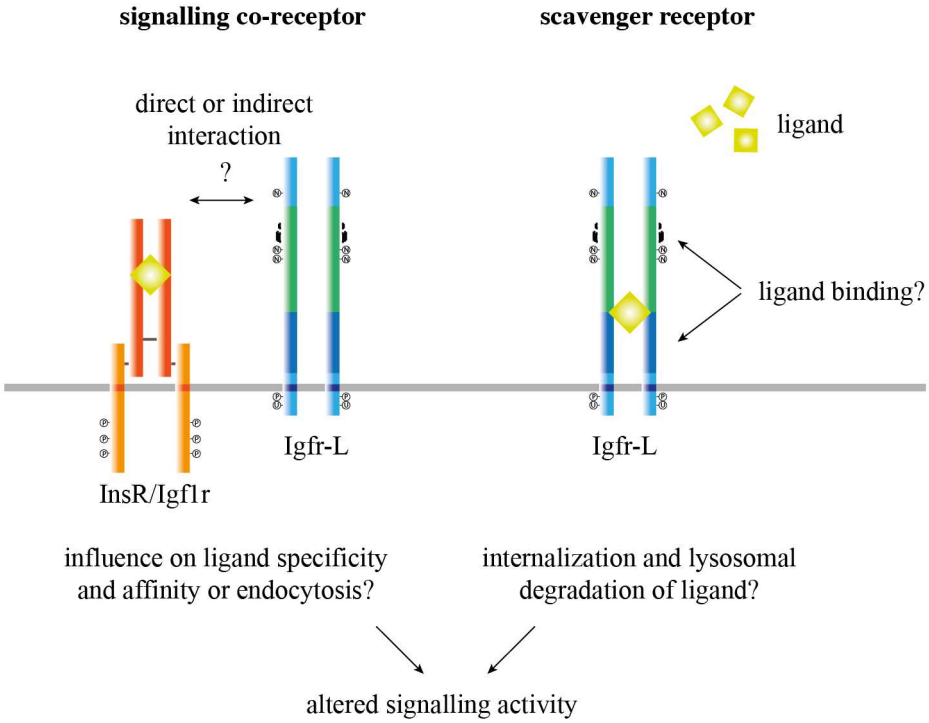

Figure 5.3: Mechanistical model of Igfr-L receptor actions influencing InsR/Igfr signalling

Another possibility how Igfr-L might control the InsR/Igfr pathway is by acting as scavenger receptor (Figure 5.3). Scavenger receptors are cell surface receptors comprising a structurally and functionally diverse group of proteins. Their common feature is the recognition and internalization of a variety of ligands including endogenous proteins, modified lipoproteins and pathogens. However, they do not transmit an intracellular response. By binding and internalizing a large repertoire of ligands, scavenger receptors regulate a broad spectrum of biological functions including endocytosis, signalling, adhesion, lipid transport, antigen presentation, and pathogen clearance (Canton, Neculai, & Grinstein, 2013; Zani et al., 2015). The CI-M6PR/Igf2r is a well-studied receptor that lacks intracellular kinase activity and functions as scavenger receptor controlling bioavailability of the Igf2 growth factor. Beside other ligands, CI-M6PR/Igf2r binds and internalizes Igf2. The Igf2-Igf2r complex is directed to pre-lysosomal areas, where Igf2 is released due to the acid pH in these compartments and further routed to the lysosome, where Igf2 is proteolytically degraded (El-Shewy & Luttrell, 2009). By depleting Igf2 from the environment, the CI-M6PR/Igf2r prevents binding of Igf2 to the Igf1r and to InsR/Igf1r hybrid receptors, thus reducing InsR/Igfr signal activity. The existence of the M6P-binding domain and the cysteine-rich region in the extracellular region of Igfr-L might imply the binding of growth

factors such as insulin or Igfs. In addition, the Igfr-L is partially transported to lysosomal areas after endocytosis, which might indicate that Igfr-L recognizes and internalizes extracellular growth factors and targets ligands to the lysosome for degradation. Clearing insulin or Igfs from the extracellular space would therefore result in the attenuation of InsR/Igf signalling activity. Further experiments will verify if the Igfr-L potentially binds ligands as mono- or dimer at the cell surface.

5.3.8 Igfr-L as potential therapeutic target

Diabetes mellitus is a major healthcare problem that affects millions of people worldwide and results from the development of insulin resistance and a loss or dysfunction of pancreatic β-cells ("WHO | *Global report on diabetes*," 2017). Until now, there is no curative medication for diabetes mellitus. Current studies aim to restore β-cell mass either by a β-cell replacement therapy or by triggering regenerative processes in existing β-cells. Insulin-producing β-cell-like cells could be differentiated from induced pluripotent stem cells (iPSCs) by recapitulating the normal developmental process of β-cells *in vitro*. Transplantation of these cells in diabetic mouse models can cure diabetes offering potential cell-replacement therapy for diabetic patients (Rezania et al., 2014). Moreover, efforts are done to trigger regenerative processes activating self-replication of remaining β-cells to increase β-cell mass (P A Halban, 2008; Philippe A. Halban, 2015). We observed that Igfr-L supresses β-cell proliferation. Therefore, blocking Igfr-L receptors via therapeutic molecules could stimulate β-cell replication and eventually lead to an increase in β-cell mass.

Current pharmacological therapies for the treatment of T2D can be classified in different categories (Bailey, 2015; Tahrani, Barnett, & Bailey, 2016). The administration of insulin and analogues substitute for the lack of insulin in the body to achieve an euglycemic state. α-glucosidase inhibitors and glycosurics (SGLT2 inhibitors) interfere with glucose uptake and excretion whereas insulin sensitizer like Metformin, Biguanides or Thiazolidinediones ameliorate effects of insulin resistance in metabolic organs. Secretagogues like Sulfonylurea and peptide analogs such as GLP1 agonists or Dipeptidylpeptidase 4 (DPP4) inhibitors elevate glucose-induced insulin secretion of remaining functional β-cells.

One of the major reasons for a dysregulated glucose metabolism is a dysfunctional InsR/Igfr system leading to insulin resistance in patients. Thus, molecules targeting the InsR/Igfr axis became an area of intense preclinical and clinical research in diabetes therapeutics (Annunziata, Granata, & Ghigo, 2011a). The in-depth characterization of the InsR/Igfr system and the understanding of its influence on glucose metabolism is crucial. We showed that Igfr-L negatively regulates the InsR/Igf1r signalling system. Additionally, heterozygous deletion of Igfr-L caused slight hyperinsulinemia and glucose intolerance as well as significantly impaired insulin sensitivity in adult male and female mice when feeding a long-term HFD. Thus, the Igfr-L is a potential target for the development of diabetes therapeutics. Molecules affecting Igfr-L mechanisms of action could possibly counteract hyperglycaemia in patients by modulating β-cell biology and/or the function of other cells in the HPA axis.

Moreover, Igfr-L heterozygous female mice developed enlarged livers and manifested decreased triglyceride plasma concentrations upon 28 weeks of HFD. In addition, GWAS studies showed that the human IGFR-L locus associates with deregulated cholesterol metabolism, dysbalanced insulin sensitivity, coronary artery disease and T2D. Thus, Igfr-like might also be a target to modulate lipid metabolism and cardiovascular disease.

In the development of anti-diabetic drugs, therapeutic antibodies received increasing clinical attention in the past. We generated monoclonal antibodies against the extracellular domain of the human Igfr-L protein that might serve as therapeutics affecting Igfr-L function. The therapeutic potential of these antibodies could be examined by analysing their potential effects on InsR/Igfr signal transduction and their influence on glucose metabolism. *In vitro* studies will verify if antibodies have an inhibitory or activating effect on intracellular InsR/Igfr signalling. Investigating their influence on glucose metabolism could include the injection of antibodies into diabetic mice such as db/db animals or in other preclinical obesity and/or diabetes mouse models. The Igfr-L is a transmembrane receptor, which is therefore, easily accessible for antibodies via the blood stream, when located at the plasma membrane of cells. Even though that the majority of Igfr-L is expressed in the Golgi apparatus, we detected a subpopulation of Igfr-L at the cell surface. However, we also showed that the turnover and internalization rate of Igfr-L is very quick and that the plasma membrane pool is constantly recycled.

But how could antibodies affect Igfr-L mode of actions? We propose that the Igfr-L might either act as signalling co-receptor or as scavenger receptor. Antibody binding to the extracellular region at the cell surface could interfere with potential complex formation of Igfr-L with RTKs such as the InsR and Igf1r including the blockage of direct or indirect interactions. This could affect ligand specificity and affinity of the corresponding signalling receptor as well as receptor internalization rates leading to a manipulated downstream signalling cascade. In the case of a potential scavenger receptor, bound antibodies could inhibit the association of Igfr-L with ligands. Altered bioavailability of endogenous ligands such as insulin or igf, would also result in changed signalling activity of the InsR/Igfr pathway.

Beside its effect on InsR/Igfr signalling, the Igfr-L receptor also supresses the activity of Ampk. Thus, inhibitory therapeutic antibodies might also operate via the activation of the metabolic sensor Ampk as it was shown for the drug Metformin. Metformin is an insulin sensitizer and one of the most widely used medication for the treatment of type 2 diabetes especially in obese patients. It diminishes hepatic glucose output due to decreased glycogenolysis/gluconeogenesis and enhances glucose uptake into peripheral tissues. Metformin acts by indirectly increasing Ampk activity through a mild and transient inhibition of the mitochondrial respiratory-chain complex 1 (Viollet et al., 2012).

In summary, the Igfr-L itself constitutes a potential therapeutic target. Understanding its mode of action as well as its influence on the InsR/Igfr signalling system and energy homeostasis will open new possibilities for drug development that might improve current therapeutic strategies. Further investigations will also reveal if the Igfr-L receptor might affect β-cell survival and regeneration.

6 Material and methods

6.1 Material

6.1.1 Equipment

Agarose gel chamber	Midi 450 (Neolab, Heidelberg)
Balances	ScoutTM Pro (OHAUS)
Biorep perfusion system	Biorep Technologies, Miami USA
Cell counter	TC20™ Automated cell counter (Biorad, Heidelberg)
Cell culture hood	BDK (Luft-und Reinraumtechnik GmbH, Sonnenbühl-Genkingen)
Centrifuges	5417R, 5430C, 5804 R (Eppendorf, Hamburg) Microcentrifuge (Roth, Karlsruhe), Micro 220 (Hettich, Tuttlingen) Universal 320R (Hettich, Tuttlingen), 6767 (Corning)
Cryostat	Ag Protect (Leica, Wetzlar)
Cytospin equipment	Cyto chambers, filter, rotor (Hettich, Tuttlingen)
Developing machine	AGFA Curix 60 developing machine (AGFA HealthCare GmbH, Bonn)
ELISA reader	PHERAastar FS (BMG Labtech GmbH, Ottenberg) Varioskan LUX (Thermo Scientific, Waltham)
FACS	BD FACSAria III (Becton and Dickinson and Company, Franklin Lakes)
Film cassettes	Hypercassette (Amersham, Munich)
Freezer	-20°C Medline, premium nofrost (Liebherr, Ochsenhausen) -80°C (Thermo Scientific, Waltham)
Fridge	4°C comfort (Liebherr, Ochsenhausen)
Gel documentation system	UVsolo TS Imaging System (Biometra, Goettingen)
Glassware	Schott-Duran (Schott, Mainz)
Glucometer	Freestyle freedom lite (Abbot Diabetes Care Oxon, UK)
Incubation systems/ovens	Thermomixer comfort, Thermomixer 5436 (Eppendorf, Hamburg) Oven (Thermo Scientific, Waltham)
Incubator	BBD6220 (Thermo Scientific, Waltham) Inkubator C16 (Labortect, Rosdorf) KBF (Binder GmbH, Tuttlingen-Möhringen) Shake'n'Stack (ThermoHybaid, Thermo Fisher Scientific Inc., Waltham)
Microscopes	Axiovert 200 M (Carl Zeiss AG, Göttingen) MS5, MZ75(Leica Microsystems GmbH, Wetzlar) TCS SP5 and Cube (heating), Brick (CO_2) (Leica Microsystems GmbH, Wetzlar)

	M80 and Dissection light (Leica, Wetzlar)
Microwave	700 W (Severin Elektrogeräte GmbH, Sundern)
N_2 tank	Biostore systems (Cryo Anlagenbau GmbH, Wilnsdorf)
NMR	EchoMRI LLC (Houston, TX, USA)
Odyssey Imaging Systems	LI-COR Biosciences, Lincoln USA
PCR machines	Personal Thermocycler, Professional Trio Thermocycler (Biometra, Goettingen)
	PXE0.2 Thermo Cycler (Thermo Fisher Scientific Inc. Waltham)
pH meter	Mettler Toledo (HANNA Instrumentes Deutschland GmbH, Kehl am Rhein)
Photometer	NanoDrop 2000c (Thermo Fisher Scientific, Waltham)
	HERAstar FS (BMG LABTECH GmbH, Ortenberg)
Pipettboy	Accu-jet® pro (Brand GmbH, Wertheim)
Pipettes	1000 µl / 100 µl / 10 µl Eppendorf Research (Eppendorf, Hamburg)
Plastic ware	(VITLAB GmbH, Großostheim)
Polyacrylamid gel chamber	Mini Trans-Blot® Cell (Biorad, Heidelberg)
Power supply (agarose gel)	Power Source 300V (VWR International, Darmstadt)
qPCR cycler	ViiA7 Real-time PCR system (Life technologies, Frankfurt)
	AB 7300 unit (BD)
Roller/Mixer	VSR 23 (VWR International, Darmstadt), Shaker DOS-10L (Neolab, Heidelberg), RMS (I), Rocker 247 (Everlast)
Sonificator	Sonoplus HD2070 (Bandelin electronic GmbH&Co.KG, Berlin)
	Elmasonic, UW 2070 (Bandelin electronics, Berlin)
Sterile hoods	MSC Advantage (Thermo Scientific, Waltham)
Stirrer	D-6011 (Neolab, Heidelberg)
Timer	Roth, Karlsruhe
Tissue Homogenizer	Ultra Turrax T25 (IKA)
Ultrasonic bath	Ultrasonic cleaner (VWR International, Darmstadt)
Vortexer	Vortexer (VWR international GmbH, Darmstadt)
Water bath	Memmert
	SWB25 (Thermo Fisher Scientific Inc., Langenselbold)
Water purification system	Millipore Q-POD, 0.22 µl filter (Merck Chemicals GmbH, Schwalbach)
Western blot semi-dry	Trans-Blot® SD, Semi Dry Transfer cell, Mini-PROTEAN® Tetra Cell, Trans-Blot® Turbo™ Blotting System (Biorad, Heidelberg)

6.1.2 Consumables

50 ml/ 15 ml tubes	Becton and Dickinson and Company, Franklin Lakes
15 cm/ 10 cm/ 6 cm dishes	Nunc (Thermo Scientific Fisher, Waltham)
6-well/ 12-well/ 24-well/48-well / 96-well plates	Nunc (straight/conical) (Thermo Scientific Fisher, Waltham)
10 cm bacterial plates	BD FalconTM (Becton Dickinson GmbH, Franklin Lakes)
EDTA-treated tubes	Microvette Di- pottasium-EDTA (Sarstedt, Kleinstadt)
8 well chambers	Uncoated and coated 8-well imaging plates (Ibidi, Planegg)
Embedding moulds	Peel-A-Way® (Roth, Karlsruhe)
50ml/ 25ml/ 10ml/5ml/ 2ml/ 1ml plastic pipettes	Greiner Bio-One GmbH, Frickenhausen
Adhesive covers	Optical adhesive covers (Life Technologies, Frankfurt)
Blotting paper	Whatman paper (GE Healthcare Buchler GmbH & Co. KG, München)
Cell scraper	Sarstedt, Nümbrecht
Cell strainer	Nylon cell stainer 70 µm (Falcon, Fisher Scientific, Waltham)
Clamp (pancreas)	Bulldog SerrefinE—Straight 35 mm (Fine Science Tools GmbH, Heidelberg)
Counting chambers	Neubauer (LO – Laboroptik GmbH, Friedrichsdorf)
Cryotubes	Sarstedt, Kleinstadt
Cover slips	VWR International, Darmstadt
Embedding molds	Peel-a-way embedding molds, S-2 (Sigma Aldrich, Hamburg)
FACS tubes	5 ml polystyrene round bottom tube with cell strainer cap and 5 ml polypropene round bottom tube (Falcon, Fisher Scientific, Waltham)
Films	Hyperfilm ECL (GE Healthcare Buchler GmbH & Co. KG, München), CEA, Rö.Blaufilm, RP new (Christiansen und Linhardt GmbH, München)
Forceps	Dumount Inox (11251-, 11252-20, Fine Science Tools GmbH, Heidelberg)
Freezing boxes	CoolCell® Alcohol-Free (BioCision LLC, USA, CA) Freezing container, Nalgene® (Sigma-Aldrich Chemie Gmbh, München)
Glass slides	Menzel Gläser superfrost plus (Thermo Scientific, Waltham)
Needles	Sterican 27G ½ ``, Sterican 30G ½ `` (B.Braun, Puchheim)
Nitrocellulose membrane	GE Healthcare Buchler GmbH & Co. KG, München
Parafilm	Pechiney Plastic Packaging
PVDF membrane	Biorad, Munich
Scalpels	Sterile (B.Braun, Tuttlingen)
Scissors	14088-10 (Fine Science Tools GmbH, Heidelberg)

Spacer	Secure-Sela, 9mm 0.12 mm deep (Life Technologies, Frankfurt)
Syringes	Omnifix 30 ml / 3 ml; Omnican 50 (B. Braun Melsungen AG, Melsungen) 30G1/2-G needle (B. Braun Melsungen AG, Melsungen)
Syringe filter	Millex-GP (Filter unit fast flow and low binding 0.22 µm)
qPCR 96-well plates	MicroAmp Fast optcal 96-well reaction plate (Life Technologies, Frankfurt)
Pasteur pipettes, plastic	Roth, Karlsruhe
Pasteur pipettes, glass	15cm/23cm (LABOR-BRAND, Gießen; Hirschmann Laborgeräte GmbH & Co. KG, Eberstadt)
PCR Tubes	Eppendorf, Hamburg
2 ml/ 1.5 ml / 0.2 ml tubes	safe-lock reaction tubes (Eppendorf, Hamburg)

6.1.3 Kits and Mastermix

5x VILO™ reaction mix and 10x SuperScript (Life Technologies, Frankfurt)

AccuBlue™ High Sensitivity dsDNA Quantitation Kits (Biotium, Fremont USA)

Click-IT EDU Alexa Fluor 647 (#C10340, Life Technologies, Freiburg)

Dynamo Color Flash SYBR Green qPCR kit (Life Technologies, Frankfurt)

ECL Clarity Western ECL substrate kit (Biorad, Munich)

Fast EvaGreen Supermix with low ROX (Biorad, Munich)

Insulin Ultra Sensitive Assay Kit, HTRF assay (Cisbio, Bedford USA)

BlutketonFreeStyle Precision H (measurement of β-ketones; Abbot Diabetes Care Oxon, UK)

LabAssay TM Triglyceride (#290-6370; WAKO Chemicals GmbH Neuss)

LabAssay™ Cholesterol (total) (#294-65801, WAKO Chemicals GmbH Neuss)

Mouse Glucagon ELISA kit (Crystal chem, Downers Grove USA)

Mouse HDL-Cholesterol Assay Kit (#79990 Crystal Chem, Chicago, USA)

Mouse LDL-Cholesterol Assay Kit (#79980 Crystal Chem, Chicago, USA)

NEFA-HR (2) R1+R2 Set (#434-91795 and # 436-91995, WAKO Chemicals GmbH Neuss)

Pierce BCA Protein Assay Kit (Thermo Fisher Scientific, Waltham)

QIAquick PCR Purification Kit (Qiagen Holding, Hilden)

Rneasy Mini Kit, Rneasy Micro Kit, miRNA Micro Kit (Qiagen Holding, Hilden)

SuperSignal West femto maximum sensitivity substrate (Life Technologies, Frankfurt)

TaqMan Fast Advanced Master Mix (Life Technologies, Frankfurt)

Ultrasensitive mouse insulin ELISA kit (Crystal Chem INC., #90080, IL, USA)

6.1.4 Chemicals

If not indicated, chemicals were purchased from Roth, Karlsruhe; Merck, Darmstadt; Sigma-Aldrich, Hamburg

A	Acetic acid
	Acrylamide/bisacrylamide (Rotiphorese)
	Agarose (Biozym Scientific)
	Ammoniumpersulfat (APS)
	L-Arginine
B	BCA
	Big Dye/ Big Dye Buffer (Life Technologies 4337457 or Lager 5000986)
	Bovine Serum Albumine (BSA)
	Bradford reagent
	Bromophenol blue
C	Calcium chloride
	Chloroform, 99+%
D	DAPI
	Developer G135 A/B (AGFA, Bonn)
	Diethylpyrocarbonate (DEPC), 121pprox.. 97%
	Dimethylsulfoxide (DMSO), >99,9%
	Dithiothreitol (DTT)
	Dithizone
	D-MEM (Gibco, Invitrogen™ Cooperation, Carlsbad, CA)
	DNAZap (Thermo Fisher Scientific, Waltham)
	dNTPs (Fermentas, Leon-Rot)
E	Ethylenediaminetetraacetic acid (EDTA)
	EdU (Life Technologies, Frankfurt)
	Ethanol, 96%
	Ethidium bromide
F	Formaldehyde
	Formamide
G	Glucose (D-)
	Glutaraldehyde
	Glycerol
	Glycin
H	HEPES (200mM, Gibco, InvitrogenTM Cooperation, Carlsbad, CA)
	Hoechst 33342 (Thermo Fisher Scientific, Waltham)
	Hydrogen chloride (HCl)
I	Isopropanol, 100%

M	Magnesium chloride
	MEM non-essential amino acids (Gibco®, InvitrogenTM Cooperation, Karlsruhe)
	Methanol, 100%
	Milk powder (Becton Dickinson GmbH, Heidelberg)
	Mounting medium – Jung Tissue Freezing medium (Leica, Wetzlar)
N	Natrium citrate
	Nitrogen(l) (Linde AG, München)
	NP-40 nonylphenoxypolyethoxyethanol (Nonidet NP-40) (Life Technologies, Frankfurt)
O	Orange G
P	Paraformaldehyde
	Polyacrylamide
	Polyvinyl-alcohol
	Potassium chloride (KCl)
	Potassium hydrogenphosphate (KH_2PO_4)
	ProLong Gold antifade reagent (Invitrogen, Carlsbad)
R	Rapid fixer G356 (AGFA, Bonn)
	RNaseZAP
	Rnase (Promega GmbH, Mannheim)
	Rnase inhibitors (Fermentas GmbH, St. Leon-Rot)
S	Sodium chloride (NaCl)
	Sodium deoxycholate ($C_{24}H_{39}O_4Na$)
	Sodium dodecyl sulphate (SDS)
	Sodium hydrogenic phosphate (Na_2HPO_4)
	Sodium hydroxide
	Sodium tetraborate ($Na_2B_2O_7$)
	Superscript II (Fermentas GmbH, St. Leon-Rot)
T	TEMED
	Tris(hydroxymethyl)aminomethane
	Triton X-100
	Tween-20
X	Xylene

6.1.5 Buffers and solutions

Western blot

10x TBST:	100 mM Tris/HCl, 1.5 M NaCl, 2.0% Tween20 (adjust to pH 7.4)
10x Tris-Glycine (running buffer):	1.0% SDS, 0.25 M Tris, 1.92 M Glycine
4x SDS-loading buffer:	200 mM Tris/HCl, pH 6.8, 8% SDS, 40% Glycerol, 0.4% bromine phenol blue (add freshly 400 mM DTT)
4x Tris-HCl/SDS buffer	1.5 M Tris, 0.4% SDS (adjust to pH 8.8)
4x Tris-HCl/SDS buffer:	0.5 M Tris, 0.4% SDS (adjust to pH 6.8)
APS:	10% APS (in ddH_2O)
Blocking solution:	5% milk powder in 1x TBST
Buffer anode I (API):	300 mM Tris/HCl, 10% Methanol (adjust to pH 10.4)
Buffer anode II (APII):	25 mM Tris/HCl, 10% Methanol (adjust to pH 10.4)
Buffer cathode (KP):	25 mM Tris/HCl, 40 mM Glycine, 10% Methanol (adjust to pH 9.4)
Femto-ECL-solution:	Solution A and B mix: 1:1 (mix shortly before usage)
Odyssey Blocking Buffer (PBS)	LI-COR Biosciences, Lincoln USA
Ponceau-solution:	0.2% PonceauS, 3% TCA
Protein ladder	PageRuler Plus Pre-Stained (Life Technologies, Frankfurt)
RIPA buffer:	50 mM Tris pH 7,5, 150 mM NaCl, 1 mM EDTA, 1% IGEPAL (Nonidet p-40), 0.1% SDS, 0.5% NaDeoxycholate

Immunostainings

10x Krebs buffer:	1.2 M NaCl, 48 mM KCl, 25 mM $CaCl_2$*$2H_2O$, 12 mM $MgCl_2$ in dH_2O
10x PBS:	1.37 M NaCl, 26.8 mM KCl, 0,101 M Na_2HPO_4, 13.8 mM KH_2PO_4
10x Tris-Borat-Buffer:	10 mM $Na_2B_2O_7$ in dH2O
1x Modified Krebs buffer:	1x Krebs buffer, 5 mM HEPES, 0.025 mM $NaHCO_3$, 0.1% BSA in H_2O (adjust to pH 7.4)
4% PFA:	1.3 M PFA in 1x PBS (adjust to pH 7.2-7.4)
50 x TAE buffer	2 M Tris, 50 mM Glacial acetic acid, 50 mM EDTA
Agarose gel DNA/RNA	
Antigen retrieval:	10N HCl in H2O
Blocking solution:	5% FCS, 1% serum (goat or donkey) in PBST, 1% BSA
DAPI:	5 mg DAPI in 25 ml PBS
DNA lysis buffer:	100 mM Tris (pH 8.5), 5mM EDTA, 0.2% SDS 200 mM Sodium chloride, 100 µg/ µl Proteinase K
Elvanol (embedding):	0.015 mM Polyvinyl-alcohol, 24 mM Tris pH 6.0, 2 g DABCO, in 90 ml H_2O and 37.8 ml Glycerol

FACS buffer:	1x PBS (-Ca/Mg), 3% FCS, 5 mM EDTA
Loading buffer DNA	100 mM EDTA, 2% SDS, 60% Glycerol, 0.2% Bromine phenol blue
Loading buffer RNA (2x)	95% Formamide, 0.025% SDS, 0.025% Bromine phenol blue, 0.025% Xylene cyanol FF, 0.025% Ethidium bromide, 0.5 mM EDTA
OCT medium	optimal cutting temperature (Leica Microsystems GmbH, Wetzlar)
PBST:	1x PBS + 0.1% Tween20 (adjust to pH7.4)
Permeabilisation (cells):	0.5% Saponin, 100 mM Glycin in dH_2O
Permeabilisation (islets):	0.5% TritonX-100, 100 mM Glycin in dH_2O
Permeabilisation (sections, cells):	0.25% TritonX-100, 100 mM Glycin in dH_2O

Cell-surface biotinylation assay:

NeutrAvidin IP beads	Pierce™ High Capacity NeutrAvidin™ Agarose (Thermo Fisher Scientific, Waltham; #29202)
Stopping solution	100 mM Glycin in PBS pH 7.5
EZ-Link Sulfo-NHS-LC-Biotin	N-Hydroxysulfosuccinimide (NHS)-biotin (Thermo Fisher Scientific, Waltham 10538723)

Others:

Bio-Gel P-4 polyacrylamide beads suspension	(Biorep Technologies, Miami USA)
ddH_2O	QPod (Millipore, Schwalbach)
DNA ladder (100 bp and 1 kb)	New England Biolabs GmbH, Frankfurt am Main
EdU for animal injections	(#A10044, Life Technologies, Freiburg)
Eosin Y solution, aqueous	HT110216 (Sigma, Hamburg)
Hematoxylin solution, Mayer´s	MHS1 (Sigma, Hamburg)
Nuclear fast red (NFR)	N3020 (Sigma, Hamburg)
QIAzol lysis reagent	Quiagen GmbH, Hilden
RNA ladder	RNA ladder 100 bp (NEB, Frankfurt)
Xylene mounting medium	Roti® Histokitt (Carl-Roth GmbH, Karlsruhe)

6.1.6 Solutions for cell culture

10 x KRH buffer stock	1.200 mM NaCl, 48 mM KCl, 25 mM $CaCl_2.2H_2O$, 12 mM $MgCl_2$
1x MEM, NEAA	non-essential amino acids, 100x (Gibco, Invitrogen, Carlsbad, CA)
CMRL1066	Gibco, Invitrogen, Carlsbad, CA; Thermo Fisher Scientific, Waltham
Collagenase (islets):	1 mg/ml Collagenase P (Roche, Pensberg) in G-solution
DMEM (1 g/l glucose)	Gibco, Invitrogen, Carlsbad, CA; Life technologies, Frankfurt
DMEM (4.5 g/l glucose)	Gibco, Invitrogen, Carlsbad, CA
DMEM without glucose	Life Technology, Frankfurt
DMEM without phenol red (1 or 4.5 g/l glucose)	Gibco, Invitrogen, Carlsbad, CA
Donkey serum	Millipore, Schwalbach
DPBS	Lonza Verviers, Belgium
DPBS (-Ca/-Mg)	Gibco, Invitrogen, Carlsbad, CA
ECM	Sigma-Aldrich, Hamburg
EdU	Life Technologies, Frankfurt
FCS	PAA (Laboratories Gesellschaft GmbH, Pasching, Österreich)
Fibronectin from bovine Plasma	Sigma-Aldrich, Hamburg
Freezing Medium:	9 ml FCS (PAN/PAA Biotech GmbH, Aidenbach), 1 ml DMSO (1x)
Goat serum	Biozol, Eching
Gradient medium (islets):	5 ml G-solution 30 µl 1M HEPES (Life Technologies, Frankfurt) 970 µl DPBS (Lonza Verviers, Belgium) 2 ml Optiprep density gradient medium (Sigma, Hamburg, D1556-250ML)
G-Solution (islets):	HBSS (Lonza Verviers, Belgium) supplemented with 1x P/S (Gibco, Invitrogen, Carlsbad, CA) and 1% BSA (Sigma, Hamburg) (5 g BSA sterile filtered)
HBSS	Lonza Verviers, Belgium
HBSS (Min6)	114 mM NaCl, 4.7 mM KCl, 1.2 mM KH_2PO_4, 1.16 mM $MgSO_4$, 20 mM Hepes, 2.5 mM $CaCl_2$, 25.5 mM $NaHCO_3$, 0.2% BSA (essentially free fatty acid), pH 7.2
HEPES (1 M)	Gibco, Invitrogen™ Cooperation, Carlsbad, CA
Human Transferrin	Sigma-Aldrich, Hamburg
KRH working solution	Final concentration: 120 mM NaCl, 4.8 mM KCl, 2.5 mM $CaCl_2.2H_2O$, 1.2 mM $MgCl_2$. For 200 ml (pH 7.4): 20 ml of 10 x

	KRB stock, 1 ml 1 M HEPES, 9.6 ml HCO_3 (0.5 M $NaHCO_3$) stock (1 M)
L-Glutamine	200 mM, Gibco, InvitrogenTM Cooperation, Carlsbad, CA
Lipofectamine2000	Thermo Fisher Scientific, Waltham
Matrigel	BD Bioscience / Neolab, Heidelberg
Nicotinamide	VWR International, Darmstadt
Opti-MEM	(Life Technologies GmbH, Frankfurt)
OptiPrep Density gradient medium	Sigma, Hamburg
Penicillin/Streptomycin (100x)	Pen/ strep (Gibco, Invitrogen™ Cooperation, Carlsbad, CA)
Perfusion assay buffer (KRBH)	120 mM NaCl, 4.8 mM KCl, 2.5 mM $CaCl_2$ $2H_2O$, 1.2 mM $MgCl_2$ $6H_2O$, 10 mM HEPES, 0.25% BSA, 24 mM $NaHCO_3$
Rat serum	Sigma-Aldrich GmbH, Hamburg
RPMI1640	Lonza Verviers, Belgium
Sodium pyruvate	Gibco, Invitrogen™ Cooperation, Carlsbad, CA
Sodium selenite	Sigma-Aldrich, Hamburg
Trypsin-EDTA	0.05% or 0.25% Trypsin, 0.53 mM EDTA4Na, Gibco, Invitrogen, Carlsbad, CA
β-mercaptoethanol (50mM)	50 mM (Gibco, Invitrogen™ Cooperation, Carlsbad, CA)

6.1.7 Enzymes, inhibitors and growth factors

Chlorpromazin	Selleckchem Houston, USA
Collagenase P	(Roche, Pensberg)
Cyclopamine	Smootened ligand inhibitor (Cyc, Sigma, Schnelldorf)
DNA-Polymerases	Thermo Fisher Scientific, Waltham (Taq DNA Polymerase, recombinant)
Filipin III	Sigma Aldrich, Hamburg (F 4767)
Igf1 ligand	Recombinant Igf1 (Eagle Biosciences, Nashua, USA)
Igf2 ligand	Recombinant Igf2 (Sigma Aldrich, Hamburg)
Insulin (cell culture)	Sigma Aldrich, Hamburg
Insulin (mice)	Actrapid penfill (Bagsværd, Denmark)
Methyl-β-cyclodextrin	Sigma Aldrich, Hamburg
Phosphatase & Proteinase inhibitors	Sigma-Aldrich GmbH, Seelze
RNase-free DNase I	Qiagen Holding, Hilden
SAG	Smoothened ligand activator (Life Sciences, Lörrach)
Shh	Recombinant mouse Shh (C25II) N-Terminus (R&D Systems, Inc., Deubel, Minneapolis, MN)

6.1.8 Antibodies

Table 6.1: List of primary antibodies used in this thesis.

WB: Western Blot, IF: Immunofluorescence

ID	Name	Generated in	company	Order #	Dilution
IDO	(SMA) Anti-alpha smooth muscle Actin	rabbit	Abcam	ab5694	IF 1:100
269	Akt (pan) (C67E7)	rabbit	Cell signaling	4691	WB 1:5000
511	Akt(pan) (40D4) Mouse mAb	mouse	Cell Signaling/NEB	2920S	WB 1:5000
270	Akt-Phospho (Ser473) (D9E)	rabbit	Cell signaling	4060	WB 1:5000
289	AMPK alpha	rabbit	Cell signaling	2532	WB 1:1000
288	AMPK-Phospho α (Thr172)	rabbit	Cell signaling	2535	WB 1:1000
513	AMPKα (F6) Mouse mAb	mouse	Cell Signaling/NEB	2793S	WB 1:5000
IDR-G	Arl13	rabbit	Proteintech/ Acris	17711-1-AP	IF 1:100
Sample	Atg12 (D88H11)	rabbit	Cell Signaling	4180	WB 1:1000
Sample	Atg16L1 (D6D5)	rabbit	Cell Signaling	8089	WB 1:1000
Sample	Atg3	rabbit	Cell Signaling	3415	WB 1:1000
Sample	Atg5 (D5F5U)	rabbit	Cell Signaling	12994	WB 1:1000
Sample	Atg7 (D12B11)	rabbit	Cell Signaling	8558	WB 1:1000
Sample	Beclin-1 (D40C5)	rabbit	Cell Signaling	3495	WB 1:1000
466	Caveolin-1	rabbit	Santa Cruz	sc 894	IF 1:100
053	CD31/PECAM1	rat	BD	553370	IF 1:300
533	Centrin-2	rabbit	Merck Millipore	ABE480	IF 1:100
	CM1	mouse	Gift from Ünal Coskun, Dresden		IF 1:300
401	Collagen IV	rabbit	Abcam	ab6586	IF 1:100
464	EEA1	rabbit	NEB	2411S	IF 1:300
489	ERGIC53	rabbit	Santa Cruz	sc-66880	IF 1:300
056	Foxa2	rabbit	Abcam	ab40874	IF 1:1000
256	GASP-2 (E14)	rabbit	Santa Cruz	sc-162842	IF 1:100
048	GFP	chicken	Aves Labs	GFP-1020	IF 1:5000
337	Ghrelin (C-18)	goat	Santa Cruz	sc-10368	WB 1:1000
576	Giantin	rabbit	BioLegend	924302	IF 1:100
147	Gli1 (L42B10)	mouse	NEB	2643	IF 1:100
201	GLI3	goat	RD	AF3690	IF 1:100
315	Glucagon	guinea pig	TAKARA	M182	IF 1:1000
091	GM130	mouse	BD	610822	IF 1:300
423	HSP90	rabbit	Cell Signaling	4874	WB 1:5000
433	IGF-I Receptor β (D23H3) XP® Rabbit mAb	rabbit	Cell Signaling	9750	WB: 1:1000
193	Insulin	guinea pig	Thermo Scientific	10520565	IF: 1:1000
302	Insulin	guinea pig	Thermo Schientific	PA1-26938	IF 1:1000
299	Insulin Rbeta (C-19)	rabbit	Santa Cruz	sc-711	WB 1:1000

262	Insulin Receptor beta (4b8)	rabbit	NEB	3025	WB 1:1000
452	InsulinReceptor/IGF1R (Tyr1158/Tyr1162/Tyr1163)-phospho	rabbit	Millipore	07-841	WB 1:1000
266	IRS-2	rabbit	NEB	4502	WB 1:1000
216	Ki67	rabbit	Abcam	ab15580	IF 1:100
163	KIF7	rabbit	abcam	ab95884	WB 1:1000
095	LAMP1	mouse	BIOMOL	VAM-EN001	IF 1:100
339	LAMP1 (D2D11) XP	rabbit	NEB	9091	WB 1:1000
482	LAMP-2 / CD107b	rabbit	Thermo fisher	PA1-655	IF 1:300
484	LC3A/B (D3U4C) XP	rabbit	Cell Signaling	12741S	WB 1:1000
Sample	LC3A/B (D3U4C) XP	rabbit	Cell Signaling	12741	WB 1:1000
446	Mannose 6 Phosphate Receptor / CD222 Antibody	rabbit	Thermo Scientific	PA3-850	IF 1:100
271	MAPK p44/p42 (Erk1/2) (1367F5)	rabbit	Cell signaling	4695	WB 1:5000
272	MAPK Phospho-p44/42 (Erk1/2) (Thr202/Tyr204)	rabbit	Cell signaling	4370	WB 1:5000
273	mTOR	rabbit	Cell signaling	2972	WB 1:5000
512	mTOR (L27D4) Mouse mAb	mouse	Cell Signaling/NEB	4517S	WB 1:5000
274	mTOR-Phospho (Ser2448) (D9C2)	rabbit	Cell signaling	5536	WB 1:5000
IDO	NG2	mouse	Abcam	ab50009	IF 1:100
213	NKX6.1	goat	R&D systems	AF5857	IF 1:300
215	Nkx6.1	rabbit	Acris/Novus	NBP1-82553	IF 1:100
593	p44/42 MAPK (Erk1/2)	rabbit	Cell Signaling	9102	WB 1:1000
594	p44/42 MAPK (Erk1/2)-Phospho (Thr202/Tyr204)	rabbit	Cell Signaling	9101	WB 1:1000
203	Patched (G-19)	goat	Santa Cruz	sc-6149	IF 1:100
174	Pericentrin	rabbit	Covance/HISS Diagn.	PRB-432C	WB 1:100
IDR	Pifo	rabbit	PhD thesis D. Padula 2014	ISO-L, 3GI, M2a	IF 1:100
257	PP	goat	Abcam	ab77192	IF 1:100
580	Rab 11A (D-3)	mouse	Santa cruz	sc-166523	IF 1:100
578	Rab7 (D95F2)	rabbit	Cell Signaling	9367	IF 1:100
456	S6 Ribosomal Protein (5G10)	rabbit	Cell Signaling	2217S	WB 1:1000
455	S6 Ribosomal Protein (Ser235/236)- Phospho	rabbit	Cell Signaling	2211S	WB 1:1000
141	Smoothened	rabbit	Abcam	ab38686	IF 1:100
214	Somatostatin (D-20)	goat	Santa Cruz	sc-7819	IF 1:500
545	Somatostatin (G-10)	mouse	Santa Cruz	sc-55565	IF 1:1000
202	Su(fu)	goat	Santa Cruz	sc-10933	WB 1:100
577	TGN46	rabbit	Abcam	ab16059	IF 1:100
079	tRFP	rabbit	Biocat/Evrogen	AB234	WB 1:1000 IF 1:100
030	Tubulin-Acetylated	mouse	Sigma	T7451	IF 1:1000
029	Tubulin-α	mouse	Sigma	T6199	WB 1:5000

Table 6.2: List of secondary antibodies used in this thesis.

WB: Western Blot, IF: Immunofluorescence

ID	Name	Labelled	Company	Order #	Dilution
015	Goat anti-mouse IgG	HRP	Dianova	115-036-062	WB 1:10000
019	Goat anti-rabbit IgG	HRP	Dianova	111-036-045	WB 1:10000
020	Donkey anti-chicken IgY	Cy5	Dianova	703-175-155	IF 1:800
023	Donkey anti-mouse IgG	488	Invitrogen	A21202	IF 1:800
024	Donkey anti-rabbit IgG	555	Invitrogen	A31572	IF 1:800
025	Donkey anti-goat IgG	488	Invitrogen	A11055	IF 1:800
026	Donkey anti-rabbit IgG	488	Invitrogen	A21206	IF 1:800
027	Donkey anti-chicken IgY	Cy3	Dianova	703-165-155	IF 1:800
037	Donkey anti-mouse IgG	Cy5	Dianova	715-175-151	IF 1:800
061	Goat anti guinea pig IgG	546	Invitrogen	A11074	IF 1:800
071	Concanavalin A (ConA)	488	Invitrogen	C11252	IF 1:100
072	Wheat Germ Agglutinin (WGA)	488	Invitrogen	W11261	IF 1:100
083	Donkey-anti-rabbit IgG, IRDye (H+L)	800CW	LI-COR Biosciences	926-32213	WB 1:5000
084	Donkey-anti-Mouse IgG (H + L), IRDye	680RD	LI-COR Biosciences	926-68072	WB 1:5000

6.1.9 Primers, Taqman probes and siRNAs

6.1.9.1 Primers

All primers were purchased from Eurofins MWG Operon, Munich.

Table 6.3:List of primers for genotyping

Name	ID	sequence
SRY	EP990	TGACTGGGATGCAGTAGTTC
	EP991	TGTGCTAGAGAGAAACCCTG
GBS-GFP	EP1111	TGCAGTGCTTCAGCCGCTAC
	EP1112	CCAGCAGGACCATGTGATCG
Kif7	EP963	CTATCCCCAATTCAAAGTAGAC
	EP964	CACCACCATGCCTGATAAAAC
	EP965	CCAAATGTGTCAGTTTCATAGC
	EP966	TTCSTCACCCAAGCTCTTATCC
ARL13B-tRFP	EP1358	GCTGAACTTGTGGCCGTTTAC
	EP1430	AGATCCAAGAAACCCGCTAAGAAC
Igfr-L	EP1583	GTGCACTCTGGGTAGTGTTC
	EP1584	GATGCCTGTCAGCCTTCATC
	EP1585	CACCTCCCCCTGAACCTGAAAC
	EP1586	GAGTGGGATGAGCTACCTCAC
RosaCre	EP485	ATGCCCAAGAAGAAGAGGAAGGT
	EP486	GAAATCAGTGCGTTCGAACGCTAGA

Table 6.4: List of primers for sequencing

Name	ID	sequence
2A-BFP-CETN2 construct part	EP181	GAACTCCAGCAGGACCATGTG
	EP183	ACGTTGTGGCTGTTGTAG
	EP1111	TGCAGTGCTTCAGCCGCTAC
	EP1112	CCAGCAGGACCATGTGATCG
	EP1320	GCCACCTGATCTGCAACTTC
	EP1450	GCGTCGCGTTAAGATACATTG
	EP1481	GCCACGCGCTTAAGATTCTTG
	EP1482	CTTCCCGGATTTCCTGTTTCTG
	EP1483	TCCAGCAGGACCATGTGATCG
	EP1484	CTGCTTGACGGCCATGATATAG
	EP1485	GAACTTGTGGCCGTTTACGTC

Table 6.5: List of primers for qPCR (SYBR Green)

Name	ID	sequence
CENT2	EP1649	CCCTCATTGCCACCTTCAGT
	EP1650	GCATCCAGTGCCCAGAGAAA
BFP	EP1655	TCTCGTTGGGGTCTTTGCTC
	EP1656	ATCATGGCCGTCAAGCAGAA
GAPDH	EP144	GGCCAAGGTCATCCATGA
	EP145	TCAGTGTAGCCCAGGATG

6.1.9.2 Taqman probes

TaqMan primer were purchased from Life Technologies, Frankfurt.

Table 6.6: List of TaqMan probes for qPCR

Gene	Box position	Order information
eGFP	A-D5	Mr04329676_mr
Gli1	A-D2	Mm00494651_m1
Ptch1	A-B6	Mm00436026_m1
Foxo1	A-A12	Mm005490672_m1
Actb	A-C4	Mm00607939_s1
Gapdh	A-D3	Mm99999915_g1
18S	A-F12	Mm03928990_g1
MafA	A-H12	Mm00845206_s1
Foxa2	B-B4	Mm01976556_s1
Slc2a2	B-C12	Mm00446229_m1
Pcsk1	C-B1	Mm00479023_m1

Gipr	C-B10	Mm01316344_m1
Nkx2.2	A-B12	Mm00839794_m1
Gck	A-C1	Mm00439129_m1
Hprt	A-D11	Mm01545399_m1
Cdkn1a	A-G5	Mm04205640_g1
Glp1r	B-A2	Mm00445292_m1
Gcgr	B-A3	Mm00433546_m1
Cdkn1b	B-B10	Mm00438168_m1
5330417C22Rik	B-B12	Mm01199801_m1
Slc2a2	B-C12	Mm00446229_m1
Dvl3	C-C5	Mm00432914_m1
Pax6	B-H4	Mm00443081_m1
Pcsk2	C-B2	Mm00500981_m1
Slc30a8	C-B4	Mm00555793_m1
Gjd3	C-B5	Mm00731344_s1
Kcnj11	C-B6	Mm00440050_s1
Abcc8	C-B7	Mm00803450_m1
Smarca1	C-B8	Mm00474150_m1
MafB	C-B9	Mm00627481_s1
Insr	C-B11	Mm01211875_m1
Insrr	C-B12	Mm00442243_m1
Il6ra	C-C1	Mm00439653_m1
Sstr3	C-C3	Mm00436695_s1
Pard6a	C-C4	Mm01247370_g1
Rhoa	C-C6	Mm00834507_g1
Rock1	C-C7	Mm00485745_m1
Neurod1	A-D12	Mm01946604_s1
Wnt5b	A-D6	Mm01183986_m1
Rock2	C-A12	Mm01270843_m1

6.1.9.3 siRNA

The ON-TARGETplus non-targeting siRNA #1 and ON-TARGETplus Mouse 5330417C22Rik (229722) siRNA – SMARTpool mix were purchased from GE Healthcare (Dharmacon, Lafayette, USA).

6.1.10 Cell lines, primary cells, explant culture, embryonic culture

EndoC-βH1α	Human pancreatic β cell line (Ravassard et al., 2011)

IMCD3	Kidney, medulla/ collecting duct stable expressing the T-large antigen of SV40 (ATCC, USA, M)
Islets	Pancreatic islets were isolated from adult mice
MCF-7	breast cancer cell line (Michigan Cancer Foundation-7) (Soule, Vazquez, Long, Albert, & Brennan, 1973)
Min6 Igfr-L control and KO clones (B7-B10, D5, E10, F9, G9, G11)	Generated at IDR-L by Dr. Amir Morshedi
Min6 WT (parental WT)	Murine insulinoma cell line MIN6 m9 (Minami et al., 2000)
Primary MEFs	Primary murine embryonic fibroblasts isolated at E13.5

6.1.11 Culture medium of cell lines, primary cells, embryos and explant organ cultures

Embryo culture medium	40% DMEM 4.5 g/L D-Glucose without Phenol Red, 50% rat serum, 2 mM L-glutamine, 100 µM 2-mercaptoethanol and 1 mM sodium pyruvate
Embryo dissecting medium	DMEM 4.5 g/L D-glucose, 10% FCS and 20 mM HEPES
EndoC-βH1α coating solution	DMEM 4.5g/L glucose, 1% penicillin /streptomycin, 2 µg/ml fibronectin, 1% ECM
EndoC-βH1α culture medium	DMEM low glucose (1 g/L), 2 % albumin from bovine serum fraction V, 50 µM 2-mercaptoethanol, 10 mM nicotinamide, 5.5 µg/ml transferrin, 6.7 ng/ml sodium selenite and penicillin (100 units/ml)/streptomycin (100 µg/ml)
EndoC-βH1α neutralization medium	80% 1x PBS, 20% FCS
Islets	RPMI1640 supplemented with 1x P/S and 10% FCS
Min6	DMEM (4.5 g/l glucose) supplemented with with penicillin (100 units/ml)/streptomycin (100 µg/ml), 1.4 mM β-mercaptoethanol and 10% FCS
Organ explant culture medium	RPMI 1640 without Phenol Red, 10% FCS, 2 mM L-glutamine, penicillin (100 units/ml)/streptomycin (100 µg/ml), 100 µM 2-mercaptoethanol, only for pancreas culturing medium 1% insulin-transferrin-seleniumA of 100x Mix, 1% NEAA of 100x
Primary MEFs and IMCD3 (feeder medium)	DMEM supplemented with 2 mM L-glutamine, 15 % FCS, 0.1 mM β-mercaptoethanol, NEAA
Spermatocytes	HTF buffer (5.9 mg/ml NaCl, 0.3 mg/ml KCl, 50 µg/ml KH_2PO_4, 49.3 µg/ml $MgSO_4$ x $7H_2O$, 0.2% sodium lactate, 0.5 mg/ml glucose, 2.1 mg/ml $NaHCO_3$, 36.5 µg/ml sodium-pyruvate, 75 µg/ ml penicillin G, 50 µg/ml streptomycin, 0.6 mg/ml $CaCl_2$ x $2H_2O$, 4 mg/ml BSA (all from Sigma, Hamburg)

6.1.12 Mouse lines

ARL13B-tRFP	Generation of mouse line in this laboratory (IDR Prof. H. Lickert, Dr. Ingo Burtscher) and in collaboration with A. Gossler, Medizinische Hochschule Hannover, Germany
C57BL/6NCrl	BL6 Mice were obtained from Charles River
CD1	Outbred strain (Helmholtz Zentrum München)
Fltp(T2AiCre)	(Lange et al., 2012)
Foxa2^{T2AiCre}	(Horn et al., 2012)
Igfr-L$^{-/-}$ and Igfr-L$^{+/-}$	ESC clone bought from the European Conditional Mouse Mutagenesis Program. The EUCOMM clone 5330417C22RIK$^{tm1a(EUCOMM)Hmgu}$ (clone number H03) was chosen for ESC aggregation.
Kif7$^{+/-}$	(Cheung et al., 2009)
R26Cre (RosaCre)	(Soriano, 1999)
Tg(GBS-eGFP)	(Balaskas et al., 2012)

6.1.13 Food of mouse lines

Kif7$^{+/-}$ and Igfr-L$^{+/-}$: High-fat diet (HFD) food pellets: 58% fat, Research Diets Inc. D12331

6.2 Methods

6.2.1 Cell culture

6.2.1.1 Culture of cell lines

Cells were washed twice with PBS (-Mg/Ca) and trypsinized with 0.05% trypsin EDTA at 37°C for 5 min, which was stopped by adding culture medium (neutralization medium EndoC-βH1α). After cells were centrifuged at 1200 rpm at RT for 4 min, cells were washed with culture medium or PBS, centrifuged, re-suspended in a suitable volume and used for further experiments or plated in a new culture dish.

Table 6.7: Cell culture details for different cell lines

Cell line	Cell splitting	Dish coating	Cell density (splitting)
Min6	1x / week	no	max 50%
IMCD3	2x / week	no	90%
MEFs	2x / week	0,2% gelatin	90%
EndoC-βH1α	1x / week	coating medium	Seeding: 70.000-75.000 cells/cm^2

6.2.1.2 Cryopreservation of cells

For cryopreservation, cells were typsinized as described before and re-suspended in freezing medium (10% DMSO and 90% FCS). After transferring cells to cryotubes, cells were frozen in

freezing boxes overnight at -80°C and then placed into liquid N_2. Cells were thawed in a 37°C water bath and transferred into a culture dish with culture medium. The next day, the medium was changed to remove residual DMSO. Cells were cultured for one week prior to an experiment.

6.2.1.3 Generation of MEFs

Head and organs of cultured E13.5 embryos were removed to isolate the embryonic skin. The skin was minced for about 30 seconds using a scalpel and trypsinzed (0,25% trypsin) to generate a single cell suspension. After adding feeder medium, clusters of cells were further separated by pipetting up and down and centrifuged at 1200 rpm for 5 min. The pellet was resuspended with feeder medium and transferred to a culture dish, which was coated with 0,2% gelatine. Cell culture was performed as described before.

6.2.1.4 Islet isolation and culture

Collagenase P solution (1 mg/ml in G-solution) was injected in the common bile duct after sealing the connection of the central pancreatic duct and the duodenum with a clamp. After the pancreas was inflated with Collagenase P solution sufficiently, it was transferred in a falcon tube and digested at 37°C in a water bath for 15 min (mixing after 7.5 min). Digestion was stopped by adding G-solution. The digested pancreas was centrifuged at 1620 rpm, 4°C for 3 min, and the pellet was washed twice with 10 ml G-solution. Subsequently, the pellet was resuspended in 5.5 ml of gradient medium containing DBPS with 40% Optiprep density gradient medium and 10 µM HEPES, which was mixed with HBSS medium containing 1% FCS (ratio of mix 3:5). The suspension (2nd phase) was added slowly on the 2.5 ml remaining gradient medium (1st phase) and 6 ml of G-solution were added slowly on top forming the 3rd phase. After a 10 min incubation step at RT, the gradient solution with digested pancreas was centrifuged at 700 rpm, RT for 10 min (acceleration 3, brake 0). This entailed the enrichment of islets in the interphase between the middle and the upper phase. The interphase with islets was filtered through a pre-wet cell strainer (70 µm), which restrained islets. By washing the cell strainer with culture medium, islets were transferred to a petri dish with culture medium. Following, islets were handpicked twice under a light microscope. For further analysis, islets were cultured overnight. Image acquisition was performed on a Leica SP5 confocal microscope equipped with an incubation system and image analysis was carried out using Leica LAS AF software.

6.2.1.5 Isolation and culture of spermatocytes

Both caudae epididymidis from male adult animals were isolated. After removing fat and big blood vessels, the caudae epididymidis were transferred into human tubal fluid (HTF) buffer, cut several times with a scalpel and incubated for 5 min at room temperature. Imaging of spermatocytes was performed using a Zeiss microscope with a 20x objective in bright field mode, and movies were recorded with a Canon eos700d camera.

6.2.1.6 Culture of embryos and explant cultures

The isolation of embryos and lung explant cultures was performed as described previously (Burtscher & Lickert, 2009). Briefly, the isolation of embryos and organs was carried out in dissecting medium. Afterwards, embryos were transferred to embryo culture medium. Isolated organs were covered with a drop of Matrigel to avoid moving of tissue during imaging. Culture medium was added on top once the Matrigel solidified. Imaging of embryos was performed about one hour after isolation, whereas organs were cultured for up to three days before movies were recorded.

6.2.1.7 Time-lapse live imaging of islets, MEFs, organ cultures and embryos

Time-lapse imaging was carried out as described by (Burtscher & Lickert, 2009). Embryos, islets and organs were isolated and cultured on glass-bottom dishes using 200 µl culture medium in a 37°C incubator with 5% CO_2 and 5% O_2. Similarly, MEFs were seeded and cultured on glass-bottom dishes. To avoid evaporation, the culture medium was covered with mineral oil. Image acquisition was performed on a Leica SP5 confocal microscope equipped with an incubation system and image analysis was carried out using Leica LAS AF software.

6.2.2 Assays

6.2.2.1 Hedgehog stimulation assay of islet and cells

MEFs were seeded in 6 well plates and cultured for two days. At day three, at a confluency of 70-80%, cells were starved in serum-free culture medium overnight. In contrast, islets were cultured in culture medium containing 11 mM glucose for 1-2 hours after the isolation procedure and starved overnight. For the Hh stimulation assay, cells were treated with 500 ng/ml Sonic hedgehog ligand (Shh, R&D systems), 1 µM SAG (Enzo Life Sciences) or 10 µM cyclopamine (Cyc, Sigma) for 24–72 hours. Following, cells were lysed with RIPA buffer containing proteinase and phosphatase inhibitor cocktails and analysed by Western blot.

6.2.2.2 Growth factor and glucose stimulation assay of Min6 cells

For the stimulation assay, Min6 cells were seeded at a concentration, which ensured that cells reached a confluency of 50% at day four. After five washing steps with 1x PBS, cells were starved in HBSS buffer for 120 min and stimulated with 45 mU insulin, 10 nM Igf1, 10 nM Igf2 ligands or with 16.7 mM glucose diluted in HBSS buffer for 15 min. Subsequently, cells were fixated in 4% paraformaldehyde (PFA) and immunostained.

6.2.2.3 Endocytosis assay of Min6 cells

Min6 cells were seeded at a concentration, which ensured that cells reached a confluency of 50% at day four. Living cells were incubated at 4 °C for 30 min to inhibit endocytic processes. Afterwards, the culture medium was complemented with an Igfr-L antibody, which recognizes the extracellular domain of the Igfr-L protein (Igfr-L ecto). This enables receptor-antibody binding at the cell surface. Cells were washed with 1x PBS five times and antibody free culture medium was added to the cells. Subsequently, cells were placed at 37 °C for up to 60 min allowing the receptor-antibody complex to be endocytosed by the cell. In immunofluorescence stainings, the endocytosed Igfr-L ecto antibody was detected by a fluorescently labelled secondary antibody. For quantification method see page 146.

6.2.2.4 Endocytosis assay with CME and caveolae inhibitors

Min6 cells were seeded at a concentration, which ensured that cells reached a confluency of 50% at day four. To explore if the Igfr-L utilizes CME or CIE, pathway specific inhibitors were used to block endocytosis in cells. Living cells were incubated with Methyl-β-cyclodextrin, Filipin-III or Chlorpromazine at 37 °C for 60 min. Subsequently, the culture medium was additionally supplemented with an Igfr-L antibody, which specifically recognizes the extracellular domain of the receptor (Igfr-L ecto antibody). This allowed the endocytosis of the antibody receptor complex from the cell surface within the next 30 min (37 °C). For further analysis, cells were fixated with 4% PFA and immunostained.

6.2.2.5 EdU labelling of Min6 cells

For EdU labelling, Min6 cells were seeded at a concentration, which ensured that cells reached a confluency of 50% at day four. Cells were treated in culture medium complemented with 10 µM EdU for two hours. After PFA fixation, cells were immunostained according to the common protocol. EdU detection on Min6 cells was carried out using the Click-IT EDU Alexa Fluor 647 kit.

6.2.2.6 siRNA transfection of Min6 cells

To decrease Igfr-L expression in Min6 cells, a si-RNA mediated knock-down was performed. Cells were seeded in 8-well Ibidi chambers at a concentration of $5x10^4$ cells per well. At day two, cells were transfected: 31 µl Opti-MEM and 100 pmol of siRNA (0,25 µl) as well as 31 µl Opti-MEM and 0,62 µl Lipofectamine 2000 were mixed and incubated at RT for 10 min. Subsequently, both solutions were mixed carefully, further incubated at RT for 20 min and added to the culture medium. After 6 hours, the medium was replaced with fresh culture medium. The next day, the transfection procedure was repeated. At day four, cells were rinsed with 1x PBS and lysed for Western blot analysis or fixated with 4% PFA for an immunofluorescence staining.

6.2.2.7 Cell-surface biotinylation assay

Living Min6 cells were cooled to 4 °C to inhibit endocytic processes and rinsed three times with ice cold 1x PBS. Afterwards, cells were incubated in N-hydroxysulfosuccinimide (not cleavable, NHS)-biotin complemented buffer (2 mM) for 10 min enabling biotin to bind to cell surface proteins. NHS-biotin is a cell impermeable compound, which covalently attaches biotin to proteins by modifying exposed primary amino groups through its succinimidyl (NHS) estergroup. The reaction was stopped by adding stopping solution (100 mM Glycine in PBS). After a washing step with ice cold 1x PBS, cells were lysed in RIPA buffer (300 µl for one well of a 6 well plate) supplemented with proteinase and phosphatase inhibitors on ice for 10 min and homogenized with a cell scraper. Following, cells were centrifuged at full speed (14,000 rpm), at 4^0 C for 10 min. The supernatant was collected and the protein concentration was measured using the Pierce BCA Protein Assay Kit. Using a neutravidin-IP pull down assay, biotin-labelled plasma membrane proteins were isolated exploiting the high binding affinity of biotin for streptavidin. Therefore, neutravidin beads were washed 5x with RIPA buffer to remove the EtOH. 200µl lysate (1 µg/ µl protein) was added to 40 µl slurry (beads) and incubated at 4°C on a rotor overnight. The remaining lysate was used to control protein amounts on a Western blot (input). The next day, beads were carefully washed 5x with RIPA buffer at 4°C. Biotinylated proteins were eluted by adding 2x SDS-loading buffer to the beads and by heating the suspension at 95°C for 5 min. Subsequently, beads were centrifuged, the supernatant was loaded on a SDS-PAGE and proteins were detected by Western blot analysis.

6.2.3 Molecular biology

6.2.3.1 Isolation of genomic DNA and genotyping of mice

The genomic DNA was isolated from mouse tail biopsies or ear punches after mice were weaned at the age of about 20 days. If not processed the same day, biopsies were stored at -20°C. The tissue was lysed in 500 µl lysis buffer complemented with proteinase K (100 µg/ml) and incubated at 55°C overnight. The next day, the lysate was vortexed and centrifuged at 14,000 rpm for 10 min (RT) to pellet the hair and other undigested fragments. Subsequently, the supernatant was mixed with 500 µl 100% isopropanol to precipitate genomic DNA and centrifuged again (14,000 rpm, 10 min). The genomic DNA was washed with 70% EtOH and pelleted (14,000 rpm, 10 min). The pellet was air-dried and resuspended in 50-100 µl nuclease-free H_2O.

This protocol was also used to isolate genomic DNA from cultured cells.

Following PCR protocols were used for genotyping of mice.

Table 6.8: PCR protocols for genotyping

Mouse strain/gene	Primers	Protocol	PCR product
RosaCre	EP485 EP486	94°C 5 min [94°C 30 sec/ 58°C 40 sec/ 72°C 90 sec] 35x - 72°C 2 min - 4°C (12°C) ∞	~450 bp
Kif7	EP 963 EP 964 EP 965 EP 966	95°C 5 min [95°C 1 min / 58°C 1 min / 72°C 1 min 20 sec] x 35 - 72°C 5 min - 4°C (12°C) ∞	mutant: 500 bp WT: 300 bp
SRY	EP990 EP991	94°C 4 min [94°C 60 sec/ 54°C 45 sec/72°C 45 sec] x 30 - 72°C 10 min - 4°C (12°C) ∞	239 bp band for males, none for females
GBS-eGFP	EP1111 EP1112	94°C 2min [94°C 30 sec/ 58°C 30 sec/ 72°C 1 min] x 30 - 72°C 10 min - 4°C (12) ∞	~450 bp
ARL13B-tRFP	EP1358 EP1430	94°C 5 min [94°C 30 sec/58°C 40 sec/72°C 60 sec] x 35 - 72°C 10 min - 4°C (12°C) ∞	342 bp
Igfr-L (Genetrap)	EP1583 EP1584	95°C 5 min [95°C 30 sec/55°C 45 sec/72°C 45 sec] x 35 - 72°C 5 min - 4°C (12°C) ∞	mutant: 203 bp WT: 239 bp
Igfr-L (ΔEx3)	EP1584 EP1585 EP1586	95°C 3 min [95°C 30 sec/64°C 45 sec/72°C 45 sec] x 1 - [95°C 30 sec/55°C 30 sec/72°C 30 sec] x 35 - 72°C 5 min - 4°C (12°C) ∞	mutant: 341 bp WT: 266 bp

PCR Mix:

DNA sample	1 µl
10X Fermentas Taq Buffer w/$(NH4)_2SO_4$- $MgCl_2$	2 µL
25mM $MgCl_2$	2 µL
10µM dNTPs	1 µL
10 pmol/µL primer	1 µL each
Taq DNA Polymerase (5U/µL)	0.25 µL
ddH_20	Add 20 µl

6.2.3.2 Gel electrophoresis

The PCR product (genotyping) was loaded on a 2% agarose gel and separated by size using gel electrophoresis. Therefore, agarose powder was dissolved in 1x TAE (Tris-acetate, EDTA) buffer in a microwave. After cooling the solution, EtBr (1:20000) was added and the mixture was poured in a gel tray, which was equipped with a comb. Prior to sample loading, the solid agarose gel was placed in a chamber and covered with TAE buffer. PCR products were mixed with Orange G in a ratio of 1:4 and loaded on the agarose gel. DNA fragments were separated by size upon applying 100 V for 30 min and detected using a gel documentation system.

6.2.3.3 DNA sequencing

The following mixture was used for one sequencing reaction

Long sequence	Short sequence	
1.0 µl	0.5 µl	Big Dye containing the polymerase
1.0 µl	2.0 µl	Big Dye buffer
10 pM	10 pM	sense or antisense primer
(n) bp/ 100 = x ng template DNA		
Σ 5.0 µl		

PCR program: 96°C 1 min [96°C 10 sec/ 50°C 5 sec/ 60°C 4 min] x 35 - 16°C ∞

For DNA precipitation (PCR product) 0.5 µl of 125 mM EDTA, 2.0 µl 3 M NaAC, and 50 µl 100% EtOH were mixed and incubated at room temperature for 15 min. After pelleting by centrifugation (11,000 rpm) at 4 °C for 30 min, the DNA was washed with 70% EtOH (11,000 rpm, 4 °C, 30 min) and air-dried. The DNA was resuspended in 25 µl HPLC-H_2O. Samples were passed on to the HMGU sequencing service.

6.2.3.4 RNA isolation and reverse Transcription

Cells were lysed in Qiazol at room temperature for 5 min. For RNA extraction, the QIAGEN miRNA micro kit or the QIAGEN miRNA mini kit were used depending on the amount of RNA. Additional to the standard protocol, the DNA was degraded by performing an on column DNase I treatment. The RNA was eluted in 15-30 µl of nuclease-free H_2O. Purified RNA was stored at -80°C.

To transcribe RNA in complementary DNA (cDNA), the 5x VILO™ reaction mix and 10x SuperScript was used. Up to 2.5 µg RNA was applied to the reaction mix: 4 µl 5 x VILO Reaction Mix, 2 µl 10 x SS Enzyme Mix and DEPC or RNAse ddH_2O add 20µl. Subsequently, the solution mixture was incubated at 25°C for 10 min, 60 min at 42°C, followed by 5 min at 85°C. The cDNA was stored at -20°C.

6.2.3.5 Quantitative real-time PCR (qPCR)

TaqMan qPCR:

The TaqMan probe consists of the oligonucleotide, a covalently attached fluorophore at the 5`end and a quencher at the 3`end. When annealing to the cDNA between the primer set, the TaqMan probe is degraded by the exonuclease activity of the Taq Polymerase. This enables the dissociation of the fluorophore resulting in a fluorescence signal due to the release from the quencher interaction.

10-25 ng cDNA per reaction was added to the Taqman qPCR reaction mix: 1–3 µl cDNA, 5.0 µl TaqMan™ Advanced master mix, 0.5 µl TaqMan probe, H_2O add 10 µl. After sealing the 96 well

plate, and the centrifugation at 1500 rpm for 5 min, the qPCR reaction was performed using ViiA7 Real-time PCR system.

Analysis: The C_t-values were transformed to normalized relative quantities (NRQs) using multiple (f) reference genes (Hellemans, Mortier, De Paepe, Speleman, & Vandesompele, 2007):

$$NRQ = \frac{2^{\Delta Ct\,(gene\ of\ interest)}}{\sqrt[f]{\prod_{p=1}^{f} 2^{\Delta Ct\,(reference\ gene)_p}}}$$

Evagreen qPCR:

10-25 ng cDNA per reaction was added to the Evagreen qPCR reaction mix: 5 µl Evagreen mix, 1 µl primer, 1 µl cDNA, add 10 µl ddH_2O. After sealing the 96 well plate, and its centrifugation at 1500 rpm for 5 min, the qPCR reaction was performed using ViiA7 Real-time PCR system. Subsequently, the PCR product was loaded on a 2% agarose gel and separated by size using gel electrophoresis.

6.2.4 Western blot

The Western blot technique enables the separation of proteins in a cell lysate according to their size (and charge) and the quantification of protein abundancy using SDS-polyacrylamide gel electrophorese (SDS-PAGE) followed by a semi-dry immunoblot. The latter includes the transfer of proteins on a membrane and subsequent protein detection by antibody and horse radish peroxidase (HRP) based labeling.

6.2.4.1 Protein extraction and determination of protein concentration

Cells and tissues were rinsed with 1x PBS and incubated with RIPA lysis buffer on ice for 10 min. Subsequently, cells were shared using a cell scraper. In contrast, islets and tissue lysates were homogenised and sonicated (5 x 1 min) on ice to ameliorate the lysis process. After cells were centrifuged at full speed (14,000 rpm), at 4^0 C for 10 min, the supernatant was collected and stored at -20°C or - 80^0 C. During all steps of lyses, samples were kept at low temperature (4°C) as well as in presence of proteinase- and phosphatase inhibitors to prevent protein degradation. For determining the protein concentration, the Pierce BCA Protein Assay Kit was used, and the assay was carried out according to the user manual. The protein concentration of the sample was calculated based on the absorption at 562 nm and on a BSA standard curve.

6.2.4.2 Denaturing SDS-polyacrylamide gel electrophorese (SDS-PAGE)

The separating gel solution was poured between two sealed glass plates and overlaid with isopropanol to ensure horizontal margins at the top end. After removing the isopropanol by

washing with H_2O, the stacking gel solution was added above the solid separating gel. Gel pockets were created by placing a comb in the solution.

Table 6.9: Ingredients for two separating and stacking gels (1 mm spacer plates)

2x separating gels	**6,5%**	**10%**	**15%**	**2x stacking gels**	
Acrylamid	3.26 ml	5 ml	7.5 ml	**Acrylamid**	650 µl
4x Tris HCl/SDS buffer pH 8.8	3.75 ml	3.75 ml	3.75 ml	**4xTris/SDS pH 6.8**	1.25 ml
H_2O	8 ml	6.25 ml	3.75 ml	**H_2O**	3.10 ml
TEMED	20 µl	20 µl	20 µl	**TEMED**	10 µl
10% APS	150 µl	150 µl	150 µl	**10% APS**	50 µl

Protein lysates were mixed with SDS/dithiothreitol (DTT) loading buffer (1:4), heated at 95^0 C for five minutes and immediately cooled on ice. Thereby, SDS denatures secondary and non-disulfide–linked tertiary structures, and additionally applies a negative charge to each protein in proportion to its mass. Afterwards, protein lysates were loaded in the pockets of a SDS poly acrylamide gel, which was placed in a chamber filled with 1x Tris glycine running buffer. Proteins were separated in the gel at 80 – 100 V for 1-1.5 hours. A protein ladder was used to identify the molecular weight of proteins after separation.

6.2.4.3 Semi-dry immunoblot and immunostaining

After protein separation using SDS-PAGE, gels were equilibrated in KP buffer for 15 min. The PVDF membrane was activated in 100% methanol for 15 sec due to their hydrophobic surface, quickly washed in H_2O for 2 min and incubated in APII buffer for 10 min. An immunoblot sandwich was set up as follows: Top/cathode, 3 x Whatman paper soaked in KP buffer, SDS-gel, PVDF membrane, 1 x Whatman paper soaked in APII buffer and 2 x Whatman paper soaked in API buffer, anode/ bottom). Blotting was performed at 0.22 A (25 V) per gel for 30 min using a semi-dry blot chamber. After blotting, the membrane was incubated in Ponceau S solution to confirm successful protein transfer. The Ponceau S staining was washed with H_2O until the colour vanished.

After proteins were transferred on a PVDF membrane, the latter was blocked with 5% milk in TBST (blocking solution) at room temperature for one hour to saturate unspecific binding sites for antibodies. Afterwards, membranes were incubated in primary antibodies diluted in blocking solution at 4^0 C overnight. The next day, membranes were washed three times with 1x TBST for 10 min and incubated with secondary antibody (in blocking solution) at 4^0 C for 1-2 hours. After washing (1x TBST, 3x 10 min), membranes were rinsed with a mix of ECL solutions (enhanced chemiluminescence; 1:1 mix) and wrapped in foil. In the dark room, films were exposed to the membranes for 1 sec – 10 min and subsequently developed using a developer machine. Secondary antibodies are coupled to horseradish peroxidase (HRP) that bind primary antibodies on the

membrane. In the chemiluminescence reaction, the HRP enzyme catalyzes the oxidation of luminol into a reagent, which releases energy in the form of light (at a wavelength of 428 nm) as it decays. Thereby, modified phenols that are supplemented to the luminol solution (ECL substrate solution) greatly enhance light emission. The emitted light can be captured on an X-Ray film.

For the detection and quantification of proteins using fluorescence-labelled secondary antibodies, the protocol was modified as follows: Blotting with nitrocellulose membrane, blocking with Odyssey blocking buffer, fluorophore-conjugated secondary antibodies, detection with Odyssey Imaging Systems (LI-COR Biosciences).

Quantification of protein abundancies were performed using the ImageJ software. Intensity values of proteins were normalized to reference proteins such as Hsp90 detected on the same membrane. Phospho-proteins were additionally normalized to intensity values of their total form.

6.2.5 Immunohistochemistry and histology

6.2.5.1 Immunostainings on cultured cells

Cells were seeded in 8-well Ibidi chambers and cultured for three days. After washing with 1x PBS, cells were fixed with 4% PFA for 5-10 min and permeabilised with 0.25% Triton X-100, 0.1 M glycine in 1x PBS for 10 min. Following, cells were incubated in blocking solution containing 0.1% Tween-20, 10% FCS, 0.1% BSA and 3% serum (donkey or goat) in PBST (0.1 % Tween-20 in 1x PBS) for one hour. Primary antibodies were diluted in blocking solution, and cells were incubated in it at 4 °C overnight. The next day, cells were washed three times with 1x PBS for 10 min. Afterwards, cells were incubated in blocking solution complemented with secondary antibodies at room temperature for 2-3 hours. Furthermore, cells were washed three times with 1x PBST for 10 min and stained with 40, 6-diamidin-2-phenylindol (DAPI) in 1x PBS (1:500) for 20 – 30 min. For embedding, cells were washed three times with 1x PBS for 10 min and then self-made Elvanol or ProLong1 Gold antifade reagent was applied. Ibidi chambers with stained cells were stored at 4°C.

6.2.5.2 Whole mount immunostainings of embryonic organs

E7.5 embryos were dissected in PBS+ (PBS containing Mg2+ and Ca2+) and organs were fixed with 2% PFA in PBS+ at room temperature for 20 min. Subsequently, embryos were rinsed with 1x PBST+ and permeabilised with 0.1 M glycine and 0.1% Triton X-100 in PBS+ for 20 min. Further steps were performed as described for cultured cells. A 100 µm spacer with holes was glued on a coverslip, and embryos were transferred in the holes. After embedding in ProLong1 Gold antifade reagent, embryos were covered with a second coverslip to be able to scan the embryos from both sides.

6.2.5.3 Immunostainings on cryosections

Dissected organs were washed with 1x PBS and fixed in 4% PFA overnight at 4°C (adult pancreas for 2 hours at 4°C). For cryoprotection, organs were incubated in a sucrose gradient at 4°C for at least 3 hours per sucrose concentration (5%, 15%, 30% sucrose in PBS and 1:1 of 30% sucrose and OCT), embedded in OCT (optimal cutting temperature) medium and frozen at -80°C. Cryo-embedded organs were cut in 15 µm sections. For immunostainings, cryosections were rehydrated in 1x PBST for one hour. Further steps were performed as described for cultured cells.

6.2.5.4 Immunostainings on islets

Immunostaining of isolated islets were carried out in a 96-well plate. Therefore, islets were washed three times with 1x PBS for 10 min, fixated with 4% PFA for 10 min and permeabilized with 0.5% Triton X-100 in PBS for 30 min. Further, immunostaining steps were performed as described for cultured cells. For mounting, islets were transferred to a cover slip equipped with a spacer (Life Technologies) and covered with ProLong Gold antifade reagent (Invitrogen) or self-made Elvanol.

6.2.5.5 Microscopy & analysis of immunofluorescence stainings

Image acquisition was performed on a Leica SP5 confocal microscope and image analysis was carried out using Leica LAS AF software and/or Imaris (Bitplane) software.

6.2.5.6 Haematoxylin and eosin (H&E) staining

To analyse the morphology of livers isolated from Igfr-$L^{+/-}$ male and female animals, cryosections were made and stained with haematoxylin and eosin. After rehydration in 1x PBS for 10 min, cryosections were washed in H_2O for 5 min and stained with freshly prepared Mayer´s solution for up to eight minutes, depending on the strength of the staining. Subsequently, slides were stained with eosin for several minutes and again washed in H_2O for 5 min. Further, cryosections were incubated in 95% EtOH for 2 min, in 100% EtOH for 10 min and in xylene. For mounting the Xylene mounting medium was used.

6.2.6 FACS sorting

Female MEFs were sorted using the FACS-Aria III system. Cultured MEFs were trypsinized (0.25% trypsin), washed with 1xPBS and fixated with 80% ice cold EtOH for 10 min at 4°C. After another washing step, MEFs were kept in FACS buffer at room temperature. Before sorting or analysis, cells were filtered through a 70 µm filter to remove cell clumps. Single cells were gated according to their SSC-A (side scatter area) and FSC-A (front scatter area). Cells without reporter expression were discriminated from cells with active reporter expression upon their 561 nm emission (tRFP). Cytometry data analysis was performed using the Diva software.

6.2.7 General mouse handling

6.2.7.1 Animal studies approvals

Animal experiments were carried out in compliance with the German Animal Protection Act, the guidelines of the Society of Laboratory Animals (GV-SOLAS) and Federation of Laboratory Animal Science Associations (FELASA). Mice were housed at an ambient temperature of 23^0C with a constant humidity and a 12 hours light - dark cycle.

6.2.7.2 Generation of ARL13B-tRFP mice

Generation of ARL13B-tRFP mice was done by Dr. Ingo Burtscher and Prof. Dr. Achim Gossler (collaboration partner). For method description see submitted publication "A novel Cre-inducible knock-in ARL13B-tRFP fusion cilium reporter"

6.2.7.3 Administration of EdU

The modified uracil analogs 5´ethynyl-2´-desoxyuridine (EdU) was used to detect proliferating cells in the endocrine pancreas of Igfr-$L^{+/-}$ mice, which were fed a HFD for 28 weeks. EdU labelling is based on the incorporation of EdU into newly synthesized DNA. 100 µg EdU per g body weight was injected intraperitoneal (i.p.) 24 hrs prior to their sacrifice (stock: 10 mg/ ml in PBS; 10 µl/ g body injected). EdU detection on cryosections of pancreata was carried out using the Click-IT EDU Alexa Fluor 647 kit.

6.2.8 Metabolic analysis of adult mice

For the analysis of metabolic parameters of adult mice (Kif7$^{+/-}$ and Igfr-$L^{+/-}$) a cohort of 16 mice (eight HET and eight WT mice) per group was set up. Metabolic parameters of Igfr-$L^{+/-}$ animals were monitored at the age of 3 months (before HFD), (12 weeks of age), after 12 weeks of HFD feeding (6 months old mice) and after 28 weeks of HFD (9 months of age). For each time point a glucose tolerance tests (GTT), an insulin secretion tests (IST), an insulin tolerance tests (ITT) and NMR spectroscopy was performed. Adult mice were fed a high-fat diet (HFD; food pellets from Research Diets Inc. D12331) with a metabolic energy content of 23 MJ/ kg, containing 58% fat, 16.4% protein and 25.5% carbohydrate, and no fibers.

6.2.8.1 NMR spectroscopy

Lean and fat mass determination of adult male and female Igfr-$L^{+/-}$ mice was assessed by NMR analysis using a EchoMRI.

6.2.8.2 IP-GTT, IST and IP-ITT

For measuring glucose clearance (IP-GTT) and insulin secretion (IST), mice were injected with 1.5 g glucose/ kg body weight after 5.5 hours starvation. Blood glucose concentration was measured at time point 0, 15, 30, 60 and 120 min after injection using a glucometer. Additionally, blood samples were collected from the tail vain at the first three timepoints using EDTA-treated tubes to determine the insulin concentration in the plasma. For plasma separation, blood samples were centrifuged at 3500 rpm at 4°C for 15 min. Subsequent determination of insulin concentration was performed using the Ultrasensitive mouse insulin ELISA kit. A similar procedure was conducted for intraperitoneal insulin tolerance test (IP-ITT). After 6 hours of starvation, mice were injected with 0,75 U insulin per kg body weight and the blood glucose concentration was measured at time point 0, 15, 30, 60 and 120 min.

6.2.8.3 Determination of β-ketones, glucagon, NEFA, LDL in blood plasma

Blood samples were collected from the tail vain of animals and plasma was separated by centrifugation at 3500 rpm at 4°C for 15 min. Plasma glucagon, LDL, HDL, total cholesterol, NEFA concentrations were measured using following kits: Mouse Glucagon ELISA kit, LabAssay™ Cholesterol (total), Mouse HDL-Cholesterol Assay Kit, Mouse LDL-Cholesterol Assay Kit and NEFA-HR (2) R1+R2 Set. The analysis was done on the blank corrected absorptions when required for the assay. For determination of plasma glucagon levels, mice were starved for six hours before sample taking. For the examination of β-ketones (β-hydroxybutyrate) concentrations in blood plasma samples BlutketonFreeStyle Precision H stripes were used.

6.2.8.4 Determination of insulin secretion (GSIS) and insulin content of isolated islets

Glucose Stimulated Insulin Secretion (GSIS) of islets – static assay:

After the overnight culture, isolated islets were collected in a conical 96 well plate and summarized according to their size. Triplicates of 10 islets were separately analyzed. Islets were incubated in 90 µl of 0.5% Albumin-Kreps-Ringer HEPES-buffered (KRH) saline, containing low glucose concentrations (2.8 mM) and incubated for one hour at 37^0C. 80 µl supernatant was collected and replaced with KRH buffer containing high glucose concentrations (16.8 mM). After one hour, the supernatant was again transferred in PCR tubes on ice. Remaining islets were lysed in 80 µl of RIPA lysis buffer supplemented with proteinase- and phosphatase inhibitors. All samples were stored at -20^0C until the insulin levels were assayed using the Ultrasensitive mouse insulin ELISA kit. The insulin concentration was determined by a standard curve, and insulin levels were normalized on the total insulin content (secreted plus remaining insulin content).

Glucose Stimulated Insulin Secretion (GSIS) of islets – perfusion assay:

In contrast to the conventional GSIS, the perfusion assay allows the analysis of insulin secretion in a time-resolved manner including first and second phase of insulin secretion. The Biorep perfusion system ensures that all components of the assay such as islets and buffer solutions are kept at 37°C. 50 islets per mouse were cultured for 24 hours after isolation, and starved in KRBH buffer containing 3 mM glucose one hour prior assay start. Subsequently, islets were transferred to a perfusion chamber containing a Bio-Gel P-4 polyacrylamide beads suspension. On top of the islets, additional bead suspension was added. This sandwich setup of islets and bead suspension contained islets and prevented clogging of the filter, which lies on the bottom of the perfusion chamber. The perfusing fluid was pushed by a peristaltic pump through the perfusion chamber, and the perfusate was collected in a 96 well plate for further analysis. To adjust islets to the new environment, islets were perfused with KRBH buffer containing 3 mM glucose for 52 min. To induce insulin secretion, islets were stimulated with KRBH buffer containing 11 mM glucose for 30 min. After a recovery phase of 20 min in 3 mM glucose KRBH buffer, islets were stimulated with 25 mM KCl for 10 min. Following the perfusion assay, the polyacrylamide bead solution containing islets were centrifuged (1200 rpm, 5 min), and the supernatant with islets was transferred to DNA lysis buffer and incubated at 55°C overnight. The next day, the genomic DNA was extracted, and the DNA concentration was measured using the AccuBlue™ High Sensitivity dsDNA Quantitation kit. Collected GSIS KRBH buffer with secreted insulin was diluted and samples were taken for insulin measurements using the Insulin Ultra Sensitive Assay Kit, HTRF assay (Cisbio, Bedford USA) kit. After kit solutions and samples were mixed in a 384 well dish, samples were incubated for 18 hours overnight, and insulin levels were quantified using the ELISA plate reader Varioskan LUX. Insulin concentration were normalized on total DNA content.

Insulin content determination of isolated islet:

Islets were isolated from adult mice and cultured in islet culture medium overnight. Subsequently, islets were lysed with RIPA, complemented with proteinase- and phosphatase inhibitors. To improve the lysis process, islet lysates were sonicated for 5 min at 4°C. Insulin content was measured using the Ultrasensitive mouse insulin ELISA kit (Crystal Chem). Insulin levels were normalized over the protein concentration, which was determined by BCA protein assay.

6.2.9 Image analysis and statistics

6.2.9.1 Colocalization studies of IF images

IF pictures (merge of channels) were exported from the Leica LAS AF software in jpeg format and imported in ImageJ software. The degree of colocalization for proteins was measured by quantifying images via the ImageJ plugin Fiji Coloc2 using Costes background subtraction. Large "black" space around cell patches in images were excluded from the analysis by defining ROI areas

(K. W. Dunn, Kamocka, & McDonald, 2011). Intensity values derived from ImageJ calculations were depicted in a scatter plot using the software R. Scatter plots graphically represent colocalizing pixels of a merged image with pixel signals plotted according to their intensity values. The cloud of colocalizing pixels can be fitted by linear regression measuring a correlation coefficient. This coefficient is expressed via the Pearson correlation coefficient (PCC, R-value) value. R-values range between +1 and -1, whereby a value of +1 indicates perfect correlation, 0 no correlation, and -1 perfect inverse correlation. Thus, a linear relationship of colocalizing pixel intensities signifies good colocalization. The PCC is a robust value but is not sensitive to differences in mean signal intensities of merged signals within an image. Deviating signal intensities often appear in immunofluorescence stainings. The Mander's overlap coefficient (MOC) value tM2 calculates the percentage of above-background pixels in image 2 (Igfr-L) that overlaps with above-background pixels in image 1 (marker) whereas tM1 represents the inverse relation. The MOC is susceptible to background immunostaining, but provides the advantage that it also considers small subpopulations of proteins that are localized apart from the main protein pool. Only one z-plane of image stacks (highest overlap represented by PCC and MCC) was chosen. 4-6 pictures per n were quantified and the average was calculated. For the scatterplot, representative data from a single merged picture are shown.

6.2.9.2 Statistics

The statistical analysis was carried out using the software Graphpad Prism. If not indicated otherwise, a two-sided and paired or unpaired Student's t-test was used. For GTT, IST and ITT two-way ANOVA analysis was performed. * indicated P-values smaller than 0.05, ** < 0.01, *** < 0.001 and **** < 0.0001.

7 List of figures and tables

7.1 Figures

7.2 Tables

8 References

Adams, T. E., Epa, V. C., Garrett, T. P. J., & Ward*, C. W. (2000). Structure and function of the type 1 insulin-like growth factor receptor. *Cellular and Molecular Life Sciences*, *57*(7), 1050–1093. https://doi.org/10.1007/PL00000744

Agarraberes, F. A., & Dice, J. F. (2001). Protein translocation across membranes. *Biochimica et Biophysica Acta (BBA) - Biomembranes*, *1513*(1), 1–24. https://doi.org/10.1016/S0304-4157(01)00005-3

Ait-Lounis, A., Baas, D., Barras, E., Benadiba, C., Charollais, A., Nlend Nlend, R., … Reith, W. (2007). Novel Function of the Ciliogenic Transcription Factor RFX3 in Development of the Endocrine Pancreas. *Diabetes*, *56*(4). Retrieved from http://diabetes.diabetesjournals.org/content/56/4/950

Alberti, K. G. M. M., & Zimmet, P. Z. (1998). Definition, diagnosis and classification of diabetes mellitus and its complications. Part 1: diagnosis and classification of diabetes mellitus. Provisional report of a WHO Consultation. *Diabetic Medicine*, *15*(7), 539–553. https://doi.org/10.1002/(SICI)1096-9136(199807)15:7<539::AID-DIA668>3.0.CO;2-S

Annunziata, M., Granata, R., & Ghigo, E. (2011a). The IGF system. *Acta Diabetologica*, *48*(1), 1–9. https://doi.org/10.1007/s00592-010-0227-z

Annunziata, M., Granata, R., & Ghigo, E. (2011b). The IGF system. *Acta Diabetologica*, *48*(1), 1–9. https://doi.org/10.1007/s00592-010-0227-z

Apte, M. V, Pirola, R. C., & Wilson, J. S. (2012). Pancreatic stellate cells: a starring role in normal and diseased pancreas. *Frontiers in Physiology*, *3*, 344. https://doi.org/10.3389/fphys.2012.00344

Aspinwall, C. A., Qian, W. J., Roper, M. G., Kulkarni, R. N., Kahn, C. R., & Kennedy, R. T. (2000). Roles of insulin receptor substrate-1, phosphatidylinositol 3-kinase, and release of intracellular Ca2+ stores in insulin-stimulated insulin secretion in beta -cells. *The Journal of Biological Chemistry*, *275*(29), 22331–8. https://doi.org/10.1074/jbc.M909647199

Babu, D., & Roy, S. (2013). Left-right asymmetry: cilia stir up new surprises in the node. *Open Biology*, *3*(5), 130052–130052. https://doi.org/10.1098/rsob.130052

Bach, L. A. (2015). Insulin-Like Growth Factor Binding Proteins--an Update. *Pediatric Endocrinology Reviews : PER*, *13*(2), 521–30. Retrieved from http://www.ncbi.nlm.nih.gov/pubmed/26841640

Bader, E., Migliorini, A., Gegg, M., Moruzzi, N., Gerdes, J., Roscioni, S. S., … Lickert, H. (2016). Identification of proliferative and mature β-cells in the islets of Langerhans. *Nature*, *535*(7612), 430–434. https://doi.org/10.1038/nature18624

Bai, Y., Bai, Y., Dong, J., Li, Q., Jin, Y., Chen, B., & Zhou, M. (2016). Hedgehog Signaling in Pancreatic Fibrosis and Cancer. *Medicine*, *95*(10), e2996. https://doi.org/10.1097/MD.0000000000002996

Bailey, C. J. (2015). The Current Drug Treatment Landscape for Diabetes and Perspectives for the Future. *Clinical Pharmacology and Therapeutics*, *98*(2), 170–84. https://doi.org/10.1002/cpt.144

Balaskas, N., Ribeiro, A., Panovska, J., Dessaud, E., Sasai, N., Page, K. M., … Ribes, V. (2012). Gene regulatory logic for reading the Sonic Hedgehog signaling gradient in the vertebrate neural tube. *Cell*, *148*(1–2), 273–84. https://doi.org/10.1016/j.cell.2011.10.047

Bangs, F., & Anderson, K. V. (2017). Primary Cilia and Mammalian Hedgehog Signaling. *Cold Spring Harbor Perspectives in Biology*, *9*(5), a028175. https://doi.org/10.1101/cshperspect.a028175

Barbieri, E., Di Fiore, P. P., & Sigismund, S. (2016). Endocytic control of signaling at the plasma membrane. *Current Opinion in Cell Biology*, *39*, 21–27. https://doi.org/10.1016/j.ceb.2016.01.012

Bass, J., Chiu, G., Argon, Y., & Steiner, D. F. (1998). Folding of insulin receptor monomers is facilitated by the molecular chaperones calnexin and calreticulin and impaired by rapid dimerization. *The Journal of Cell Biology*, *141*(3), 637–46. Retrieved from http://www.ncbi.nlm.nih.gov/pubmed/9566965

Bastidas-Ponce, A., Scheibner, K., Lickert, H., & Bakhti, M. (2017). Cellular and molecular mechanisms coordinating pancreas development. *Development*, *144*(16), 2873–2888. https://doi.org/10.1242/dev.140756

Belfiore, A., Frasca, F., Pandini, G., Sciacca, L., & Vigneri, R. (2009). Insulin receptor isoforms and insulin receptor/insulin-like growth factor receptor hybrids in physiology and disease. *Endocrine Reviews*, *30*(6), 586–623. https://doi.org/10.1210/er.2008-0047

Bell, E., Cao, X., Moibi, J. A., Greene, S. R., Young, R., Trucco, M., … Wolf, B. A. (2003). Rapamycin has a deleterious effect on MIN-6 cells and rat and human islets. *Diabetes*, *52*(11), 2731–9. Retrieved from http://www.ncbi.nlm.nih.gov/pubmed/14578291

Benmerah, A. (2013). The ciliary pocket. *Current Opinion in Cell Biology*, *25*(1), 78–84. https://doi.org/10.1016/j.ceb.2012.10.011

Bergers, G., & Song, S. (2005). The role of pericytes in blood-vessel formation and maintenance. *Neuro-Oncology*, *7*(4), 452–64. https://doi.org/10.1215/S1152851705000232

Bernal-Mizrachi, E., Wen, W., Stahlhut, S., Welling, C. M., & Permutt, M. A. (2001). Islet beta cell expression of constitutively active Akt1/PKB alpha induces striking hypertrophy, hyperplasia, and hyperinsulinemia. *The Journal of Clinical Investigation*, *108*(11), 1631–8. https://doi.org/10.1172/JCI13785

Bianchi, M. E., Calogero, S., Grassi, F., Aguzzi, A., Voigtländer, T., Ferrier, P., & Ferrari, S. (1999). The lack of chromosomal protein Hmg1 does not disrupt cell growth but causes lethal hypoglycaemia in newborn mice. *Nature Genetics*, *22*(3), 276–280. https://doi.org/10.1038/10338

Birkenfeld, A. L., & Shulman, G. I. (2014). Nonalcoholic fatty liver disease, hepatic insulin resistance, and type 2 Diabetes. *Hepatology*, *59*(2), 713–723. https://doi.org/10.1002/hep.26672

Blanchard, F., Duplomb, L., Raher, S., Vusio, P., Hoflack, B., Jacques, Y., & Godard, A. (1999). Mannose 6-Phosphate/Insulin-like growth factor II receptor mediates internalization and degradation of leukemia inhibitory factor but not signal transduction. *The Journal of Biological Chemistry*, *274*(35), 24685–93. Retrieved from http://www.ncbi.nlm.nih.gov/pubmed/10455136

Bleekemolen, J. E., Stein, M., von Figura, K., Slot, J. W., & Geuze, H. J. (1988). The two mannose 6-phosphate receptors have almost identical subcellular distributions in U937 monocytes. *European Journal of Cell Biology*, *47*(2), 366–72. Retrieved from http://www.ncbi.nlm.nih.gov/pubmed/2854064

Boothe, T., Lim, G. E., Cen, H., Skovsø, S., Piske, M., Li, S. N., … Johnson, J. D. (2016). Inter-domain tagging implicates caveolin-1 in insulin receptor trafficking and Erk signaling bias in pancreatic beta-cells. *Molecular Metabolism*, *5*(5), 366–78. https://doi.org/10.1016/j.molmet.2016.01.009

Boulant, S., Kural, C., Zeeh, J.-C., Ubelmann, F., & Kirchhausen, T. (2011). Actin dynamics counteract membrane tension during clathrin-mediated endocytosis. *Nature Cell Biology*, *13*(9), 1124–31. https://doi.org/10.1038/ncb2307

Boura-Halfon, S., & Zick, Y. (2009). Phosphorylation of IRS proteins, insulin action, and insulin resistance. *AJP: Endocrinology and Metabolism*, *296*(4), E581–E591. https://doi.org/10.1152/ajpendo.90437.2008

Brandizzi, F., & Barlowe, C. (2013). Organization of the ER–Golgi interface for membrane traffic control. *Nature Reviews Molecular Cell Biology*, *14*(6), 382–392. https://doi.org/10.1038/nrm3588

Braun, M. (2014). The Somatostatin Receptor in Human Pancreatic β-Cells. In *Vitamins and hormones* (Vol. 95, pp. 165–193). https://doi.org/10.1016/B978-0-12-800174-5.00007-7

Briscoe, J., & Th?rond, P. P. (2013). The mechanisms of Hedgehog signalling and its roles in development and disease. *Nature Reviews Molecular Cell Biology*, *14*(7), 418–431. https://doi.org/10.1038/nrm3598

Briscoe, J., & Thérond, P. P. (2013). The mechanisms of Hedgehog signalling and its roles in development and disease. *Nature Reviews. Molecular Cell Biology*, *14*(7), 416–29. https://doi.org/10.1038/nrm3598

Brissova, M., Fowler, M. J., Nicholson, W. E., Chu, A., Hirshberg, B., Harlan, D. M., & Powers, A. C. (2005). Assessment of human pancreatic islet architecture and composition by laser scanning confocal microscopy. *The Journal of Histochemistry and Cytochemistry : Official Journal of the Histochemistry Society*, *53*(9), 1087–97. https://doi.org/10.1369/jhc.5C6684.2005

Brown, J., Jones, E. Y., & Forbes, B. E. (2009). Interactions of IGF-II with the IGF2R/cation-independent mannose-6-phosphate receptor mechanism and biological outcomes. *Vitamins and Hormones*, *80*, 699–719. https://doi.org/10.1016/S0083-6729(08)00625-0

Brown, J., Jones, E. Y., & Forbes, B. E. (2009). Keeping IGF-II under control: lessons from the IGF-II-IGF2R crystal structure. *Trends in Biochemical Sciences*, *34*(12), 612–9. https://doi.org/10.1016/j.tibs.2009.07.003

Burgess, A. W., Cho, H.-S., Eigenbrot, C., Ferguson, K. M., Garrett, T. P. J., Leahy, D. J., … Yokoyama, S. (2003). An open-and-shut case? Recent insights into the activation of EGF/ErbB receptors. *Molecular Cell*, *12*(3), 541–52. Retrieved from http://www.ncbi.nlm.nih.gov/pubmed/14527402

Burtscher, I., & Lickert, H. (2009). Foxa2 regulates polarity and epithelialization in the endoderm germ layer of the mouse embryo. *Development*, *136*(6), 1029–1038. https://doi.org/10.1242/dev.028415

Cantley, J., Choudhury, A. I., Asare-Anane, H., Selman, C., Lingard, S., Heffron, H., … Withers, D. J. (2007). Pancreatic deletion of insulin receptor substrate 2 reduces beta and alpha cell mass and impairs glucose homeostasis in mice. *Diabetologia*, *50*(6), 1248–1256. https://doi.org/10.1007/s00125-007-0637-9

Canton, J., Neculai, D., & Grinstein, S. (2013). Scavenger receptors in homeostasis and immunity. *Nature Reviews Immunology*, *13*(9), 621–634. https://doi.org/10.1038/nri3515

Capuani, F., Conte, A., Argenzio, E., Marchetti, L., Priami, C., Polo, S., … Ciliberto, A. (2015). Quantitative analysis reveals how EGFR activation and downregulation are coupled in normal but not in cancer cells. *Nature Communications*, *6*, 7999. https://doi.org/10.1038/ncomms8999

Carpentier, J. L., Fehlmann, M., Van Obberghen, E., Gorden, P., & Orci, L. (n.d.). Insulin receptor internalization and recycling: mechanism and significance. *Biochimie*, *67*(10–11), 1143–5. Retrieved from http://www.ncbi.nlm.nih.gov/pubmed/3907718

Cerf, M. E. (2013). Beta cell dynamics: beta cell replenishment, beta cell compensation and diabetes. *Endocrine*, *44*(2), 303–311. https://doi.org/10.1007/s12020-013-9917-y

Cerf, M. E. (2015). High fat programming of beta cell compensation, exhaustion, death and dysfunction. *Pediatric Diabetes*, *16*(2), 71–78. https://doi.org/10.1111/pedi.12137

Cervantes, S., Lau, J., Cano, D. A., Borromeo-Austin, C., & Hebrok, M. (2010). Primary cilia regulate Gli/Hedgehog activation in pancreas. *Proceedings of the National Academy of Sciences*, *107*(22), 10109–10114. https://doi.org/10.1073/pnas.0909900107

Chadda, R., Howes, M. T., Plowman, S. J., Hancock, J. F., Parton, R. G., & Mayor, S. (2007). Cholesterol-sensitive Cdc42 activation regulates actin polymerization for endocytosis via the GEEC pathway. *Traffic (Copenhagen, Denmark)*, *8*(6), 702–17. https://doi.org/10.1111/j.1600-0854.2007.00565.x

Chait, A., Bierman, E. L., & Albers, J. J. (1979). Low-density lipoprotein receptor activity in cultured human skin fibroblasts. Mechanism of insulin-induced stimulation. *The Journal of Clinical Investigation*, *64*(5), 1309–19. https://doi.org/10.1172/JCI109587

Chan, E. Y. W., Nasir, J., Gutekunst, C.-A., Coleman, S., Maclean, A., Maas, A., … Hayden, M. R. (2002). Targeted disruption of Huntingtin-associated protein-1 (Hap1) results in postnatal death due to depressed feeding behavior. *Human Molecular Genetics*, *11*(8), 945–59. Retrieved from http://www.ncbi.nlm.nih.gov/pubmed/11971876

Chen, W., Kirkbride, K. C., How, T., Nelson, C. D., Mo, J., Frederick, J. P., … Blobe, G. C. (2003). -Arrestin 2 Mediates Endocytosis of Type III TGF- Receptor and Down-Regulation of Its Signaling. *Science*, *301*(5638), 1394–1397. https://doi.org/10.1126/science.1083195

Chen, W., Ren, X.-R., Nelson, C. D., Barak, L. S., Chen, J. K., Beachy, P. A., … Lefkowitz, R. J. (2004). Activity-dependent internalization of smoothened mediated by beta-arrestin 2 and GRK2. *Science (New York, N.Y.)*, *306*(5705), 2257–60. https://doi.org/10.1126/science.1104135

Cheng, I., Stram, D. O., Burtt, N. P., Gianniny, L., Garcia, R. R., Pooler, L., … Haiman, C. A. (2009). IGF2R missense single-nucleotide polymorphisms and breast cancer risk: the multiethnic cohort study. *Cancer Epidemiology, Biomarkers & Prevention : A Publication of the American Association for Cancer Research, Cosponsored by the American Society of Preventive Oncology*, *18*(6), 1922–4. https://doi.org/10.1158/1055-9965.EPI-09-0253

Cheung, H. O.-L., Zhang, X., Ribeiro, A., Mo, R., Makino, S., Puviindran, V., … Hui, C. -c. (2009). The Kinesin Protein Kif7 Is a Critical Regulator of Gli Transcription Factors in Mammalian Hedgehog Signaling. *Science Signaling*, *2*(76), ra29-ra29. https://doi.org/10.1126/scisignal.2000405

Chimienti, F., Favier, A., & Seve, M. (2005). ZnT-8, A Pancreatic Beta-Cell-Specific Zinc Transporter. *BioMetals*, *18*(4), 313–317. https://doi.org/10.1007/s10534-005-3687-9

Chow, J. C., Condorelli, G., & Smith, R. J. (1998). Insulin-like growth factor-I receptor internalization regulates signaling via the Shc/mitogen-activated protein kinase pathway, but not the insulin receptor substrate-1 pathway. *The Journal of Biological Chemistry*, *273*(8), 4672–80. Retrieved from http://www.ncbi.nlm.nih.gov/pubmed/9468528

Choy, S. W., & Cheng, S. H. (2012). Hedgehog Signaling. In *Vitamins and hormones* (Vol. 88, pp. 1–23). https://doi.org/10.1016/B978-0-12-394622-5.00001-8

Citri, A., & Yarden, Y. (2006). EGF–ERBB signalling: towards the systems level. *Nature Reviews Molecular Cell Biology*, *7*(7), 505–516. https://doi.org/10.1038/nrm1962

Cochrane, C., Szczepny, A., Watkins, D., & Cain, J. (2015). Hedgehog Signaling in the Maintenance of Cancer Stem Cells. *Cancers*, *7*(3), 1554–1585. https://doi.org/10.3390/cancers7030851

Collins, B. M., McCoy, A. J., Kent, H. M., Evans, P. R., & Owen, D. J. (2002). Molecular Architecture and Functional Model of the Endocytic AP2 Complex. *Cell*, *109*(4), 523–535. https://doi.org/10.1016/S0092-8674(02)00735-3

Corbit, K. C., Aanstad, P., Singla, V., Norman, A. R., Stainier, D. Y. R., & Reiter, J. F. (2005).

Vertebrate Smoothened functions at the primary cilium. *Nature*, *437*(7061), 1018–1021. https://doi.org/10.1038/nature04117

Dahmane, N., & Ruiz i Altaba, A. (1999). Sonic hedgehog regulates the growth and patterning of the cerebellum. *Development (Cambridge, England)*, *126*(14), 3089–100. Retrieved from http://www.ncbi.nlm.nih.gov/pubmed/10375501

Darlington, G. J. (1999). Molecular mechanisms of liver development and differentiation. *Current Opinion in Cell Biology*, *11*(6), 678–82. Retrieved from http://www.ncbi.nlm.nih.gov/pubmed/10600708

Day, E. A., Ford, R. J., & Steinberg, G. R. (2017). AMPK as a Therapeutic Target for Treating Metabolic Diseases. *Trends in Endocrinology & Metabolism*. https://doi.org/10.1016/j.tem.2017.05.004

De Meyts, P., & Whittaker, J. (2002). Structural biology of insulin and IGF1 receptors: implications for drug design. *Nature Reviews. Drug Discovery*, *1*(10), 769–83. https://doi.org/10.1038/nrd917

Del Prato, S. (2009). Role of glucotoxicity and lipotoxicity in the pathophysiology of Type 2 diabetes mellitus and emerging treatment strategies. *Diabetic Medicine*, *26*(12), 1185–1192. https://doi.org/10.1111/j.1464-5491.2009.02847.x

Deng, L., Broaddus, R. R., McCampbell, A., Shipley, G. L., Loose, D. S., Stancel, G. M., … Davies, P. J. A. (2005). Identification of a novel estrogen-regulated gene, EIG121, induced by hormone replacement therapy and differentially expressed in type I and type II endometrial cancer. *Clinical Cancer Research : An Official Journal of the American Association for Cancer Research*, *11*(23), 8258–64. https://doi.org/10.1158/1078-0432.CCR-05-1189

Deng, L., Feng, J., & Broaddus, R. R. (2010). The novel estrogen-induced gene EIG121 regulates autophagy and promotes cell survival under stress. *Cell Death & Disease*, *1*(4), e32. https://doi.org/10.1038/cddis.2010.9

Dennis, P. A., & Rifkin, D. B. (1991). Cellular activation of latent transforming growth factor beta requires binding to the cation-independent mannose 6-phosphate/insulin-like growth factor type II receptor. *Proceedings of the National Academy of Sciences of the United States of America*, *88*(2), 580–4. Retrieved from http://www.ncbi.nlm.nih.gov/pubmed/1846448

Di Guglielmo, G. M., Drake, P. G., Baass, P. C., Authier, F., Posner, B. I., & Bergeron, J. J. (1998). Insulin receptor internalization and signalling. *Molecular and Cellular Biochemistry*, *182*(1–2), 59–63. Retrieved from http://www.ncbi.nlm.nih.gov/pubmed/9609114

Donnelly, M. L., Hughes, L. E., Luke, G., Mendoza, H., ten Dam, E., Gani, D., & Ryan, M. D. (2001). The "cleavage" activities of foot-and-mouth disease virus 2A site-directed mutants and naturally occurring "2A-like" sequences. *The Journal of General Virology*, *82*(Pt 5), 1027–41. https://doi.org/10.1099/0022-1317-82-5-1027

Dunn, K. W., Kamocka, M. M., & McDonald, J. H. (2011). A practical guide to evaluating colocalization in biological microscopy. *American Journal of Physiology. Cell Physiology*, *300*(4), C723-42. https://doi.org/10.1152/ajpcell.00462.2010

Dunn, W. A., Hubbard, A. L., & Aronson, N. N. (1980). Low temperature selectively inhibits fusion between pinocytic vesicles and lysosomes during heterophagy of 125I-asialofetuin by the perfused rat liver. *The Journal of Biological Chemistry*, *255*(12), 5971–8. Retrieved from http://www.ncbi.nlm.nih.gov/pubmed/6155379

Dutta, D., & Donaldson, J. G. (2012). Search for inhibitors of endocytosis. *Cellular Logistics*, *2*(4), 203–208. https://doi.org/10.4161/cl.23967

Ekholm, S. V, & Reed, S. I. (2000). Regulation of G(1) cyclin-dependent kinases in the mammalian cell cycle. *Current Opinion in Cell Biology*, *12*(6), 676–84. Retrieved from

http://www.ncbi.nlm.nih.gov/pubmed/11063931

El-Shewy, H. M., Johnson, K. R., Lee, M.-H., Jaffa, A. A., Obeid, L. M., & Luttrell, L. M. (2006). Insulin-like growth factors mediate heterotrimeric G protein-dependent ERK1/2 activation by transactivating sphingosine 1-phosphate receptors. *The Journal of Biological Chemistry*, *281*(42), 31399–407. https://doi.org/10.1074/jbc.M605339200

El-Shewy, H. M., Lee, M.-H., Obeid, L. M., Jaffa, A. A., & Luttrell, L. M. (2007). The insulin-like growth factor type 1 and insulin-like growth factor type 2/mannose-6-phosphate receptors independently regulate ERK1/2 activity in HEK293 cells. *The Journal of Biological Chemistry*, *282*(36), 26150–7. https://doi.org/10.1074/jbc.M703276200

El-Shewy, H. M., & Luttrell, L. M. (2009). Insulin-like growth factor-2/mannose-6 phosphate receptors. *Vitamins and Hormones*, *80*, 667–97. https://doi.org/10.1016/S0083-6729(08)00624-9

El?Ouaamari, A., Dirice, E., Gedeon, N., Hu, J., Zhou, J.-Y., Shirakawa, J., … Kulkarni, R. (2016). SerpinB1 Promotes Pancreatic ? Cell Proliferation. *Cell Metabolism*, *23*(1), 194–205. https://doi.org/10.1016/j.cmet.2015.12.001

Escher, C., Cymer, F., & Schneider, D. (2009). Two GxxxG-Like Motifs Facilitate Promiscuous Interactions of the Human ErbB Transmembrane Domains. *Journal of Molecular Biology*, *389*(1), 10–16. https://doi.org/10.1016/j.jmb.2009.04.002

Eskelinen, E.-L. (2006). Roles of LAMP-1 and LAMP-2 in lysosome biogenesis and autophagy. *Molecular Aspects of Medicine*, *27*(5–6), 495–502. https://doi.org/10.1016/j.mam.2006.08.005

Estrella, J. S., Ma, L. T., Milton, D. R., Yao, J. C., Wang, H., Rashid, A., & Broaddus, R. R. (2014). Expression of Estrogen-Induced Genes and Estrogen Receptor β in Pancreatic Neuroendocrine Tumors. *Pancreas*, *43*(7), 996–1002. https://doi.org/10.1097/MPA.0000000000000203

Fabian, S. L., Penchev, R. R., St-Jacques, B., Rao, A. N., Sipilä, P., West, K. A., … Humphreys, B. D. (2012). Hedgehog-Gli Pathway Activation during Kidney Fibrosis. *The American Journal of Pathology*, *180*(4), 1441–1453. https://doi.org/10.1016/j.ajpath.2011.12.039

Fatrai, S., Elghazi, L., Balcazar, N., Cras-Méneur, C., Krits, I., Kiyokawa, H., & Bernal-Mizrachi, E. (2006). Akt induces beta-cell proliferation by regulating cyclin D1, cyclin D2, and p21 levels and cyclin-dependent kinase-4 activity. *Diabetes*, *55*(2), 318–25. Retrieved from http://www.ncbi.nlm.nih.gov/pubmed/16443763

Faure, A., & Sutter-Dub, M. T. (1979). Insulin secretion from isolated pancreatic islets in the female rat. Short and long term oestradiol influence. *Journal de Physiologie*, *75*(3), 289–95. Retrieved from http://www.ncbi.nlm.nih.gov/pubmed/387949

Ferrannini, E. (2010). The Stunned β Cell: A Brief History. *Cell Metabolism*, *11*(5), 349–352. https://doi.org/10.1016/j.cmet.2010.04.009

Foretz, M., Ancellin, N., Andreelli, F., Saintillan, Y., Grondin, P., Kahn, A., … Viollet, B. (2005). Short-term overexpression of a constitutively active form of AMP-activated protein kinase in the liver leads to mild hypoglycemia and fatty liver. *Diabetes*, *54*(5), 1331–9. Retrieved from http://www.ncbi.nlm.nih.gov/pubmed/15855317

Foti, M., Moukil, M. A., Dudognon, P., & Carpentier, J.-L. (2004). Insulin and IGF-1 receptor trafficking and signalling. *Novartis Foundation Symposium*, *262*, 125-41–7, 265–8. Retrieved from http://www.ncbi.nlm.nih.gov/pubmed/15562826

Fujimoto, T., Hayashi, M., Iwamoto, M., & Ohno-Iwashita, Y. (1997). Crosslinked plasmalemmal cholesterol is sequestered to caveolae: analysis with a new cytochemical probe. *The Journal of Histochemistry and Cytochemistry : Official Journal of the Histochemistry Society*, *45*(9),

1197–205. https://doi.org/10.1177/002215549704500903

Fujita, A., Cheng, J., Tauchi-Sato, K., Takenawa, T., & Fujimoto, T. (2009). A distinct pool of phosphatidylinositol 4,5-bisphosphate in caveolae revealed by a nanoscale labeling technique. *Proceedings of the National Academy of Sciences of the United States of America*, *106*(23), 9256–61. https://doi.org/10.1073/pnas.0900216106

Gao, C., Cai, Y., Wang, Y., Kang, B.-H., Aniento, F., Robinson, D. G., & Jiang, L. (2014a). Retention mechanisms for ER and Golgi membrane proteins. *Trends in Plant Science*, *19*(8), 508–515. https://doi.org/10.1016/j.tplants.2014.04.004

Gao, C., Cai, Y., Wang, Y., Kang, B.-H., Aniento, F., Robinson, D. G., & Jiang, L. (2014b). Retention mechanisms for ER and Golgi membrane proteins. *Trends in Plant Science*, *19*(8), 508–515. https://doi.org/10.1016/j.tplants.2014.04.004

Garcia, D., & Shaw, R. J. (2017). AMPK: Mechanisms of Cellular Energy Sensing and Restoration of Metabolic Balance. *Molecular Cell*, *66*(6), 789–800. https://doi.org/10.1016/j.molcel.2017.05.032

Garg, N., Thakur, S., Alex McMahan, C., & Adamo, M. L. (2011). High fat diet induced insulin resistance and glucose intolerance are gender-specific in IGF-1R heterozygous mice. *Biochemical and Biophysical Research Communications*, *413*(3), 476–480. https://doi.org/10.1016/j.bbrc.2011.08.123

Garrett, T. P., McKern, N. M., Lou, M., Frenkel, M. J., Bentley, J. D., Lovrecz, G. O., … Ward, C. W. (1998). Crystal structure of the first three domains of the type-1 insulin-like growth factor receptor. *Nature*, *394*(6691), 395–9. https://doi.org/10.1038/28668

Gegg, M., Böttcher, A., Burtscher, I., Hasenoeder, S., Van Campenhout, C., Aichler, M., … Lickert, H. (2014). Flattop regulates basal body docking and positioning in mono- and multiciliated cells. *eLife*, *3*. https://doi.org/10.7554/eLife.03842

Gerber, D., Sal-Man, N., & Shai, Y. (2004). Two motifs within a transmembrane domain, one for homodimerization and the other for heterodimerization. *The Journal of Biological Chemistry*, *279*(20), 21177–82. https://doi.org/10.1074/jbc.M400847200

Gerdes, J. M., Christou-Savina, S., Xiong, Y., Moede, T., Moruzzi, N., Karlsson-Edlund, P., … Berggren, P.-O. (2014). Ciliary dysfunction impairs beta-cell insulin secretion and promotes development of type 2 diabetes in rodents. *Nature Communications*, *5*, 5308. https://doi.org/10.1038/ncomms6308

Gerdes, J. M., Davis, E. E., & Katsanis, N. (2009). The Vertebrate Primary Cilium in Development, Homeostasis, and Disease. *Cell*, *137*(1), 32–45. https://doi.org/10.1016/j.cell.2009.03.023

Gerhartz, C., Dittrich, E., Stoyan, T., Rose-John, S., Yasukawa, K., Heinrich, P. C., & Graeve, L. (1994). Biosynthesis and half-life of the interleukin-6 receptor and its signal transducer gp130. *European Journal of Biochemistry*, *223*(1), 265–74. Retrieved from http://www.ncbi.nlm.nih.gov/pubmed/8033901

Ghosh, P., Dahms, N. M., & Kornfeld, S. (2003). Mannose 6-phosphate receptors: new twists in the tale. *Nature Reviews Molecular Cell Biology*, *4*(3), 202–213. https://doi.org/10.1038/nrm1050

Giddings, S. J., & Carnaghi, L. R. (1992). Insulin receptor gene expression during development: developmental regulation of insulin receptor mRNA abundance in embryonic rat liver and yolk sac, developmental regulation of insulin receptor gene splicing, and comparison to abundance of insulin-like growth factor 1 receptor mRNA. *Molecular Endocrinology*, *6*(10), 1665–1672. https://doi.org/10.1210/mend.6.10.1448116

Gil-Campos, M., Aguilera, C. M., Cañete, R., & Gil, A. (2017). Ghrelin: a hormone regulating food intake and energy homeostasis. https://doi.org/10.1079/BJN20061787

Ginsberg, H. N. (1991). Lipoprotein physiology in nondiabetic and diabetic states. Relationship to atherogenesis. *Diabetes Care*, *14*(9), 839–55. Retrieved from http://www.ncbi.nlm.nih.gov/pubmed/1959476

Girnita, L., Girnita, A., & Larsson, O. (2003). Mdm2-dependent ubiquitination and degradation of the insulin-like growth factor 1 receptor. *Proceedings of the National Academy of Sciences of the United States of America*, *100*(14), 8247–52. https://doi.org/10.1073/pnas.1431613100

Girnita, L., Shenoy, S. K., Sehat, B., Vasilcanu, R., Girnita, A., Lefkowitz, R. J., & Larsson, O. (2005). {beta}-Arrestin is crucial for ubiquitination and down-regulation of the insulin-like growth factor-1 receptor by acting as adaptor for the MDM2 E3 ligase. *The Journal of Biological Chemistry*, *280*(26), 24412–9. https://doi.org/10.1074/jbc.M501129200

Glass, C., & Olefsky, J. (2012). Inflammation and Lipid Signaling in the Etiology of Insulin Resistance. *Cell Metabolism*, *15*(5), 635–645. https://doi.org/10.1016/j.cmet.2012.04.001

Goetz, S. C., & Anderson, K. V. (2010). The primary cilium: a signalling centre during vertebrate development. *Nature Reviews Genetics*, *11*(5), 331–344. https://doi.org/10.1038/nrg2774

Goginashvili, A., Zhang, Z., Erbs, E., Spiegelhalter, C., Kessler, P., Mihlan, M., … Ricci, R. (2015). Insulin secretory granules control autophagy in pancreatic cells. *Science*, *347*(6224), 878–882. https://doi.org/10.1126/science.aaa2628

Goh, L. K., & Sorkin, A. (2013). Endocytosis of Receptor Tyrosine Kinases. *Cold Spring Harbor Perspectives in Biology*, *5*(5), a017459–a017459. https://doi.org/10.1101/cshperspect.a017459

Goldberg, I. J. (2001). Diabetic Dyslipidemia: Causes and Consequences. *The Journal of Clinical Endocrinology & Metabolism*, *86*(3), 965–971. https://doi.org/10.1210/jcem.86.3.7304

Goldfine, A. B., & Kulkarni, R. N. (2012). Modulation of β-cell function: a translational journey from the bench to the bedside. *Diabetes, Obesity & Metabolism*, *14 Suppl 3*, 152–60. https://doi.org/10.1111/j.1463-1326.2012.01647.x

Gomez-Navarro, N., & Miller, E. (2016a). Protein sorting at the ER–Golgi interface. *The Journal of Cell Biology*, *215*(6), jcb.201610031. https://doi.org/10.1083/jcb.201610031

Gomez-Navarro, N., & Miller, E. A. (2016b). COP-coated vesicles. *Current Biology*, *26*(2), R54–R57. https://doi.org/10.1016/j.cub.2015.12.017

Goto, H., Inaba, H., & Inagaki, M. (2017). Mechanisms of ciliogenesis suppression in dividing cells. *Cellular and Molecular Life Sciences : CMLS*, *74*(5), 881–890. https://doi.org/10.1007/s00018-016-2369-9

Grapin-Botton, A. (2005). Ductal cells of the pancreas. *The International Journal of Biochemistry & Cell Biology*, *37*(3), 504–510. https://doi.org/10.1016/j.biocel.2004.07.010

Gunasekaran, U., & Gannon, M. (2011). Type 2 diabetes and the aging pancreatic beta cell. *Aging*, *3*(6), 565–75. https://doi.org/10.18632/aging.100350

Gustavsson, J., Parpal, S., Karlsson, M., Ramsing, C., Thorn, H., Borg, M., … Strålfors, P. (1999). Localization of the insulin receptor in caveolae of adipocyte plasma membrane. *FASEB Journal : Official Publication of the Federation of American Societies for Experimental Biology*, *13*(14), 1961–71. Retrieved from http://www.ncbi.nlm.nih.gov/pubmed/10544179

Halban, P. A. (2008). Cell therapy for type 2 diabetes: is it desirable and can we get it? *Diabetes, Obesity & Metabolism*, *10 Suppl 4*, 205–11. https://doi.org/10.1111/j.1463-1326.2008.00957.x

Halban, P. A. (2015). 50 years forward: beta cells. *Diabetologia*, *58*(8), 1688–1692.

https://doi.org/10.1007/s00125-015-3601-0

Hamer, I., Foti, M., Emkey, R., Cordier-Bussat, M., Philippe, J., De Meyts, P., … Carpentier, J.-L. (2002). An arginine to cysteine252 mutation in insulin receptors from a patient with severe insulin resistance inhibits receptor internalisation but preserves signalling events. *Diabetologia*, *45*(5), 657–667. https://doi.org/10.1007/s00125-002-0798-5

Han, H.-S., Kang, G., Kim, J. S., Choi, B. H., & Koo, S.-H. (2016). Regulation of glucose metabolism from a liver-centric perspective. *Experimental & Molecular Medicine*, *48*(3), e218. https://doi.org/10.1038/emm.2015.122

HAO, K., TIAN, X.-D., QIN, C.-F., XIE, X.-H., & YANG, Y.-M. (2013). Hedgehog signaling pathway regulates human pancreatic cancer cell proliferation and metastasis. *Oncology Reports*, *29*(3), 1124–1132. https://doi.org/10.3892/or.2012.2210

Hardie, D. G. (2008). AMPK: a key regulator of energy balance in the single cell and the whole organism. *International Journal of Obesity (2005)*, *32 Suppl 4*, S7-12. https://doi.org/10.1038/ijo.2008.116

Hashimoto, N., Kido, Y., Uchida, T., Asahara, S., Shigeyama, Y., Matsuda, T., … Kasuga, M. (2006). Ablation of PDK1 in pancreatic β cells induces diabetes as a result of loss of β cell mass. *Nature Genetics*, *38*(5), 589–593. https://doi.org/10.1038/ng1774

Hassan, A. B. (2003). Keys to the hidden treasures of the mannose 6-phosphate/insulin-like growth factor 2 receptor. *The American Journal of Pathology*, *162*(1), 3–6. https://doi.org/10.1016/S0002-9440(10)63791-1

Hauge-Evans, A. C., King, A. J., Carmignac, D., Richardson, C. C., Robinson, I. C. A. F., Low, M. J., … Jones, P. M. (2009). Somatostatin secreted by islet delta-cells fulfills multiple roles as a paracrine regulator of islet function. *Diabetes*, *58*(2), 403–11. https://doi.org/10.2337/db08-0792

Haumaitre, C., Lenoir, O., & Scharfmann, R. (2009). Directing cell differentiation with small-molecule histone deacetylase inhibitors: the example of promoting pancreatic endocrine cells. *Cell Cycle (Georgetown, Tex.)*, *8*(4), 536–44. https://doi.org/10.4161/cc.8.4.7610

Heaton, J. H., & Gelehrter, T. D. (1981). Desensitization of hepatoma cells to insulin action. Evidence for a post-receptor mechanism. *The Journal of Biological Chemistry*, *256*(23), 12257–62. Retrieved from http://www.ncbi.nlm.nih.gov/pubmed/7028753

Hebrok, M., Kim, S. K., & Melton, D. A. (1998). Notochord repression of endodermal Sonic hedgehog permits pancreas development. *Genes & Development*, *12*(11), 1705–13. Retrieved from http://www.ncbi.nlm.nih.gov/pubmed/9620856

Hebrok, M., Kim, S. K., St Jacques, B., McMahon, A. P., & Melton, D. A. (2000). Regulation of pancreas development by hedgehog signaling. *Development (Cambridge, England)*, *127*(22), 4905–13. Retrieved from http://www.ncbi.nlm.nih.gov/pubmed/11044404

Heine, P. A., Taylor, J. A., Iwamoto, G. A., Lubahn, D. B., & Cooke, P. S. (2000). Increased adipose tissue in male and female estrogen receptor-alpha knockout mice. *Proceedings of the National Academy of Sciences*, *97*(23), 12729–12734. https://doi.org/10.1073/pnas.97.23.12729

Hellemans, J., Mortier, G., De Paepe, A., Speleman, F., & Vandesompele, J. (2007). qBase relative quantification framework and software for management and automated analysis of real-time quantitative PCR data. *Genome Biology*, *8*(2), R19. https://doi.org/10.1186/gb-2007-8-2-r19

Henquin, J. C. (2000). Triggering and amplifying pathways of regulation of insulin secretion by glucose. *Diabetes*, *49*(11), 1751–60. Retrieved from http://www.ncbi.nlm.nih.gov/pubmed/11078440

Henquin, J. C. (2009). Regulation of insulin secretion: a matter of phase control and amplitude modulation. *Diabetologia*, *52*(5), 739–751. https://doi.org/10.1007/s00125-009-1314-y

Heppner, K. M., Habegger, K. M., Day, J., Pfluger, P. T., Perez-Tilve, D., Ward, B., … Tschöp, M. (2010). Glucagon regulation of energy metabolism. *Physiology & Behavior*, *100*(5), 545–548. https://doi.org/10.1016/j.physbeh.2010.03.019

Hildebrandt, F., Benzing, T., Katsanis, N., & Katsanis, N. (2011). Ciliopathies. *The New England Journal of Medicine*, *364*(16), 1533–43. https://doi.org/10.1056/NEJMra1010172

Hiroshima, M., Saeki, Y., Okada-Hatakeyama, M., & Sako, Y. (2012). Dynamically varying interactions between heregulin and ErbB proteins detected by single-molecule analysis in living cells. *Proceedings of the National Academy of Sciences of the United States of America*, *109*(35), 13984–9. https://doi.org/10.1073/pnas.1200464109

Horn, S., Kobberup, S., Jørgensen, M. C., Kalisz, M., Klein, T., Kageyama, R., … Jensen, J. N. (2012). Mind bomb 1 is required for pancreatic β-cell formation. *Proceedings of the National Academy of Sciences of the United States of America*, *109*(19), 7356–61. https://doi.org/10.1073/pnas.1203605109

Horner, V. L., & Caspary, T. (2011). Disrupted dorsal neural tube BMP signaling in the cilia mutant Arl13bhnn stems from abnormal Shh signaling. *Developmental Biology*, *355*(1), 43–54. https://doi.org/10.1016/j.ydbio.2011.04.019

Howard, B. V. (1999). Insulin resistance and lipid metabolism. *The American Journal of Cardiology*, *84*(1A), 28J–32J. Retrieved from http://www.ncbi.nlm.nih.gov/pubmed/10418856

Huang, Q., & Szebenyi, D. M. E. (2010). Structural Basis for the Interaction between the Growth Factor-binding Protein GRB10 and the E3 Ubiquitin Ligase NEDD4. *Journal of Biological Chemistry*, *285*(53), 42130–42139. https://doi.org/10.1074/jbc.M110.143412

Hubbard, S. R., & Till, J. H. (2000). Protein Tyrosine Kinase Structure and Function. *Annual Review of Biochemistry*, *69*(1), 373–398. https://doi.org/10.1146/annurev.biochem.69.1.373

Hui, C., & Angers, S. (2011). Gli Proteins in Development and Disease. *Annual Review of Cell and Developmental Biology*, *27*(1), 513–537. https://doi.org/10.1146/annurev-cellbio-092910-154048

Ingham, P. W., & McMahon, A. P. (2001). Hedgehog signaling in animal development: paradigms and principles. *Genes & Development*, *15*(23), 3059–3087. https://doi.org/10.1101/gad.938601

Ishikawa, T. (2017). Axoneme Structure from Motile Cilia. *Cold Spring Harbor Perspectives in Biology*, *9*(1), a028076. https://doi.org/10.1101/cshperspect.a028076

Islam, M. S. (2010). *The islets of Langerhans*. Springer.

Jaillard, S., Akloul, L., Beaumont, M., Hamdi-Roze, H., Dubourg, C., Odent, S., … Ravel, C. (2016). Array-CGH diagnosis in ovarian failure: identification of new molecular actors for ovarian physiology. *Journal of Ovarian Research*, *9*(1), 63. https://doi.org/10.1186/s13048-016-0272-5

Janikiewicz, J., Hanzelka, K., Kozinski, K., Kolczynska, K., & Dobrzyn, A. (2015). Islet β-cell failure in type 2 diabetes – Within the network of toxic lipids. *Biochemical and Biophysical Research Communications*, *460*(3), 491–496. https://doi.org/10.1016/j.bbrc.2015.03.153

Jia, Y., Wang, Y., & Xie, J. (2015). The Hedgehog pathway: role in cell differentiation, polarity and proliferation. *Archives of Toxicology*, *89*(2), 179–191. https://doi.org/10.1007/s00204-014-1433-1

Jiang, J., & Hui, C. (2008). Hedgehog Signaling in Development and Cancer. *Developmental Cell*, *15*(6), 801–812. https://doi.org/10.1016/j.devcel.2008.11.010

Jung, B., Padula, D., Burtscher, I., Landerer, C., Lutter, D., Theis, F., … Lickert, H. (2016). Pitchfork and Gprasp2 Target Smoothened to the Primary Cilium for Hedgehog Pathway Activation. *PloS One*, *11*(2), e0149477. https://doi.org/10.1371/journal.pone.0149477

Kang, H. S., Kim, Y.-S., ZeRuth, G., Beak, J. Y., Gerrish, K., Kilic, G., … Jetten, A. M. (2009). Transcription factor Glis3, a novel critical player in the regulation of pancreatic beta-cell development and insulin gene expression. *Molecular and Cellular Biology*, *29*(24), 6366–79. https://doi.org/10.1128/MCB.01259-09

Kang, J. M., Park, S., Kim, S. J., Kim, H., Lee, B., Kim, J., … Kim, S.-J. (2015). KIAA1324 Suppresses Gastric Cancer Progression by Inhibiting the Oncoprotein GRP78. *Cancer Research*, *75*(15), 3087–97. https://doi.org/10.1158/0008-5472.CAN-14-3751

Katz, M., Amit, I., & Yarden, Y. (2007). Regulation of MAPKs by growth factors and receptor tyrosine kinases. *Biochimica et Biophysica Acta*, *1773*(8), 1161–76. https://doi.org/10.1016/j.bbamcr.2007.01.002

Kenney, A. M., Cole, M. D., & Rowitch, D. H. (2003). Nmyc upregulation by sonic hedgehog signaling promotes proliferation in developing cerebellar granule neuron precursors. *Development (Cambridge, England)*, *130*(1), 15–28. Retrieved from http://www.ncbi.nlm.nih.gov/pubmed/12441288

Kenney, A. M., & Rowitch, D. H. (2000). Sonic hedgehog promotes G(1) cyclin expression and sustained cell cycle progression in mammalian neuronal precursors. *Molecular and Cellular Biology*, *20*(23), 9055–67. Retrieved from http://www.ncbi.nlm.nih.gov/pubmed/11074003

Khan, A. H., & Pessin, J. E. (2002). Insulin regulation of glucose uptake: a complex interplay of intracellular signalling pathways. *Diabetologia*, *45*(11), 1475–83. https://doi.org/10.1007/s00125-002-0974-7

Khandekar, N., Berning, B. A., Sainsbury, A., & Lin, S. (2015). The role of pancreatic polypeptide in the regulation of energy homeostasis. *Molecular and Cellular Endocrinology*, *418*, 33–41. https://doi.org/10.1016/j.mce.2015.06.028

Kim, A., Miller, K., Jo, J., Kilimnik, G., Wojcik, P., & Hara, M. (2009). Islet architecture: A comparative study. *Islets*, *1*(2), 129–36. https://doi.org/10.4161/isl.1.2.9480

Kim, S.-J., Winter, K., Nian, C., Tsuneoka, M., Koda, Y., & McIntosh, C. H. S. (2005). Glucose-dependent Insulinotropic Polypeptide (GIP) Stimulation of Pancreatic β-Cell Survival Is Dependent upon Phosphatidylinositol 3-Kinase (PI3K)/Protein Kinase B (PKB) Signaling, Inactivation of the Forkhead Transcription Factor Foxo1, and Down-regulation of *bax* Expression. *Journal of Biological Chemistry*, *280*(23), 22297–22307. https://doi.org/10.1074/jbc.M500540200

Kinzel, D., Boldt, K., Davis, E. E., Burtscher, I., Trümbach, D., Diplas, B., … Lickert, H. (2010). Pitchfork Regulates Primary Cilia Disassembly and Left-Right Asymmetry. *Developmental Cell*, *19*(1), 66–77. https://doi.org/10.1016/j.devcel.2010.06.005

Kirchhausen, T. (2000). Clathrin. *Annual Review of Biochemistry*, *69*(1), 699–727. https://doi.org/10.1146/annurev.biochem.69.1.699

Kirkbride, K. C., Ray, B. N., & Blobe, G. C. (2005). Cell-surface co-receptors: emerging roles in signaling and human disease. *Trends in Biochemical Sciences*, *30*(11), 611–621. https://doi.org/10.1016/j.tibs.2005.09.003

Kishi, K., Mawatari, K., Sakai-Wakamatsu, K., Yuasa, T., Wang, M., Ogura-Sawa, M., … Ebina, Y. (2007). APS-mediated ubiquitination of the insulin receptor enhances its internalization,

but does not induce its degradation. *Endocrine Journal*, *54*(1), 77–88. Retrieved from http://www.ncbi.nlm.nih.gov/pubmed/17102568

Kitamura, T., Kahn, C. R., & Accili, D. (2003). Insulin Receptor Knockout Mice. *Annual Review of Physiology*, *65*(1), 313–332. https://doi.org/10.1146/annurev.physiol.65.092101.142540

Kohn, A. D., Summers, S. A., Birnbaum, M. J., & Roth, R. A. (1996). Expression of a constitutively active Akt Ser/Thr kinase in 3T3-L1 adipocytes stimulates glucose uptake and glucose transporter 4 translocation. *The Journal of Biological Chemistry*, *271*(49), 31372–8. Retrieved from http://www.ncbi.nlm.nih.gov/pubmed/8940145

Komatsu, Y., & Mishina, Y. (2013). Establishment of left?right asymmetry in vertebrate development: the node in mouse embryos. *Cellular and Molecular Life Sciences*, *70*(24), 4659–4666. https://doi.org/10.1007/s00018-013-1399-9

Kornfeld, S. (1992). Structure and function of the mannose 6-phosphate/insulinlike growth factor II receptors. *Annual Review of Biochemistry*, *61*(1), 307–30. https://doi.org/10.1146/annurev.bi.61.070192.001515

Kotoulas, O. B., Kalamidas, S. A., & Kondomerkos, D. J. (2006). Glycogen autophagy in glucose homeostasis. *Pathology - Research and Practice*, *202*(9), 631–638. https://doi.org/10.1016/j.prp.2006.04.001

Kovacs, J. J., Hara, M. R., Davenport, C. L., Kim, J., & Lefkowitz, R. J. (2009). Arrestin development: emerging roles for beta-arrestins in developmental signaling pathways. *Developmental Cell*, *17*(4), 443–58. https://doi.org/10.1016/j.devcel.2009.09.011

Kovacs, J. J., Whalen, E. J., Liu, R., Xiao, K., Kim, J., Chen, M., … Lefkowitz, R. J. (2008). Beta-arrestin-mediated localization of smoothened to the primary cilium. *Science (New York, N.Y.)*, *320*(5884), 1777–81. https://doi.org/10.1126/science.1157983

Kubota, N., Terauchi, Y., Tobe, K., Yano, W., Suzuki, R., Ueki, K., … Noda, T. (2004). Insulin receptor substrate 2 plays a crucial role in β cells and the hypothalamus. *Journal of Clinical Investigation*, *114*(7), 917–927. https://doi.org/10.1172/JCI21484

Kulkarni, R. N., Brüning, J. C., Winnay, J. N., Postic, C., Magnuson, M. A., & Kahn, C. R. (1999a). Tissue-specific knockout of the insulin receptor in pancreatic beta cells creates an insulin secretory defect similar to that in type 2 diabetes. *Cell*, *96*(3), 329–39. Retrieved from http://www.ncbi.nlm.nih.gov/pubmed/10025399

Kulkarni, R. N., Brüning, J. C., Winnay, J. N., Postic, C., Magnuson, M. A., & Kahn, C. R. (1999b). Tissue-specific knockout of the insulin receptor in pancreatic beta cells creates an insulin secretory defect similar to that in type 2 diabetes. *Cell*, *96*(3), 329–39. Retrieved from http://www.ncbi.nlm.nih.gov/pubmed/10025399

Kulkarni, R. N., Holzenberger, M., Shih, D. Q., Ozcan, U., Stoffel, M., Magnuson, M. A., & Kahn, C. R. (2002). beta-cell-specific deletion of the Igf1 receptor leads to hyperinsulinemia and glucose intolerance but does not alter beta-cell mass. *Nature Genetics*, *31*(1), 111–5. https://doi.org/10.1038/ng872

Kulkarni, R. N., Holzenberger, M., Shih, D. Q., Ozcan, U., Stoffel, M., Magnuson, M. A., & Kahn, C. R. (2002). β-cell–specific deletion of the Igf1 receptor leads to hyperinsulinemia and glucose intolerance but does not alter β-cell mass. *Nature Genetics*, *31*(1), 111–5. https://doi.org/10.1038/ng872

Kuma, A., Hatano, M., Matsui, M., Yamamoto, A., Nakaya, H., Yoshimori, T., … Mizushima, N. (2004). The role of autophagy during the early neonatal starvation period. *Nature*, *432*(7020), 1032–1036. https://doi.org/10.1038/nature03029

Kumari, S., Mg, S., & Mayor, S. (2010). Endocytosis unplugged: multiple ways to enter the cell. *Cell Research*, *20*(3), 256–75. https://doi.org/10.1038/cr.2010.19

Kunze, M., & Berger, J. (2015). The similarity between N-terminal targeting signals for protein import into different organelles and its evolutionary relevance. *Frontiers in Physiology*, *6*, 259. https://doi.org/10.3389/fphys.2015.00259

Lambert, J. E., Ramos–Roman, M. A., Browning, J. D., & Parks, E. J. (2014). Increased De Novo Lipogenesis Is a Distinct Characteristic of Individuals With Nonalcoholic Fatty Liver Disease. *Gastroenterology*, *146*(3), 726–735. https://doi.org/10.1053/j.gastro.2013.11.049

Lan, A., Qi, Y., & Du, J. (2014). Akt2 mediates TGF-β1-induced epithelial to mesenchymal transition by deactivating GSK3β/snail signaling pathway in renal tubular epithelial cells. *Cellular Physiology and Biochemistry : International Journal of Experimental Cellular Physiology, Biochemistry, and Pharmacology*, *34*(2), 368–82. https://doi.org/10.1159/000363006

Landsman, L., Parent, A., & Hebrok, M. (2011). Elevated Hedgehog/Gli signaling causes ?-cell dedifferentiation in mice. *Proceedings of the National Academy of Sciences*, *108*(41), 17010–17015. https://doi.org/10.1073/pnas.1105404108

Landsman, L., Parent, A., & Hebrok, M. (2011). Elevated Hedgehog/Gli signaling causes beta-cell dedifferentiation in mice. *Proceedings of the National Academy of Sciences of the United States of America*, *108*(41), 17010–5. https://doi.org/10.1073/pnas.1105404108

Lange, A., Gegg, M., Burtscher, I., Bengel, D., Kremmer, E., & Lickert, H. (2012). Fltp(T2AiCre): a new knock-in mouse line for conditional gene targeting in distinct mono- and multiciliated tissues. *Differentiation; Research in Biological Diversity*, *83*(2), S105-13. https://doi.org/10.1016/j.diff.2011.11.003

Lau, J., & Hebrok, M. (2010). Hedgehog Signaling in Pancreas Epithelium Regulates Embryonic Organ Formation and Adult -Cell Function. *Diabetes*, *59*(5), 1211–1221. https://doi.org/10.2337/db09-0914

Lau, J., & Hebrok, M. (2010a). Hedgehog signaling in pancreas epithelium regulates embryonic organ formation and adult beta-cell function. *Diabetes*, *59*(5), 1211–21. https://doi.org/10.2337/db09-0914

Lau, J., & Hebrok, M. (2010b). Hedgehog signaling in pancreas epithelium regulates embryonic organ formation and adult beta-cell function. *Diabetes*, *59*(5), 1211–21. https://doi.org/10.2337/db09-0914

Lau, M. M., Stewart, C. E., Liu, Z., Bhatt, H., Rotwein, P., & Stewart, C. L. (1994). Loss of the imprinted IGF2/cation-independent mannose 6-phosphate receptor results in fetal overgrowth and perinatal lethality. *Genes & Development*, *8*(24), 2953–63. Retrieved from http://www.ncbi.nlm.nih.gov/pubmed/8001817

Lee, P. S. W., Wang, Y., Dominguez, M. G., Yeung, Y. G., Murphy, M. A., Bowtell, D. D., & Stanley, E. R. (1999). The Cbl protooncoprotein stimulates CSF-1 receptor multiubiquitination and endocytosis, and attenuates macrophage proliferation. *The EMBO Journal*, *18*(13), 3616–3628. https://doi.org/10.1093/emboj/18.13.3616

Lee, S. J., & Nathans, D. (1988). Proliferin secreted by cultured cells binds to mannose 6-phosphate receptors. *The Journal of Biological Chemistry*, *263*(7), 3521–7. Retrieved from http://www.ncbi.nlm.nih.gov/pubmed/2963825

Leibiger, B., Wahlander, K., Berggren, P. O., & Leibiger, I. B. (2000). Glucose-stimulated insulin biosynthesis depends on insulin-stimulated insulin gene transcription. *The Journal of Biological Chemistry*, *275*(39), 30153–6. https://doi.org/10.1074/jbc.M005216200

Leibiger, I. B., Leibiger, B., & Berggren, P.-O. (2008). Insulin signaling in the pancreatic beta-cell. *Annual Review of Nutrition*, *28*(1), 233–51. https://doi.org/10.1146/annurev.nutr.28.061807.155530

Li, F., Duman-Scheel, M., Yang, D., Du, W., Zhang, J., Zhao, C., … Xin, S. (2010). Sonic Hedgehog Signaling Induces Vascular Smooth Muscle Cell Proliferation via Induction of the G1 Cyclin-Retinoblastoma Axis. *Arteriosclerosis, Thrombosis, and Vascular Biology*, *30*(9), 1787–1794. https://doi.org/10.1161/ATVBAHA.110.208520

Li, Y., Wei, Q., Zhang, Y., Ling, K., & Hu, J. (2010). The small GTPases ARL-13 and ARL-3 coordinate intraflagellar transport and ciliogenesis. *The Journal of Cell Biology*, *189*(6), 1039–1051. https://doi.org/10.1083/jcb.200912001

Liang, Y., Meng, D., Zhu, B., & Pan, J. (2016). Mechanism of ciliary disassembly. *Cellular and Molecular Life Sciences*, *73*(9), 1787–1802. https://doi.org/10.1007/s00018-016-2148-7

Liem, K. F., He, M., Ocbina, P. J. R., & Anderson, K. V. (2009). Mouse Kif7/Costal2 is a cilia-associated protein that regulates Sonic hedgehog signaling. *Proceedings of the National Academy of Sciences of the United States of America*, *106*(32), 13377–82. https://doi.org/10.1073/pnas.0906944106

Liu, J. P., Baker, J., Perkins, A. S., Robertson, E. J., & Efstratiadis, A. (1993). Mice carrying null mutations of the genes encoding insulin-like growth factor I (Igf-1) and type 1 IGF receptor (Igf1r). *Cell*, *75*(1), 59–72. Retrieved from http://www.ncbi.nlm.nih.gov/pubmed/8402901

Lonn, S., Rothman, N., Shapiro, W. R., Fine, H. A., Selker, R. G., Black, P. M., … Inskip, P. D. (2008). Genetic variation in insulin-like growth factors and brain tumor risk. *Neuro-Oncology*, *10*(4), 553–559. https://doi.org/10.1215/15228517-2008-026

Lu, H., Toh, M. T., Narasimhan, V., Thamilselvam, S. K., Choksi, S. P., & Roy, S. (2015). A function for the Joubert syndrome protein Arl13b in ciliary membrane extension and ciliary length regulation. *Developmental Biology*, *397*(2), 225–236. https://doi.org/10.1016/j.ydbio.2014.11.009

Ludwig, T., Eggenschwiler, J., Fisher, P., D'Ercole, A. J., Davenport, M. L., & Efstratiadis, A. (1996). Mouse mutants lacking the type 2 IGF receptor (IGF2R) are rescued from perinatal lethality in Igf2 and Igf1r null backgrounds. *Developmental Biology*, *177*(2), 517–35. https://doi.org/10.1006/dbio.1996.0182

Lund, P. K., Moats-Staats, B. M., Hynes, M. A., Simmons, J. G., Jansen, M., D'Ercole, A. J., & Van Wyk, J. J. (1986). Somatomedin-C/insulin-like growth factor-I and insulin-like growth factor-II mRNAs in rat fetal and adult tissues. *The Journal of Biological Chemistry*, *261*(31), 14539–44. Retrieved from http://www.ncbi.nlm.nih.gov/pubmed/3771541

Ma, W., & Goldberg, J. (2013). Rules for the recognition of dilysine retrieval motifs by coatomer. *The EMBO Journal*, *32*(7), 926–37. https://doi.org/10.1038/emboj.2013.41

Ma, X., Guan, Y., & Hua, X. (2014). Glucagon-like peptide 1-potentiated insulin secretion and proliferation of pancreatic β -cells. *Journal of Diabetes*, *6*(5), 394–402. https://doi.org/10.1111/1753-0407.12161

Manning, B. D., & Cantley, L. C. (2007). AKT/PKB signaling: navigating downstream. *Cell*, *129*(7), 1261–74. https://doi.org/10.1016/j.cell.2007.06.009

Manning, B. D., & Toker, A. (2017a). AKT/PKB Signaling: Navigating the Network. *Cell*, *169*(3), 381–405. https://doi.org/10.1016/j.cell.2017.04.001

Manning, B. D., & Toker, A. (2017b). AKT/PKB Signaling: Navigating the Network. *Cell*, *169*(3), 381–405. https://doi.org/10.1016/j.cell.2017.04.001

Mariani, L. E., Bijlsma, M. F., Ivanova, A. I., Suciu, S. K., Kahn, R. A., & Caspary, T. (2016). Arl13b regulates Shh signaling from both inside and outside the cilium. *Molecular Biology of the Cell*, *27*(23), 3780. https://doi.org/10.1091/mbc.E16-03-0189

Marshall, J. D., Maffei, P., Collin, G. B., & Naggert, J. K. (2011). Alström syndrome: genetics and clinical overview. *Current Genomics*, *12*(3), 225–35.

https://doi.org/10.2174/138920211795677912

Marshall, W. F. (2008). Basal bodies platforms for building cilia. *Current Topics in Developmental Biology*, *85*, 1–22. https://doi.org/10.1016/S0070-2153(08)00801-6

Maruyama, I. (2014). Mechanisms of Activation of Receptor Tyrosine Kinases: Monomers or Dimers. *Cells*, *3*(2), 304–330. https://doi.org/10.3390/cells3020304

Maruyama, I. N. (2015). Activation of transmembrane cell-surface receptors via a common mechanism? The "rotation model." *BioEssays*, *37*(9), 959–967. https://doi.org/10.1002/bies.201500041

Mauvais-Jarvis, F., Clegg, D. J., & Hevener, A. L. (2013). The Role of Estrogens in Control of Energy Balance and Glucose Homeostasis. *Endocrine Reviews*, *34*(3), 309–338. https://doi.org/10.1210/er.2012-1055

McInnes, C., & Sykes, B. D. (1997). Growth factor receptors: Structure, mechanism, and drug discovery. *Biopolymers*, *43*(5), 339–366. https://doi.org/10.1002/(SICI)1097-0282(1997)43:5<339::AID-BIP2>3.0.CO;2-W

McMahon, A. P., Ingham, P. W., & Tabin, C. J. (2003). Developmental roles and clinical significance of hedgehog signaling. *Current Topics in Developmental Biology*, *53*, 1–114. Retrieved from http://www.ncbi.nlm.nih.gov/pubmed/12509125

Minami, K., Yano, H., Miki, T., Nagashima, K., Wang, C. Z., Tanaka, H., … Seino, S. (2000). Insulin secretion and differential gene expression in glucose-responsive and -unresponsive MIN6 sublines. *American Journal of Physiology. Endocrinology and Metabolism*, *279*(4), E773-81. Retrieved from http://www.ncbi.nlm.nih.gov/pubmed/11001758

Monami, G., Emiliozzi, V., & Morrione, A. (2008). Grb10/Nedd4-mediated multiubiquitination of the insulin-like growth factor receptor regulates receptor internalization. *Journal of Cellular Physiology*, *216*(2), 426–437. https://doi.org/10.1002/jcp.21405

Moses, A. C., Nissley, S. P., Short, P. A., Rechler, M. M., White, R. M., Knight, A. B., & Higa, O. Z. (1980). Increased levels of multiplication-stimulating activity, an insulin-like growth factor, in fetal rat serum. *Proceedings of the National Academy of Sciences of the United States of America*, *77*(6), 3649–53. Retrieved from http://www.ncbi.nlm.nih.gov/pubmed/6932040

Muoio, D. M., & Newgard, C. B. (2008). Mechanisms of disease: Molecular and metabolic mechanisms of insulin resistance and ?-cell failure in type 2 diabetes. *Nature Reviews Molecular Cell Biology*, *9*(3), 193–205. https://doi.org/10.1038/nrm2327

Myatt, S. S., & Lam, E. W.-F. (2007). The emerging roles of forkhead box (Fox) proteins in cancer. *Nature Reviews. Cancer*, *7*(11), 847–59. https://doi.org/10.1038/nrc2223

Nagase, T., Nagase, M., Machida, M., & Fujita, T. (2008). Hedgehog signalling in vascular development. *Angiogenesis*, *11*(1), 71–77. https://doi.org/10.1007/s10456-008-9105-5

Nakayama, S., Arakawa, M., Uchida, T., Ogihara, T., Kanno, R., Ikeda, F., … Watada, H. (2008). Dose-dependent requirement of patched homologue 1 in mouse pancreatic beta cell mass. *Diabetologia*, *51*(10), 1883–92. https://doi.org/10.1007/s00125-008-1080-2

Nolan, C. J., & Prentki, M. (2008). The islet β-cell: fuel responsive and vulnerable. *Trends in Endocrinology & Metabolism*, *19*(8), 285–291. https://doi.org/10.1016/j.tem.2008.07.006

Nystrom, F. H., Chen, H., Cong, L.-N., Li, Y., & Quon, M. J. (1999). Caveolin-1 Interacts with the Insulin Receptor and Can Differentially Modulate Insulin Signaling in Transfected Cos-7 Cells and Rat Adipose Cells. *Molecular Endocrinology*, *13*(12), 2013–2024. https://doi.org/10.1210/mend.13.12.0392

Oh, E. C., Vasanth, S., & Katsanis, N. (2015). Metabolic regulation and energy homeostasis

through the primary Cilium. *Cell Metabolism*, *21*(1), 21–31. https://doi.org/10.1016/j.cmet.2014.11.019

Onishi, H., & Katano, M. (2014). Hedgehog signaling pathway as a new therapeutic target in pancreatic cancer. *World Journal of Gastroenterology*, *20*(9), 2335–42. https://doi.org/10.3748/wjg.v20.i9.2335

Orth, J. D., Krueger, E. W., Weller, S. G., & McNiven, M. A. (2006). A novel endocytic mechanism of epidermal growth factor receptor sequestration and internalization. *Cancer Research*, *66*(7), 3603–10. https://doi.org/10.1158/0008-5472.CAN-05-2916

Otani, K., Kulkarni, R. N., Baldwin, A. C., Krutzfeldt, J., Ueki, K., Stoffel, M., … Polonsky, K. S. (2004). Reduced beta-cell mass and altered glucose sensing impair insulin-secretory function in betaIRKO mice. *American Journal of Physiology. Endocrinology and Metabolism*, *286*(1), E41-9. https://doi.org/10.1152/ajpendo.00533.2001

Oud, M., Lamers, I., & Arts, H. (2016). Ciliopathies: Genetics in Pediatric Medicine. *Journal of Pediatric Genetics*, *6*(1), 018–029. https://doi.org/10.1055/s-0036-1593841

Pak, E., & Segal, R. (2016). Hedgehog Signal Transduction: Key Players, Oncogenic Drivers, and Cancer Therapy. *Developmental Cell*, *38*(4), 333–344. https://doi.org/10.1016/j.devcel.2016.07.026

Papaioannou, V. E., & Behringer, R. (2005). *Mouse phenotypes : a handbook of mutation analysis*. Cold Spring Harbor Laboratory Press.

Pazour, G. J., & Witman, G. B. (2003). The vertebrate primary cilium is a sensory organelle. *Current Opinion in Cell Biology*, *15*(1), 105–10. Retrieved from http://www.ncbi.nlm.nih.gov/pubmed/12517711

Pedersen, L. B., & Rosenbaum, J. L. (2008). Intraflagellar transport (IFT) role in ciliary assembly, resorption and signalling. *Current Topics in Developmental Biology*, *85*, 23–61. https://doi.org/10.1016/S0070-2153(08)00802-8

Petrova, R., & Joyner, A. L. (2014). Roles for Hedgehog signaling in adult organ homeostasis and repair. *Development (Cambridge, England)*, *141*(18), 3445–57. https://doi.org/10.1242/dev.083691

Pettersson, U. S., Wald?n, T. B., Carlsson, P.-O., Jansson, L., & Phillipson, M. (2012). Female Mice are Protected against High-Fat Diet Induced Metabolic Syndrome and Increase the Regulatory T Cell Population in Adipose Tissue. *PLoS ONE*, *7*(9), e46057. https://doi.org/10.1371/journal.pone.0046057

Plotnikova, O. V., Pugacheva, E. N., & Golemis, E. A. (2009). Primary Cilia and the Cell Cycle. In *Methods in cell biology* (Vol. 94, pp. 137–160). https://doi.org/10.1016/S0091-679X(08)94007-3

Plotnikova, O. V, Nikonova, A. S., Loskutov, Y. V, Kozyulina, P. Y., Pugacheva, E. N., & Golemis, E. A. (2012). Calmodulin activation of Aurora-A kinase (AURKA) is required during ciliary disassembly and in mitosis. *Molecular Biology of the Cell*, *23*(14), 2658–70. https://doi.org/10.1091/mbc.E11-12-1056

Pola, R., Ling, L. E., Silver, M., Corbley, M. J., Kearney, M., Blake Pepinsky, R., … Isner, J. M. (2001). The morphogen Sonic hedgehog is an indirect angiogenic agent upregulating two families of angiogenic growth factors. *Nature Medicine*, *7*(6), 706–11. https://doi.org/10.1038/89083

Polishchuk, R. S., Capestrano, M., & Polishchuk, E. V. (2009). Shaping tubular carriers for intracellular membrane transport. *FEBS Letters*, *583*(23), 3847–3856. https://doi.org/10.1016/j.febslet.2009.10.031

Praefcke, G. J. K., & McMahon, H. T. (2004). The dynamin superfamily: universal membrane

tubulation and fission molecules? *Nature Reviews. Molecular Cell Biology*, *5*(2), 133–47. https://doi.org/10.1038/nrm1313

Prentki, M., & Nolan, C. J. (2006). Islet cell failure in type 2 diabetes. *Journal of Clinical Investigation*, *116*(7), 1802–1812. https://doi.org/10.1172/JCI29103

Ran, X., Zhou, P., & Zhang, K. (2017). Autophagy plays an important role in stemness mediation and the novel dual function of EIG121 in both autophagy and stemness regulation of endometrial carcinoma JEC cells. *International Journal of Oncology*. https://doi.org/10.3892/ijo.2017.4047

Ravassard, P., Hazhouz, Y., Pechberty, S., Bricout-Neveu, E., Armanet, M., Czernichow, P., & Scharfmann, R. (2011). A genetically engineered human pancreatic β cell line exhibiting glucose-inducible insulin secretion. *Journal of Clinical Investigation*, *121*(9), 3589–3597. https://doi.org/10.1172/JCI58447

Rezania, A., Bruin, J. E., Arora, P., Rubin, A., Batushansky, I., Asadi, A., … Kieffer, T. J. (2014). Reversal of diabetes with insulin-producing cells derived in vitro from human pluripotent stem cells. *Nature Biotechnology*, *32*(11), 1121–1133. https://doi.org/10.1038/nbt.3033

Rhodes, C. J., White, M. F., Leahy, J. L., & Kahn, S. E. (2013). Direct autocrine action of insulin on β-cells: does it make physiological sense? *Diabetes*, *62*(7), 2157–63. https://doi.org/10.2337/db13-0246

Riant, E., Waget, A., Cogo, H., Arnal, J.-F., Burcelin, R., & Gourdy, P. (2009). Estrogens Protect against High-Fat Diet-Induced Insulin Resistance and Glucose Intolerance in Mice. *Endocrinology*, *150*(5), 2109–2117. https://doi.org/10.1210/en.2008-0971

Ribas, V., Nguyen, M. T. A., Henstridge, D. C., Nguyen, A.-K., Beaven, S. W., Watt, M. J., & Hevener, A. L. (2010). Impaired oxidative metabolism and inflammation are associated with insulin resistance in ERalpha-deficient mice. *American Journal of Physiology. Endocrinology and Metabolism*, *298*(2), E304-19. https://doi.org/10.1152/ajpendo.00504.2009

Rice, L. M., & Agard, D. A. (2002). Centriole duplication: centrin in on answers? *Current Biology : CB*, *12*(18), R618-9. Retrieved from http://www.ncbi.nlm.nih.gov/pubmed/12372266

Röder, P. V, Wu, B., Liu, Y., & Han, W. (2016). Pancreatic regulation of glucose homeostasis. *Experimental & Molecular Medicine*, *48*(3), e219. https://doi.org/10.1038/emm.2016.6

Roith, D. Le. (2003). The Insulin-Like Growth Factor System. *Experimental Diabesity Research*, *4*(4), 205–212. https://doi.org/10.1155/EDR.2003.205

Rorsman, P., & Braun, M. (2013). Regulation of insulin secretion in human pancreatic islets. *Annual Review of Physiology*, *75*(1), 155–79. https://doi.org/10.1146/annurev-physiol-030212-183754

Roskoski, R. (2012). ERK1/2 MAP kinases: Structure, function, and regulation. *Pharmacological Research*, *66*(2), 105–143. https://doi.org/10.1016/j.phrs.2012.04.005

Rothberg, K. G., Heuser, J. E., Donzell, W. C., Ying, Y. S., Glenney, J. R., & Anderson, R. G. (1992). Caveolin, a protein component of caveolae membrane coats. *Cell*, *68*(4), 673–82. Retrieved from http://www.ncbi.nlm.nih.gov/pubmed/1739974

Rui, L. (2014). Energy metabolism in the liver. *Comprehensive Physiology*, *4*(1), 177–97. https://doi.org/10.1002/cphy.c130024

Sanchez, I., & Dynlacht, B. D. (2016). Cilium assembly and disassembly. *Nature Cell Biology*, *18*(7), 711–717. https://doi.org/10.1038/ncb3370

Salani, B., Briatore, L., Garibaldi, S., Cordera, R., & Maggi, D. (2008). Caveolin-1 Down-Regulation Inhibits Insulin-Like Growth Factor-I Receptor Signal Transduction in H9C2 Rat Cardiomyoblasts. *Endocrinology*, *149*(2), 461–465. https://doi.org/10.1210/en.2007-0312

Salani, B., Passalacqua, M., Maffioli, S., Briatore, L., Hamoudane, M., Contini, P., … Maggi, D. (2010). IGF-IR Internalizes with Caveolin-1 and PTRF/Cavin in Hacat Cells. *PLoS ONE*, *5*(11), e14157. https://doi.org/10.1371/journal.pone.0014157

Samuel, V. T., Shulman, G. I., Chung, S. K., Cresser, J. H., Sweeney, G., Wong, R. L., … al., et. (2012). Mechanisms for insulin resistance: common threads and missing links. *Cell*, *148*(5), 852–71. https://doi.org/10.1016/j.cell.2012.02.017

Sanders, M., Grondin, P., Hegarty, B., Snowden, M., & Carling, D. (2007). Investigating the mechanism for AMP activation of the AMP-activated protein kinase cascade. *Biochemical Journal*, *403*(1), 139–148. https://doi.org/10.1042/BJ20061520

Sankar, S., Mahooti-Brooks, N., Centrella, M., McCarthy, T. L., & Madri, J. A. (1995). Expression of transforming growth factor type III receptor in vascular endothelial cells increases their responsiveness to transforming growth factor beta 2. *The Journal of Biological Chemistry*, *270*(22), 13567–72. Retrieved from http://www.ncbi.nlm.nih.gov/pubmed/7768960

Sara, V. R., Hall, K., Misaki, M., Fryklund, L., Christensen, N., & Wetterberg, L. (1983). Ontogenesis of somatomedin and insulin receptors in the human fetus. *The Journal of Clinical Investigation*, *71*(5), 1084–94. Retrieved from http://www.ncbi.nlm.nih.gov/pubmed/6304143

Scheuner, D., Song, B., McEwen, E., Liu, C., Laybutt, R., Gillespie, P., … Kaufman, R. J. (2001). Translational control is required for the unfolded protein response and in vivo glucose homeostasis. *Molecular Cell*, *7*(6), 1165–76. Retrieved from http://www.ncbi.nlm.nih.gov/pubmed/11430820

Schlumbrecht, M. P., Xie, S.-S., Shipley, G. L., Urbauer, D. L., & Broaddus, R. R. (2011). Molecular clustering based on ERα and EIG121 predicts survival in high-grade serous carcinoma of the ovary/peritoneum. *Modern Pathology : An Official Journal of the United States and Canadian Academy of Pathology, Inc*, *24*(3), 453–62. https://doi.org/10.1038/modpathol.2010.211

Scholey, J. M. (2008). Intraflagellar transport motors in cilia: moving along the cell's antenna. *The Journal of Cell Biology*, *180*(1), 23–29. https://doi.org/10.1083/jcb.200709133

Seeger-Nukpezah, T., Liebau, M. C., Höpker, K., Lamkemeyer, T., Benzing, T., Golemis, E. A., & Schermer, B. (2012). The centrosomal kinase Plk1 localizes to the transition zone of primary cilia and induces phosphorylation of nephrocystin-1. *PloS One*, *7*(6), e38838. https://doi.org/10.1371/journal.pone.0038838

Sehat, B., Andersson, S., Girnita, L., & Larsson, O. (2008). Identification of c-Cbl as a New Ligase for Insulin-like Growth Factor-I Receptor with Distinct Roles from Mdm2 in Receptor Ubiquitination and Endocytosis. *Cancer Research*, *68*(14), 5669–5677. https://doi.org/10.1158/0008-5472.CAN-07-6364

Seino, S., & Bell, G. I. (1989). Alternative splicing of human insulin receptor messenger RNA. *Biochemical and Biophysical Research Communications*, *159*(1), 312–6. Retrieved from http://www.ncbi.nlm.nih.gov/pubmed/2538124

Senzen, S. (1978). Effects of ovariectomy and treatment with progesterone or oestradiol-17 beta on the secretion of insulin by the perfused rat pancreas. *The Journal of Endocrinology*, *78*(1), 153–4. Retrieved from http://www.ncbi.nlm.nih.gov/pubmed/355588

Shahi, M. H., Afzal, M., Sinha, S., Eberhart, C. G., Rey, J. A., Fan, X., & Castresana, J. S. (2010). Regulation of sonic hedgehog-GLI1 downstream target genes PTCH1, Cyclin D2, Plakoglobin, PAX6 and NKX2.2 and their epigenetic status in medulloblastoma and astrocytoma. *BMC Cancer*, *10*(1), 614. https://doi.org/10.1186/1471-2407-10-614

Shalom, O., Shalva, N., Altschuler, Y., & Motro, B. (2008). The mammalian Nek1 kinase is involved in primary cilium formation. *FEBS Letters*, *582*(10), 1465–70.

https://doi.org/10.1016/j.febslet.2008.03.036

Sharpe, S., Barber, K. R., & Grant, C. W. M. (2002). Interaction between ErbB-1 and ErbB-2 transmembrane domains in bilayer membranes. *FEBS Letters*, *519*(1–3), 103–7. Retrieved from http://www.ncbi.nlm.nih.gov/pubmed/12023026

Sheng, G., Chang, G., Lin, J. Y., Yu, Z.-X., Fang, Z.-H., Rong, J., … Li, X.-J. (2006). Hypothalamic huntingtin-associated protein 1 as a mediator of feeding behavior. *Nature Medicine*, *12*(5), 526–33. https://doi.org/10.1038/nm1382

Shi, H., & Clegg, D. J. (2009). Sex differences in the regulation of body weight. *Physiology & Behavior*, *97*(2), 199–204. https://doi.org/10.1016/j.physbeh.2009.02.017

Shi, Y., Kanaani, J., Menard-Rose, V., Ma, Y. H., Chang, P. Y., Hanahan, D., … Baekkeskov, S. (2000). Increased expression of GAD65 and GABA in pancreatic beta-cells impairs first-phase insulin secretion. *American Journal of Physiology. Endocrinology and Metabolism*, *279*(3), E684-94. Retrieved from http://www.ncbi.nlm.nih.gov/pubmed/10950838

Siddle, K. (2011). Signalling by insulin and IGF receptors: supporting acts and new players. *Journal of Molecular Endocrinology*, *47*(1), R1-10. https://doi.org/10.1530/JME-11-0022

Sigismund, S., Algisi, V., Nappo, G., Conte, A., Pascolutti, R., Cuomo, A., … Di Fiore, P. P. (2013). Threshold-controlled ubiquitination of the EGFR directs receptor fate. *The EMBO Journal*, *32*(15), 2140–57. https://doi.org/10.1038/emboj.2013.149

Singla, V., & Reiter, J. F. (2006). The primary cilium as the cell's antenna: signaling at a sensory organelle. *Science (New York, N.Y.)*, *313*(5787), 629–33. https://doi.org/10.1126/science.1124534

Sklar, M. M., Kiess, W., Thomas, C. L., & Nissley, S. P. (1989). Developmental expression of the tissue insulin-like growth factor II/mannose 6-phosphate receptor in the rat. Measurement by quantitative immunoblotting. *The Journal of Biological Chemistry*, *264*(28), 16733–8. Retrieved from http://www.ncbi.nlm.nih.gov/pubmed/2550455

Slaaby, R. (2015). Specific insulin/IGF1 hybrid receptor activation assay reveals IGF1 as a more potent ligand than insulin. *Scientific Reports*, *5*(1), 7911. https://doi.org/10.1038/srep07911

Sohar, I., Sleat, D., Gong Liu, C., Ludwig, T., & Lobel, P. (1998). Mouse mutants lacking the cation-independent mannose 6-phosphate/insulin-like growth factor II receptor are impaired in lysosomal enzyme transport: comparison of cation-independent and cation-dependent mannose 6-phosphate receptor-deficient mice. *The Biochemical Journal*, *330 (Pt 2)*, 903–8. Retrieved from http://www.ncbi.nlm.nih.gov/pubmed/9480908

Song, J., Xu, Y., Hu, X., Choi, B., & Tong, Q. (2010). Brain expression of Cre recombinase driven by pancreas-specific promoters. *Genesis*, *48*(11), 628–634. https://doi.org/10.1002/dvg.20672

Soos, M. A., & Siddle, K. (1989). Immunological relationships between receptors for insulin and insulin-like growth factor I. Evidence for structural heterogeneity of insulin-like growth factor I receptors involving hybrids with insulin receptors. *The Biochemical Journal*, *263*(2), 553–63. Retrieved from http://www.ncbi.nlm.nih.gov/pubmed/2480779

Soriano, P. (1999). Generalized lacZ expression with the ROSA26 Cre reporter strain. *Nature Genetics*, *21*(1), 70–71. https://doi.org/10.1038/5007

Soule, H. D., Vazquez, J., Long, A., Albert, S., & Brennan, M. (1973). A Human Cell Line From a Pleural Effusion Derived From a Breast Carcinoma 2. *JNCI: Journal of the National Cancer Institute*, *51*(5), 1409–1416. https://doi.org/10.1093/jnci/51.5.1409

Stenvers, K. L., Tursky, M. L., Harder, K. W., Kountouri, N., Amatayakul-Chantler, S., Grail, D., … Zhu, H.-J. (2003). Heart and liver defects and reduced transforming growth factor beta2

sensitivity in transforming growth factor beta type III receptor-deficient embryos. *Molecular and Cellular Biology*, *23*(12), 4371–85. Retrieved from http://www.ncbi.nlm.nih.gov/pubmed/12773577

Stoscheck, C. M., & Carpenter, G. (1984). Characterization of the metabolic turnover of epidermal growth factor receptor protein in A-431 cells. *Journal of Cellular Physiology*, *120*(3), 296–302. https://doi.org/10.1002/jcp.1041200306

Straface, G., Aprahamian, T., Flex, A., Gaetani, E., Biscetti, F., Smith, R. C., … Pola, R. (2009). Sonic hedgehog regulates angiogenesis and myogenesis during post-natal skeletal muscle regeneration. *Journal of Cellular and Molecular Medicine*, *13*(8B), 2424–35. https://doi.org/10.1111/j.1582-4934.2008.00440.x

Sturgill, T. W. (2008). MAP kinase: it's been longer than fifteen minutes. *Biochemical and Biophysical Research Communications*, *371*(1), 1–4. https://doi.org/10.1016/j.bbrc.2008.04.002

Sun, X. J., & Liu, F. (2009). Phosphorylation of IRS proteins Yin-Yang regulation of insulin signaling. *Vitamins and Hormones*, *80*, 351–87. https://doi.org/10.1016/S0083-6729(08)00613-4

Suspitsin, E. N., & Imyanitov, E. N. (2016). Bardet-Biedl Syndrome. *Molecular Syndromology*, *7*(2), 62–71. https://doi.org/10.1159/000445491

Suzuki, T., Imai, J., Yamada, T., Ishigaki, Y., Kaneko, K., Uno, K., … Katagiri, H. (2011). Interleukin-6 Enhances Glucose-Stimulated Insulin Secretion From Pancreatic -Cells: Potential Involvement of the PLC-IP3-Dependent Pathway. *Diabetes*, *60*(2), 537–547. https://doi.org/10.2337/db10-0796

Tahrani, A. A., Barnett, A. H., & Bailey, C. J. (2016). Pharmacology and therapeutic implications of current drugs for type 2 diabetes mellitus. *Nature Reviews Endocrinology*, *12*(10), 566–592. https://doi.org/10.1038/nrendo.2016.86

Tang, T., Li, L., Tang, J., Li, Y., Lin, W. Y., Martin, F., … de Sauvage, F. J. (2010). A mouse knockout library for secreted and transmembrane proteins. *Nature Biotechnology*, *28*(7), 749–755. https://doi.org/10.1038/nbt.1644

Taniguchi, C. M., Emanuelli, B., & Kahn, C. R. (2006). Critical nodes in signalling pathways: insights into insulin action. *Nature Reviews. Molecular Cell Biology*, *7*(2), 85–96. https://doi.org/10.1038/nrm1837

Taniguchi, C. M., Ueki, K., & Kahn, C. R. (2005). Complementary roles of IRS-1 and IRS-2 in the hepatic regulation of metabolism. *Journal of Clinical Investigation*, *115*(3), 718–727. https://doi.org/10.1172/JCI23187

Tao, R.-H., & Maruyama, I. N. (2008). All EGF(ErbB) receptors have preformed homo- and heterodimeric structures in living cells. *Journal of Cell Science*, *121*(Pt 19), 3207–17. https://doi.org/10.1242/jcs.033399

Tatulian, S. A. (2015). Structural Dynamics of Insulin Receptor and Transmembrane Signaling. *Biochemistry*, *54*(36), 5523–5532. https://doi.org/10.1021/acs.biochem.5b00805

Tazat, K., Hector-Greene, M., Blobe, G. C., & Henis, Y. I. (2015). TβRIII independently binds type I and type II TGF-β receptors to inhibit TGF-β signaling. *Molecular Biology of the Cell*, *26*(19), 3535–45. https://doi.org/10.1091/mbc.E15-04-0203

Thirone, A. C. P., Huang, C., & Klip, A. (2006). Tissue-specific roles of IRS proteins in insulin signaling and glucose transport. *Trends in Endocrinology & Metabolism*, *17*(2), 72–78. https://doi.org/10.1016/j.tem.2006.01.005

Thomas, M. K., Lee, J. H., Rastalsky, N., & Habener, J. F. (2001). Hedgehog Signaling Regulation of Homeodomain Protein Islet Duodenum Homeobox-1 Expression in Pancreatic β-Cells [1].

Endocrinology, *142*(3), 1033–1040. https://doi.org/10.1210/endo.142.3.8007

Thomas, M. K., Rastalsky, N., Lee, J. H., & Habener, J. F. (2000). Hedgehog signaling regulation of insulin production by pancreatic beta-cells. *Diabetes*, *49*(12), 2039–47. Retrieved from http://www.ncbi.nlm.nih.gov/pubmed/11118005

Thompson, S., Clarke, A. R., Pow, A. M., Hooper, M. L., & Melton, D. W. (1989). Germ line transmission and expression of a corrected HPRT gene produced by gene targeting in embryonic stem cells. *Cell*, *56*(2), 313–21. Retrieved from http://www.ncbi.nlm.nih.gov/pubmed/2912572

Tiano, J. P., & Mauvais-Jarvis, F. (2012). Importance of oestrogen receptors to preserve functional β-cell mass in diabetes. *Nature Reviews. Endocrinology*, *8*(6), 342–51. https://doi.org/10.1038/nrendo.2011.242

Traub, L. M. (2009a). Tickets to ride: selecting cargo for clathrin-regulated internalization. *Nature Reviews Molecular Cell Biology*, *10*(9), 583–596. https://doi.org/10.1038/nrm2751

Traub, L. M. (2009b). Tickets to ride: selecting cargo for clathrin-regulated internalization. *Nature Reviews. Molecular Cell Biology*, *10*(9), 583–96. https://doi.org/10.1038/nrm2751

Turgeon, B., & Meloche, S. (2009). Interpreting neonatal lethal phenotypes in mouse mutants: insights into gene function and human diseases. *Physiological Reviews*, *89*(1), 1–26. https://doi.org/10.1152/physrev.00040.2007

Tuttle, R. L., Gill, N. S., Pugh, W., Lee, J.-P., Koeberlein, B., Furth, E. E., … Birnbaum, M. J. (2001). Regulation of pancreatic beta-cell growth and survival by the serine/threonine protein kinase Akt1/PKBalpha. *Nature Medicine*, *7*(10), 1133–1137. https://doi.org/10.1038/nm1001-1133

Uchizono, Y., Alarcón, C., Wicksteed, B. L., Marsh, B. J., & Rhodes, C. J. (2007). The balance between proinsulin biosynthesis and insulin secretion: where can imbalance lead? *Diabetes, Obesity & Metabolism*, *9 Suppl 2*(s2), 56–66. https://doi.org/10.1111/j.1463-1326.2007.00774.x

Ullrich, S. (2015). IGF-1 and Insulin-Receptor Signalling in Insulin-Secreting Cells: From Function to Survival. In *Islets of Langerhans* (pp. 659–685). Dordrecht: Springer Netherlands. https://doi.org/10.1007/978-94-007-6686-0_26

Varjosalo, M., & Taipale, J. (2008). Hedgehog: functions and mechanisms. *Genes & Development*, *22*(18), 2454–2472. https://doi.org/10.1101/gad.1693608

Vasudevan, K. M., & Garraway, L. A. (2010). AKT signaling in physiology and disease. *Current Topics in Microbiology and Immunology*, *347*, 105–33. https://doi.org/10.1007/82_2010_66

Viollet, B., Guigas, B., Garcia, N. S., Leclerc, J., Foretz, M., & Andreelli, F. (2012). Cellular and molecular mechanisms of metformin: an overview. *Clinical Science*, *122*(6), 253–270. https://doi.org/10.1042/CS20110386

Wang, G., Zhang, Z., Xu, Z., Yin, H., Bai, L., Ma, Z., … Wu, G. (2010). Activation of the sonic hedgehog signaling controls human pulmonary arterial smooth muscle cell proliferation in response to hypoxia. *Biochimica et Biophysica Acta*, *1803*(12), 1359–67. https://doi.org/10.1016/j.bbamcr.2010.09.002

Wang, Y. J., Schug, J., Won, K.-J., Liu, C., Naji, A., Avrahami, D., … Kaestner, K. H. (2016). Single-Cell Transcriptomics of the Human Endocrine Pancreas. *Diabetes*, *65*(10), 3028–38. https://doi.org/10.2337/db16-0405

Wang, Z.-Q., Fung, M. R., Barlow, D. P., & Wagner, E. F. (1994). Regulation of embryonic growth and lysosomal targeting by the imprintedIgf2/Mpr gene. *Nature*, *372*(6505), 464–467. https://doi.org/10.1038/372464a0

Ward, A. (1997). Beck-Wiedemann syndrome and Wilms' tumour. *Molecular Human Reproduction*, *3*(2), 157–68. Retrieved from http://www.ncbi.nlm.nih.gov/pubmed/9239720

Ward, C. W., Hoyne, P. A., & Flegg, R. H. (1995). Insulin and epidermal growth factor receptors contain the cysteine repeat motif found in the tumor necrosis factor receptor. *Proteins*, *22*(2), 141–53. https://doi.org/10.1002/prot.340220207

Ward, C. W., Lawrence, M. C., Streltsov, V. A., Adams, T. E., & McKern, N. M. (2007). The insulin and EGF receptor structures: new insights into ligand-induced receptor activation. *Trends in Biochemical Sciences*, *32*(3), 129–37. https://doi.org/10.1016/j.tibs.2007.01.001

Wechsler-Reya, R. J., & Scott, M. P. (1999). Control of neuronal precursor proliferation in the cerebellum by Sonic Hedgehog. *Neuron*, *22*(1), 103–14. Retrieved from http://www.ncbi.nlm.nih.gov/pubmed/10027293

Whiteman, E. L., Cho, H., & Birnbaum, M. J. (2002). Role of Akt/protein kinase B in metabolism. *Trends in Endocrinology and Metabolism: TEM*, *13*(10), 444–51. Retrieved from http://www.ncbi.nlm.nih.gov/pubmed/12431841

WHO | *Global report on diabetes*. (2017). *WHO*. Retrieved from http://www.who.int/diabetes/global-report/en/

Wicksteed, B., Brissova, M., Yan, W., Opland, D. M., Plank, J. L., Reinert, R. B., … Dempsey, P. J. (2010). Conditional gene targeting in mouse pancreatic ß-Cells: analysis of ectopic Cre transgene expression in the brain. *Diabetes*, *59*(12), 3090–8. https://doi.org/10.2337/db10-0624

Willmann, S. J., Mueller, N. S., Engert, S., Sterr, M., Burtscher, I., Raducanu, A., … Lickert, H. (2016). The global gene expression profile of the secondary transition during pancreatic development. *Mechanisms of Development*, *139*, 51–64. https://doi.org/10.1016/j.mod.2015.11.004

Winder, W. W., & Hardie, D. G. (1999). AMP-activated protein kinase, a metabolic master switch: possible roles in type 2 diabetes. *The American Journal of Physiology*, *277*(1 Pt 1), E1-10. Retrieved from http://www.ncbi.nlm.nih.gov/pubmed/10409121

Xie, J., & Herbert, T. P. (2012). The role of mammalian target of rapamycin (mTOR) in the regulation of pancreatic β-cell mass: implications in the development of type-2 diabetes. *Cellular and Molecular Life Sciences*, *69*(8), 1289–1304. https://doi.org/10.1007/s00018-011-0874-4

Xu, J., Li, H., Wang, B., Xu, Y., Yang, J., Zhang, X., … Esteban, M. A. (2010). VHL inactivation induces HEF1 and Aurora kinase A. *Journal of the American Society of Nephrology : JASN*, *21*(12), 2041–6. https://doi.org/10.1681/ASN.2010040345

Xuan, S., Kitamura, T., Nakae, J., Politi, K., Kido, Y., Fisher, P. E., … Efstratiadis, A. (2002). Defective insulin secretion in pancreatic beta cells lacking type 1 IGF receptor. *The Journal of Clinical Investigation*, *110*(7), 1011–9. https://doi.org/10.1172/JCI15276

Yang, J.-S., Lee, S. Y., Gao, M., Bourgoin, S., Randazzo, P. A., Premont, R. T., & Hsu, V. W. (2002). ARFGAP1 promotes the formation of COPI vesicles, suggesting function as a component of the coat. *The Journal of Cell Biology*, *159*(1), 69–78. https://doi.org/10.1083/jcb.200206015

York, S. J., Arneson, L. S., Gregory, W. T., Dahms, N. M., & Kornfeld, S. (1999). The rate of internalization of the mannose 6-phosphate/insulin-like growth factor II receptor is enhanced by multivalent ligand binding. *The Journal of Biological Chemistry*, *274*(2), 1164–71. Retrieved from http://www.ncbi.nlm.nih.gov/pubmed/9873065

Yovos, J. G. (2011). The role of α-, δ- and F cells in insulin secretion and action. *Diabetes Research*

and Clinical Practice, *93*, S25–S26. https://doi.org/10.1016/S0168-8227(11)70009-2

Zang, G., Sandberg, M., Carlsson, P.-O., Welsh, N., Jansson, L., & Barbu, A. (2015). Activated pancreatic stellate cells can impair pancreatic islet function in mice. *Upsala Journal of Medical Sciences*, *120*(3), 169–80. https://doi.org/10.3109/03009734.2015.1032453

Zani, I., Stephen, S., Mughal, N., Russell, D., Homer-Vanniasinkam, S., Wheatcroft, S., & Ponnambalam, S. (2015). Scavenger Receptor Structure and Function in Health and Disease. *Cells*, *4*(2), 178–201. https://doi.org/10.3390/cells4020178

Zeslawski, W., Beisel, H. G., Kamionka, M., Kalus, W., Engh, R. A., Huber, R., … Holak, T. A. (2001). The interaction of insulin-like growth factor-I with the N-terminal domain of IGFBP-5. *The EMBO Journal*, *20*(14), 3638–3644. https://doi.org/10.1093/emboj/20.14.3638

Zhang, Q., Berggren, P. O., & Tally, M. (1997). Glucose increases both the plasma membrane number and phosphorylation of insulin-like growth factor II/mannose 6-phosphate receptors. *The Journal of Biological Chemistry*, *272*(38), 23703–6. https://doi.org/10.1074/JBC.272.38.23703

Zick, Y. (2005). Ser/Thr Phosphorylation of IRS Proteins: A Molecular Basis for Insulin Resistance. *Science Signaling*, *2005*(268), pe4-pe4. https://doi.org/10.1126/stke.2682005pe4

Zisman, A., Peroni, O. D., Abel, E. D., Michael, M. D., Mauvais-Jarvis, F., Lowell, B. B., … Kahn, B. B. (2000). Targeted disruption of the glucose transporter 4 selectively in muscle causes insulin resistance and glucose intolerance. *Nature Medicine*, *6*(8), 924–8. https://doi.org/10.1038/78693

9 Acknowledgments

First of all, I am very grateful to my PhD advisor, Prof. Dr. Heiko Lickert for the interesting and fascinating research project, his patience, inspiration and continuous scientific support. The joy and enthusiasm he has for his research is contagious and motivational. I would like to show my appreciation to Dr. Aurelia Raducanu for all her brilliant ideas, the fruitful discussions and the opportunity to learn from her. I have greatly benefited from her knowledge. My sincere gratitude goes to Dr. Ingo Burtscher who greatly supported me in the characterization of the ARL13B-tRPF mouse line and who helped me publishing this project! Furthermore, I would like to thank the receptor and GTT team including Dr. Aurelia Raducanu, Fataneh Fathi Far, Sarah Homberg, Dr. Amir Morshedi, Katharina Wißmiller, Robert Fimmen, Jürgen Schultheiß, Alexandra Aliluev for the great teamwork and support. A big thank you also to Robert Fimmen for his excellent technical assistance. I want to pay my regards to Dr. Anika Böttcher who patiently answered thousands of questions and gave me lots of input. I would also like to deeply thank Alexandra Aliluev and Michael Sterr for their great friendship, encouragement and scientific help (especially all the bioinformatics). We spend many nights out and had a lot of fun together during the last five years. Additionally, I would like to acknowledge Dr. Jantje Gerdes and Francesco Volta for sharing their expertise on the cilia and metabolism field as well as Dr. Bomi Jung for introducing me to many techniques in the laboratory in the beginning of my PhD. I would like to thank Prof. Dr. Heiko Lickert, Dr. Mostafa Bakhti, Dr. Aurelia Raducanu, Dr. Ingo Burtscher, Dr. Pallavi Mahaddalkar, Dr. Julia Scerbo, Alexandra Aliluev, Michael Sterr, Dr. Silvia Engert and Bomi Jung for correcting my thesis and giving me insightful comments and suggestions. Moreover, I appreciate the technical support received from the animal care takers and many coworkers including Kerstin Diemer, Gabriele Glaser, Anne Theis and Bianca Vogel. Many thanks goes to all my fellow labmates for the stimulating scientific discussions, good advices, collaborations and great moments at lunchtime. I wish to present my special thanks to all collaboration partners including Prof. Dr. Achim Gossler and Dr. Michael Stauber as well as to all members of the thesis committee for their valuable comments and input to my project (Prof. Dr. Heiko Lickert, Prof. Dr. Martin Hrabě de Angelis, Prof. Dr. Roland Schmid and Dr. Paul Pfluger).

My sincere gratitude to my family and friends for their continuous love and warm encouragements. You make my life colourful! Finally, am I deeply grateful to Cuno for his endless love, patients, his believe in me and his support during wonderful and difficult times of my PhD thesis.

10 Attachment

See CD with movies attached at the cover of the thesis.

11 List of publications

Bug S, **Schmitz F**, Nevinny-Stickel-Hinzpeter C. The Correct Genetic Diagnosis Has Already Been Determined More Often Than We Think, Let's Report It to the Parents! Clin Pediatr (Phila) [Internet]. 2014 Jan 22 [cited 2017 Aug 11];53(1):8–10. Available from: http://www.ncbi.nlm.nih.gov/pubmed/23613176

Bug, S, **Schmitz, F** & Nevinny-Stickel-Hinzpeter, C. Imbalancen im Genom: Eine Ursache mit oft großer Wirkung auf das klinische Erscheinungsbild. Pädiatrix 1, 14-17 (2013)

Bug S, Solfrank B, **Schmitz F**, Pricelius J, Stecher M, Craig A, et al. Diagnostic utility of novel combined arrays for genome-wide simultaneous detection of aneuploidy and uniparental isodisomy in losses of pregnancy. Mol Cytogenet [Internet]. 2014 [cited 2017 Aug 11];7(1):43. Available from: http://www.ncbi.nlm.nih.gov/pubmed/25013457

Schmitz F, Roscioni S, Lickert H. Repurposing an Osteoporosis Drug for β Cell Regeneration in Diabetic Patients. Cell Metab [Internet]. 2015 Jul 7 [cited 2017 Aug 18];22(1):58–9. Available from: http://linkinghub.elsevier.com/retrieve/pii/S1550413115002673

Schmitz F, Burtscher I, Stauber M, Gossler A, Lickert H. A novel Cre-inducible knock-in ARL13B-tRFP fusion cilium reporter. (2017) *Submitted to the journal Genesis*